#### OFFICIAL JOURNAL OF THE SCIENTIFIC SOCIETY OF ANATOMISTS, HISTOLOGISTS, EMBRYOLOGISTS AND TOPOGRAPHIC ANATOMISTS OF UKRAINE

DOI: 10.31393 ISSN 1818-1295 eISSN 2616-6194

# BICHИК МОРФОЛОГІЇ REPORTS OF MORPHOLOGY

VOL. 31, №1, 2025

Scientific peer-reviewed journal in the fields of normal and pathological anatomy, histology, cytology and embryology, topographical anatomy and operative surgery, biomedical anthropology, ecology, molecular biology, biology of development

Published since 1993 Periodicity: 4 times a year

#### ВІСНИК МОРФОЛОГІЇ - REPORTS OF MORPHOLOGY

Founded by the "Scientific Society of Anatomists, Histologists, Embryologists, and Topographic Anatomists of Ukraine" and National Pyrogov Memorial Medical University, Vinnytsya in 1993

Certificate of state registration KB №9310 from 02.11.2004

Professional scientific publication of Ukraine in the field of medical sciences in specialties 221, 222, 228, 229

According to the list of professional scientific publications of Ukraine, approved by the order of the Ministry of Education and Science of Ukraine No. 1188 of 24.09.2020

Professional scientific publication of Ukraine in the field of biological sciences in specialty 091

According to the list of professional scientific publications of Ukraine, approved by the order of the Ministry of Education and Science of Ukraine No. 1471 of 26.11.2020

Chairman of the Editorial Board - Gunas I.V. (Vinnytsya)

Vice-Chairman of Editorial Board - Berenshtein E.L. (Jerusalem), Kovalchuk O.I. (Kyiv)

Secretary - Kaminska N.A. (Vinnytsya)

#### **Editorial Board Members:**

Byard R. (Adelaida), Graeb C. (Hof), Gunas V.I. (Vinnytsya), Juenemann A. (Rostock), Maievskyi O.Ye. (Kyiv), Moskalenko R.A. (Sumy), Nebesna Z.M. (Ternopil), Pivtorak V.I. (Vinnytsya), Rejdak R. (Lublin), Romaniuk A.M. (Sumy), Shinkaruk-Dykovytska M.M. (Vinnytsya), Skibo G.G. (Kyiv), Vlasenko O.V. (Vinnytsya)

#### **Editorial Council:**

Appelhans O.L. (Odessa), Bulyk R.Ye. (Chernivtsi), Dgebuadze M.A. (Tbilisi), Fedonyuk L.Ya. (Ternopil), Fomina L.V. (Vinnytsya), Furman Yu.M. (Vinnytsya), Gerasymyuk I.Ye. (Ternopil), Golovatskyy A.S. (Uzhgorod), Guminskyi Yu.Y. (Vinnytsya), Herashchenko S.B. (Ivano-Frankivsk), Kostylenko Yu.P. (Poltava), Kryvko Yu.Ya. (Lviv), Lutsyk O.D. (Lviv), Mateshuk-Vatseba L.R. (Lviv), Mishalov V.D. (Kyiv), Ocheredko O.M. (Vinnytsya), Olkhovskyy V.O. (Kharkiv), Piskun R.P. (Vinnytsya), Rudyk S.K. (Kyiv), Sarafyniuk L.A. (Vinnytsya), Shepitko V.I. (Poltava), Sherstyuk O.O. (Poltava), Shevchuk Yu.G. (Vinnytsya), Shkolnikov V.S. (Vinnytsya), Sikora V.Z. (Sumy), Slobodian O.M. (Chernivtsi), Sokurenko L.M. (Kyiv), Stechenko L.O. (Kyiv), Tereshchenko V.P. (Kyiv), Topka E.G. (Dnipro), Tverdokhlib I.V. (Dnipro), Tykholaz V.O. (Vinnytsya), Yatsenko V.P. (Kviv), Yeroshenko G.A. (Poltava)

Approved by the Academic Council of National Pyrogov Memorial Medical University, Vinnytsya, protocol №7 from 27.02.2025.

*Indexation:* Scopus, CrossRef, Index Copernicus, Google Schoolar Metrics, National Library of Ukraine Vernadsky

Address editors and publisher:

Pyrogov Str. 56, Vinnytsya, Ukraine - 21018 Tel.: +38 (0432) 553959 E-mail: nila@vnmu.edu.ua Computer page-proofs - Slobodianiuk L.M. Translator - Gunas V.I. Technical support - Levenchuk S.S. Scientific editing - editorship

The site of the magazine - https://morphology-journal.com

## CONTENT

Petrushko M. P., Piniaiev V. I., Yurchuk T. O.  Morphological and morphometric characteristics of human oocytes' Zona pellucida:  effect on embryological and cryobiological outcomess
<b>Tsubanova N. A., Voloshchuk N. I., Zastryzhna M. L.</b> Study of the effect of Saponaria officinalis herb extract on histological changes in the marginal vein of the ear under conditions of experimental thrombophlebitis
Kritsak M. Yu., Dzyubanovsky I. Ya., Golovata T. K., Gargula T. I., Yasinovskyi O. B., Palamar S. A. Structural changes in the diaphragm under conditions of obstructive jaundice (an experimental study)22
Bartiuk R. S., Smolko D. G., Smotrytska T. V., Marunkevych Ya. Yu., Starynets N. H., Fiks D. O., Moskovko S. P. Characteristics of cerebral morphometric parameters in acute stroke patients and its associations with 90 days stroke outcome
Vynnychenko O. I., Moskalenko Yu. V., Piddubnyi A. M., Moskalenko R. A.  Distribution of M1 and M2 macrophages and their impact on survival in non-small cell lung cancer
Yakubov M. Z.  Morphometric indices of thickness of artificial vagina created from colon
Polyviana O. A., Stetsuk E. V., Shepitko V. I., Vilkhova O. V., Boruta N. V., Rud M. V., Pelypenko L. B., Lysachenko O. D., Voloshyna O. V., Dvornyk I. L., Morokhovets H. Yu. Studies of changes in rat hepatocytes under conditions of central blockade of luteinizing hormone synthesis with the additional quercetin
Nyzova O. A., Chaika H. V., Berenshtein E. L., Kryvonis T. G., Kyrychenko V. I., Sorokoumov V. P., Gunas I. V.  Discriminant models of the possibility of genital endometriosis in Ukrainian young women depending on the features of the structure and body size
Strafun S. S., Bohdan S. V., Savosko S. I., Yuriychuk L. M.  A correlation between cartilage degradation and inflammation of the synovial membrane of shoulder joint in a rabbit model of collagenase-induced osteoarthritis
Mizyakina K. V., Dzyak L. A., Tverdokhlib I. V.  Morphological changes in the cingulate gyrus in rats with various neurocognitive disorders after traumatic brain injury

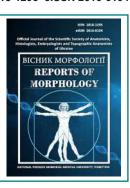
ISSN 1818-1295 eISSN 2616-6194



#### REPORTS OF MORPHOLOGY

Official Journal of the Scientific Society of Anatomists, Histologists, Embryologists and Topographic Anatomists of Ukraine

journal homepage: https://morphology-journal.com



## Morphological and morphometric characteristics of human oocytes' Zona pellucida: effect on embryological and cryobiological outcomes

Petrushko M. P.1, Piniaiev V. I.1, Yurchuk T. O.1,2

<sup>1</sup>Institute for Problems of Cryobiology and Cryomedicine of the National Academy of Sciences of Ukraine, Kharkiv, Ukraine <sup>2</sup>Institute of Animal Reproduction and Food Research of the Polish Academy of Sciences in Olsztyn, 10-748 Olsztyn, Poland

#### **ARTICLE INFO**

Received: 4 June 2024 Accepted: 11 November 2024

UDC: 612.017.1:576.33:577.21

#### **CORRESPONDING AUTHOR**

e-mail: petrushkomarina@gmail.com Petrushko M. P.

#### **CONFLICT OF INTEREST**

The authors have no conflicts of interest to declare.

#### **FUNDING**

The study was carried out within the framework of the state scientific theme of the National Academy of Sciences of Ukraine (State Registration No. 0120U100546).

#### **DATA SHARING**

Data are available upon reasonable request to corresponding author.

Cryobiological approaches are widely applied enabling the preservation of the viability of reproductive cells and tissues in order to improve the success rates of infertility treatment cycles using assisted reproductive technologies. Cryopreservation offers patients the opportunity to store biological material for an extended period of time. This is especially important for those with cancer or other conditions that may affect fertility. At the same time, the search for cryoresistance markers has become an important area of focus, as it allows for identifying which cells are best suited for low-temperature storage. Research on gametes cryoresistance is helping to identify factors that influence cellular resilience to freezing and thawing, including membrane structural features, cellular lipid composition, and the presence of specific proteins and antioxidant systems. This enables the optimization of storage conditions and the selection of the most effective cryoprotectants for each cell type. The aim of the study was to investigate the effect of the morphological and morphometric characteristics of the Zona pellucida (ZP) on oocyte survival, fertilization, and development to the blastocyst stage. After oocytes isolation and denudation, the morphological (transparency, integrity) and morphometric (thickness) characteristics were assessed. The survival rate of oocytes post-cryopreservation was evaluated regarding their morphological characteristics. Fisher's criterion was used to assess the significance of differences among study groups, with data considered significant at p<0.05. The study found that normal ZP morphological characteristics, specifically high transparency and structural integrity, were most common in oocytes from the youngest patient group aged 29.81±3.53 years. This group also exhibited the highest oocyte survival rates post-cryopreservation. There was significantly higher chance to retrieve oocytes without ZP in group of women aged 38.50±3.65 years old had compared to the youngest group. The total dose of folliclestimulating hormone required for superovulation induction also increased with patient age and was the highest in the group with ZP abnormalities. The highest survival rate post-cryopreservation was observed in oocytes with a normal ZP structure (93 %), whereas oocytes with absent or abnormal ZP showed significantly lower survival rates, indicating a negative impact of ZP defects on cryoresistance (42 % in the group with completely absent ZP). ZP thickness was shown to influence cryoprotectant saturation and oocyte survival after cryopreservation. Structurally intact ZP allowed normal cryoprotectant saturation, while increasing ZP thickness prolonged the required equilibration time. Oocytes with ZP thickness up to 10 µm required 5 minutes, those with 11-15 μm needed 7.5 minutes, 16-20 μm required 10 minutes, and ZP thicker than 20 µm needed 12.5 minutes for optimal results. Prolonging exposure time adversely affected oocytes with thinner ZP, indicating their increased sensitivity to cryoprotectants. Thus, ZP thickness is a critical factor in oocyte survival post-cryopreservation, and adjusting cryoprotectant exposure time accordingly to ZP morphometric characteristics can improve fertility preservation outcomes.

**Keywords:** human oocytes, morphology, morphometry, cryopreservation, Zona pellucida.

#### Introduction

Oocyte cryopreservation is an important method for preserving fertility in patients planning to undergo gonadotoxic therapy, such as cancer treatment [7, 25]. At the same time, the physical and chemical factors involved in this process may cause cellular damage, negatively affecting the structural and functional characteristics of oocytes [17, 23]. The effectiveness of oocyte cryopreservation depends on their initial morphological state, stage of development, and the patient's age [25]. The morphological and morphometric characteristics of cellular structures, particularly the Zona pellucida (ZP), can also significantly impact oocyte cryoresistance.

ZP is an extracellular matrix that forms around the oocyte during primary follicle development, with a thickness ranging from 5 to 20  $\mu$ m [20]. It consists of four glycoproteins that create a mesh-like structure [13]. The ZP ensures the stability of contacts between cumulus cell projections and oocyte microvilli, which pass through the ZP and form gap junctions, known to be important for efficient oocyte maturation [10]. The ZP also plays a crucial role in fertilization; in particular, the cortical reaction following sperm-oocyte fusion prevents additional sperm penetration [31, 32].

It is known that the elasticity and stiffness of the extracellular matrix affect fundamental cellular processes. including growth, proliferation, migration, differentiation, and organoid formation [5]. These properties also play a crucial role in protecting cells from potential damage caused by ice crystal formation during cryopreservation [6]. A key step in the cryopreservation process is the equilibration of cells with cryoprotectants. Oocytes are particularly sensitive to increased osmolarity, a factor that is partially regulated by the ZP [2]. The structural and functional characteristics of the ZP play an important role in this process, influencing cryoprotectant permeability and osmotic balance. It is known that specific ZP features, such as elasticity, thickness, and morphological characteristics, can significantly affect oocyte competence [16] and subsequent embryological development [19].

However, it remains an open question how the morphological features of the ZP or even its complete absence – affect cryopreservation efficiency. Understanding these effects is crucial for optimizing cryopreservation protocols, as current protocols are developed using a generalized approach rather than being adapted to individual oocyte characteristics [8].

The aim of this study was to investigate the influence of the morphological and morphometric characteristics of the ZP on oocyte survival, fertilization, and development to the blastocyst stage.

#### Materials and methods

The study was conducted at the ART Clinic for Reproductive Medicine in Kharkiv. Embryological protocols of patients undergoing infertility treatment using ART methods were retrospectively analyzed.

All experiments were carried out in compliance with the

principles of biomedical ethics. Written informed consent was obtained from all patients for the use of their oocytes and embryos in the study. All procedures adhered to the Order of the Ministry of Health of Ukraine dated 09.09.2013 No. 787, "On Approval of the Procedure for the Use of Assisted Reproductive Technologies in Ukraine," and the European Protocol for the Protection of Embryos [9]. The study was conducted in accordance with the principles of the Declaration of Helsinki on Human Rights, the Council of Europe Convention on Human Rights and Biomedicine, and the recommendations of ESHRE and ASRM [11, 18]. The study was approved by the Bioethics Committee of the Institute for Problems of Cryobiology and Cryomedicine of the National Academy of Sciences of Ukraine (Protocol No. 1, 2019).

Superovulation induction and ART procedures were performed according to standard protocols [11]. Follicles were aspirated 36 hours after the administration of 10.000 IU hCG (Ovitrel, Switzerland) using a single-lumen aspiration needle (Wallace, Smiths Medical International, UK) under reduced pressure (150 mm Hg). The collected oocytes were evaluated for nuclear maturity under a stereomicroscope (Olympus Co., Japan). Oocyte maturity was assessed using a stripper (Cook, USA) and 80 IU hyaluronidase (SuperSurgical, USA). Oocytes with a clearly visible first polar body under a light microscope were considered mature (metaphase II).

Denuded oocytes were placed in a drop of Global Total fertilization culture medium (CooperSurgical, USA) in 30 mm Petri dishes (Thermo Fisher Scientific, Denmark).

For detailed visualization of the ZP, an Olympus IX-71 inverted microscope (Olympus, Japan) with ×400 magnification was used. Oocytes were photographed from different angles using a universal 5.0-megapixel Olympus SC50 camera (Olympus, Japan) to obtain a comprehensive view of the morphological and morphometric characteristics of the ZP.

The images were processed using ImageJ software (NIH, USA) for morphometric analysis. The thickness of the ZP was measured by determining the distance between its outer and inner borders at five points on each image to ensure data representativeness (Fig. 1).

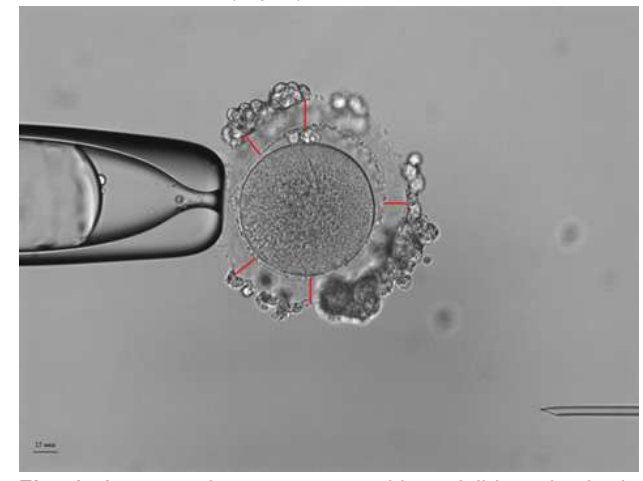


**Fig. 1.** A mature human oocyte with a visible polar body, perivitelline space, and cumulus cells on the ZP.

At the first stage of the study, oocytes were divided into three groups based on the morphological characteristics of the ZP. The survival rate, fertilization, and development of the resulting zygotes to the blastocyst stage *in vitro* were analyzed in relation to ZP morphology. Group I (54 oocytes): ZP intact, transparent, smooth homogeneous structure with a perivitelline space; group II (37 oocytes): these oocytes had a heterogeneous ZP, showing variability in structure, density, or appearance; less transparent with an asymmetric perivitelline space; in group III (12 oocytes) ZP completely absent (Fig. 2).



**Fig. 2.** Human oocytes with different morphological characteristics of the ZP. A – structurally intact, transparent, and smooth ZP with a uniform perivitelline space; B – enlarged ZP with an asymmetrical perivitelline space; C – absence of ZP.

In the second series of experiments, oocytes were divided into four groups based on ZP thickness: Group 1: (16 oocytes with a ZP thickness of up to 10  $\mu$ m), Group 2 (65 oocytes with a ZP thickness of 11-15  $\mu$ m), Group 3 (58 oocytes with a ZP thickness of 16-20  $\mu$ m), and Group 4 (30 oocytes with a ZP thickness exceeding 20  $\mu$ m).

Oocytes were cryopreserved using the CryoTech method (Cryotech, Japan). They were initially equilibrated in a solution containing 7.5 % ethylene glycol (EG) and 7.5 % dimethylsulfoxide (DMSO) in Global general medium (CooperSurgical, USA) for varying durations (5, 7.5, 10, and 12.5 min) at room temperature. This was followed by 1 min vitrification in 15 % EG, 15 % DMSO and 0.5 M sucrose. Each oocyte was individually placed on a Cryotech carrier (Cryotech, Japan) and immediately immersed in liquid nitrogen for storage for at least one week.

Thawing was performed by immersing oocytes in a 1.0 M sucrose solution in Global general medium at 37 °C. After 1 minute, oocytes were sequentially transferred to 0.75 M, 0.5 M, and 0.25 M sucrose solutions, spending two minutes in each. Post-thaw survival was assessed based on the integrity of the ZP, plasma membrane, and volume recovery. Surviving oocytes were cultured in Global Total medium for fertilization under standard CO<sub>2</sub> incubator conditions. After 2 hours, intracytoplasmic sperm injection (ICSI) was

performed. Fertilization was confirmed 16-18 hours after ICSI by the presence of two pronuclei in the ooplasm.

Embryos were cultured *in vitro* in a  $CO_2$  incubator (37 °C, 5 %  $CO_2$ ) for 5 days. The number of blastocysts formed, as well as the morphological characteristics of the inner cell mass and trophectoderm, were evaluated according to Gardner's criteria [27].

To assess statistical significance between groups, Fisher's exact test was used, with a significance threshold of p<0.05. Statistical analysis was performed using GraphPad Prism software (version 9.02, GraphPad Software Inc., USA).

#### Results

The age of patients whose oocytes were analyzed, the cumulative FSH doses administered for ovulation induction, and the average number of oocytes retrieved per superovulation cycle showed no significant differences between groups I and II. However, patients in group III were significantly older and required a significantly higher cumulative FSH dose compared to groups I and II. Overall, patients whose oocytes lacked a ZP had a significantly lower number of aspirated oocytes (Table 1).

**Table 1.** Clinical and embryological characteristics of the study groups (M±m).

Parameters	Group			
Parameters	I (n=54)	II (n=37)	III (n=12)	
Average age of donors, years (M ± m)	29.81±3.53	31.99±3.38	38.50±3.65*	
Total FSH dose, IU	1650±275	2250±225	3000±375*	
Average number of oocytes per cycle, (M ± m)	9.667±6.256	8.865±1.337	3.167±1.267*	
Survival rate after cryopreservation, %	92.5 (50/54)	72.9 (27/37)	41.6 (5/12)	
Fertilization rate, %	94.0 (47/50)	92.6 (25/27)	60.0 (3/5)**	
Blastocyst development rate, %	85.1 (40/47)	76.0 (19/25)	66.7 (2/3)**	

**Notes:** \* – significant difference compared to group I, p<0.05; \*\* – significant difference compared to all other groups, p<0.05.

Oocytes with normal ZP morphology were most frequently observed in the youngest patients. The average age of women whose oocytes lacked a ZP was significantly higher than that of the other study groups. Additionally, the cumulative FSH dose required for superovulation increased with patient age. Group III had a significantly lower mean number of retrieved oocytes (only 3.167±1.267 oocytes per cycle), suggesting a decline in ovarian reserve in older patients and a higher incidence of oocytes without ZP (see Table 1).

The highest survival rate was observed in group I. In contrast, group III exhibited the lowest survival rate (42 %,

Vol. 31, №1, Page 5-11

p<0.05). Structurally intact, transparent oocytes with a uniform perivitelline space (group I) demonstrated superior cryoresistance, while oocytes with abnormal ZP were associated with a lower number of retrieved oocytes and reduced post-cryopreservation survival. The absence of ZP had a pronounced negative effect on oocyte cryoresistance, significantly reducing survival rates compared to groups I and II (see Table 1).

Embryological analysis revealed that group I oocytes had the highest fertilization rate. The embryo development rate to the blastocyst stage in group I was 85.1 %. In contrast, embryos with dysmorphic features and lacking ZP demonstrated a diminished capacity to reach the blastocyst stage (Fig. 3).



**Fig. 3.** Morphological characteristics of the oocyte and embryo without ZP on the first (a), second (b), third (c) and fifth (d) days of in vitro culture.

In the next series of experiments, the retrieved oocytes were divided into four groups depending on the thickness of the ZP: group 1 (16 oocytes with a thickness of up to 10  $\mu m$ ), group 2 (65 oocytes with a thickness of 11 to 15  $\mu m$ ), group 3 (58 oocytes with a thickness of 16 to 20  $\mu m$ ), and group 4 (30 oocytes with a ZP thickness of more than 20  $\mu m$ ) (Fig. 4). Each group of oocytes was exposed to the cryoprotectant solution for different periods of time: 5, 7.5, 10, and 12.5 minutes.

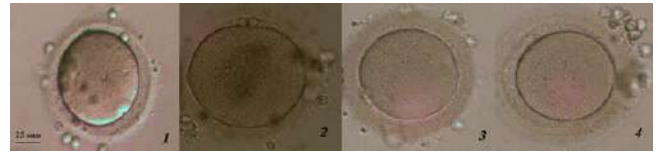


Fig. 4. Oocytes of the studied groups with different ZP thickness: 1-8  $\mu m,~2\text{--}13~\mu m,~3\text{--}18~\mu m,~4\text{--}21~\mu m.$ 

The study found that increasing the exposure time in the cryoprotectant solution negatively affected the survival rate of oocytes with thinner ZP. This suggests that oocytes with a thin ZP required less time to achieve cryoprotectant saturation and were more sensitive to prolonged exposure.

In group 2, survival rates also varied with exposure time but were significantly higher compared to group 1 at the

same durations. These findings indicate that oocytes with a ZP thickness of 10-15  $\mu m$  required a longer exposure period to ensure adequate cryoprotectant penetration and maintain high survival rates.

In group 3, the highest survival rate was observed with a 10-minute exposure to the cryoprotectant solution, while significantly lower survival was recorded at only 5 minutes. This suggests that oocytes with a ZP thickness of 16-20  $\mu m$  require extended exposure time for optimal cryoprotectant equilibration.

For group 4 (ZP thickness >20  $\mu$ m), the longest exposure time was necessary to achieve adequate cryoprotectant saturation and maximize survival rates (Fig. 5).

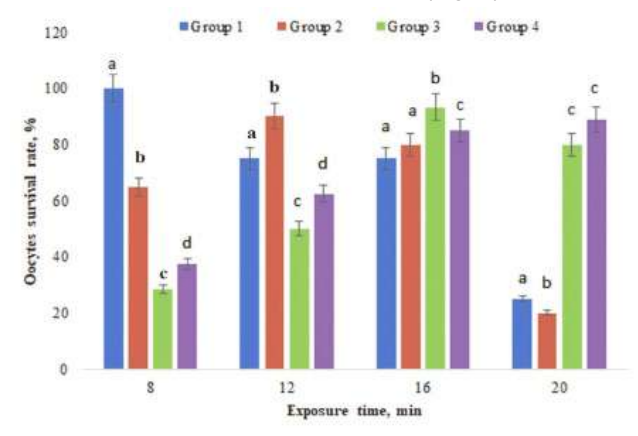


**Fig. 5.** Oocyte survival rate depending on the exposure time in the equilibrium cryoprotectant solution. Different letters indicate statistically significant differences between groups at a specific equilibrium time.

The study of the influence of ZP thickness on the frequency of oocyte survival after cryopreservation revealed a significant effect of this factor on the efficiency of the cryoprotectant exposure time and oocyte viability. The results of the experiment indicate that oocytes with different ZP thicknesses require an individual approach to determining the exposure time with a cryoprotectant to achieve maximum survival after thawing.

#### **Discussion**

Modern ART is continuously accompanied by the search for predictors of successful infertility treatment cycles. Scientific evidence suggests that the morphological and morphometric characteristics of the ZP can serve as clinical indicators of oocyte quality and embryonic developmental potential [12]. Some studies associate ZP thickness with embryo implantation rates [1]. A retrospective study revealed a potential link between cumulus cell apoptosis and ZP thickness, with higher apoptosis rates observed in cumulus cells exhibiting pronounced ZP dysmorphism [15].

Our study found that age may influence the frequency of ZP morphological dysmorphism, with older patients more frequently exhibiting its absence. The quality of the oocyte ZP declines with age and increasing doses of ovarian stimulation drugs, which aligns with findings from other researchers [3].

Our results emphasize the significant role of ZP morphology in oocyte cryoresistance. ZP dysmorphism, observed in patients undergoing ART, may result from external factors such as controlled ovarian stimulation protocols or internal factors, including inherited molecular defects and patient age [26]. Group I, in which oocvtes exhibited a well-defined, smooth, and uniform ZP structure, had the highest survival rate after cryopreservation (93 %). These findings are consistent with studies demonstrating that an intact ZP can act as a physical barrier, protecting the oocyte from external influences during cryopreservation. A study by J. Choi highlighted the crucial biophysical role of ZP in shielding oocytes during vitrification, partly due to its stronger mechanical properties compared to the oocyte plasma membrane [6]. Additionally, microencapsulation of various mammalian cells lacking ZP in a ZP-like hydrogel has been shown to be an effective strategy for enhancing their survival after vitrification.

Oocytes without ZP are generally not used in ART cycles. There are only a few reports of successful pregnancies following the transfer of embryos derived from fertilized oocytes lacking ZP [28, 29]. The primary etiopathogenesis of such oocytes remains unclear, although genetic factors are believed to play a significant role in this process [14]. Studies have shown that oocytes without ZP fertilize and develop into the blastocyst stage as successfully as intact ones [30]. However, our results indicate that structural defects or the complete absence of ZP can negatively affect oocyte cryoresistance, as uneven cryoprotectant penetration into the oocyte cytoplasm may lead to intracellular damage. This represents a promising area for further research, particularly in developing specialized cryopreservation protocols for such oocytes.

ZP plays a crucial role in fertilization and early embryonic development. Even during ICSI, where the sperm is directly injected into the oocyte cytoplasm, bypassing the need for penetration, ZP still provides structural protection against mechanical intervention [22]. Additionally, ZP ensures a stable microenvironment that may be essential for proper cell division. Its absence can disrupt cleavage, leading to irregular division or developmental arrest, potentially reducing embryo quality [21].

In this study, we evaluated the impact of ZP morphometric characteristics on oocyte cryoresistance. Previous studies have indicated that oocyte morphometric parameters do not affect survival rates after vitrification, whereas increased oocyte size, structural changes in the polar body, and compromised ZP integrity negatively impact fertilization rates [4]. It has been suggested that morphometric assessment does not play a significant role in predicting oocyte maturation and fertilization outcomes [24]. Our study demonstrated that ZP thickness influences oocyte cryoresistance. Oocytes with a thin ZP require a shorter exposure time to cryoprotectant solutions for effective cryopreservation. However, prolonged exposure can lead to osmotic and toxic stress, reducing their survival rates. Conversely, oocytes with a thick ZP require a longer cryoprotectant exposure time. Based on our findings, incorporating ZP morphological characteristics, particularly thickness, may allow for the development of more tailored oocyte vitrification protocols.

Future research should focus on identifying new biomarkers of oocyte cryoresistance and developing individualized cryopreservation protocols.

#### Conclusions

- 1. The morphological and morphometric characteristics of ZP are critical for human oocyte cryoresistance. The highest survival rates were observed in the group with normal ZP characteristics, whereas abnormal structure or the absence of ZP was associated with a significant decrease in post-vitrification survival. Thus, ZP morphological and morphometric parameters may serve as predictors of oocyte cryoresistance.
- 2. The absence or dysmorphism of ZP negatively affects embryological parameters such as fertilization and in vitro embryo development. A normal ZP structure is associated with higher fertilization success and improved embryo progression to the blastocyst stage.
- 3. The time required for cryoprotectant saturation of oocytes is significantly influenced by the thickness of the ZP. To improve oocyte survival after cryopreservation, it is essential to consider ZP thickness when optimizing cryoprotectant exposure times.

#### References

- [1] Alhelou, Y., Hamdan, M., Razali, N., Adenan, N., & Ali, J. (2023). Novel image analyser-assisted morphometric methodology offer unique opportunity for selection of embryos with potential for implantation. BMC Pregnancy and Childbirth, 23(1), 698. doi: 10.1186/s12884-023-06025-2
- [2] Baltz, J. M., & Tartia, A. P. (2010). Cell volume regulation in oocytes and early embryos: connecting physiology to successful culture media. Human Reproduction Update, 16(2), 166-176. doi: 10.1093/humupd/dmp045
- [3] Bomba-Warczak, E. K., Velez, K. M., Zhou, L. T., Guillermier, C., Edassery, S., Steinhauser, M. L., ... & Duncan, F. E. (2024). Exceptional longevity of mammalian ovarian and oocyte macromolecules throughout the reproductive lifes-
- pan. eLife, 13, RP93172. doi: 10.7554/eLife.93172
- [4] Camargos, M. G. R. S., Rodrigues, J. K., Lobach, V. N., El Cury-Silva, T., Nunes, M. E. G., Camargos, A. F., & Reis, F. M. (2019). Human oocyte morphometry before and after cryopreservation: a prospective cohort study. Cryobiology, 88, 81-86. doi: 10.1016/j.cryobiol.2019.03.007
- [5] Chaudhuri, O., Cooper-White, J., Janmey, P. A., Mooney, D. J., & Shenoy, V. B. (2020). Effects of extracellular matrix viscoelasticity on cellular behaviour. Nature, 584(7822), 535-546. doi: 10.1038/s41586-020-2612-2
- [6] Choi, J. K., Yue, T., Huang, H., Zhao, G., Zhang, M., & He, X. (2015). The crucial role of Zona pellucida in cryopreservation of oocytes by vitrification. Cryobiology, 71(2), 350-355.

Vol. 31, №1, Page 5-11

- doi: 10.1016/j.cryobiol.2015.08.012
- [7] Cobo, A., García-Velasco, J. A., Remohí, J., & Pellicer, A. (2021). Oocyte vitrification for fertility preservation for both medical and nonmedical reasons. *Fertil. Steril*, 115(5), 1091-1101. doi: 10.1016/j.fertnstert.2021.02.006
- [8] Coello, A., Pellicer, A., & Cobo, A. (2018). Vitrification of human oocytes. *Minerva Ginecol*, 70(4), 415-423. doi: 10.23736/S0026-4784.18.04218-1
- [9] Council of Europe. (2003). Protocol on Embryo Protection: A working Party of the 24th Meeting of the Steering Committee on Bioethics.
- [10] Crozet, F., Letort, G., Bulteau, R., Da Silva, C., Eichmuller, A., Tortorelli, A. F., ... & Terret, M. E. (2023). Filopodia-like protrusions of adjacent somatic cells shape the developmental potential of oocytes. *Life Sci, Alliance, 6*(6), e202301963. doi: 10.26508/lsa.202301963
- [11] ESHRE Guideline Group on Good Practice in IVF Labs, De los Santos, M. J., Apter, S., Coticchio, G., Debrock, S., Lundin, K., ... & Vermeulen, N. (2016). Revised guidelines for good practice in IVF laboratories (2015). *Human Reproduction*, 31(4), 685-686. doi: 10.1093/humrep/dew016
- [12] Fang, J., Sun, H., Chen, L., Wang, J., Lin, F., Xu, Z., ... & Wang, S. (2024). Embryological characteristics and clinical outcomes of oocytes with different degrees of abnormal Zona pellucida during assisted reproductive treatment. *Zygote (Cambridge, England)*, 32(1), 7-13. doi: 10.1017/S0967199423000515
- [13] Gupta, S. K. (2021). Human Zona pellucida glycoproteins: binding characteristics with human spermatozoa and induction of acrosome reaction. *Front. Cell. Dev. Biol.*, 9, 619868. doi: 10.3389/fcell.2021.619868
- [14] Gupta, S. K. (2018). The human egg's Zona pellucida. Current Topics in Developmental Biology, 130, 379-411. doi: 10.1016/bs.ctdb.2018.01.001
- [15] Høst, E., Gabrielsen, A., Lindenberg, S., & Smidt-Jensen, S. (2002). Apoptosis in human cumulus cells in relation to Zona pellucida thickness variation, maturation stage, and cleavage of the corresponding oocyte after intracytoplasmic sperm injection. Fertility and Sterility, 77(3), 511-515. doi: 10.1016/s0015-0282(01)03006-0
- [16] Hu, J., Wang, H., Jiang, R., Yang, G., Zhang, T., Zhang, J., & Yao, G. (2023). Effects of indented Zona pellucida on oocyte growth and development explored from changes of gene expression in cumulus cells. *Arch. Gynecol. Obstetr.*, 308(3), 1023-1033. doi: 10.1007/s00404-023-07104-7
- [17] Jaiswal, A. N., & Vagga, A. (2022). Cryopreservation: A Review Article. *Cureus*, 14(11), e31564. doi: 10.7759/ cureus.31564
- [18] Kottow Lang, M. H. (2017). Critical analysis of the Council for International Organizations of Medical Sciences 2016 International Guidelines for health-related research involving humans. *Medwave*, 17(4), e6956. doi: 10.5867/medwave.2017.04.6956
- [19] Lamas-Toranzo, I., Fonseca Balvís, N., Querejeta-Fernández, A., Izquierdo-Rico, M. J., González-Brusi, L., Lorenzo, P. L., ... & Bermejo-Álvarez P. (2019). ZP4 confers struc-

- tural properties to the Zona pellucida essential for embryo development. *Elife*, *8*, e48904. doi: 10.7554/eLife.48904
- [20] Litscher, E. S. &Wassarman, P. M. (2020). Zona pellucida proteins, fibrils, and matrix. *Annual Review of Biochemistry*, 89, 695-715. doi: 10.1146/annurev-biochem-011520-105310
- [21] Moghadam, A. R. E., Moghadam, M. T., Hemadi, M., & Saki, G. (2022). Oocyte quality and aging. *JBRA Assisted Reproduction*, 26(1), 105-122. doi: 10.5935/1518-0557.20210026
- [22] Moros-Nicolás, C., Chevret, P., Jiménez-Movilla, M., Algarra, B., Cots-Rodríguez, P., González-Brusi, L., ... & Izquierdo-Rico, M. J. (2021). New insights into the mammalian egg Zona pellucida. *International Journal of Molecular Sciences*, 22(6), 3276. doi: 10.3390/ijms22063276
- [23] Murray, K. A., & Gibson, M. I. (2022). Chemical approaches to cryopreservation. *Nature Reviews. Chemistry*, 6(8), 579-593. doi: 10.1038/s41570-022-00407-4
- [24] Nazari, S., Khalili, M. A., Esmaielzadeh, F., & Mohsenzadeh, M. (2011). Maturation capacity, morphology and morphometric assessment of human immature oocytes after vitrification and in-vitro maturation. *Iranian Journal of Reproductive Medicine*, 9(3), 209-216.
- [25] Pai, H. D., Baid, R., Palshetkar, N. P., Pai, A., Pai, R. D., & Palshetkar, R. (2021). Oocyte Cryopreservation Current Scenario and Future Perspectives: A Narrative Review. J. Hum. Reprod. Sci., 14(4), 340-349. doi: 10.4103/jhrs.jhrs\_173\_21
- [26] Pan, C., & Zhang, H. (2020). Embryological characteristics and clinical outcomes of oocytes with heterogeneous Zona pellucida during assisted reproduction treatment: a retrospective study. Medical Science Monitor: International Medical Journal of Experimental and Clinical Research, 26, e924316. doi: 10.12659/MSM.924316
- [27] Pierson, H. E., Invik, J., Meriano, J., & Pierson, R. A. (2023). A novel system for rapid conversion of Gardner embryo grades to linear scale numeric variables. *Repro*ductive Biomedicine Online, 46(5), 808-818. doi: 10.1016/j. rbmo.2023.01.008
- [28] Shu, Y., Peng, W., & Zhang, J. (2010). Pregnancy and live birth following the transfer of vitrified-warmed blastocysts derived from zona- and corona-cell-free oocytes. *Reproduc*tive Biomedicine Online, 21(4), 527-532. doi: 10.1016/j. rbmo.2010.04.033
- [29] Stanger, J. D., Stevenson, K., Lakmaker, A., & Woolcott, R. (2001). Pregnancy following fertilization of zona-free, coronal cell intact human ova: Case Report. *Human Re*production, 16(1), 164-167. doi: 10.1093/humrep/16.1.164
- [30] Ueno, S., Bodri, D., Uchiyama, K., Okimura, T., Okuno, T., Kobayashi, T., & Kato, K. (2014). Developmental potential of Zona pellucida-free oocytes obtained following mild in vitro fertilization. *Fertility and Sterility*, 102(6), 1602-1607. doi: 10.1016/j.fertnstert.2014.08.025
- [31] Wassarman, P. M., & Litscher, E. S. (2022). Female fertility and the Zona pellucida. eLife, 11, e76106. doi: 10.7554/ eLife.76106
- [32] Wassarman, P. M., & Litscher, E. S. (2024). Female fertility and the mammalian egg's Zona pellucida. Histology and Histopathology, 39(10), 1273-1284. doi: 10.14670/HH-18-728

#### МОРФОЛОГІЧНІ ТА МОРФОМЕТРИЧНІ ХАРАКТЕРИСТИКИ ZONA PELLUCIDA ООЦИТІВ ЛЮДИНИ: ВПЛИВ НА ЕМБРІОЛОГІЧНІ ТА КРІОБІОЛОГІЧНІ РЕЗУЛЬТАТИ

Петрушко М. П., Піняєв В. І., Юрчук Т. О.

Кріобіологічні підходи широко застосовуються для збереження життєздатності репродуктивних клітин і тканин з метою підвищення успішності циклів лікування безпліддя за допомогою допоміжних репродуктивних технологій. Кріоконсервування надає пацієнтам можливість зберігати біологічний матеріал протягом тривалого часу, що особливо важливо для осіб, які стикаються з онкологічними чи іншими станами, що можуть негативно впливати на фертильність.

Водночас пошук маркерів кріорезистентності стає важливим напрямом досліджень, оскільки це дозволяє визначати, які клітини найкраще підходять для зберігання при низьких температурах. Дослідження кріорезистентності допомагають визначити фактори, що впливають на стійкість клітин до заморожування і відтавання, зокрема структурні особливості мембран, ліпідний склад клітин, наявність специфічних білків та антиоксидантних систем. Це дозволяє оптимізувати умови зберігання та підібрати найефективніші кріопротектори для кожного типу клітин. Метою роботи було дослідити вплив морфологічних і морфометричних характеристик Zona pellucida (ZP) на виживання, запліднення та розвиток ооцитів до стадії бластоцисти. Після ізоляції та денудації ооцитів оцінювали морфологічні (прозорість, цілісність) та морфометричні (товщина) характеристики. Виживання ооцитів після кріоконсервування оцінювали з урахуванням їхніх морфологічних характеристик. Для оцінки достовірності різниць між групами використовували критерій Фішера, статистично значимими вважали дані при р<0.05. Дослідження показало, що нормальні морфологічні характеристики ZP. зокрема висока прозорість і структурна цілісність, найчастіше спостерігалися в ооцитах наймолодшої групи пацієнток віком 29,81±3,53 років. Ця група також демонструвала найвищі показники виживання ооцитів після кріоконсервування. У групі жінок віком 38,50±3,65 років було значно більше ооцитів без ZP порівняно з наймолодшою групою. Загальна доза фолікулостимулюючого гормону, необхідного для індукції суперовуляції, також збільшувалася з віком пацієнток і була найвищою у групі з аномаліями ZP. Найвищий рівень виживання після кріоконсервування спостерігався в ооцитах з нормальною структурою ZP (93 %), тоді як ооцити з відсутньою або аномальною ZP демонстрували значно нижчі показники виживання, що вказує на негативний вплив дефектів ZP на кріорезистентність (42 % у групі з повністю відсутньою ZP). Було показано, що товщина ZP впливає на насичення кріопротекторами та виживання ооцитів після кріоконсервування. Структурно інтактна ZP сприяла кращому насиченню кріопротекторами, при цьому збільшення товщини ZP подовжувало необхідний час для рівноваги. Ооцити з товщиною ZP до 10 мкм потребували 5 хв, з товщиною 11-15 мкм – 7,5 хв, з товщиною 16-20 мкм – 10 хв, а для ZP товщиною понад 20 мкм було необхідно 12,5 хв для оптимального результату. Продовження експозиції негативно впливало на ооцити з тоншою ZP, що свідчить про їхню підвищену чутливість до кріопротекторів. Отже, товщина ZP є критичним фактором виживання ооцитів після кріоконсервування, а адаптація часу експозиції до кріопротекторів відповідно до морфометричних характеристик ZP може покращити результати збереження фертильності.

Ключові слова: ооцити людини, морфологія, морфометрія, кріоконсервування, Zona pellucida.

#### Author's contribution:

Petrushko M. P. – data curation, investigation, methodology, visualization, conceptualization, validation, writing.

Piniaiev V. I. - investigation, writing, review & editing.

Yurchuk T. O. – methodology, investigation, visualization, data curation, formal analysis.

Vol. 31, №1, Page 5-11

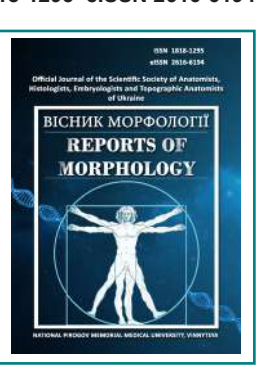
ISSN 1818-1295 eISSN 2616-6194



#### REPORTS OF MORPHOLOGY

Official Journal of the Scientific Society of Anatomists, Histologists, Embryologists and Topographic Anatomists of Ukraine

journal homepage: https://morphology-journal.com



#### Study of the effect of Saponaria officinalis herb extract on histological changes in the marginal vein of the ear under conditions of experimental thrombophlebitis

Tsubanova N. A.1, Voloshchuk N. I.2, Zastryzhna M. L.2

<sup>1</sup>Andrei Krupynskyi Lviv Medical Academy, Lviv, Ukraine

#### **ARTICLE INFO**

Received: 22 February 2024 Accepted: 14 November 2024

**UDC:** 615:616.1.615.3:633.8.616-08

#### **CORRESPONDING AUTHOR**

e-mail: tsubanova19@gmail.com Tsubanova N. A.

#### **CONFLICT OF INTEREST**

The authors have no conflicts of interest to declare.

#### **FUNDING**

Not applicable.

#### **DATA SHARING**

Data are available upon reasonable request to corresponding author.

Thrombophlebitis is recognized as one of the most common complications of chronic venous insufficiency (CVI). Its course is characterized by inflammation of the venous wall and the formation of blood clots in the lower extremities of varicose veins. Thrombophlebitis is diagnosed according to various data in 5-60 % of patients with CVI. The number of drugs with a phleboprotective effect and the ability to reduce the processes of thrombus formation in veins on the pharmaceutical market of Ukraine and the world is extremely limited. As a promising object, as a new phleboprotective drug, medicinal plant raw materials can be considered, namely the extract of the herb Saponaria officinalis, for which venotonic and antiexudative effects have been established in previous studies. The aim of this work was to study the effect of Saponaria officinalis herb extract on changes in the histological parameters of the ear vein in rabbits under conditions of experimental thrombophlebitis. Experimental thrombophlebitis was modeled on rabbits according to the standard method with applying a ligature to the marginal vein of the animal's ear and injecting Lugol's solution. Histological changes after phytocomposition administration (ETML) (20 mg/ kg intragastrically) were compared with the effectiveness of the reference drug Eskuvit (7.2 mg/kg for escin intragastrically). It was established that the therapeutic and prophylactic administration of ETML at a dose of 20 mg/kg significantly prevented thrombus formation in the marginal ear vein of rabbits, contributing to the softening of the thrombus material, thrombolysis, preventing the acquisition of an obliterating character for thrombotic masses. in all rabbits of the group. probably reduces the clinical indicators of transudative edema, which developed as a result of acute venostasis. ETML prevented the destruction of the vascular wall, reduced or eliminated degenerative changes and inflammatory reaction in the surrounding tissues. Significant advantages of ETML over the comparison drug Eskuvit have been established. Under the conditions of experimental thrombophlebitis, the therapeutic and prophylactic administration of ETML at a dose of 20 mg/kg has a powerful phleboprotective effect, reduces the processes of thrombus formation in the vein. The effect of ETML is statistically significantly higher than the effectiveness of the comparison drug Eskuvit. Keywords: Saponaria officinalis herb extract, experimental thrombophlebitis, histological changes, Escuvit, phleboprotective effect, anti-inflammatory effect, medicinal plants.

#### Introduction

The thrombotic and associated inflammatory process in the veins, leading to the development of thrombophlebitis, can affect both varicose-altered and non-varicose veins. In clinical practice, this distinction has led to the classification of thrombosis of varicose-altered superficial veins (varicothrombophlebitis) and thrombosis of non-varicose

superficial veins [41, 42, 43].

The prognosis of the disease and the treatment strategy for patients with varicothrombophlebitis and thrombosis of non-varicose superficial veins exhibit certain differences. However, therapeutic recommendations include both pharmacological agents with phleboprotective properties

and those capable of reducing thrombus size [33, 37, 38].

The most common risk factor for thrombophlebitis is the presence of varicose veins of the lower extremities. Transformation of superficial veins in patients with thrombophlebitis is detected in up to 80 % of cases. Conversely, thrombophlebitis develops in 5-60 % of patients with varicose vein disease of the lower extremities [21, 24].

The major etiological risk factors for thrombophlebitis include age, obesity, tobacco use, a history of deep vein thrombosis or thrombophlebitis, pregnancy and the postpartum period, oral hormonal contraceptive use, hormone replacement therapy, immobilization, recent surgeries and trauma, and oncological diseases. For instance, within the first month postpartum, the risk of developing de novo thrombophlebitis significantly increases. A positive correlation between thrombophlebitis and oncological diseases has been established in 10-18 % of patients [10].

Genetic factors play a significant role in the etiopathogenesis of thrombophlebitis. Hereditary thrombophilia, particularly Leiden factor V mutation, prothrombin gene mutation G20210A, and deficiencies of antithrombin III (AT III), protein C, and protein S, significantly increase the risk of thrombophlebitis [41].

In patients with thrombotic vein lesions, oxidative stress and dyslipidemia play a crucial role, increasing the risk of recurrent thrombophlebitis fivefold in cases of untimely or inadequate treatment [31, 34].

The most dangerous complications of thrombophlebitis include thrombus extension into the deep veins and the development of pulmonary embolism. According to various authors, the incidence of thrombus propagation into deep veins reaches 18-20 % (95 % CI 13.9-23.3), while the frequency of symptomatic pulmonary embolism in thrombophlebitis cases is reported at 6.5-7.5 % (95 % CI 3.9-11.8). It is crucial to consider the risk of thrombophlebitis extending into the deep venous system, which ranges from 7 % to 32 % [36, 38, 39, 41].

The pharmacotherapy of thrombophlebitis includes various drugs with different mechanisms of action, such as anticoagulants, anti-inflammatory agents, venotonic drugs (which stimulate venous blood flow), and phleboprotective agents (which restore venous wall integrity) [30, 32].

Pathogenetically justified pharmacotherapy of thrombophlebitis involves the use of drugs with membrane-protective, venotonic, antioxidant, and anti-inflammatory properties [23].

Given the chronic nature of venous insufficiency with periodic episodes of thrombophlebitis, an important task for pharmacology is the development of an effective phleboprotective agent suitable for long-term and safe use. Phytoniring-based drugs (agents derived from medicinal plant raw materials) meet these requirements. These preparations contain a complex of biologically active substances with multifunctional properties, membrane-stabilizing effects on affected veins, normalization of hemostatic processes (anticoagulant action), reduced thrombus formation risk, a

broad therapeutic dose range, and low toxicity.

A promising medicinal plant raw material for the development of a novel domestic phleboprotective agent is the thick extract of *Saponaria officinalis* (soapwort) herb (SOTE), developed by Doctor of Pharmaceutical Sciences, Professor Marchyshyn S. M. (I. Horbachevsky Ternopil National Medical University, Ukraine). Pharmacognostic studies have demonstrated that the investigated *Saponaria officinalis* extract contains a significant amount of triterpene saponins and other biologically active compounds, whose biological activity correlates with the pathogenesis of venous system disorders [5, 12].

The aim of this study was to evaluate the effect of Saponaria officinalis herb extract on changes in the histological parameters of the ear vein in rabbits under experimental thrombophlebitis conditions.

#### Materials and methods

To model experimental thrombophlebitis in rabbits, a comprehensive thrombophlebitis methodology in rabbits was selected [16]. The methodology includes ligation to induce blood stasis, as well as the administration of a chemical agent (Lugol's solution) to damage the vascular intima, given the proven greater effectiveness of using multiple thrombogenic factors in experiments.

The experiment was conducted on 24 rabbits weighing 2-2.5 kg. The animals were housed under standard vivarium conditions at the National Pirogov Memorial Medical University, Vinnytsia, with ad libitum access to food and water. The study was conducted in accordance with the National "General Ethical Principles of Animal Experimentation" (Ukraine, 2001), which comply with the provisions of the "European Convention for the Protection of Vertebrate Animals Used for Experimental and Other Scientific Purposes" (Strasbourg, 1986) [26]. The Bioethics Committee of the National Pirogov Memorial Medical University, Vinnytsia, found no violations of ethical standards in the conduct of the research (Protocol No. 11 dated November 18, 2024). The experiments were conducted with consideration of circadian and seasonal rhythms, and all procedures were performed under standard conditions from 9:00 to 10:00 a.m. A ligature was applied to the marginal ear vein of the rabbits after preliminary depilation and disinfection. Above the ligature, 0.1 mL of a 2 % Lugol's solution was introduced into the vein lumen. Following the administration of Lugol's solution, the ligatures were removed to restore blood circulation in the vessel. The laboratory animals were distributed as follows (six rabbits per group):

Group 1 – intact control;

Group 2 – pathological control (thrombophlebitis);

Group 3 – thrombophlebitis + therapeutic-prophylactic administration of SOTE at a dose of 20 mg/kg;

Group 4 – thrombophlebitis + therapeutic-prophylactic administration of Escuvit at a dose of 7.2 mg/kg based on escin content.

The tested SOTE extract and the reference drug Escuvit

Vol. 31, №1, Page 12-21

were finely ground into powder, thoroughly mixed with distilled water to form a suspension, and administered intragastrically to the animals using a metal probe with an olive tip. The administration was performed once daily, starting seven days before pathology induction and continuing for ten days during its progression.

Rabbits from all groups were euthanized on the 10th day of the experiment via air embolism. The excised samples (approximately 3 cm from the ligation site) were fixed in a 10 % formalin solution, dehydrated in ethanol of increasing concentrations, and embedded in paraffin. The sections were stained with hematoxylin and eosin. Microscopic examination of the histological specimens was performed using a Granum microscope. Microphotography was conducted with a Granum DCM 310 digital video camera, and the images were processed on a Pentium 2.4 GHz computer using the Toup View software.

#### Results

The histological structure of the examined ear region in animals from the intact control group is characterized by a normally appearing epidermis lining both the outer and inner surfaces. The dermis of the skin proper contains hair follicles and sebaceous glands. Near the cartilage plate, transverse profiles of the external marginal ear vein are visible. The vessel lumen is narrow, and the venous wall is thin. The vessel wall consists of the intima (elongated endothelial cell nuclei), a very thin media (almost devoid of muscular components, with very fine and sparse collagen fibers), and an indistinct adventitia. The surrounding tissues of the vein showed no signs of inflammation or edema (Fig. 1).

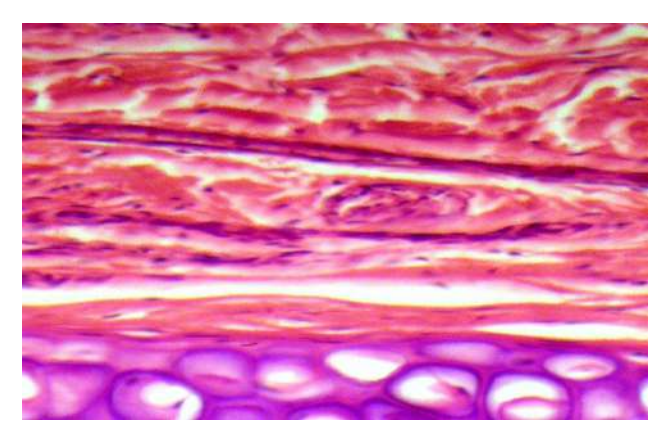


**Fig. 1.** External marginal ear vein of an intact rabbit. The condition of the vessel and surrounding tissues (indicated by arrows) corresponds to the norm. Hematoxylin-eosin. ×100.

In animals of the control pathology group, on the 10th day of experimental thrombophlebitis development, significant necrosis of the epidermis, dermis, and even the cartilage plate, as well as a diffuse inflammatory reaction, were observed in the injured area (Fig. 2a).

In areas adjacent to the necrosis, the venous lumen is markedly dilated and filled with a relatively dense red

thrombus. In certain regions, the venous wall is damaged, with visible adhesion of the thrombus to the destructed remnants of the vein. The surrounding dermis exhibits an inflammatory reaction of varying intensity and degenerative edema of collagen fibers (Fig. 2b).

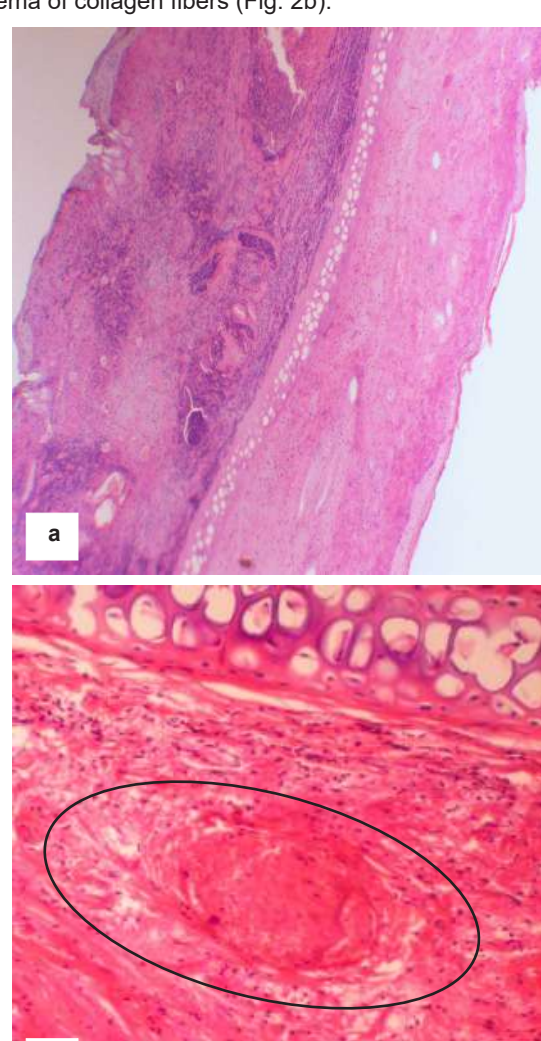


**Fig. 2.** Control pathology group. External marginal ear vein of the rabbit on the 10th day of thrombophlebitis development: a – extensive necrosis of all tissues in the injured area (×100); b – barrel-shaped dilation of the vascular lumen, occluded by a red thrombus (outlined), vascular wall partially destroyed, collagen fibers of the dermis in a state of degenerative edema, inflammatory reaction in the dermis (×200). Hematoxylin-eosin.

Additionally, in animals from the control pathology group, various stages of thrombus organization were observed along almost the entire examined segment of the ear vein. These stages ranged from the breakdown of erythrocytes and leukocytes and the appearance of connective tissue cells to partial or complete obliteration with lumen overgrowth by connective tissue. Moreover, perivascular tissue fibrosis and signs of inflammation in the dermis were detected (Fig. 3).

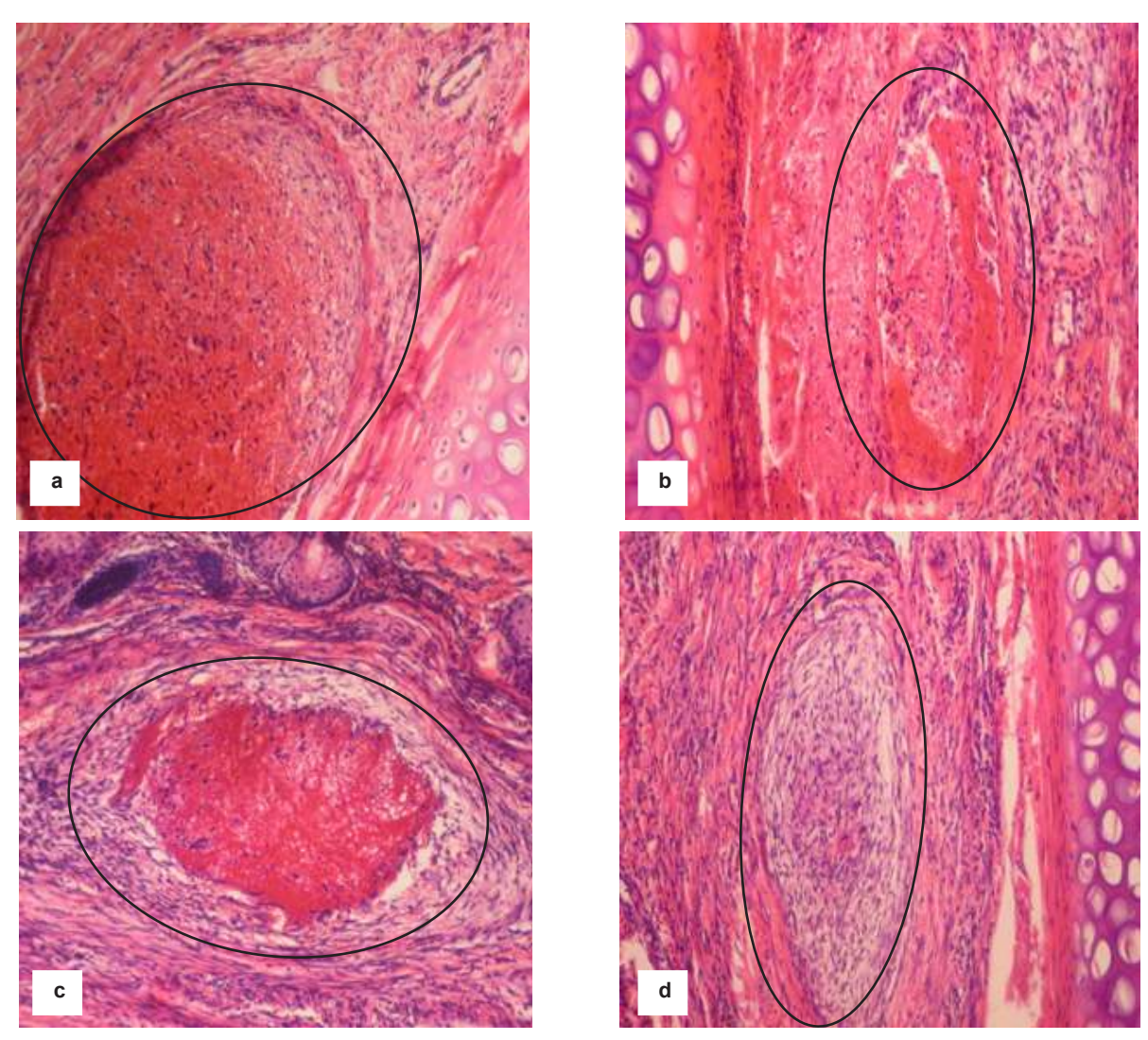


**Fig. 3.** Control pathology group. External marginal ear vein of a rabbit on day 10 of thrombo-phlebitis development. Lysis of thrombotic masses (outlined) (a), stages of thrombus organization (outlined) (b-c), complete obliteration of the vascular lumen (outlined) (d). Inflammatory reaction of varying intensity and perivascular fibrosis. Hematoxylin-eosin. ×250.

In rabbits that received SOTE at a dose of 20 mg/kg in a therapeutic-prophylactic regimen, no necrosis of the vein tissues was observed in the injury zone. The lumen of the external marginal ear vein was widened, but the thrombus did not occlude the vein and was parietal in nature. The thrombotic masses appeared significantly softened, and in some specimens, they were lysed.

The vein wall remained intact. The collagen stroma of the dermis was slightly edematous, but the inflammatory response was not pronounced (Fig. 4). Further along the vein, in areas more distant from the site of injury, no thrombus was observed in the vascular lumen. Various residual erythrocyte masses of different volumes and densities were present but did not obstruct blood flow. The condition of the vein wall was close to that of an intact vessel, and no fibrosis of the perivascular tissue was detected. Signs of inflammation in the ear tissues were either absent or significantly reduced (Fig. 5).

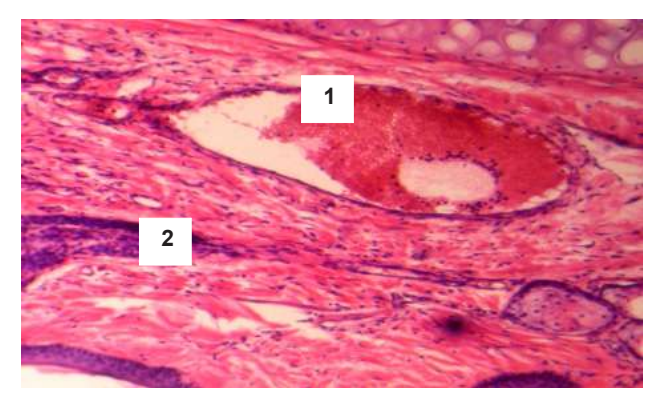


**Fig. 4.** External marginal ear vein of a rabbit that received SOTE at a dose of 20 mg/kg in a therapeutic-prophylactic regimen on day 10 of thrombophlebitis development. 1 – parietal thrombus in the widened vascular lumen, liquefaction of thrombotic masses; in some areas, 2 – initial infiltration of thrombotic masses by leukocytes. Hematoxylin-eosin. ×200.

Vol. 31, №1, Page 12-21

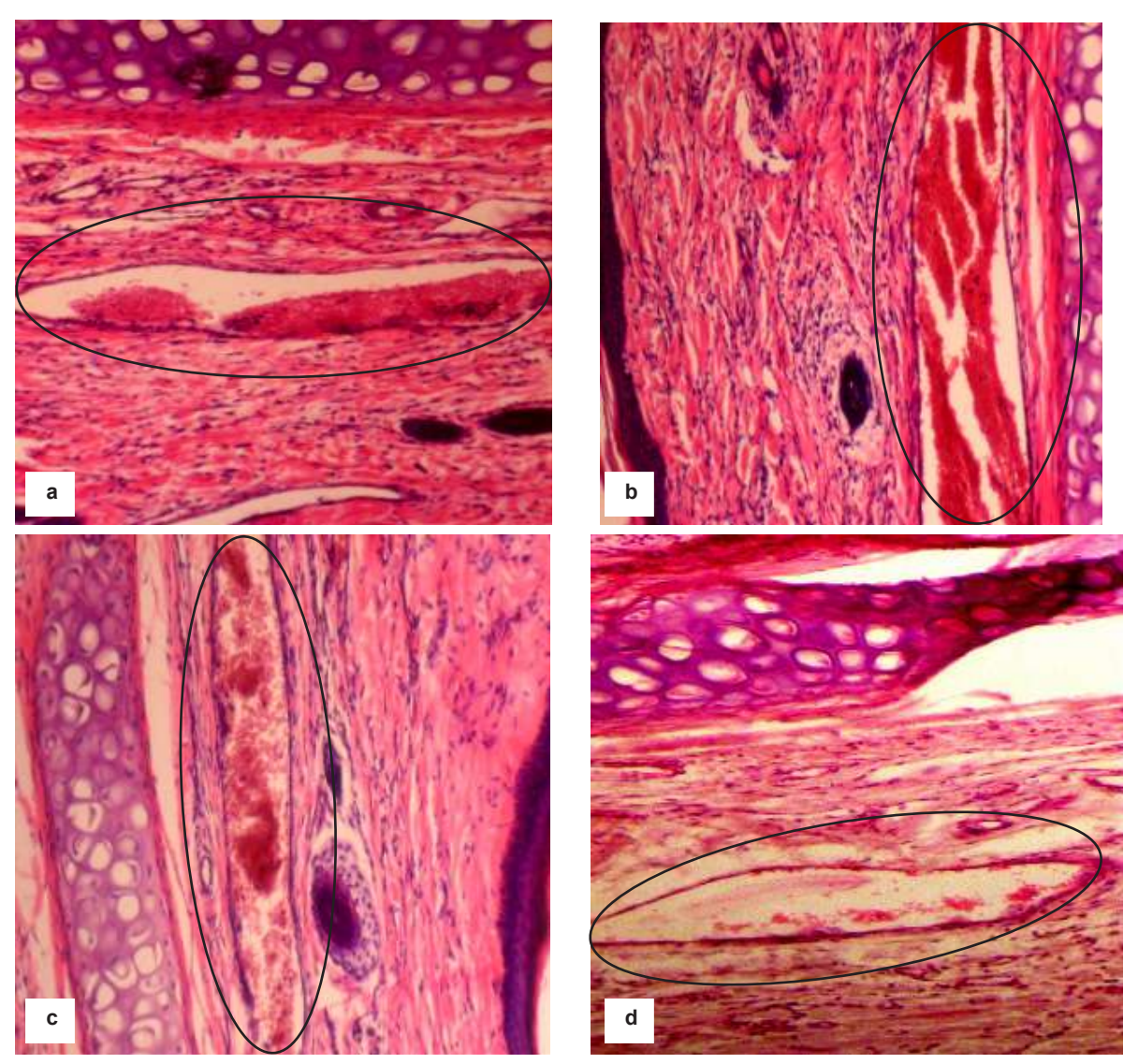


**Fig. 5.** External marginal ear vein of a rabbit that received SOTE at a dose of 20 mg/kg in a therapeutic-prophylactic regimen on day 10 of thrombophlebitis development. Vascular normalization: various volumes of liquefied erythrocyte masses (outlined) in the vascular lumen (a-d), vessel wall condition approaching normal, and a marked reduction in signs of inflammation in surrounding tissues. Hematoxylin-eosin. ×200.

The administration of the comparative drug Eskuvit in the same regimen prevented the formation of necrotic zones in the venous injury area. The expanded lumen of the marginal ear vein is filled with a thrombus of varying size. The thrombotic masses are not uniformly dense, with areas that are cracked and softened (which may allow blood flow in these regions), and some areas are infiltrated by leukocytes. The vessel wall is partially damaged, and the perivascular tissue is swollen. The tissues of the ear itself are infiltrated with inflammatory cells (Fig. 6).

Further along the vein, in some histological samples of the examined segment of the ear, the thrombus was still present. Processes of its organization were observed, and in parallel with the organization, distinct signs of canalization were found – the appearance of newly formed capillaries in the connective tissue that replaced the thrombus, which restored blood flow in this section of the vein. Closer to the edge of the ear, the state of the marginal vein in these rabbits was close to normal. In other cases, only erythrocyte masses of varying volumes were visible in the lumen of the vein. The condition of the collagen fibers in the dermis slightly normalized (Fig. 7).

#### **Discussion**

Chronic venous insufficiency (CVI) is one of the most prevalent diseases of modern times. The World Health Organization has included varicose veins in its list of "diseases of civilization": according to its data, this pathology affects 40 % of women and 32 % of men worldwide.

Varicose veins are the most common visible symptom of

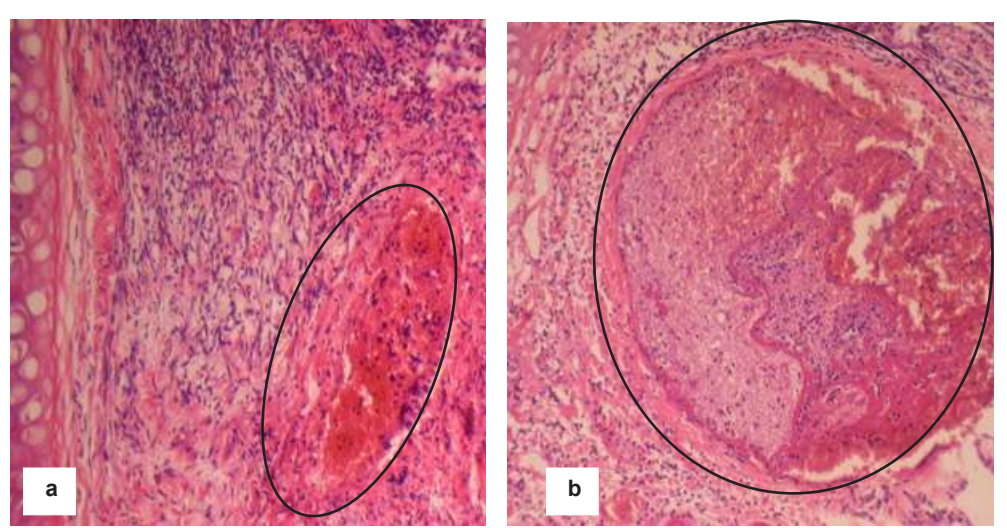


**Fig. 6.** The external marginal vein of the ear in the rabbit, which received Eskuvit at a dose of 7.2 mg/kg as escin in the therapeutic and prophylactic regimen, on the 10th day of experimental thrombophlebitis. Thrombotic masses of varying size (outlined by a line), which are not uniformly dense (a – b), fill the vessel lumen. The vessel wall is partially damaged. Hematoxylin-eosin. ×200.

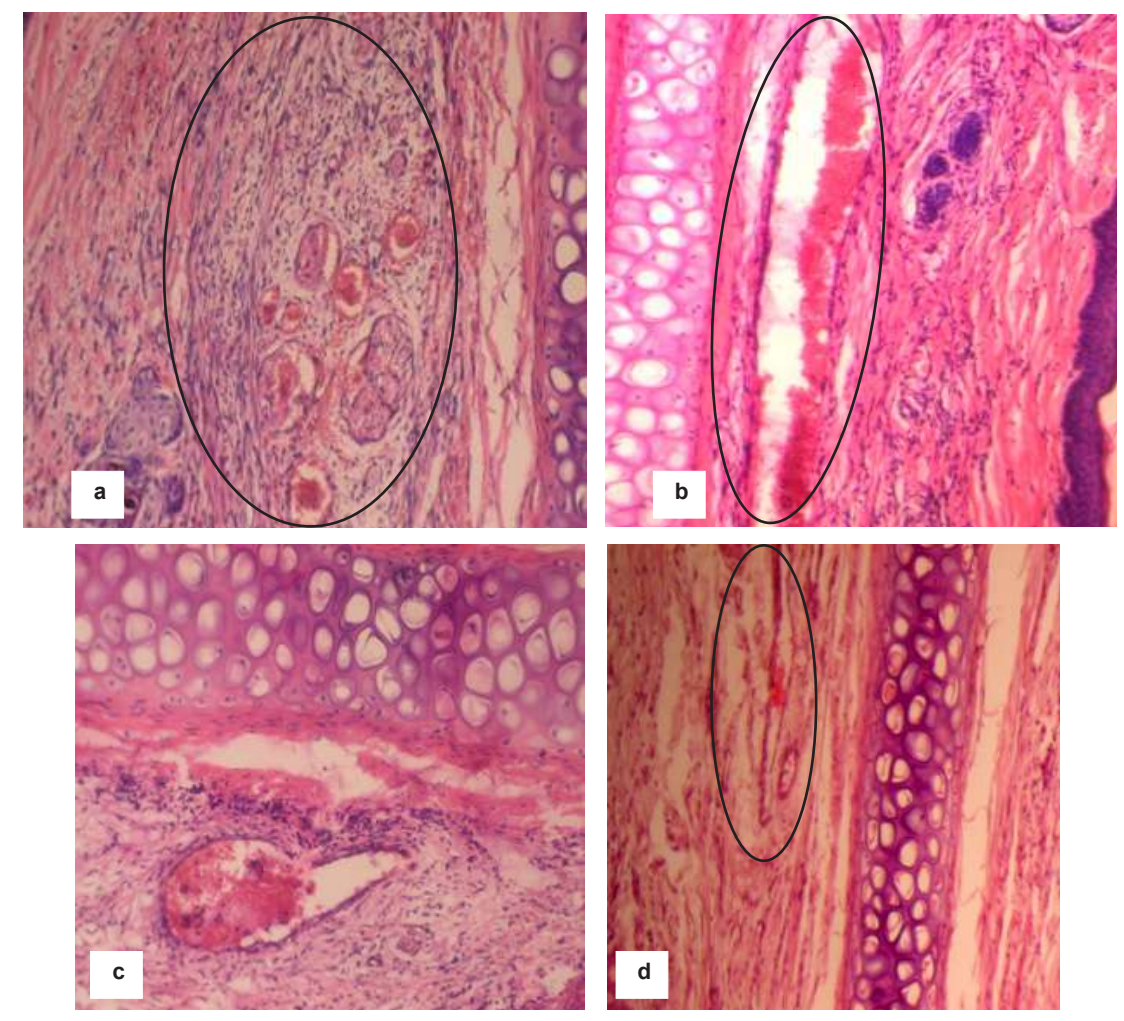


**Fig. 7.** External marginal vein of the rabbit's ear, which received Escuvit at a dose of 7.2 mg/kg as escin in a therapeutic-preventive regimen, on the 10th day of thrombo-phlebitis development. Organization of the thrombus (outlined with a line) and canalization of the thrombus (arrow) (a); remnants of erythrocytic masses (outlined with a line) in the lumen of the vessel (b); lysis of erythrocytes (c); vein with a small thrombus (outlined with a line) (d). Hematoxylin-eosin. ×200.

Vol. 31, №1, Page 12-21

venous insufficiency, but they do not occur in every patient. Deep vein insufficiency is less common and is often caused by deep vein thrombosis. CVI imposes a significant economic burden on society in the form of medication and surgical treatment costs and, importantly, an immeasurable loss of work productivity due to pain and disability [18].

CVI is a multifactorial disease associated with endothelial dysfunction, inflammation, venous wall remodeling, valve incompetence, venous hypertension, and reflux [6]. Other causes include venous outflow obstruction and calf muscle pump failure due to obesity or leg immobility.

Pharmacological treatment is an essential component of conservative CVI management; therefore, the indications and benefits of this therapeutic approach in patients with venous system disorders are indisputable. The goals of pharmacological treatment include [13]: increasing venous emptying; affecting vascular walls and interstitial tissue; restoring metabolic balance (eliminating oxidative stress); reducing thrombotic predisposition in the lymphatic system; and minimizing cellular damage.

An important aspect of CVI treatment is the use of modern phlebotropic agents (venotonics, phleboprotectors) as first-line therapy. This is a substantial group of pharmacological agents, usually of natural origin, with the ability to enhance venous outflow from the lower limbs.

A crucial contribution to CVI therapy effectiveness is the use of modern venotonic agents (phleboprotectors). This is a large group of pharmacological agents, typically of natural origin, whose primary feature is their ability to enhance venous outflow from the lower limbs. This effect results from a synergistic influence on various components of the microcirculatory system and/or a direct impact on venous wall tone. Their mechanism of action is usually pleiotropic and includes stimulation of lymphatic flow, anti-inflammatory and antioxidant activity, improvement of hemorheology, and endothelial protection.

The most commonly used venotonics belong to four main groups of drugs, including flavonoids (hesperidin, diosmin, rutin, esculin), saponins (escin, horse chestnut extract, Ginkgo biloba), coumarins, synthetic venotonics, or combination drugs (calcium dobesilate, tribenoside, naftazone, benzarone).

However, the evidence base for the effectiveness of phleboprotective agents has been confirmed only for certain drugs from the extremely broad list of phleboprotectors. Therefore, despite extensive experience, comparisons of the clinical efficacy of pharmacotherapy for CVI symptoms using various venotonic drugs from different pharmacological groups do not allow for the definitive identification of the most effective drug. This is due to the insufficient number of randomized clinical trials and the significantly limited range of drugs available for comparison, which justifies the need for further research in this direction [14].

In our opinion, a promising addition to the arsenal of modern natural phleboprotective agents could be the use of an extract from the plant Saponaria officinalis L. (Caryophyllaceae), commonly known as common soapwort, which is widely distributed worldwide [19]. Phytopreparations derived from various parts of Saponaria officinalis are used in traditional medicine: the root as a blood-purifying, diaphoretic, and diuretic agent; the sap for liver diseases and to enhance bile outflow: and the leaves and roots for skin diseases [27, 28]. Literature data indicate that Saponaria officinalis contains a high level of saponins. The saponin fraction of common soapwort has demonstrated anti-inflammatory activity in vitro in a carrageenan-induced edema model in rats and has been shown to inhibit prostaglandin synthetase [17]. Purified saponins from the Saponaria officinalis fraction have demonstrated a hypocholesterolemic effect in vitro, which is believed to result from the saponins' ability to form an insoluble complex with cholesterol [4]. In addition to saponins, common soapwort also contains tannins, quillaic acid, flavonoids, sulfur-containing compounds, various phenolic compounds, and essential oils [20]. Experimental research data indicate that soapwort saponin extracts possess antibacterial and antifungal activity [1, 7].

Our results demonstrated the high phleboprotective efficacy of soapwort herb extract in an experimental model of thrombophlebitis. Microscopic findings confirmed the development of experimental thrombophlebitis, as evidenced by pathological changes both in the vessel itself and in the surrounding tissues, which occur due to temporary cessation of blood flow in a limited area of the ear, along with the simultaneous injection of Lugol's solution into the marginal vein cavity. By the 10th day of experimental thrombophlebitis development in animals from the control pathology group, thrombosis of the marginal vein was observed, characterized by lumen obstruction, vascular wall destruction, degenerative and inflammatory changes in the surrounding dermal tissues. Signs of different stages of thrombus organization were recorded - from erythrocyte and leukocyte breakdown, and the appearance of connective tissue cells, to complete occlusion of the lumen by connective tissue, cessation of blood flow in this area, and the development of vascular wall sclerosis of varying severity, as well as perivascular fibrosis.

The extract of Saponaria officinalis herb, when administered in a prophylactic-therapeutic regimen, significantly prevented thrombus formation in the marginal vein, promoting the softening of thrombotic material, thrombolysis, and preventing thrombotic masses from becoming obliterative in all rabbits in the group. As a result, the degradation products of the thrombus were "washed away" by the blood flow, and unlike in the control pathology group, hemocirculation was restored in the examined area of the ear. SOTE prevented vascular wall destruction, reduced or eliminated degenerative changes in the surrounding tissues, and exhibited anti-inflammatory effects.

The prophylactic effect of the reference drug Escuvit in this experimental model of thrombophlebitis varied among animals. In some cases, thrombosis in the marginal ear vein was prevented, while in others, active thrombus formation followed by its canalization was observed, facilitating the

restoration of blood flow in the thrombosed vessel. Under the influence of Escuvit, inflammatory and sclerotic changes in the ear tissues were reduced. Thus, in terms of the positive impact on the morphological manifestations of experimental thrombophlebitis, the reference drug Escuvit was significantly inferior to the studied SOTE.

The established pharmacological activity of SOTE in experimental thrombophlebitis, which significantly surpasses the reference drug Escuvit in restoring the histological parameters of the vein, is presumably realized through the additive synergy of the biologically active compounds (BAC) of Saponaria officinalis herb extract [5, 12]. These include triterpene saponins (4 % in the extract), hydroxycinnamic acids (7.36 % in the extract), and flavonoids (15.8 % in the extract).

The corticosteroid-like action of the saponins present in SOTE (saponaroside A, saponaroside D, saponrubin) suppresses the synthesis of pro-inflammatory intermediates (interleukins IL-1, IL-2, IL-6, IL-8, vascular endothelial growth factors, tumor necrosis factor- $\alpha$  (TNF- $\alpha$ ), and interferon- $\gamma$ ), which promote inflammatory and phlogogenic responses [3, 11]. An important aspect of the phleboprotective action of saponins, including escin, is their ability to stimulate the synthesis of prostaglandin F<sub>2 $\alpha$ </sub>, which exerts a venotonic effect and, according to Gallelli L. [8], prevents hypoxia-induced disruptions in the normal expression and distribution of endothelial cell platelet adhesion molecule-1 in the vein [3, 15].

The reduction of thrombus formation processes in the vein under the prophylactic-therapeutic administration of SOTE is likely also mediated by the normalizing effect of saponins on hemostatic processes in the damaged area. This includes inhibition of the coagulation component of hemostasis, direct inhibition of thrombin, and a reduction in thrombus formation in the vein [3].

The venotonic and antithrombotic effects of saponins are most likely the key mechanisms underlying the phleboprotective action of SOTE in experimental thrombophlebitis.

Hydroxycinnamic acids (chlorogenic acid, syringic acid, caffeic acid, quinic acid) and flavonoids (quercetin, isoquercetin, kaempferol), which are present in significant amounts in the Saponaria officinalis extract, as reported by Ullah R. et al. [29], Yang X. et al. [35], Shabbir U. et al. [25], and Zhao L. et al. [40], exhibit substantial anti-exudative and anti-inflammatory effects, contributing to the phleboprotective activity of the studied extract.

#### References

- [1] Abdolreza, N. (2013). Antibacterial effects of Saponaria officinalis extracts against avian pathogenic Escherichia coli (APEC). African Journal of Agricultural Research, 8(18), 2068-2071. doi: 10.5897/ajar11.1390
- [2] Bekendam, R. H., & Flaumenhaft, R. (2016). Inhibition of Protein Disulfide Isomerase in Thrombosis. *Basic Clin. Pharmacol. Toxicol.*, 119(3), 42-48. doi: 10.1111/bcpt.12573
- [3] Biswas, T., & Dwivedi, U. N. (2019). Plant triterpenoid saponins: biosynthesis, in vitro production, and pharmacological relevance. *Protoplasma*, 256(6), 1463-1486. doi: 10.1007/s00709-019-01411-0

The marked reduction in thrombus size under the prophylactic-therapeutic administration of SOTE in experimental thrombophlebitis can also be explained by the normalizing effect of SOTE flavonoids on the coagulation system. The anticoagulant mechanism of flavonoids involves their ability to inhibit platelet aggregation and prolong blood clotting time through the blockade of IIb/ IIIa platelet receptors and inhibition of the thromboxane A2 synthesis cascade. Additionally, the anticoagulant effect of flavonoids is associated with the inhibition of serine proteases [9, 22]. Quercetin, the primary flavonoid in Saponaria officinalis extract, has been shown by Bekendam R. H. and Flaumenhaft R. [2] to inhibit protein disulfide isomerase activity and block thrombus formation.

Thus, further in-depth preclinical and clinical studies of SOTE appear promising, as they may establish this phytopharmaceutical as an effective venotonic and phlebotropic drug with a pleiotropic mechanism of action.

#### **Conclusions**

- 1. Experimental thrombophlebitis in rabbits is characterized by the development of pathological changes both in the vein and in the surrounding tissues. Histologically, a picture of thrombophlebitis of the marginal vein was established, with occlusion of the vein lumen by a thrombus, destruction of the vascular wall, degenerative and inflammatory changes in the tissues surrounding the vessel, and the presence of varying degrees of vascular wall sclerosis and perivascular fibrosis.
- 2. The administration of SOTE in a therapeutic-preventive regimen at a dose of 20 mg/kg significantly prevented thrombus formation in the marginal vein, promoted softening of thrombotic material, activated thrombolysis, and prevented the formation of obliterating thrombi in all rabbits of the group. The extract of Saponaria officinalis herb prevented the destruction of the vascular wall, reduced or eliminated degenerative changes and inflammatory reactions in the surrounding tissues. The potent phleboprotective effect of the studied extract of Saponaria officinalis herb, according to histological examination, exceeded the effectiveness of Escuvit (at a dose of 7.2 mg/kg as escin).
- 3. The phleboprotective effect of SOTE is likely realized due to the additive synergy of its main groups of biologically active substances (triterpenoid saponins, hydroxycinnamic acids, flavonoids).
- [4] Böttger, S., & Melzig, M. F. (2011). Triterpenoid saponins of the Caryophyllaceae and Illecebraceae family. *Phytochemistry Letters*, 4(2), 59-68. doi: 10.1016/j.phytol.2010.08.003
- [5] Budniak, L., Slobodianiuk, L., Marchyshyn, S., Kostyshyn, L. & Horoshko, O. (2021) Determination of composition of fatty acids in saponaria officinalis L. ScienceRise: Pharmaceutical Science, 29(1), 25-30. doi: 10.15587/2519-4852.2021
- [6] Castro-Ferreira, R., Cardoso, R., Leite-Moreira, A., & Mansilha, A. (2018). The role of endothelial dysfunction and inflammation in chronic venous disease. Ann. Vasc. Surg., 46, 380-393. doi: 10.1016/j.avsg.2017.06.131

Vol. 31, №1, Page 12-21

- [7] Czaban, J., Mołdoch, J., Wróblewska, B., Szumacher-Strabel, M., Cieślak, A., & Oleszek, W. (2013). Effect of triterpenoid saponins of field scabious, alfalfa, red clover and common soapwort on growth of Gaeumannomyces graminis var. tritici and Fusarium culmorum. Allelopathy Journal, 32, 79-90. do i: 10.1080/14786419.2017.1350668
- [8] Gallelli, L. (2019). Escin: a review of its anti-edematous, anti-inflammatory, and venotonic properties. Drug Des. Devel. Ther,. (13), 3425-3437. doi: 10.2147/DDDT.S207720
- [9] Guglemone, H. A., Agnese, A. M., & Montya, S. C. (2002). Anticoagulant effect and action mechanism of sulphated flavonoids from Flaveria bidentis. Thrombosis Researsh, 105(2), 183-188. doi: 10.1016/s0049-3848(01)00419-4
- [10] Heit, J. A., Spencer, F. A., & White, R. H. (2016). The epidemiology of venous thromboembolism. J. Thromb. Thrombolysis, 41(1), 3-14. doi: 10.1007/s11239-015-1311-6
- [11] Ishaq, M., DeGray, G., Mou, K., Aguilera, A., Yang, J., Lempicki, R. A., ... & Natarajan, V. (2007). Zap70 signaling pathway mediates glucocorticoid receptor-dependent transcriptional activation: role in the regulation of annexin 1 expression in T cells. *J. Immunol.*, 179(6), 3851-3858. doi: 10.4049/jimmunol.179.6.3851
- [12] Kostyshyn, L. V., Slobodianiuk, L. V., Marchyshyn, S. M., Demydiak, O. L. & Liashenko, L. Yu. (2020). Дослідження органічних кислот у траві та підземних органах Saponaria officinalis L. [Study of organic acids in herb and underground organs of saponaria officinalis L.]. Медична та клінічна хімія=Medical and Clinical Chemistry, 22(4), 77-82. doi: 10.11603/mcch.2410-681X.2020.i4.11743
- [13] Krasinski, Z., Krasińska, A., Markiewicz, S., & Zieliński, M. (2021). Patients with chronic venous insufficiency in the times of COVID-19 and the risk of thrombus formation suggestions on conservative treatment of such patients based on the principles of pathophysiology. Pol. Przegl. Chir., 93(2), 43-52. doi: 10.5604/01.3001.0014.8500
- [14] Lindner, I., Meier, C., Url, A., Unger, H., Grassauer, A., Prieschl-Grassauer, E., & Doerfle, P. (2010). Beta-escin has potent anti-allergic efficacy and reduces allergic airway inflammation. BMC Immunol., 11(1), 24. doi: 10.1186/1471-2172-11-24
- [15] Lorent, J. H., Quetin-Leclercq, J., & Mingeot-Leclercq, M. P. (2014). The amphiphilic nature of saponins and their effects on artificial and biological membranes and potential consequences for red blood and cancer cells. Org. Biomol. Chem., 44(12), 8803-8822. doi: 10.1039/c4ob01652a
- [16] Maloshtan L. M., Artemova K. O., Borodina N. V., & Kukht-enko A. S. (2023). Study of pharmacological activity of dry extract of Sakhalin willow shoots against the background of experimental thrombophlebitis. ScienceRise: Pharmaceutical Science, 4(44), 97-103. doi: 10.15587/2519-4852.2023.286723
- [17] Moniuszko-Szajwaj, B., Pecio, L., Kowalczyk, M., Simonet, A. M., Macias, F. A., Szumacher-Strabel, M., ... & Stochmal, A. (2013). New Triterpenoid Saponins from the Roots of Saponaria officinalis. Natural Product Communications, 12(8), 1687-1690. doi: 10.1177/1934578x1300801207
- [18] Ouriel, K. (2018). Central Venous Pathologies: Treatments and Economic Impact. Methodist Debakey Cardiovasc J., 14(3), 166-172. doi: 10.14797/mdcj-14-3-166
- [19] Pavela, R. (2016). Extract from the roots of Saponaria officinalis as a potential acaricide against Tetranychus urticae. Journal of Pest Science, 90(2), 683-692. doi: 10.1007/ s10340-016-0828-6

- [20] Petrović, G. M., Ilić, M. D., Stankov-Jovanović, V. P., Stojanović, G. S., & Jovanović, S. Č. (2017). Phytochemical analysis of Saponaria officinalis L. shoots and flowers essential oils. Natural Product Research, 32(3), 331-334. doi: 10.1080/14786419.2017.1350668
- [21] Pihlaja, T., Romsi, P., Ohtonen, P., Jounila, J., & Pokela, M. (2020). Post-procedural Compression vs. No Compression After Radiofrequency Ablation and Concomitant Foam Sclerotherapy of Varicose Veins: A Randomised Controlled Non-inferiority Trial. Eur. J. Vasc. Endovasc. Surg., 59(1), 73-80. doi: 10.1016/j.ejvs.2019.08.020
- [22] Rakhmatullina, A. A., Turaev, R. G., & Kiselev, L. V. (2015). The influence of camphene derivatives on coagulation processes blood. Medical Journal, 96(3), 455-458.
- [23] Robertson, N. U., Schoonees, A., Brand, A., & Visser, J. (2020). Pine bark (Pinus spp.) extract for treating chronic disorders. Cochrane Database Syst. Rev., 9(9), CD008294-CD008298. doi: 10.1002/14651858
- [24] Saberianpour, S., Modaghegh, M. H. S., Rahimi, H., & Kamyar, M. M. (2021). Role of mechanosignaling on pathology of varicose vein. Biophys. Rev., 13(1), 139-145. doi: 10.1007/s12551-021-00783-z
- [25] Shabbir, U., Rubab, M., & Daliri, E. B. (2021). Curcumin, Quercetin, Catechins and Metabolic Diseases: The Role of Gut Microbiota. Nutrients, 13(1), 206-212. doi: 10.3390/ nu13010206
- [26] Sneddon, L. U., Halsey, L. G., & Bury, N. R. (2017). Considering aspects of the 3Rs principles within experimental animal biology. J. Exp. Biol., (220), 3007-3016. doi: 10.1242/jeb.147058
- [27] Subbarayappa, B. V. (2001). The roots of ancient medicine: an historical outline. Journal of Biosciences, 26(2), 135-143. doi: 10.1007/bf02703637
- [28] Talluri, M. R., Gummadi, V. P., & Battu, G. R. (2018). Chemical Composition and Hepatoprotective Activity of Saponaria officinalis on Paracetamol-Induced Liver Toxicity in Rats. Pharmacognosy Journal, 10(6s), s129-s134. doi: 10.5530/pj.2018.6s.24
- [29] Ullah, R., Nadeem, M., Khalique A., & Imran, M. (2016). Nutritional and therapeutic perspectives of Chia (Salvia hispanica L.): a review. J. Food Sci. Technol., (4),1750-1758. doi: 10.1007/s13197-015-1967-0
- [30] Vazquez-Padron, R. I., & Allon, M. (2016). New Insights into Dialysis Vascular Access: Impact of Preexisting Arterial and Venous Pathology on AVF and AVG Outcomes. Clin. J. Am. Soc. Nephrol., 11(8), 1495-1503. doi: 10.2215/ CJN.01860216
- [31] Weaver, J. C., Krilis, S. A., & Giannakopoulos, B. (2018). Oxidative post-translational modification of βeta 2-glycoprotein I in the pathophysiology of the anti-phospholipid syndrome. Free Radic Biol. Med., 125, 98-103. doi: 10.1016/j. freeradbiomed.2018.03.048
- [32] Winter, M. P., Schernthaner, G. H., & Lang, I. M. (2017.). Chronic complications of venous thromboembolism. J. Thromb. Haemost., 15(8), 1531-1540. doi: 10.1111/jth.13741
- [33] Woller, S. C., Stevens, S. M., Kaplan, D., Wang, T. F., Branch, D. W., Groat, D., ... & Elliott, C. G. (2022). Apixaban compared with warfarin to prevent thrombosis in thrombotic antiphospholipid syndrome: a randomized trial. Blood Adv., 6(6),1661-1670. doi: 10.1182/bloodadvances.2021005808
- [34] Yang, X., Feng, Y., & Liu, Y. (2021). Fuzheng Jiedu Xiaoji formulation inhibits hepatocellular carcinoma progression in patients by targeting the AKT/CyclinD1/p21/p27 path-

- way. Phytomedicine, (87), 153575-153579. doi: 10.1016/j. phymed.2021.153575
- [35] Yang, X., Li, Y., Li, Y., Ren, X., Zhang, X., Hu, D., ... & Shang, H. (2017). Oxidative Stress-Mediated Atherosclerosis: Mechanisms and Therapies. Front. Physiol., 8, 600. doi: 10.3389/fphys.2017.00600
- [36] Zabczyk, M., Natorska, J., & Undas, A. (2021). Factor XIII and Fibrin Clot Properties in Acute Venous Thromboembolism. Int. J. Mol. Sci., 22(4),1607. doi: 10.3390/ iims22041607
- [37] Zanza, C., Racca, F., Longhitano, Y., Piccioni, A., Franceschi, F., & Artico, M. (2021). Risk Management and Treatment of Coagulation Disorders Related to COVID-19 Infection Risk Management and Treatment of Coagulation Disorders Related to COVID-19 Infection. Int. J. Environ. Res. Public Health, 18(3), 1268-1274. doi: 10.3390/ijerph18031268
- [38] Zhang, L., Kong, Y. H., Wang, D. W., Li, K. T., & Yu, H. P. (2021). Anticoagulant management by low-dose of low molecular weight heparin in patients with nonvalvular atrial fibrillation following hemorrhagic transformation and complicated with venous thrombosis: Five case reports and literature review. Medicine, 100(7), e24189 doi: 10.1097/MD.0000000000024189

- [39] Zhang, R., Ni, L., Di, X., Wang, X., & Ma, B. (2021). Systematic review and meta-analysis of the prevalence of venous thromboembolic events in novel coronavirus disease-2019 patients. J. Vasc. Surg. Venous Lymphat. Disord., 9(2), 289-298. doi: 10.1016/j.jvsv.2020.11.023
- [40] Zhao, L., Wang, H., & Du, X. (2021). The therapeutic use of quercetin in ophthalmology: recent applications. Biomed. Pharmacother., (137), 111371-111378. doi: 10.3389/ fcvm.2021.596506
- [41] Zhu, V. W., Zhao J. J., Gao, Y., Syn, N. L., & Zhang, S. S. (2021). Thromboembolism in ALK+ and ROS1+ NSCLC patients: A systematic review and meta-analysis. Lung Cancer, (157), 147-155. doi: 10.1016/j.lungcan.2021.05.019
- [42] Zielsdorf, S., Narayanan, L., Kantymyr, S., Barbetta, A., & Kwon, Y. (2021). Surgical shunts for extrahepatic portal vein obstruction in pediatric patients: a systematic review. HPB (Oxford), 23(5), 656-665. doi: 10.1016/j.hpb.2020.11.1149
- [43] Zoccarato, M., Nardetto, L., Basile, A. M., Giometto, B., Zagonel, V., & Lombardi, G. (2021). Seizures, Edema, Thrombosis, and Hemorrhages: An Update Review on the Medical Management of Gliomas. Front. Oncol., 11, 617-966. doi: 10.3389/fonc.2021.617966

## ДОСЛІДЖЕННЯ ВПЛИВУ ЕКСТРАКТУ ТРАВИ SAPONARIA OFFICINALIS НА ГІСТОЛОГІЧНІ ЗМІНИ КРАЙОВОЇ ВЕНИ ВУХА ЗА УМОВ ЕКСПЕРИМЕНТАЛЬНОГО ТРОМБОФЛЕБІТУ Цубанова Н. А., Волощук Н. І., Застрижна М. Л.

Тромбофлебіт визнано одним із найбільш розповсюджених ускладнень хронічної венозної недостатності (ХВН). Його перебіг характеризує запалення венозної стінки з подальшим тромбоутворенням у варикозно розширених венах нижніх кінцівок. Тромбофлебіт діагностують за різним даними у 5-60 % пацієнтів із ХВН. Кількість лікарських засобів, які здатні зменшувати процеси тромбоутворення у венах (флебопротектори), недостатньо представлена як в Україні, так і на фармацевтичному ринку інших країн. Найбільш перспективними флебопротекторами вважають засоби рослинного походження, серед яких важливе місце займає екстракт трави Saponaria officinalis, для якого у попередніх дослідженнях встановлено венотонізуючу та антиексудативну дію. Метою даної роботи було вивчити вплив екстракту трави Saponaria officinalis на зміну гістологічних показників вени вуха у кролів за умов експериментального тромбофлебіту. Експериментальний тромбофлебіт моделювали на кролях за стандартною методикою з накладанням лігатури на крайову вену вуха тварини та введенням розчину Люголя. Гістологічні зміни на тлі досліджуваної фітокомпозиції (20 ма/кг в/шл) порівнювали з дієвістю референс-препарату Ескувіту (7,2 ма/ка за есцином в/шл). Показано, що екстракт трави Saponaria officinalis за умов лікувально-профілактичного введення в значній мірі попереджував тромбоутворення у крайовій вені вуха кролів, сприяючи розм'якшенню матеріалу тромбу, тромболізису, запобігаючи набуттю облітеруючого характеру для тромбічних мас у всіх кролів дослідної групи, зменшував клінічні показники транссудативного набряку, який розвинувся внаслідок гострого веностазу. Таким чином, екстракт трави Saponaria officinalis перешкоджав руйнуванню судинної стінки, викликав депресію або повне нівелювання дегенеративних та запальних змін в оточуючих тканинах. За умов експериментального тромбофлебіту лікувально-профілактичне введення екстракт трави Saponaria officinalis у дозі 20 мг/кг чинить потужну флебопротекторну дію, зменшує процеси тромбоутворення у вені. Дія екстракт трави Saponaria officinalis значуще перевищує ефективність препарату порівняння Ескувіту.

**Ключові слова:** екстракт трави Saponaria officinalis, експериментальний тромбофлебіт, гістологічні зміни, Ескувіт, флебопротекторна дія, протизапальна активність, лікарські рослини.

#### Author's contribution

Tsubanova N. A. – conceptualization, research, review writing and editing, formal analysis and validation.

Voloshchuk N. I. – project administration, conceptualization, supervision, editing, verification.

Zastryzhna M. L. - research, methodology and writing of the original draft, data visualization, resources, software.

Vol. 31, №1, Page 12-21

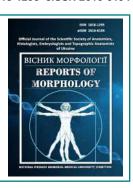
ISSN 1818-1295 eISSN 2616-6194



#### REPORTS OF MORPHOLOGY

Official Journal of the Scientific Society of Anatomists, Histologists, Embryologists and Topographic Anatomists of Ukraine

journal homepage: https://morphology-journal.com



## Structural changes in the diaphragm under conditions of obstructive jaundice (an experimental study)

Kritsak M. Yu., Dzyubanovsky I. Ya., Golovata T. K., Gargula T. I., Yasinovskyi O. B., Palamar S. A. I. Horbachevsky Ternopil National Medical University, Ternopil, Ukraine

#### ARTICLE INFO

Received: 10 April 2024 Accepted: 19 November 2024

**UDC:** 616.26-091.8:616.36-008.5]-092.9

#### **CORRESPONDING AUTHOR**

e-mail: kricakmy@tdmu.edu.ua Kritsak M. Yu..

#### **CONFLICT OF INTEREST**

The authors have no conflicts of interest to declare.

#### **FUNDING**

Not applicable.

#### **DATA SHARING**

Data are available upon reasonable request to corresponding author.

Obstructive jaundice is a prevalent condition in surgical wards. Despite the possibility of surgical removal of biliary obstruction, the high incidence of multiorgan damage during the postoperative period and the associated mortality remain significant challenges for clinical practice. The animal model of obstructive jaundice constitutes a significant component of the study of alterations in human organs, including the diaphragm. The aim of this study was to examine the impact of jaundice on the histological structure of the diaphragm, with a particular focus on the lumbar part, which is the most functionally important, and the costal and tendon components in the experimental rat model. The study was conducted on 30 adult rats weighing 225.0±20.0 g and aged 6 months. All animals were divided into 2 groups: intact and main. The intact group included animals that were not modeling with any pathological process. In the second group of animals, obstructive jaundice was modeling by ligation of the common bile duct, using laparotomic access under general anesthesia. The digital material was subjected using the software "Excel" and "STATISTICA" 5.5 using parametric methods for evaluating the obtained data. The results demonstrated significant destructive and degenerative alterations. In the main group, particular attention was directed towards circulatory disturbances in the microcirculatory system and medium-sized vessels. Capillaries, venules, and arterioles exhibited full blood content, accompanied by all indications of rheohemodynamic disorders, manifesting as blood stasis, erythrocyte sludge, and their parietal adhesion. The arterioles appeared to be thickened as a result of plasma saturation. The endothelium exhibited modifications, with the appearance of rounded cells with vacuolated cytoplasm. Some of these cells were exfoliated. Additionally, edema and smooth muscle dystrophy were observed in the vessel walls, with these changes being more pronounced in the lumbar part of the diaphragm. In the presence of jaundice, the tendon part of the diaphragm exhibited a distinct ratio of structural components compared to the intact group. The tendon layer demonstrated an increase in thickness, which was attributed to edematous loosening. The collagen fibres exhibited a tortuous appearance, and the unevenness of colour became more pronounced compared to the intact group. Additionally, increased cellular infiltration was observed, both diffuse and with the formation of focal infiltrates. The presence of macrophages was observed in the structure of infiltrates, alongside conventional cells. A statistically significant increase was identified in the morphometric parameters of the muscular part of the diaphragm, including the average diameter of the muscle fibre, the nuclei area, the cross-sectional area of the muscle fibre, and the nuclear-cytoplasmic ratio, in the primary group. Furthermore, under the conditions of experimental jaundice, microcirculation disorders with impaired rheohemodynamics, endothelial dysfunction, and dystrophic-destructive changes in the muscle and tendon components occur in parts of the diaphragm, and these are more severe in the muscles of the crus of diaphragm. Key words: jaundice, diaphragm, histology, rats, experiment.

#### Introduction

Obstructive jaundice is a type of clinically common disease that is mainly associated with impaired bile flow

[11, 23, 25]. The bile ducts are either significantly narrowed or completely blocked, resulting in the obstruction of bile

from entering the digestive tract [3, 17]. This can lead to pathophysiological disorders of the body, ultimately resulting in an imbalance and dysfunction of the intestinal flora, which is accompanied by severe septic shock and systemic multiorgan failure [7, 29, 30]. The disease is frequently characterised by an acute onset, rapid progression and high mortality [16, 17].

The animal model of obstructive jaundice is a vital component of the study of this disease. It provides a foundation for investigating the pathogenesis of various bodily changes, evaluating the therapeutic effect, and developing new drugs [4, 6, 11]. The majority of existing animal models of obstructive jaundice are established through bile duct ligation, which not only poses challenges during surgery but also results in a low survival rate [12, 22].

The high incidence of multiorgan damage during the postoperative period and the associated mortality remains a problem in clinical practice. Previous studies have shown that changes in intestinal barrier function based on obstructive jaundice led to the migration of bacteria and endotoxins to various organ systems [9, 19, 21]. In animal models, these toxins and molecules increase the amount of lipid peroxidation products via oxidative stress. This, in turn, affects extrahepatic tissues such as the kidneys, lungs and brain, including the diaphragm [5]. A complete understanding of the pathophysiological changes in obstructive jaundice remains a challenge for planning current and future treatment [1, 8, 10].

The aim of this study is to investigate the effect of jaundice on the histological structure of different parts of the diaphragm, the lumbar part of the diaphragm as the most functional, the costal and tendon parts in the experimental rat model.

#### Materials and methods

In order to achieve this objective, a random selection of 30 sexually mature rats, aged 6 months and weighing 225.0±20.0 g, was made. The experimental animals were kept in the vivarium of the I. Horbachevsky Ternopil National Medical University of the Ministry of Health of Ukraine. During the experimental study, the animals were divided into two groups of 10 animals each. Group I was designated as the intact group, for which no pathological process was modelled. Group II was designated as the main group, for which obstructive jaundice was modelled for a period of seven days [17]. The temporal frame selected for this study was not arbitrary. According to extant literature, a duration of five to seven days is deemed sufficient to elicit the desired severity of jaundice in rats, thus facilitating the observation of changes in organs and body systems. This timeframe is considered optimal for the study of this pathology [14, 15]. The presence of jaundice was assessed by the following signs: yellowing of the sclerae, change in urine colour, presence of acholic faeces. During the diaphragm sampling, a jaundiced tint of the internal organs and dilation of the extrahepatic bile ducts were noted.

All surgical procedures were carried out in a warm room by the same experimenter, who employed the same

technique throughout. The rats were not fed 12 hours prior to anaesthesia, but had free access to water; two hours before anaesthesia, water was removed from the cage. The rats were induced into drug-induced sleep by means of an intramuscular injection of 10 mg/kg Xylazine plus 90 mg/kg Ketamine Solutions. The animals were then fixed to a table in a supine position, and the abdominal wall was shaved and disinfected with a 10 % povidone-iodine solution before being covered with sterile napkins. A midline laparotomy was performed, and the common bile duct was identified by gentle caudal stretching of the stomach and duodenum after entering the abdominal cavity (Fig. 1).

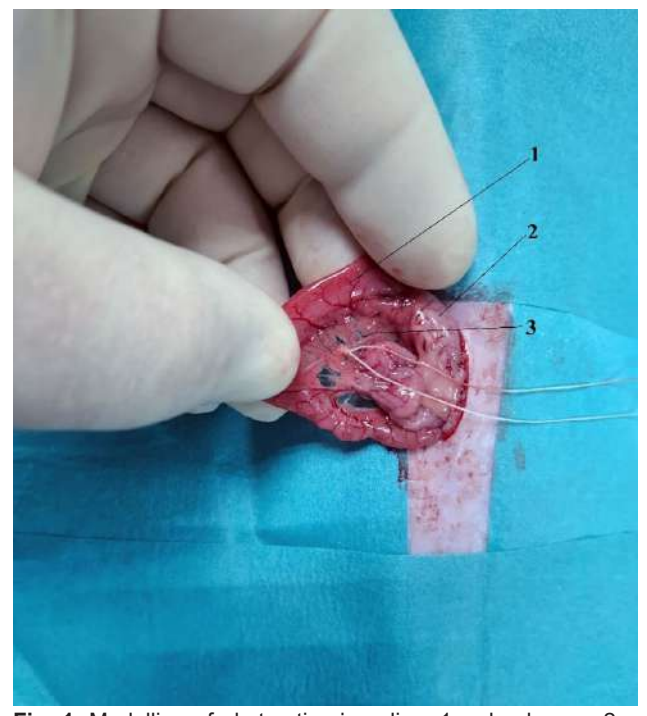


**Fig. 1.** Modelling of obstructive jaundice: 1 – duodenum; 2 – pyloric part of the stomach; 3 – common bile duct with ligature.

All animal manipulations were performed in the morning indoors at a temperature of 20-22°C and relative humidity of 60-80 %. The induction of euthanasia was achieved through the intraperitoneal injection of high doses of Thiopental sodium, at a rate of 75 mg/kg body weight. Following the conclusion of the experiment, the diaphragm of the rat was taken in accordance with the copyright certificate for the work No. 126059 of 29 April 2024. A macro section of the diaphragm is shown in Figure 2.

The experimental animals were used in accordance with the provisions of the Law of Ukraine 'On the Protection of Animals from Cruelty', the European Convention for the Protection of Vertebrate Animals Used for Experimental and Other Scientific Purposes of 18.03.1986, and Council of Europe Directive 2010/63/EU. The Bioethics Commission of the I. Horbachevsky Ternopil National Medical University (protocol No. 74 dated May 16, 2024) did not identify any violations of moral and ethical norms during this study.

Vol. 31, №1, Page 22-29

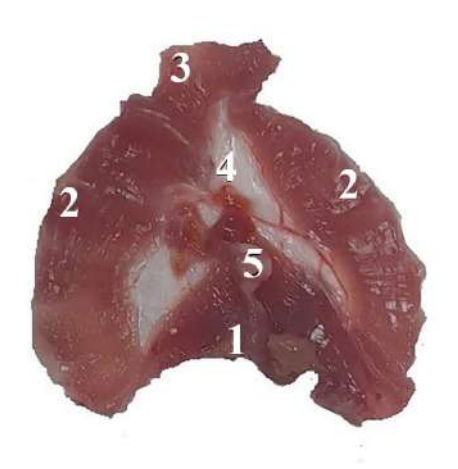


**Fig. 2.** Removed macrosection of the diaphragm: 1 – lumbar part; 2 – costal part; 3 – sternal part; 4 – tendon part; 5 – residual part of the esophagus.

On the macro preparations of the diaphragm, the tendon, costal and lumbar parts were separately isolated and placed in a 10 % solution of neutral formalin (see Fig. 2). The thoracic part was not isolated, as it was hypothesised that similar changes would occur as in the costal part. The cruses of diaphragm were isolated separately, as it was determined that they represent the most functionally loaded part of the respiratory muscle. Following fixation, the histological material was dehydrated in ethyl alcohols of increasing concentration and embedded in paraffin. Histological sections (5-7 µm thick) were prepared from each paraffin block using a microtome, following deparaffinisation and staining with hematoxylin and eosin [2].

Two rats from the primary cohort perished on the fifth and sixth days following the surgical intervention. Obstructive jaundice is a grave disease that can lead to multiorgan failure and high mortality. This experiment is consistent with this pattern. The rats that died during the experimental procedure were excluded from the analysis of the study, and no new rats were added to replace them. All other rats were euthanised at the conclusion of the experiment. Consequently, bile duct dilation was detected in all rats at the conclusion of the experiment.

The digital material was subjected to statistical processing on a computer using the software "Excel" (Microsoft, USA) and "STATISTICA" 5.5 (Statsoft, USA) with the use of parametric methods of data evaluation.

#### Results

Histologically, the costal part of the diaphragm is composed of transversely striated muscle fibres that form a dense layer. In longitudinal sections, these fibres exhibit a distinctive appearance, typical of this particular muscle type. The thickness of the muscle fibres varies slightly, and the sarcoplasm is light eosinophilic in colour. However, the tintorial

properties demonstrate heterogeneity, frequently resulting in a grooved structure within the sarcoplasm. The elongated oval-shaped nuclei were located beneath the sarcolemma and were not always evenly spaced or oriented parallel to the fibre. Transverse striation in the form of straight or arcuate stripes is also distinguishable in longitudinal sections (Fig. 3).

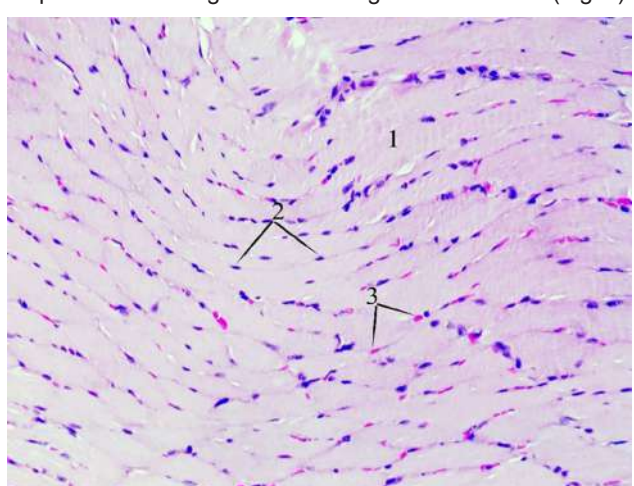


**Fig. 3.** Histological structure of the costal part of the diaphragm of an intact rat: 1 – sarcoplasm; 2 – nuclei; 3 – capillaries located in the endomysium. Hematoxylin and eosin staining. ×200.

In the primary cohort, the focus was directed towards the identification of circulatory disturbances within the microcirculatory system and medium-sized vessels. The capillaries, venules and arterioles exhibited signs of rheohemodynamic dysfunction, manifesting as blood stasis, erythrocyte sludge and their parietal adhesion. The arterioles appeared thickened, indicative of plasma saturation. The endothelium exhibited modifications, characterised by the presence of rounded cells with vacuolated cytoplasm. Some of these cells were exfoliated, and the vessel walls demonstrated signs of edema and smooth muscle dystrophy. Perivascular spaces were observed to be expanded due to stromal edema. Additionally, small lymphocytic infiltrates were detected in the endo- and perimysium. A greater heterogeneity was observed in the muscle fibres compared to the previous experimental group. On longitudinal sections, transverse striation was often weakly expressed or not visualised, and there were foci of sarcoplasmic disintegration and fragmentation of the fibres themselves (Fig. 4).

The muscle tissue of the cruses of diaphragm in intact rats exhibited an identical histological structure to the costal part; however, the heterogeneity of muscle fibres, myofibril disruption and the presence of adipose tissue in the perimysium were more pronounced (Fig. 5).

The morphological picture in this area in cases of jaundice was characterised by the presence of oedema, and foci of dystrophic and degenerative changes in muscle fibres were more frequently detected. The fibres themselves were thickened due to intracellular oedema. Cellular infiltrates were common, and their structure was dominated by lymphocytes (Fig. 6).

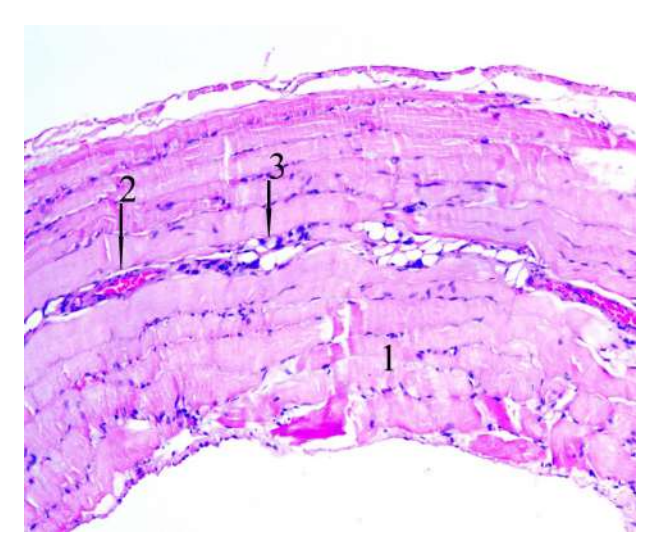


**Fig. 4.** Histological structure of the costal part of the diaphragm of a rat from the main group: 1 – muscle fibres with sarcoplasmic disintegration; 2 – full blood vessels; 3 – oedema, fatty tissue and cellular infiltrates in the stroma. Hematoxylin and eosin staining. ×100.

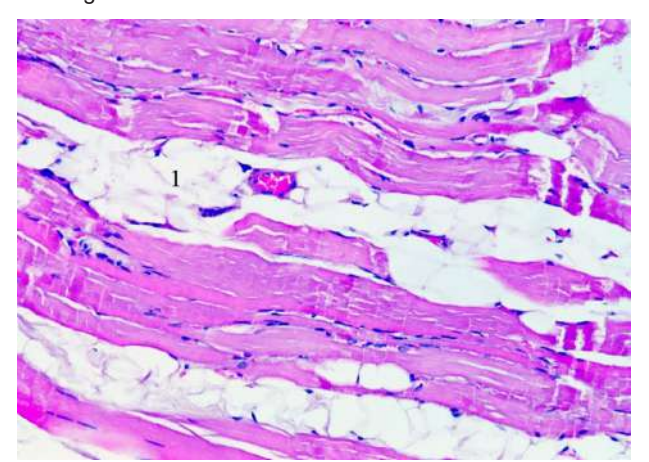


**Fig. 5.** Histological structure the crus of the diaphragm of an intact rat: 1 – adipose tissue in the perimysium. Hematoxylin and eosin staining. ×200.

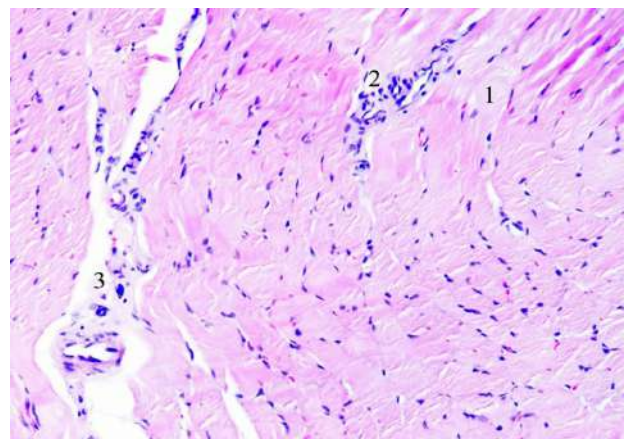


**Fig. 6.** Histological structure the crus of the diaphragm of the main group rat: 1 – disintegration of muscle fibre sarcoplasm; 2 – cellular infiltrates; 3 – severe stromal oedema. Hematoxylin and eosin staining. ×100.

The tendinous part of the diaphragm of intact rats is constituted primarily by dense bundles of collagen fibres that form the aponeurotic sheet, with slight variations in thickness observed across different sections. Microscopically, the tendinous tissue exhibits a friable consistency and contains fatty tissue. On the side of the thoracic cavity, the connective tissue is covered by the diaphragmatic fascia, and below it is a thin sheet of parietal peritoneum. The collagen fibres are homogeneously eosinophilic, with slight variations in intensity, and often exhibit signs of disintegration without compromising their structural integrity. The cellular component is minimal, comprising fibroblasts, fibrocytes, and histiocytes (Fig. 7).

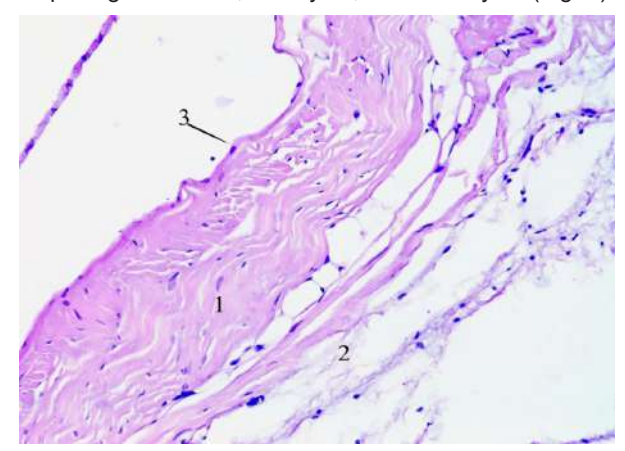


**Fig. 7.** Histological structure of the tendon part of the diaphragm of an intact rat: 1 – dense bundles of collagen fibres; 2 – loose fibre of the thoracic surface; 3 – parietal peritoneum. Hematoxylin and eosin staining. ×200.

In the presence of jaundice, the tendon part of the diaphragm exhibited an identical composition, but differed in the ratio of structural components. In general, the thickness of the tendon layer increased, which was due to edematous loosening. The collagen fibres had a tortuous appearance, and the unevenness of the colour became more pronounced compared to the intact group. Increased cellular infiltration was observed, both diffuse and with the formation of focal infiltrates. Macrophages were observed within the structure of the infiltrates, in conjunction with traditional cells (Fig. 8).

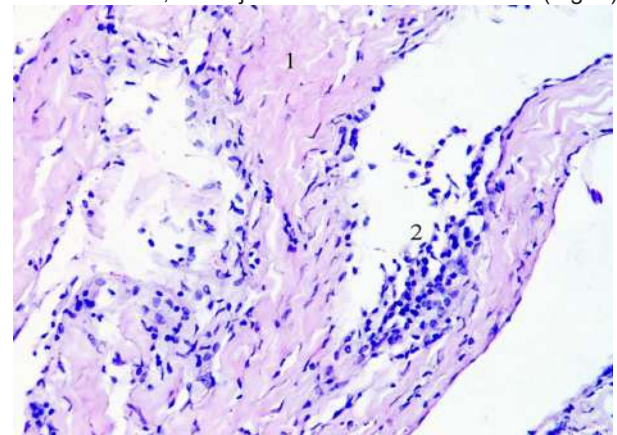


**Fig. 8.** Histological structure of the tendon part of the diaphragm of the main group rat: 1 – tortuous and unevenly coloured collagen fibres; 2 – cellular infiltrate. Hematoxylin and eosin staining. ×200.

Vol. 31, №1, Page 22-29 **25** 

As illustrated in Table 1, the morphometric data obtained from the two experimental groups indicates that the average diameter (d) of the muscle fibre in the intact group was 0.3 % larger in the cruses than in the costal part, though this difference was not statistically significant (p>0.005). A similar trend was observed in the main group. A statistically significant increase in muscle fibre diameter was observed in both the costal and lumbar regions of the two study groups, with respective increases of 3.4 % and 3.5 % (p<0.01 and p<0.001, respectively).

**Table 1.** Morphometric parameters of the diaphragm parts of the experimental groups (M±m).

		,			
	Group of animals				
Indicator	Intact group		Main group		
	Costal part	Lumbar part	Costal part	Lumbar part	
d, µm	40.37±0.08	40.46±0.11 (p <sub>1</sub> >0.05)	41.81±0.22 (p <sub>2</sub> <0.01)	41.94±0.19 (p <sub>1</sub> >0.05) (p <sub>3</sub> <0.001)	
s <sub>s,</sub> µm²	1296±7	1297±9 (p <sub>1</sub> >0,05)	1360±16 (p <sub>2</sub> <0.01)	1361±16 (p <sub>1</sub> >0.05) (p <sub>3</sub> <0.01)	
s <sub>n,</sub> µm²	62.36±0.04	62.36±0.05 (p <sub>1</sub> >0.05)	62.73±0.11 (p <sub>2</sub> <0.01)	62.79±0.11 (p <sub>1</sub> >0.05) (p <sub>3</sub> <0.01)	
s <sub>n</sub> /s <sub>s</sub>	0.048±0.0003	0.048±0.0003 (p <sub>1</sub> >0.05)	0,046±0,001 (p <sub>2</sub> <0.01)	0,046±0,001 (p <sub>1</sub> >0.05) (p <sub>3</sub> <0.01)	

**Notes:**  $p_1$  – is the reliability of indicators within one study group;  $p_2$  – reliability of the values compared to the group of intact animals;  $p_3$  – reliability of the indicators compared to the group of intact animals.

The cross-sectional area of the muscle fibre (Ss) of the diaphragm and its cruses within the same group increased, though this increase was not significant (p>0.005). However, the values of these parameters between the experimental groups increased in the direction of animals with jaundice. Consequently, the cross-sectional area of the fibres of the costal part of the diaphragm and animals with jaundice exhibited a statistically significant increase of 4.7 % (p<0.01), while the lumbar part of the diaphragm demonstrated a similar increase of 4.7 % (p<0.01).

A slight (p>0.005) increase in the area of muscle fibre nuclei (Sn) of the cruses of diaphragm in relation to its costal part by 0.1 % was found in animals with jaundice. In the group of intact animals, this indicator remained almost unchanged; however, a comparison between the groups revealed a significant difference. The diameter of the fibre nuclei of the costal part of the diaphragm increased by 0.6 % (p<0.01), and of the muscle fibres of the cruses by 0.7 % (p<0.01) in animals with jaundice.

A comparable tendency was identified in the course of a comparison of the values of the nuclear-cytoplasmic ratio (Sn/Ss). While the values remained constant (p>0.05), then the comparison between the groups showed a significant decrease in animals with jaundice of 4.0 % (p<0.01) in both parts of the diaphragm.

#### **Discussion**

Therefore, when comparing the results between groups, it was observed that there were destructive and dystrophic changes present in all parts of the diaphragm in the presence of jaundice. The present study investigated structural changes in a rat model of acute cholestasis by ligation of the bile ducts, which resulted in cholestatic liver dysfunction. In other words, morphological signs of endothelial dysfunction in the diaphragm were observed, caused by the direct toxic effect of bilirubin and which led to the above pathological manifestations.

A comprehensive review of the extant literature revealed that this is the inaugural study to examine histopathological changes in the respiratory muscle in animals with modelled obstructive jaundice. The study all the animals of the main group revealed the presence of blood circulation disorders in the microcirculatory system and medium-sized vessels, as well as oedema and foci of dystrophic and degenerative changes in muscle fibres. These changes were more pronounced in the lumbar part of the diaphragm. Morphometric parameters (average diameter, nucleus area and cross-sectional area of muscle fibre, nuclear-cytoplasmic ratio) statistically significantly increased in the main group.

Obstructive jaundice is a prevalent condition within the domain of hepatobiliary surgery [1, 28]. Despite the surgical intervention for biliary obstruction being a well-established procedure, the significant postoperative incidence of multiorgan damage and the resultant mortality rates continue to present significant challenges to clinical practice [18, 20, 26]. It is especially important that 90 % of operations are performed laparoscopically, which involves the creation of another pathological condition in the human body – pneumoperitoneum with carbon dioxide [8]. It is therefore evident that further research is necessary to study the morphological structure of the diaphragm in conditions of jaundice and carboxyperitoneum.

Multiorgan lesions have been demonstrated to be closely associated with intestinal mucosal barrier dysfunction, enteroendocrine dysfunction, and bacterial translocation [13, 24]. In studies where duct ligation was performed, total serum bilirubin and direct bilirubin in rats peaked on day 5. as expected [11, 27]. Despite the advent of new medical and surgical treatments, this pathology continues to demonstrate high morbidity and mortality rates [10]. This study unveils significant alterations and illuminates hitherto unexplored aspects of the pathogenesis of destructive diaphragmatic changes. Numerous studies have underscored structural changes in organs, predominantly the liver [22, 27]. Although the mechanisms and details of these disorders are not fully understood. Despite the absence of a comprehensive understanding of the mechanisms and specifics of these disorders, several studies have been published by experienced scientists, revealing significant details about the

progression of the disease. These findings have subsequently inspired researchers to conduct new studies [3, 25].

In the study of the intestine in jaundice, the following observations were made: thinning of the intestinal muscle layer with thinning of the villi, atrophy, uneven height, fusion of villi, partial detachment of the villi epithelium and significant lymphocyte infiltration [13, 24]. Conversely, our observations included a thickening of muscle fibres, primarily due to oedema, as well as a pronounced cellular infiltration. This finding suggests that the diaphragm may be subject to greater functional stress compared to the intestinal musculature, given its active involvement in the act of breathing.

A thorough examination of the structural changes in the liver revealed that the sinusoidal structure was disrupted, and focal inflammation, fragmentary necrosis, and congestive necrosis were evident [20, 27]. Oedema, neutrophil infiltration, and marked proliferation of the bile ducts can be observed [7]. In obstructive jaundice, the lung tissue also undergoes changes in the form of moderate to intense neutrophilic infiltration of leukocytes, perivascular oedema, and partial destruction of the lung structure in some places [28]. These data correlate with our data, where destruction and oedema are observed, but we did not observe complete destruction of the diaphragm structure. Ya-Wei Yuan et al. [28] in their study provided substantial evidence for the hypothesis that obstructive jaundice can cause vascular hyporeactivity. The objective of the study was to investigate the mechanisms of the MaxiK and  $K_{\text{ATP}}$  channels underlying cholestasis-induced vascular dysfunction [28], a hypothesis that was confirmed by the data, which showed impaired circulation. The study

revealed that chronic cholestasis instigates several structural changes in the epididymis, which are characterised by a decrease in tubular diameter, thickening of the basement membrane of the tubules and regression of the main cells. These changes were accompanied by a decrease in major cellular organelles, cytoplasmic vacuolation, nuclear changes and loss of stereovilli. The results of the study demonstrate that chronic cholestasis instigates structural changes in the epididymis due to androgen deficiency [12, 15].

#### **Conclusions**

- 1. In experimental jaundice, microcirculatory disorders manifest with impaired rheohemodynamics, endothelial dysfunction and dystrophic-destructive changes in the muscle fibres of the diaphragm, with more intense changes in the muscles of the crus. In the tendon part of the diaphragm, there are signs of disorganisation of collagen fibres and reactive inflammatory infiltration to the damage.
- 2. In the context of jaundice-induced alterations in muscle fibres of the diaphragm, significant increases in fibre diameter (p<0.01) were observed, ranging from 3.4 % to 3.5 %, along with corresponding increases in nuclear area (0.6 % to 0.7 %), predominantly in the costal and lumbar regions. Additionally, a substantial expansion (4.7 %) in the fibre's cross-sectional area was documented, affecting both regions. Consequently, the nuclear-cytoplasmic ratio in the main group exhibited a decline of 4.0 %. These observations can be attributed to the compensatory restructuring of the damaged structural components of the diaphragm under conditions of bilirubin intoxication.

#### References

- [1] Aoki, H. (2024). Changes over time in treatment for obstructive jaundice. *World Journal of Gastrointestinal Surgery*, 16(10), 3074-3077. doi: 10.4240/wjgs.v16.i10.3074
- [2] Bahriy, M. M., Dibrova, V. A., Popadynets, O. H., & Hryshchuk, M. I. (2016). Методики морфологічних досліджень: Монографія [Methods of Morphological Research: Monograph]. Вінниця: Нова книга = Vinnytsya: A new book.
- [3] Chen, H. L., Wu, S. H., Hsu, S. H., Liou, B. Y., Chen, H. L., & Chang, M. H. (2018). Jaundice revisited: recent advances in the diagnosis and treatment of inherited cholestatic liver diseases. *Journal of Biomedical Science*, 25(1), 1-13. doi: 10.1186/s12929-018-0475-8
- [4] Chen, J., Dong, J. T., Li, X. J., Gu, Y., Cheng, Z. J., & Cai, Y. K. (2015). Glucagon-like peptide-2 protects impaired intestinal mucosal barriers in obstructive jaundice rats. World Journal of Gastroenterology, 21(2), 484-490. doi: 10.3748/wjg.v21.i2.484
- [5] Demircioglu, M. K., Demircioglu, Z. G., Cakir, O., Yanar, K., Ozguven, M. B. Y., Atukeren, P., ... & Yazici, P. (2024). Antioxidant effect of Rosa pimpinellifolia L. fruit extract on cholestatic liver injury: an experimental study. *Revista da Associacao Medica Brasileira*, 70(1), e20230720. doi: 10.1590/1806-9282.20230720
- [6] Dilektasli, E., Ozmen, M. M., Gundogdu, E., Dizen, H., Besler, H. T., & Ozogul, C. (2016). The effects of obstructive jaundice on the brain: An experimental study. Asian Journal of Surgery, 39(3), 155-163. doi: 10.1016/j.asjsur.2015.03.014

- [7] Kaya, O., Koca, Y. S., Barut, İ., Baspinar, S., & Sabuncuoglu, M. Z. (2015). L-carnitine reduces acute lung injury in experimental biliary obstruction. *Saudi Medical Journal*, 36(9), 1046-1052. doi: 10.15537/smj.2015.9.12206
- [8] Kuzman, M., Bhatti, K. M., Omar, I., Khalil, H., Yang, W., Thambi, P., ... & Mahawar, K. (2022). Solve study: a study to capture global variations in practices concerning laparoscopic cholecystectomy. *Surgical Endoscopy*, 36(12), 9032-9045. doi: 10.1007/s00464-022-09367-8
- [9] Liu, J. J., Sun, Y. M., Xu, Y., Mei, H. W., Guo, W., & Li, Z. L. (2023). Pathophysiological consequences and treatment strategy of obstructive jaundice. *World Journal of Gastrointestinal Surgery*, 15(7), 1262-1276. doi: 10.4240/wjgs. v15.i7.1262
- [10] Lu, H., Liang, B., Xia, X., & Zheng, C. (2024) Efficacy Analysis of PTCD + TACE vs PTCD + Apatinib in the Treatment of HCC with Obstructive Jaundice: A Retrospective Study. Anticancer Agents Med. Chem., 24(17), 1241-1252. doi: 10.2174/0118715206313132240712101607
- [11] Lv, Y., Yue, J., Gong, X., Han, X., Wu, H., Deng, J., & Li, Y. (2018). Spontaneous remission of obstructive jaundice in rats: Selection of experimental models. *Experimental and Therapeutic Medicine*, 15(6), 5295-5301. doi: 10.3892/etm.2018.6119
- [12] Mahmoud, Y. I., & Abo-Zeid, F. S. (2018) Epididymal ultrastructural changes associated with chronic cholestasis after bile duct ligation in adult rats. *Ultrastruct. Pathol.*, 42(4),

Vol. 31, №1, Page 22-29 **27** 

- 344-349. doi: 10.1080/01913123.2018.1488789
- [13] Oguz, S., Salt, O., Ibis, A. C., Gurcan, S., Albayrak, D., Yalta, T., ... & Erenoglu, C. (2018). Combined effectiveness of honey and immunonutrition on bacterial translocation secondary to obstructive jaundice in rats: experimental study. Medical Science Monitor: International Medical Journal of Experimental and Clinical Research, 24, 3374. doi: 10.12659/MSM.907977
- [14] Onalan, A. K., Tuncal, S., Kilicoglu, S., Celepli, S., Durak, E., Kilicoglu, B., & Kismet, K. (2016). Effect of silymarin on oxidative stress and liver histopathology in experimental obstructive jaundice model. *Acta Cirurgica Brasileira*, 31(12), 801-806. doi: 10.1590/S0102-865020160120000004
- [15] Ozozan, O. V., Dinc, T., Vural, V., Ozogul, C., Ozmen, M. M., & Coskun, F. (2020). An electron microscopy study of liver and kidney damage in an experimental model of obstructive jaundice. *Annali Italiani di Chirurgia*, 91, 122-130.
- [16] Pavlidis, E. T., & Pavlidis, T. E. (2018) Pathophysiological consequences of obstructive jaundice and perioperative management. *Hepatobiliary Pancreat Dis. Int.*, 17(1), 17-21. doi: 10.1016/j.hbpd.2018.01.008
- [17] Reznikov, O. G. (2003). Загальні етичні принципи експериментів на тваринах [The fundamental ethical principles ofexperiments on animals]. Ендокринологія = Endocrinology, 8(1), 142-145.
- [18] Şahan, M. H., & Akşamoğlu, M. (2025). Clinical Results of Percutaneous Transhepatic Biliary Drainage With Different Hepatic Access and Methods in the Treatment of Obstructive Jaundice. Surgical Laparoscopy Endoscopy & Percutaneous Techniques, 35(1), e1335. doi: 10.1097/ SLE.00000000000001335
- [19] Shen, X., Zhang, X., Li, K., Huang, G., Li, X., Hou, Y., & Ge, X. (2024). Combined bacterial translocation and cholestasis aggravates liver injury by activation pyroptosis in obstructive jaundice. *Heliyon*, 10(16), e35793. doi: 10.1016/j. heliyon.2024.e35793
- [20] Solmaz, A., Gülçiçek, O. B., Erçetin, C., Yiğitbaş, H., Yavuz, E., Arıcı, S., ... & Çelebi, F. (2016). Nesfatin-1 alleviates extrahepatic cholestatic damage of liver in rats. *Bosnian Journal of Basic Medical Sciences*, 16(4), 247-253. doi: 10.17305/bjbms.2016.1465
- [21] Tang, X., Ma, W., Zhan, W., Wang, X., Dong, H., Zhao, H., ... & Wang, N. (2018). Internal biliary drainage superior to external biliary drainage in improving gut mucosa barrier because of goblet cells and mucin-2 up-regulation. *Bioscience Reports*, 38(3), BSR20171241. doi: 10.1042/BSR20171241
- [22] Unal, Y., Tuncal, S., Kosmaz, K., Kucuk, B., Kismet, K.,

- Cavusoglu, T., ... & Hucumenoglu, S. (2019). The effect of calcium dobesilate on liver damage in experimental obstructive jaundice. *Journal of Investigative Surgery*, *32*(3), 238-244. doi: 10.1080/08941939.2018.1451936
- [23] Van Campenhout, S., Van Vlierberghe, H., & Devisscher, L. (2019). Common Bile Duct Ligation as Model for Secondary Biliary Cirrhosis. *Methods Mol. Biol.*, 1981, 237-247. doi: 10.1007/978-1-4939-9420-5 15
- [24] Wang, C., Fan, W., Feng, X., Zhang, Y., Liu, C., & Liu, Z. (2021). The roles of the glucagon-like peptide-2 and the serum TGF-β1 levels in the intestinal barrier and immune functions in rats with obstructive jaundice. *American Journal of Translational Research*, 13(9), 10449-10458. PMID: 34650714
- [25] Wu, Y. L., Li, Z. L., Zhang, X. B., & Liu, H. (2019). Yinchenhao decoction attenuates obstructive jaundice-induced liver injury and hepatocyte apoptosis by suppressing protein kinase RNA-like endoplasmic reticulum kinase-induced pathway. World Journal of Gastroenterology, 25(41), 6205-6221. doi: 10.3748/wjg.v25.i41.6205
- [26] Yang, R., Zhu, S., Pischke, S. E., Haugaa, H., Zou, X., & Tonnessen, T. I. (2018). Bile and circulating HMGB1 contributes to systemic inflammation in obstructive jaundice. *The Journal of Surgical Research*, 228, 14-19. doi: 10.1016/j.jss.2018.02.049
- [27] Yilmaz, E. E., Arikanoğlu, Z., Turkoğlu, A., Kiliç, E., Yüksel, H., & Gümüş, M. (2016). The protective effects of pomegranate on liver and remote organs caused by experimental obstructive jaundice model. *European Review for Medical & Pharmacological Sciences*, 20(4) 767-772.
- [28] Yuan, Y. W., Wang, L., Lu, Z. Y., Long, Y., Jiao, Y. F., Xia, Q., ... & Yu, W. F. (2016). Overexcited MaxiK and KATP channels underlie obstructive jaundice-induced vasoconstrictor hyporeactivity of arterial smooth muscle. *Scientific Reports*, 6(1), e39246. doi: 10.1038/srep39246
- [29] Zhang, C. X., Shu, C. M., Zhang, X. Y., Lin, X. T., Guan, Q. H., Zhang, F., & Zhi, X. T. (2021). Effect and mechanism of omega-3 polyunsaturated fatty acids on intestinal injury in rats with obstructive jaundice. *European Review for Medical & Pharmacological Sciences*, 25(19), 6077-6092. doi: 10.26355/eurrev 202110 26886
- [30] Zhang, C., Yin, Z., Hu, F., Lin, X., Guan, Q., Zhang, F., & Zhang, X. (2024). Omega-3 Polyunsaturated Fatty Acids Alleviate Intestinal Barrier Dysfunction in Obstructive Jaundice Rats. *Molecular Biotechnology*, 66(8), 1954-1960. doi: 10.1007/s12033-023-00829-5

### СТРУКТУРНІ ЗМІНИ ДІАФРАГМИ ЗА УМОВ МЕХАНІЧНОЇ ЖОВТЯНИЦІ (ЕКСПЕРИМЕНТАЛЬНЕ ДОСЛІДЖЕННЯ) Кріцак М. Ю., Дзюбановський І. Я., Головата Т. К., Гаргула Т. І., Ясіновський О. Б., Паламар С. А.

Механічна жовтяниця є поширеним захворюванням у хірургічних відділеннях. Хоча непрохідність жовчовивідних шляхів можна усунути хірургічним шляхом, велика частота поліорганних ушкоджень під час післяопераційного періоду та пов'язана з ними смертність залишаються складними для клінічної практики. Тваринна модель механічної жовтяниці є важливою частиною досліджень змін органів організму людини в тому числі і діафрагми. Мета дослідження — вивчити вплив жовтяниці на гістологічну структуру різних частин діафрагми, поперекову частину діафрагми, як найбільш функціональну, реберну та сухожильну частини в експериментальній моделі на щурах. Роботу виконано на 30 дорослих щурах масою 225,0±20,0 гр., віком 6 місяців. Всіх тварин розподілили на 2 групи: інтактну та основну. До інтактної групи увійшли тварини, котрим не моделювали жодного патологічного процесу. У другій групі тварин проведено моделювання механічної жовтяниці шляхом перев'язки загальної жовчної протоки лапаротомним доступом під загальним знечуленням. Цифровий матеріал оброблений за допомогою програмних забезпечень «Excel» і «STATISTICA» 5.5 з використанням параметричних методів оцінки отриманих даних. В отриманих результатах спостерігали виражені деструктивні та дегенеративні зміни. У основній групі звертали увагу розлади кровообігу в системі гемомікроциркуляторного русла і судин середнього калібру. Капіляри, венули та артеріоли були повнокровними з усіма ознаками розладу реогемодинаміки

у вигляді стазу крові, сладжу еритроцитів та їх пристінкової адгезії. Артеріоли виглядали потовщеними за рахунок їх просякання плазмою. Видозмінювався ендотелій — з'являлися округлі клітини з вакуолізованою цитоплазмою. Частина з них злущувалася. В стінках судин з'являвся набряк, дистрофія гладких міоцитів. Дані зміни більш виражені у поперековій частині діафрагми. За наявності жовтяниці сухожилкова частина діафрагми різнилась співвідношенням структурних компонентів порівняно з інтактною групою. Товщина сухожилкового пласту збільшувалася, що було зумовлено набряковим розрихленням. Колагенові волокна мали звивистий вигляд, а нерівномірність забарвлення ставала більш виразною порівняно з інтактною групою. Звертала увагу посилена клітинна інфільтрація як дифузна, так із формуванням осередкових інфільтратів. В структурі інфільтратів поряд із традиційними клітинами з'являлися макрофаги. Морфометричні показники м'язової частини діафрагми такі як: пересічний діаметр м'язового волокна, площа ядер, площа поперечного перерізу м'язового волокна, ядерно-цитоплазматичне співвідношення статистично достовірно зростали в основній групі. В умовах експериментальної жовтяниці в частинах діафрагми виникають розлади мікроциркуляції з порушенням реогемодинаміки, ендотеліальної дисфункції і дистрофічно-деструктивні зміни м'язового та сухожильного компоненту, причому в м'язах ніжок вони були виражені більш інтенсивно.

Ключові слова: жовтяниця, діафрагма, гістологія, щурі, експеримент.

#### Author's contribution

Kritsak M. Yu. – work concept and design, data collection and analysis, writing the article.

Dzyubanovsky I. Ya. - formal analysis and verification, supervision, research, peer review, review and editing.

Golovata T. K. - data visualization, critical review.

Gargula T. I. – editing, project administration.

Yasinovskyi O. B. - conceptualization, methodology and writing of the original project.

Palamar S. A. - responsibility for statistical analysis.

Vol. 31, №1, Page 22-29

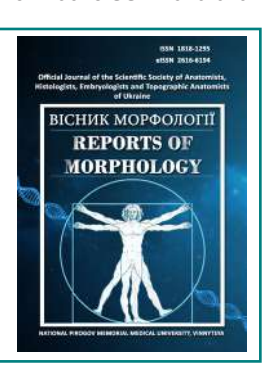
ISSN 1818-1295 eISSN 2616-6194



#### REPORTS OF MORPHOLOGY

Official Journal of the Scientific Society of Anatomists, Histologists, Embryologists and Topographic Anatomists of Ukraine

journal homepage: https://morphology-journal.com



## Characteristics of cerebral morphometric parameters in acute stroke patients and its associations with 90 days stroke outcome

Bartiuk R. S., Smolko D. G., Smotrytska T. V., Marunkevych Ya. Yu., Starynets N. H., Fiks D. O., Moskovko S. P.

National Pirogov Memorial Medical University, Vinnytsia, Ukraine

#### ARTICLE INFO

Received: 3 April 2024 Accepted: 26 November 2024

UDC: 616.45-091.8:616.5-001.17-06]-

085.36

#### **CORRESPONDING AUTHOR**

e-mail: rambrs88@gmail.com Bartiuk R. S.

#### **CONFLICT OF INTEREST**

The authors have no conflicts of interest to declare.

#### **FUNDING**

Not applicable.

#### **DATA SHARING**

Data are available upon reasonable request to corresponding author.

Brain morphometry is widely used to diagnose and predict mainly neurodegenerative diseases, but cerebrovascular diseases have received much less attention, especially for predicting long-term consequences of stroke. The aim of the research was to investigate the associations between changes in brain morphometric parameters and stroke outcome at 90 days. 294 consecutive patients with acute stroke were recruited. All participants underwent brain magnetic resonance imaging and/or computed tomography assessment as well as clinical-neurological evaluation. Statistical analysis was performed in the program The Jamovi project (2022), Jamovi (Version 2.3) [Computer Software], Sydney, Australia using parametric and nonparametric statistical methods. We found that enlarged ventricular and cortical morphometric parameters are associated with unfavorable stroke outcome at 90 days. In the univariable analysis, enlarged third ventricle index (the regression coefficient b=-2.6, p=0.014), Shlatenbrandt-Nurenberger index (the regression coefficient b=0.6, p=0.007), bicaudate index (the regression coefficient b=-1.5, p=0.006), higher width of the longitudinal cerebral fissure in the anterior part of the frontal lobes (the regression coefficient b=-3.5, p=0.005), higher width of the cerebral fissure in the area of the skull vault (the regression coefficient b=-3.5, p=0.006) significantly associated with lower Barthel index at 90 days. In the multivariable analysis, significant association was found between enlarged third ventricle index and Barthel index at 90 days (the regression coefficient b=-2.6, p=0.045). In the other model of multivariable analysis, enlarged bicaudate index significantly associated with higher level of functional dependence at 90 days (odds ratio=1.1, p=0.031). Our findings confirmed that enlarged cerebral morphometric indices are associated with unfavorable short-term stroke outcome at 90 days.

**Key words:** nervous system disorders, stroke, brain morphometry, bicaudate index, ventricular index.

#### Introduction

Measurements of brain morphometry, like cortical thickness and subcortical brain volumes are widely used in clinical and scientific practice. Individual differences in morphometric parameters have been linked to aging, brain diseases and behavior [17, 35]. Moreover, morphometric distinct "signature" patterns of brain anatomical changes are useful for prognosis and long-term outcome surveillance [8, 23], including cerebrovascular disease [40]. However, most of the studies were devoted to neurodegenerative disorders, like Alzheimer disease, fronto-temporal dementia, etc. [7, 15, 33]. Still, the association between stroke outcome and morphological brain changes has not been studied

exhaustively. Some research showed changes of brain anatomical parameters in response to external manipulations [3, 22]. Therefore, it can be highly informative to study stroke outcome and structural plasticity based on basic morphological brain "profile" for diagnostic and predictive purposes.

Cerebrovascular diseases are major contributors to death, long-term disability, cognitive decline and dementia [1, 2, 19]. There are well-known stroke outcome predictors, such as stroke severity at admission, admission systolic and diastolic blood pressure, baseline comorbidities, etc. [1, 41], but less attention was given to underlying structural

non-stroke lesion changes and its associations with stroke outcome. Brain morphological changes reflect global underlying pathological changes and brain fragility for both cerebrovascular and neurodegenerative disorders [13]. Hence, assessment of deep and cortical morphometrics can be clinically valuable predictors for a long-term stroke outcome

We tested a hypothesis that altered brain morphometric indices predict unfavorable stroke outcome at 90 days.

The aim of the research was to investigate associations between brain morphometric changes and 90 days stroke outcome.

#### Materials and methods

Subjects. 294 consecutive patients between December 2016 and December 2019 were enrolled (115 females and 179 males). The study was based at specialized stroke department (Stroke Unit) № 22 of the Vinnytsia Regional Psychoneurological Hospital named after acad. O. I. Yushchenko. The mean age of the patients was 61.94±10.11 years, mRS on admission – 4 (4-5) scores. The study was approved by the local ethics committee (Protocol № 9 of November 14, 2016). All patients signed informed consent before the participation. It was a prospective single-center cohort study. We thoroughly assessed neuroimaging data as well as clinical-neurological status.

The criteria for the selection of the patients were confirmed diagnosis of stroke, good quality of neuroimaging scans and absence of neuroimaging artifacts, as well as obtained informed consent to participate in the study.

Neuroimaging. Among 294 participants, 120 underwent MRI, 174 – CT. Some of them were imaged with either MRI or CT, some of them – with MRI and CT both. MRI was performed on a Philips Achieva 1.5T. The brain scanning protocol included the following whole brain scans: T1-weighted, T2-weighted, FRAIR and DWI sequences, slice thickness was 3.5-5 mm. CT was performed on a General Electric CT/e (Italy) with a tomographic slices of 3-7 mm.

Measurements of the brain morphometry. We visually measured deep ventricular indices, that are Evans index, third ventricle index, fourth ventricle index, ventricular index, Shlatenbrandt-Nurenberger index, bicaudate index, cella media index (also known as Schiersmann's index), and Huckman number. We also assessed cortical morphometrics: longitudinal cerebral fissure in the anterior part of the frontal lobes (FI), the width of the right (ICR) and left insular cisterns (ICL), and their sum (ICRL), width of the cerebral fissure in the area of the skull vault (SW), and the maximum width of the cerebellar fissure (CFW) [11] (Fig. 1). For the assessment we used computer software "The Horos Project".

Clinical assessment. We gathered demographics and stoke risk factors: age, gender, comorbidities with Charlson comorbidity index [21], smoking, alcohol overuse, body mass index (BMI), history of previous stroke. We performed comprehensive neurological examination for stroke patients on patients admission and at discharge: NIHSS score [42],

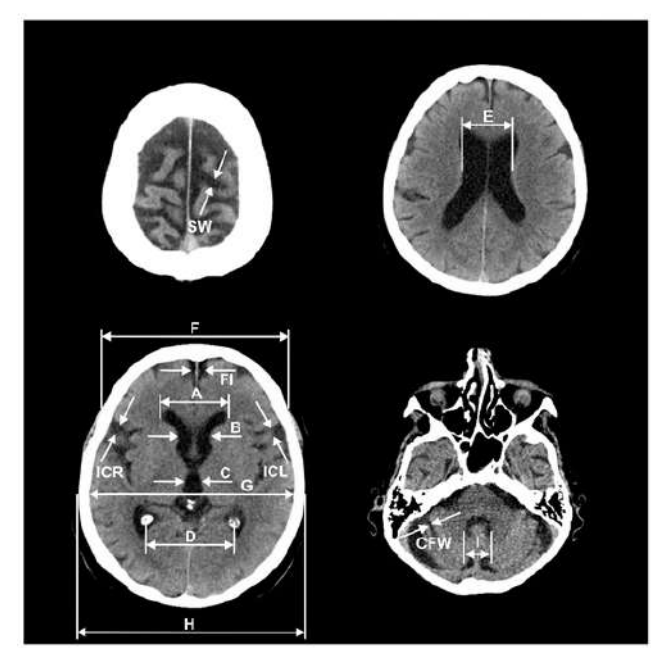


**Fig. 1.** Brain morphometry measurements. A – the frontal horns greatest width; B – intercaudate distance; C – the third ventricle distance; D – the choroid plexuses distance; E – the lateral ventricles greatest width at the level of cella media; I – the fourth ventricle distance; ICL – the left insular cistern width; ICR – the right insular cistern width; FI – the longitudinal cerebral fissure width in anterior part; SW – the cerebral sulci greatest width at the skull vault; CFW – the cerebellar fissures greatest width; G – the temporal bones greatest external distance; F – the frontal bone greatest external distance.

modified Rankin scale (mRS) score [30], Barthel index score (BI) [26], Glasgow coma scale (GCS) [10], MMSE score [20]. The stroke subtypes were determined based on the TOAST criteria [12]. The 90-day functional outcome was assessed with the mRS and BI by telephone interviews. Also, the functional outcome was measured with the mRS at 90 days as favorable (mRS $\leq$ 2) or unfavorable (mRS $\geq$ 2) [5].

Statistical analysis. Statistical analysis was performed by The Jamovi project (2022), Jamovi (Version 2.3) [Computer Software]. Sydney, Australia. Linear variables were presented as mean (M) ± standard deviation (SD). A two groups comparison was performed by nonparametric Mann-Whitney U-test. To calculate the associations between brain morphometric parameters and 90 days stroke outcome we employed univariable and multivariable regression analysis. The results are shown as odds ratio (OR) and 95 % confidence intervals (CI) or as the regression coefficient b (b) and 95 % CI in case of linear regression.

#### Results

The baseline cerebral morphometric parameters in men and women are shown in Table 1.

In Table 1 and Figure 2, Evans index, bicaudal index, ventricular index, Shlatenbrandt index, third ventricle index, Huckman number and FI are significantly different in favorable

Vol. 31, №1, Page 30-36 **31** 

**Table 1.** Comparison of brain morphometric parameters between patients with favorable (mRS 0-2) and unfavorable (mRS>2, functional dependence) stroke outcome at 90 days, distributed by gender.

	Men, (M±SD)		Women, (M±SD)	
Morphometric indices	favorable outcome, (n= 114)	unfavorable outcome, (n=55)	favorable outcome, (n=74)	unfavorable outcome, (n=34)
Evans index	27.26±3.26	28.28±2.88*	26.45±4.68	26.85±4.98
3rd ventricle index	4.947±1.730	5.627±1.687*	4.710±1.790	5.314±1.987
Shlatenbrandt- Nurenberger index	23.23±9.51	19.45±6.10*	24.49±9.56	21.42±8.30
4th ventricle index	12.42±1.62	12.48±1.97	12.51±1.90	12.44±2.29
Bicaudate index	15.51±2.98	16.99±3.34*	14.29±3.75	15.60±4.30
Ventricular index	16.45±2.07	15.76±1.73*	16.89±3.32	16.67±3.30
Schiersmann index	5.017±1.014	5.015±1.293	5.449±1.238	5.425±1.451
Huckman number	58.05±7.89	61.14±7.93*	53.55±10.33	54.87±11.79
FI	5.505±1.497	6.038±1.627*	5.143±1.355	5.806±1.620t
ICR	7.167±2.600	7.191±2.579	7.078±2.693	7.179±2.605
ICL	7.746±2.729	7.991±2.458	7.481±2.685	7.909±2.321
ICRL	14.91±4.835	15.182±4.559	14.56±4.81	15.18±4.77
sw	4.252±1.337	4.596±1.421	4.041±1.359	4.732±1.960t
CFW	2.552±1.161	2.505±1.367	2.586±1.016	2.500±1.174

**Note:** \* – significant differences between brain morphometric parameters in favorable (mRS 0-2) and unfavorable (mRS 3-6) 90 days stroke outcome (p<0.05); t – trend towards significance (p<0.1).

(mRS 0-2, functional independence) vs. unfavorable (mRS 3-6, functional dependence) stroke outcome in men. In women, trends towards statistical significance were found for FI  $(5.143\pm1.355 \text{ vs. } 5.806\pm1.620, \text{ p=0.091})$  and SW  $(4.041\pm1.359 \text{ vs. } 4.732\pm1.960, \text{ p=0.071})$ .

According to the univariable analysis, the third ventricle index (b=-2.6; 95 % CI -4.7 – -0.5, p=0.014), Shlatenbrandt-Nurenberger index (b=0.6; 95 % CI 0.2 – 1.0, p=0.007), bicaudate index (b=-1.5; 95 % CI -2.5 – -0.4, p=0.006), FI (b=-3.5; 95 % CI -5.9 – -1.1, p=0.005), SW (b=-3.5; 95 % CI -6.1 – -1.0, p=0.006) significantly associated with poorer BI at 90 days.

After adjusting for age and sex, nearly significant association was found between FI and BI at 90 days (b=-2.1;

95 % CI -4.6 - 0.4, p=0.095).

In the next model, adjusted for age, sex, history of smoking, comorbidity index, body mass index, history of stroke, hyperlipidemia, presence of complications, index stroke severity by NIHSS, significant association was found between the third ventricle index and BI at 90 days (b=-2.6; 95 % CI -3.4 - -0.1, p=0.045). In this model, Shlatenbrandt-Nurenberger index, the fourth ventricle index, bicaudate index, FI and SW showed near-marginal significance (p<0.1).

Further, multifactorial analysis was performed, adjusted for age and sex along with all morphometric indices to evaluate their associations with the unfavorable stroke outcome. Both crude and adjusted odds ratio are shown in Table 2.

**Table 2.** Brain morphometric indices and their associations with the unfavorable stroke outcome (functional dependence, mRS>2) at discharge.

Brain measurement	Crude OR (95 % Cl, p)	Adjusted OR (95 % Cl, p)
Evans index	1.0 (1.0-1.11, p=0.143)	1.0 (1.0-1.1, p=0.412)
The third ventricle index	1.1 (1.00-1.3, p=0.096)	1.1 (0.9-1.2, p=0.484)
Shlatenbrandt- Nurenberger index	1.0 (0.9-1.0, p=0.096)	1.0 (0.99-1.1, p=0.579)
The fourth ventricle index	1.0 (0.9-1.1, p=0.901)	1.0 (0.9-1.2, p=0.945)
Bicaudate index	1.1 (1.0-1.2, p=0.004)	1.1 (1.0-1.2, p=0.031)
Ventricular index	0.9 (0.8-1.0, p=0.090)	0.9 (0.8-1.0, p=0.192)
Cella media index (Schiersmann's index)	0.9 (0.8-1.1, p=0.382)	1.0 (0.8-1.2, p=0.889)
Huckman number	1.0 (1.0-1.1, p=0.090)	1.0 (0.9-1.0, p=0.306)
FI	1.2 (1.0-1.4, p=0.034)	1.0 (1.1-1.3, p=0.161)
ICR	1.1 (1.0-1.2, p=0.311)	1.0 (0.9-1.1, p=0.687)
ICL	1.0 (0.9-1.1, p=0.678)	1.0 (0.9-1.0, p=0.994)
ICRL	1.0 (0.9-1.1, p=0.374)	1.0 (0.9-1.1, p=0.994)
SW	1.2 (1.0-1.4, p=0.027)	1.1 (0.9-1.3, p=0.171)
CFW	1.1 (0.9-1.3, p=0.475)	1.0 (0.9-1.3, p=0.702)

As seen in Table 2, bicaudate index, FI and SW were significantly associated with unfavorable stroke outcome at 90 days. After adjusting for age and sex, only bicaudate

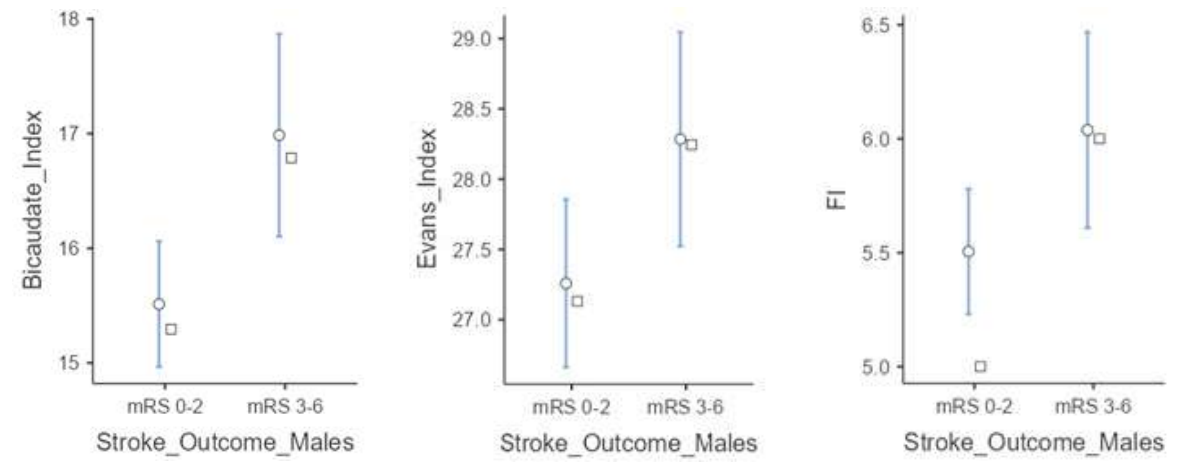
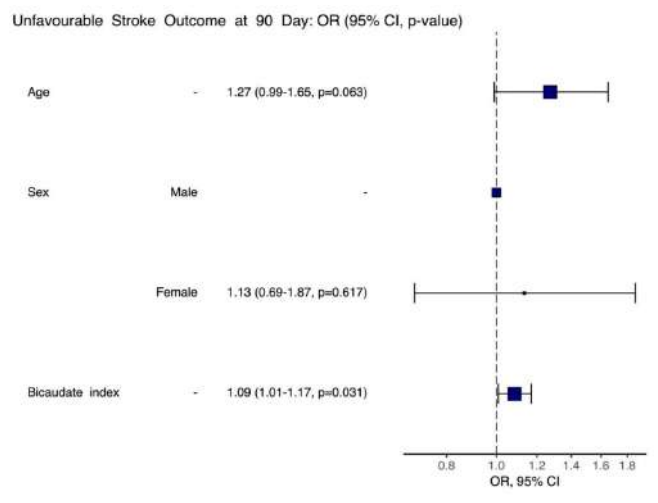


Fig. 2. Significant differences in morphometric parameters depending on the stroke outcome in men.  $\bigcirc$  – mean,  $\square$  – median.

index was significantly associated with unfavorable stroke outcome at 90 days, as shown in Fig. 3.



**Fig. 3.** Forest-plot adjusted for age and sex of bicaudate index association with unfavorable stroke outcome at 90 days.

#### **Discussion**

Previously we found that altered cerebral morphometric parameters significantly associated with short-term stroke outcome at discharge. In the current paper we investigated associations between brain morphometrics and 90 days stroke outcome.

In the two-groups comparison analysis, in men almost all ventricular indices and FI were significantly higher in the group of unfavorable stroke outcome at day 90, while in women, FI and SW were close to significance. These results can be explained by different sample sizes (169 men, 108 women), but vascular risk factors, which are more common in men, may be of greater importance. Hence, more severe baseline subcortical and cortical atrophic brain changes can worsen 90 days stroke outcome.

Increased ventricular indices represent enlarged deep cerebrospinal fluid spaces, and on the other hand – atrophy of frontal, parietal lobes and shrinking of basal ganglia, including caudate nuclei. Enlarged FI represents frontal lobes cortical atrophy, SW – parietal lobes cortical atrophy. Therefore, frontal and parietal lobes atrophy is one the most important predictors for post-stroke rehabilitation and restoration of lost brain functions. As it is known, there are complicated neural circuits, which connect basal ganglia (extrapyramidal system) and frontal cortex, which is crucial for motor, cognitive and emotional functioning [27]. Altered morphometric indices reflect reduced brain reserve for neuroplasticity and neurogenesis and are direct predictors of impaired abilities for post-stroke recovery.

In the univariable analysis our results showed that enlarged subcortical indices - the third ventricle index, Shlatenbrandt-Nurenberger index, bicaudate index, as well as cortical parameters - FI, SW were significantly associated with poorer BI at 90 days.

In the multivariable analysis, adjusted for age and sex,

nearly significant association was found between FI and BI at 90 days (b=-2.1, p=0.095).

In the next multivariable model, adjusted for age, sex, history of smoking, comorbidity index, body mass index, history of stroke, hyperlipidemia, presence of complications, index stroke severity by NIHSS, significant association was found between the third ventricle index and BI at 90 days (b=-2.6, p=0.045). In this model, Shlatenbrandt-Nurenberger index, the fourth ventricle index, bicaudate index, FI and SW showed near-marginal significance (p<0.1).

We also found that bicaudate index – (OR=1.1, p=0.004), FI – (OR=1.2, p=0.034) and SW – (OR=1.2, p=0.027) were significantly associated with unfavorable stroke outcome (mRS 3-6) at 90 days. After adjusting for age and sex, only enlargement of bicaudate index was significantly associated with unfavorable stroke outcome at 90 days – (OR=1.1, p=0.031).

Our results are consistent with the others findings, such as J. Y. Zhou et al. [42], who demonstrated that brain atrophy is an independent predictor of unfavorable stroke outcome at 90 days. However, in the study by S. H. Lee et al. [25], increased intercaudate distance was associated with a protective effect on the outcomes of large cerebral infarct with a trend of saving patients from a malignant clinical outcome. A. K. Tam et al. [37] demonstrated that the severity of brain atrophy was associated with worse outcome of subarachnoid hemorrhage at 6 weeks. In the study by J. P. Appleton et al. [2], brain atrophy as a component of the "brain frailty" was associated with unfavorable outcomes of both territorial and lacunar stroke at 90 days.

A series of studies have shown the associations of cerebral atrophy and stroke outcome after reperfusion therapy, which were quite heterogeneous: in the study by F. Arba et al. [6], the presence of severe cerebral atrophy more than doubled the odds of unfavorable functional outcome at 90 days. In another study by F. Arba et al. [4], no significant association with brain atrophy was found. In the study by C. Delcourt et al. [14], the presence of any degree of atrophy was significantly associated with a decreased likelihood of a good functional outcome according to mRS at 90 days. In the study by W. K. Diprose et al. [16], increasing cerebrospinal fluid volume associated with a reduced likelihood of good functional outcome (mRS 0-2) at 90 days. In the work of I. Lauksio et al. [24] cerebral atrophy was a significant predictor of mortality at 90 days. S. Mönch et al. [29] found no association between atrophic changes of the brain and stroke outcomes and mortality at 90 days. M. I. Pedraza et al. [31] found cortical atrophy to be significantly associated with unfavorable stroke outcome after recanalization. O. Tschirret et al. [38] found no association between brain atrophy and stroke outcomes at 3 months.

The mechanisms by which brain atrophy and enlarged cerebral morphometrics may affect functional recovery after stroke are still not well understood. It is possible that the association may be mediated by a decrease of the brain's reserve capacity for functional recovery [32, 34]. Brain

Vol. 31, №1, Page 30-36

atrophy, manifested by dilation of the ventricles and cortical sulci span, is often associated with leukoaraiosis, lacunes, and enlarged perivascular spaces, which are hallmarks of cerebral small vessel disease [39]. These features have been shown to be associated with endothelial dysfunction, impaired cerebral blood flow, and loss neuronal connectivity, which may hinder functional recovery and lead to worse outcomes after stroke. In addition, brain atrophy is also associated with cognitive impairment and dementia, which are known to be predictors of poor functional outcome after stroke [9].

As we previously speculated, altered cerebral morphometric parameters could possibly lead to loss of functional brain connectivity, which, in turn, deteriorates post-stroke recovery [18].

Besides, increased deep morphometric indices, which represent white matter shrinking, can diminish processing speed and cause executive dysfunction, and cortical indices deterioration can lead to loss of higher brain functions, as consequence – impaired motor and cognitive post-stroke recovery [28, 36].

For future research, it can be of interest to investigate the associations between brain morphometrics and ultra long-term stroke outcome – beyond 90 days, for instance, in a year or more.

#### **Conclusions**

- 1. Enlarged cerebral morphometric indices significantly associated with unfavorable 90 days stroke outcome.
- 2. The most important brain morphometric predictors of unfavorable stroke outcome at 90 days are Bicaudate index, Ventricular index, frontal and parietal lobes fissure width.
- 3. Measurement of cerebral morphometrics can be of interest to predict stroke outcome and select patients for treatment and preventive strategies.

#### References

- [1] Abujaber, A. A., Albalkhi, I., Imam, Y., Nashwan, A. J., Yaseen, S., Akhtar, N., & Alkhawaldeh, I. M. (2023). Predicting 90-Day Prognosis in Ischemic Stroke Patients Post Thrombolysis Using Machine Learning. *Journal of Personalized Medicine*, 13(11), 1555. doi: 10.3390/jpm13111555
- [2] Appleton, J. P., Woodhouse, L. J., Adami, A., Becker, J. L., Berge, E., Cala, L. A., ... & Wardlaw, J. M. (2020). Imaging markers of small vessel disease and brain frailty, and outcomes in acute stroke. *Neurology*, 94(5), e439-e452. doi: 10.1212/WNL.000000000008881
- [3] Arachchige, P. R. W., Karunarathna, S., Wataru, U., Ryo, U., Median, A. C., Yao, D., ... & Senoo, A. (2021). Changes in brain morphometry after motor rehabilitation in chronic stroke. Somatosensory & Motor Research, 38(4), 277-286. doi: 10.1080/08990220.2021.1968369
- [4] Arba, F., Inzitari, D., Ali, M., Warach, S. J., Luby, M., Lees, K. R., & STIR/VISTA Imaging Collaboration (2017). Small vessel disease and clinical outcomes after IV rt-PA treatment. Acta Neurologica Scandinavica, 136(1), 72-77. doi: 10.1111/ane.12745
- [5] Arba, F., Palumbo, V., Boulanger, J. M., Pracucci, G., Inzitari, D., Buchan, A. M., ... & CASES Investigators (2016). Leukoaraiosis and lacunes are associated with poor clinical outcomes in ischemic stroke patients treated with intravenous thrombolysis. *International Journal of Stroke: Official Journal of the International Stroke Society*, 11(1), 62-67. doi: 10.1177/1747493015607517
- [6] Arba, F., Testa, G. D., Limbucci, N., Nappini, S., Renieri, L., Pracucci, G., ... & Inzitari, D. (2019). Small vessel disease and clinical outcomes after endovascular treatment in acute ischemic stroke. Neurological Sciences: Official Journal of the Italian Neurological Society and of the Italian Society of Clinical Neurophysiology, 40(6), 1227-1235. doi: 10.1007/ s10072-019-03824-4
- [7] Bachmann, T., Schroeter, M. L., Chen, K., Reiman, E. M., Weise, C. M., & Alzheimer's Disease Neuroimaging Initiative (2023). Longitudinal changes in surface based brain morphometry measures in amnestic mild cognitive impairment and Alzheimer's disease. *NeuroImage*, 38, 103371. doi: 10.1016/j.nicl.2023.103371
- [8] Bejanin, A., Tammewar, G., Marx, G., Cobigo, Y., Iaccarino, L., Kornak, J., ... & Rabinovici, G. D. (2020). Longitudi-

- nal structural and metabolic changes in frontotemporal dementia. *Neurology*, 95(2), e140-e154. doi: 10.1212/WNL.0000000000009760
- [9] Béjot, Y., Duloquin, G., Crespy, V., Durier, J., Garnier, L., Graber, M., & Giroud, M. (2020). Influence of Preexisting Cognitive Impairment on Clinical Severity of Ischemic Stroke: The Dijon Stroke Registry. Stroke, 51(6), 1667-1673. doi: 10.1161/STROKEAHA.119.028845
- [10] Bodien, Y. G., Barra, A., Temkin, N. R., Barber, J., Foreman, B., Vassar, M., ... & Edlow, B. L. (2021). Diagnosing Level of Consciousness: The Limits of the Glasgow Coma Scale Total Score. *Journal of Neurotrauma*, 38(23), 3295-3305. doi: 10.1089/neu.2021.0199
- [11] Chrzan, R., Gleń, A., Bryll, A., & Urbanik, A. (2019). Computed Tomography Assessment of Brain Atrophy in Centenarians. International Journal of Environmental Research and Public Health, 16(19), 3659. doi: 10.3390/ijerph16193659
- [12] Chung, J. W., Park, S. H., Kim, N., Kim, W. J., Park, J. H., Ko, Y., ... & Bae, H. J. (2014). Trial of ORG 10172 in Acute Stroke Treatment (TOAST) classification and vascular territory of ischemic stroke lesions diagnosed by diffusionweighted imaging. *Journal of the American Heart Association*, 3(4), e001119. doi: 10.1161/JAHA.114.001119
- [13] De Guio, F., Duering, M., Fazekas, F., De Leeuw, F. E., Greenberg, S. M., Pantoni, L., ... & Jouvent, E. (2020). Brain atrophy in cerebral small vessel diseases: Extent, consequences, technical limitations and perspectives: The HARNESS initiative. Journal of Cerebral Blood Flow and Metabolism: Official Journal of the International Society of Cerebral Blood Flow and Metabolism, 40(2), 231-245. doi: 10.1177/0271678X19888967
- [14] Delcourt, C., Wang, X., Zhou, Z., Wardlaw, J. M., Mair, G., Robinson, T. G., ... & Lindley, R. I. (2020). Brain imaging abnormalities and outcome after acute ischaemic stroke: the ENCHANTED trial. *Journal of Neurology, Neurosur-gery, and Psychiatry*, 91(12), 1290-1296. doi: 10.1136/jnnp-2020-323015
- [15] Diaz-Torres, S., Ogonowski, N., García-Marín, L. M., Bonham, L. W., Duran-Aniotz, C., Yokoyama, J. S., & Rentería, M. E. (2023). Genetic overlap between cortical brain morphometry and frontotemporal dementia risk. *Cerebral Cortex*, 33(12), 7428-7435. doi: 10.1093/cercor/bhad049

- [16] Diprose, W. K., Diprose, J. P., Wang, M. T. M., Tarr, G. P., McFetridge, A., & Barber, P. A. (2019). Automated Measurement of Cerebral Atrophy and Outcome in Endovascular Thrombectomy. *Stroke*, 50(12), 3636-3638. doi: 10.1161/ STROKEAHA.119.027120
- [17] Elliott, M. L., Hanford, L. C., Hamadeh, A., Hilbert, T., Kober, T., Dickerson, B. C., ... & Buckner, R. L. (2023). Brain morphometry in older adults with and without dementia using extremely rapid structural scans. *NeuroImage*, 276, 120173. doi: 10.1016/j.neuroimage.2023.120173
- [18] Fan, F., Liao, X., Lei, T., Zhao, T., Xia, M., Men, W.,... & He, Y. (2021). Development of the default-mode network during childhood and adolescence: A longitudinal restingstate fMRI study. *NeuroImage*, 226, 117581. doi: 10.1016/j. neuroimage.2020.117581
- [19] Feigin, V. L., Brainin, M., Norrving, B., Martins, S., Sacco, R. L., Hacke, W., ... & Lindsay, P. (2022). World Stroke Organization (WSO): Global Stroke Fact Sheet 2022. International Journal of Stroke: Official Journal of the International Stroke Society, 17(1), 18-29. doi: 0.1177/17474930211065917
- [20] Folstein, M. F., Folstein, S. E., & McHugh, P. R. (1975). "Mini-mental state". A practical method for grading the cognitive state of patients for the clinician. *Journal of Psychiatric Research*, 12(3), 189-198. doi: 10.1016/0022-3956(75)90026-6
- [21] Goldstein, L. B., Samsa, G. P., Matchar, D. B., & Horner, R. D. (2004). Charlson Index comorbidity adjustment for ischemic stroke outcome studies. *Stroke*, 35(8), 1941-1945. doi: 10.1161/01.STR.0000135225.80898.1c
- [22] Hanakawa, T., Goldfine, A. M., & Hallett, M. (2017). A Common Function of Basal Ganglia-Cortical Circuits Subserving Speed in Both Motor and Cognitive Domains. eNeuro, 4(6), ENEURO.0200-17.2017. doi: 10.1523/EN-EURO.0200-17.2017
- [23] Keret, O., Staffaroni, A. M., Ringman, J. M., Cobigo, Y., Goh, S. M., Wolf, A., ... & Vöglein, J. (2021). Pattern and degree of individual brain atrophy predicts dementia onset in dominantly inherited Alzheimer's disease. *Alzheimer's & Dementia*, 13(1), e12197. doi: 10.1002/dad2.12197
- [24] Lauksio, I., Lindström, I., Khan, N., Sillanpää, N., Hernesniemi, J., Oksala, N., & Protto, S. (2021). Brain atrophy predicts mortality after mechanical thrombectomy of proximal anterior circulation occlusion. *Journal of Neurointerventional Surgery*, 13(5), 415-420. doi: 10.1136/ neurintsurg-2020-016168
- [25] Lee, S. H., Oh, C. W., Han, J. H., Kim, C. Y., Kwon, O. K., Son, Y. J., ... & Chung, Y. S. (2010). The effect of brain atrophy on outcome after a large cerebral infarction. *Journal* of Neurology, Neurosurgery, and Psychiatry, 81(12), 1316-1321. doi: 10.1136/jnnp.2009.197335
- [26] Li, F., Li, D., Yu, J., Jia, Y., Jiang, Y., Chen, T., ... & Zeng, R. (2020). Barthel Index as a Predictor of Mortality in Patients with Acute Coronary Syndrome: Better Activities of Daily Living, Better Prognosis. *Clinical interventions in aging*, 15, 1951-1961. doi: 10.2147/CIA.S270101
- [27] Li, J., Wen, H., Wang, S., Che, Y., Zhang, N., & Guo, L. (2022). Altered Brain Morphometry in Cerebral Small Vessel Disease with Cerebral Microbleeds: An Investigation Combining Univariate and Multivariate Pattern Analyses. Frontiers in Neurology, 13, 819055. doi: 10.3389/fneur.2022.819055
- [28] Lyden, P. (2017). Using the National Institutes of Health Stroke Scale: A Cautionary Tale. Stroke, 48(2), 513-519.

- doi: 10.1161/STROKEAHA.116.015434
- [29] Mönch, S., Sepp, D., Hedderich, D., Boeckh-Behrens, T., Berndt, M., Maegerlein, C., ... & Friedrich, B. (2020). Impact of brain volume and intracranial cerebrospinal fluid volume on the clinical outcome in endovascularly treated stroke patients. *Journal of Stroke and Cerebrovascular Diseases:* the Official Journal of National Stroke Association, 29(7), 104831. doi: 10.1016/j.jstrokecerebrovasdis.2020.104831
- [30] Nobels-Janssen, E., Postma, E. N., Abma, I. L., van Dijk, J. M. C., Haeren, R., Schenck, H., ... & Boogaarts, H. D. (2022). Inter-method reliability of the modified Rankin Scale in patients with subarachnoid hemorrhage. *Journal* of Neurology, 269(5), 2734-2742. doi: 10.1007/s00415-021-10880-4
- [31] Pedraza, M. I., de Lera, M., Bos, D., Calleja, A. I., Cortijo, E., Gómez-Vicente, B., ... & Arenillas, J. F. (2020). Brain Atrophy and the Risk of Futile Endovascular Reperfusion in Acute Ischemic Stroke. *Stroke*, *51*(5), 1514-1521. doi: 10.1161/ STROKEAHA.119.028511
- [32] Rabinstein, A. A., Albers, G. W., Brinjikji, W., & Koch, S. (2019). Factors that may contribute to poor outcome despite good reperfusion after acute endovascular stroke therapy. *International journal of stroke: official journal of the International Stroke Society*, 14(1), 23-31. doi: 10.1177/1747493018799979
- [33] Rahmani, F., Jindal, S., Raji, C. A., Wang, W., Nazeri, A., Perez-Carrillo, G. G., ... & Benzinger, T. L. S. (2023). Validity Assessment of an Automated Brain Morphometry Tool for Patients with De Novo Memory Symptoms. *American Journal of Neuroradiology*, 44(3), 261-267. doi: 10.3174/ ajnr.A7790
- [34] Rastogi, A., Weissert, R., & Bhaskar, S. M. (2023). Brain atrophy in acute ischaemic stroke patients treated with reperfusion therapy: a systematic review. Acta Radiologica (Stockholm, Sweden: 1987), 64(1), 257-266. doi: 10.1177/02841851211060427
- [35] Smith, S. M., Elliott, L. T., Alfaro-Almagro, F., McCarthy, P., Nichols, T. E., Douaud, G., & Miller, K. L. (2020). Brain aging comprises many modes of structural and functional change with distinct genetic and biophysical associations. *eLife*, 9, e52677. doi: 10.7554/eLife.52677
- [36] Swardfager, W., Cogo-Moreira, H., Masellis, M., Ramirez, J., Herrmann, N., Edwards, J. D., ... & Black, S. E. (2018). The effect of white matter hyperintensities on verbal memory: Mediation by temporal lobe atrophy. *Neurology*, 90(8), e673e682. doi: 10.1212/WNL.000000000004983
- [37] Tam, A. K., Kapadia, A., Ilodigwe, D., Li, Z., Schweizer, T. A., & Macdonald, R. L. (2013). Impact of global cerebral atrophy on clinical outcome after subarachnoid hemorrhage. *Journal of Neurosurgery*, 119(1), 198-206. doi: 10.3171/2013.3.JNS121950
- [38] Tschirret, O., Moreno Legast, G., Mansuy, A., Mewton, N., Buisson, M., Hannoun, S., ... & Mechtouff, L. (2018). Impact of Brain Atrophy on Early Neurological Deterioration and Outcome in Severe Ischemic Stroke Treated by Intravenous Thrombolysis. *European Neurology*, 79(5-6), 240-246. doi: 10.1159/000487668
- [39] Wardlaw, J. M., Smith, C., & Dichgans, M. (2013). Mechanisms of sporadic cerebral small vessel disease: insights from neuroimaging. *The Lancet. Neurology*, 12(5), 483-497. doi: 10.1016/S1474-4422(13)70060-7
- [40] Wiegand, T. L. T., Sollmann, N., Bonke, E. M., Umeasalugo, K. E., Sobolewski, K. R., Plesnila, N., ... & Koerte, I. K.

Vol. 31, №1, Page 30-36 **35** 

(2022). Translational neuroimaging in mild traumatic brain injury. *Journal of Neuroscience Research*, *100*(5), 1201-1217. doi: 10.1002/jnr.24840

[41] Zhou, J. Y., Shi, Y. B., Xia, C., Lu, C. Q., Tang, T. Y., Lu, T., ... & Ju, S. H. (2022). Beyond collaterals: brain frailty additionally improves prediction of clinical outcome in acute ischemic stroke. *European Radiology*, 32(10), 6943-6952.

doi: 10.1007/s00330-022-08792-6

[42] Zhu, H., Lu, H., Wang, F., Liu, S., Shi, Z., Gan, J., ... & Ji, Y. (2022). Characteristics of Cortical Atrophy and White Matter Lesions Between Dementia with Lewy Bodies and Alzheimer's Disease: A Case-Control Study. Frontiers in Neurology, 12, 779344. doi: 10.3389/fneur.2021.779344

## ХАРАКТЕРИСТИКА ЦЕРЕБРАЛЬНИХ МОРФОМЕТРИЧНИХ ПАРАМЕТРІВ У ПАЦІЄНТІВ З ГОСТРИМ МОЗКОВИМ ІНСУЛЬТОМ ТА ЇХ ЗВ'ЯЗКИ ІЗ НАСЛІДКОМ ІНСУЛЬТУ НА 90-ТУ ДОБУ

Бартюк Р. С., Смолко Д. Г., Смотрицька Т. В., Марункевич Я. Ю., Старинець Н. Г., Фікс Д. О., Московко С. П. Морфометрію головного мозку широко використовують для діагностики та прогнозування переважно нейродегенеративних захворювань. У той же час, цереброваскулярним захворюванням приділялось значно менше уваги, особливо для прогнозування довготривалих наслідків інсульту. Метою нашого дослідження було дослідити залежності між змінами морфометричних показників головного мозку та наслідком інсульту на 90-ту добу. До дослідження були послідовно набрані 294 пацієнта з гострим інсультом. Усім хворим була проведена комп'ютерна томографія та/або магнітно-резонансна томографія головного мозку, а також клініко-неврологічна оцінка стану хворих. Статистичний аналіз проводили у програмі The Jamovi project (2022), Jamovi (Version 2.3) [Computer Software], Sydney, Australia з використанням параметричних і непараметричних методів оцінки отриманих результатів. Нами встановлено, що збільшені шлуночкові та кіркові морфометричні параметри асоціюються із неблагоприємним наслідком інсульту на 90-ту добу. В однофакторному аналізі підвищені індекс третього шлуночка (коефіцієнт регресії b=-2,6, p=0,014), Шлатенбрандт-Нюренбергера (коефіцієнт регресії b=0,6, p=0,007), бікаудальний індекс (коефіцієнт регресії b=-1,5, р=0,006), збільшені ширина поздовжньої церебральної щілини у передній частині лобних часток (коефіцієнт регресії b=-3,5, p=0,005), ширина мозкової щілини в ділянці склепіння черепа (коефіцієнт регресії b=-3,5, p=0,006) достовірно асоціювалися з нижчим індексом Бартел на 90-ту добу. У багатофакторному аналізі достовірні асоціації були знайдені між збільшеним індексом третього шлуночка та індексом Бартел на 90-ту добу (коефіцієнт регресії b=-2,6, p=0,045). В іншій багатофакторній моделі, збільшений бікаудальний індекс достовірно асоціювався із вищим ступенем функціональної залежності на 90-ту добу (відношення шансів=1,1, р=0,031). Отже, наші дані підтвердили, що збільшені церебральні морфометричні індекси асоціюються з несприятливим наслідком інсульту на 90-ту добу.

**Ключові слова:** захворювання нервової системи, інсульт, церебральна морфометрія, бікаудальний індекс, шлуночковий індекс.

#### Author's contribution

Bartiuk R. S. – research, data visualization, writing an original article, software.

Smolko D. G. - conceptualization, editing, resources.

Marunkevych Ya. Yu. - formal analysis and verification, methodology, writing an original article.

Starynets N. H. - methodology, review, resources.

Smotrytska T. V. – research, formal analysis and verification.

Fiks D. O. – data visualization, methodology, writing an original article.

Moskovko S. P. - conceptualization, review, editing.

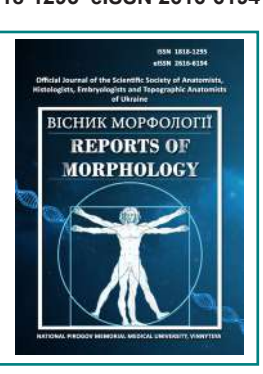
ISSN 1818-1295 eISSN 2616-6194



#### REPORTS OF MORPHOLOGY

Official Journal of the Scientific Society of Anatomists, Histologists, Embryologists and Topographic Anatomists of Ukraine

journal homepage: https://morphology-journal.com



# Distribution of M1 and M2 macrophages and their impact on survival in non-small cell lung cancer

Vynnychenko O. I.1, Moskalenko Yu. V.2, Piddubnyi A. M.3, Moskalenko R. A.2,3

<sup>1</sup>Communal non-profit enterprise of the Sumy Regional Council Sumy Regional Clinical Oncology Center, Sumy, Ukraine <sup>2</sup>Sumy State University, Sumy, Ukraine

<sup>3</sup>Ukrainian-Swedish Research Center SUMEYA, Sumy, Ukraine

#### **ARTICLE INFO**

Received: 16 April 2024 Accepted: 5 December 2024

**UDC:** 616.24-006-033.2-07-052(477.52)

#### CORRESPONDING AUTHOR

e-mail: r.moskalenko@med.sumdu.edu.ua Moskalenko R.

#### **CONFLICT OF INTEREST**

The authors have no conflicts of interest to declare.

#### **FUNDING**

This research has been performed with the financial support of grants of the external aid instrument of the European Union for the fulfillment of Ukraine's obligations in the Framework Program of the European Union for Scientific Research and Innovation "Horizon 2020" No. RN/11-2023 "The role of the DNA repair system in the pathogenesis and immunogenicity of lung cancer".

#### **DATA SHARING**

Data are available upon reasonable request to corresponding author.

Tumor-associated macrophages play an essential role in carcinogenesis and metastasis. Our study aimed to evaluate the distribution of M1 and M2 macrophages in tumor islets and stroma and establish the impact on recurrence-free survival and overall survival in patients with surgically resected non-small cell lung cancer (NSCLC). 42 surgically treated NSCLC patients were recruited from the Sumy Regional Clinical Oncology Center. The inclusion criteria were age over 18, stages IA-IIIB of NSCLC, and absence of severe cardiovascular, pulmonary, or autoimmune diseases. Antibodies against CD68+ and CD163+ were used to determine the macrophage phenotype and their distribution in tumor islets and stroma. For each sample, six fields of view with a diameter of 1 mm were analyzed, focusing on the "hot spots" in the tumor stroma and islets. The average values method determined the cut-off value for macrophages M1 and M2. The cut-off values for total macrophages M1 was 28 cells/mm², macrophages M1 in tumor islets – 18 cells/mm², macrophages M1 in the stroma – 11 cells/mm<sup>2</sup>, total macrophages M2 – 38 cells/mm<sup>2</sup>, macrophages M2 in tumor islets - 13 cells/mm<sup>2</sup>, macrophages M2 in the stroma - 24 cells/mm<sup>2</sup>. All data about the clinicopathological characteristics of patients were collected from the medical records. The long-term follow-up period continued for at least 60 months. The difference between the studied groups was assessed using the Student's t-test and the Mann-Witney test. The Cox proportional hazards model was used to assess the impact of several clinicopathological characteristics on patient survival. Most M1 and M2 macrophages accumulated in the stroma (p<0.001). The total number of M1 macrophages was higher in men than women (p=0.0082). Pro-inflammatory macrophages were more prevalent in men than women in both the tumor islets (p=0.0192) and stroma (p=0.0226). Patients with the T1a-2a category had more total M1 macrophages than those with the T2b-4 category (p=0.0486). The tumor stroma also observed this trend (p=0.0205). Current and former smokers had a significantly higher number of M1 macrophages in tumor islets (p=0.0485). In squamous cell carcinomas, the total number of M2 macrophages was higher than in adenocarcinomas (p=0.0343), especially in the tumor stroma (p=0.0006). In conclusion, high M1 macrophage infiltration of tumor islets is associated with better recurrence-free survival. A low total number of M2 macrophages and their low expression in the stroma are associated with better overall survival in surgically treated NSCLC patients. **Keywords:** M1 macrophages, M2 macrophages, lung cancer, islets, stroma, survival.

#### Introduction

According to the International Agency for Research on Cancer, in 2022, lung cancer ranked first among men and second among women in both incidence and mortality rates. Statistics indicate that one in five deaths from malignant

neoplasms worldwide is associated with lung cancer [3]. Despite significant progress in drug therapy, not all patients benefit from treatment [4, 14].

Modern understanding suggests that molecular properties

of cancer cells and the tumor microenvironment play a crucial role in carcinogenesis and metastasis. The tumor microenvironment includes tumor-associated macrophages (TAMs), fibroblasts, stromal cells, B cells, T cells, and NK cells. However, TAMs are key players in disease progression [18]. They constitute the majority of immune cells infiltrating solid tumors, sometimes accounting for up to 50 % of the tumor mass. These macrophages actively produce cytokines and enhance the metastatic potential of malignant tumors [23].

One of the most important characteristics of macrophages is their functional and phenotypic heterogeneity. Depending on the pathological context, they can polarize into two types: pro-inflammatory (M1) and anti-inflammatory (M2). M1 macrophages produce cytokines that eliminate microorganisms and exert an anti-tumor effect. In contrast, M2 macrophages promote connective tissue remodeling, suppress inflammatory responses, and stimulate tumor growth, invasion, and metastasis to lymph nodes and distant organs [24]. The polarization of M1 macrophages is driven by type 1 T-helper (Th1) cytokines, such as tumor necrosis factor (TNF) and interferon-gamma (IFN-γ). Meanwhile, type 2 T-helper (Th2) cytokines, including interleukin-13 (IL-13), interleukin-10 (IL-10), and interleukin-4 (IL-4), induce M2 macrophage polarization [20].

The role of macrophages in cancer development is ambiguous due to the dual effects of the cytokines they produce. For instance, IFN-γ has a positive effect by inhibiting neoangiogenesis and tumor cell metastasis. At the same time, its negative impact may manifest in impairing NK cell-mediated recognition and destruction of tumor cells, as well as facilitating the transmission of antiapoptotic and proliferative signals [11]. TNF, which drives M1 macrophage polarization, stimulates anti-tumor immunity by activating CD8+ T cells and NK cells. However, under certain conditions, it can sustain chronic inflammation and contribute to carcinogenesis [5].

The role of macrophages in the development of nonsmall cell lung cancer (NSCLC) remains unclear. Given that various cytokines exert dual effects, macrophages may either suppress or promote lung cancer progression and metastasis.

The aim of our study was to assess the degree of M1 and M2 macrophage infiltration in tumor clusters and stroma and to establish their relationship with recurrence-free survival (RFS) and overall survival (OS) in patients with radically treated NSCLC.

#### Material and methods

The study was approved by the Local Ethics Committee of the Sumy Regional Clinical Oncology Center (Protocol No. 20 dated December 21, 2023). All requirements of the 59th Declaration of Helsinki of the General Assembly of the World Medical Association (6th edition, revised in 2008, Seoul) and the Universal Declaration on Bioethics and Human Rights (2006) were met. All living patients at the start of the study

signed an informed consent form.

Study design. The study included 42 patients with non-small cell lung cancer (NSCLC) who were treated at the Sumy Regional Clinical Oncology Center from 2015 to 2018. Inclusion criteria were age over 18 years, stage IA-IIIB NSCLC, absence of severe cardiovascular or pulmonary pathology, absence of autoimmune diseases, and the availability of postoperative tumor tissue in the form of a paraffin block. Exclusion criteria included stage IV disease, severe comorbidities, prior neoadjuvant chemotherapy or chemoradiotherapy, and infectious postoperative complications. The lung cancer stage was determined according to the 8th edition of the TNM Classification of Malignant Tumors [15], while tumor differentiation grade and histological type were classified based on WHO recommendations for lung tumor classification [16].

Patients with stage IB-IIIB disease received platinum-based adjuvant chemotherapy. In addition to platinum agents, pemetrexed or vinorelbine was used for adenocarcinoma treatment, while docetaxel, paclitaxel, or gemcitabine was used for squamous cell carcinoma, in accordance with drugspecific guidelines. Each patient received between 2 and 4 cycles of chemotherapy. Patients in the N2 category were also prescribed external beam gamma therapy with a total focal dose of 30 Gray.

Clinical and pathological data, including age, sex, disease stage, T category, N category, ECOG (Eastern Cooperative Oncology Group) performance status, extent of surgical intervention, adjuvant chemotherapy and radiotherapy, tumor histological type, and differentiation grade, were extracted from medical records.

Follow-up period. Long-term follow-up lasted at least 60 months. During the first two years after radical treatment, CT scans of the chest and abdominal organs were performed every three months, and in the subsequent three years, every six months, according to local practice standards. After the five-year follow-up period, patients underwent annual chest X-rays. In cases of suspected disease recurrence, unplanned CT scans were performed. If there were symptoms of central nervous system metastasis, an MRI was conducted. RFS was defined as the time interval between the date of surgery and the date of documented disease progression. OS was calculated as the difference between the date of death due to disease progression or any other cause and the date of surgery. The database was closed on July 1, 2024.

Histology and immunohistochemistry. Lung cancer tissue samples were fixed in a 10 % neutral formalin solution for 24 hours before being embedded in paraffin blocks using standard techniques. For immunohistochemical (IHC) analysis of NSCLC tissues, serial 4-µm-thick sections were prepared using a rotary microtome and mounted on SuperFrost adhesive slides (Thermo Scientific, Waltham, MA, USA). The deparaffinized sections underwent antigen retrieval via heat treatment in 0.1 M citrate buffer (pH 6.0) at 95-98 °C for 30 minutes. The In Vitro visualization system (Master Diagnostica, Granada, Spain) was used for IHC

visualization. To determine macrophage phenotypes, the study employed anti-CD68 mouse monoclonal antibodies (Clone KP-1, Master-Diagnostica, Spain, ready-to-use) and anti-CD163 rabbit monoclonal antibodies (Clone EP324, Master-Diagnostica, Spain, ready-to-use). Antibody incubation was performed at room temperature for 10 minutes, followed by three washes in distilled water.

For quality control of the IHC analysis, both active control (using tissues with previously established positive and negative reactions) and passive control of obtained results were conducted. For each sample, six 1-mm-diameter fields of view, representing "hot spots" within tumor stroma and tumor nests, were analyzed. Threshold values for M1 and M2 macrophages were determined using mean values: total M1 macrophages=28 cells/mm², M1 macrophages in tumor nests=18 cells/mm², M1 macrophages in stroma=11 cells/mm², total M2 macrophages=38 cells/mm², M2 macrophages in tumor nests=13 cells/mm², M2 macrophages in stroma=24 cells/mm².

Statistical analysis. Statistical analysis was performed using Stata V.18.0 (StataCorp, Texas, USA; https://www.stata.com, 2024). The normality of data distribution was assessed using the Shapiro-Wilk test. Differences between two study groups were evaluated using the Student's t-test (for parametric variables) and the Mann-Whitney test (for nonparametric variables). A Cox proportional hazards model was used to assess the impact of multiple clinical and pathological characteristics on patient survival. Results were considered statistically significant at p<0.05.

#### Results

Characteristics of the study group. The study included 42 patients with radically treated NSCLC. The clinical characteristics of the patients and pathological characteristics of the tumors are presented in Table 1.

Immunohistochemical analysis of NSCLC tissue using CD68+ antibodies revealed an intense positive cytoplasmic reaction in macrophages of the tumor microenvironment. Macrophages were predominantly located in the stroma surrounding the tumor tissue, with some infiltrating between solid layers of squamous tumor epithelium (Fig. 1, first column, top row). In adenocarcinoma tissue, CD68-positive cells were localized among atypical tumor glands in the fibrous stroma. Some individual macrophages and clusters were identified within the tumor parenchyma, specifically within clusters of atypical glandular cells (Fig. 1, second column, top row).

To confirm the presence of M2 phenotype macrophages in NSCLC tissue, an immunohistochemical study with CD163+ antibodies was conducted. A high number of CD163-positive cells were found in the tumor microenvironment of squamous cell carcinoma (see Fig. 1, first column, bottom row). CD163-positive cells with intensely stained cytoplasm and partially stained membranes were also located among glandular complexes of adenocarcinoma (see Fig. 1, second column, bottom row).

**Table 1.** Baseline clinical and pathological characteristics of patients and tumors.

Baseline clinicopathological characteristics	Total number of patients (n, %)
Age: <60 ≥60	22 (52.4) 20 (47.6)
Sex: Female Male	8 (19.0) 34 (81.0)
Stage: IA-IIA IIB-IIIB	15 (35.7) 17 (64.3)
Category T: T1a-2a T2b-4	19 (45.2) 23 (54.8)
Category N: N0 N1-2	24 (57.1) 18 (42.9)
Histology: Adenocarcinoma Squamous cell carcinoma	20 (47.6) 22 (52.4)
Differentiation: Well or moderate Poor	26 (61.9) 16 (38.1)
Smoking history: Never smokers Current or former smokers	8 (19.0) 34 (81.0)
Performance status: 0 1	3 (7.1) 39 (92.9)
Surgery type: Lobectomy Pneumonectomy	25 (59.5) 17 (40.5)
Adjuvant chemotherapy: Yes No	36 (85.7) 6 (14.3)
Adjuvant radiation therapy: Yes No	5 (11.9) 37 (88.1)
Total macrophages M1: ≥28 cells/mm² (high) <28 cells/mm² (low)	15 (35.7) 27 (64.3)
Macrophages M1 in tumor islets: ≥18 cells/mm² (high) <18 cells/mm² (low)	16 (38.1) 26 (61.9)
Macrophages M1 in the stroma: ≥11 cells/mm² (high) <11 cells/mm² (low)	18 (42.9) 24 (57.1)
Total macrophages M2: ≥38 cells/mm² (high) <38 cells/mm² (low)	21 (50.0) 21 (50.0)
Macrophages M2 in tumor islets: ≥13 cells/mm² (high) <13 cells/mm² (low)	15 (35.7) 27 (64.3)
Macrophages M2 in the stroma: ≥24 cells/mm² (high) <24 cells/mm² (low)	21 (50.0) 21 (50.0)

Association between M1 and M2 macrophages and clinicopathological characteristics in radically treated NSCLC patients. M1 and M2 macrophages were found in both the stroma and tumor nests, but they predominantly accumulated in the stroma (p<0.001). The ratio of pro-inflammatory and anti-inflammatory macrophages in tumor nests and stroma differed significantly. M2 macrophages were more prevalent in the stroma (p<0.001), while M1 macrophages dominated in tumor nests (p<0.001).

Vol. 31, №1, Page 37-44

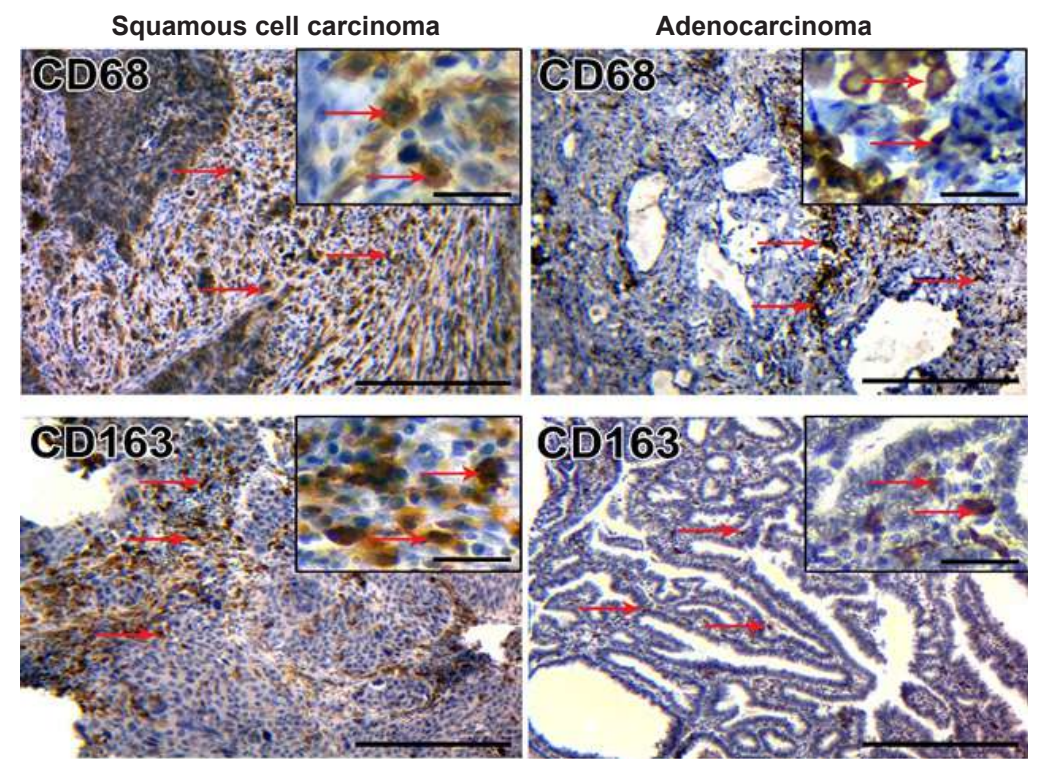


**Fig. 1.** Immunohistochemical Analysis of NSCLC Tissue (Squamous Cell Carcinoma and Adenocarcinoma) with CD68+ and CD163+Antibodies. Red arrows indicate stained macrophages. Nuclear counterstaining was performed using Mayer's hematoxylin. The magnification is specified in the bottom right corner of each image, with scale markers corresponding to 200 μm in the main microphotographs and 50 μm in the insets.

In male patients, the total number of M1 macrophages was higher than in female patients (p=0.0082; Table 2). Interestingly, the infiltration of pro-inflammatory macrophages in men was significantly higher in both tumor nests (p=0.0192) and stroma (p=0.0226; Table 3). Additionally, patients with T1a–2a tumors had a higher total number of M1 macrophages compared to patients with T2b–4 tumors (p=0.0486; see Table 2). A similar trend was observed in the tumor stroma (p=0.0205; see Table 3).

There was no significant difference in the total number of M1 macrophages between smokers and non-smokers (p=0.0586; see Table 2). However, current and former smokers had a significantly higher number of M1 macrophages in tumor nests (p=0.0485; see Table 3).

In squamous cell carcinoma, the total number of M2 macrophages was significantly higher compared to adenocarcinoma (p=0.0343; see Table 2). Moreover, M2 macrophages predominantly accumulated in the tumor stroma (p=0.0006; Table 4). No significant association was found between total M1 and M2 macrophage counts, their distribution in tumor nests and stroma, and other clinicopathological characteristics such as age, disease stage, N category, tumor differentiation grade, and ECOG performance status.

Association between M1 and M2 macrophage infiltration and survival in radically treated NSCLC patients. The mean follow-up duration was 57.9±4.2 months. At the time of data analysis, disease recurrence was recorded in 19 patients. A

**Table 2.** Association between total M1, M2 macrophage counts and clinicopathological characteristics.

Baseline clinicopathological characteristics	Macrophages M1, cells/ mm²	р	Macrophages M2, cells/ mm²	р			
Age: <60 ≥60	25 (4-73) 32 (7-76)	0.2032	40 (16-63) 36 (18-57)	0.4064			
Sex: Female Male	16 (4-47) 31 (9-76)	0.0082	38 (23-48) 38 (16-63)	0.9397			
Stage: IA-IIA IIB-IIIB	24 (7-54) 31 (4-76)	0.3182	37 (16-63) 39 (18-57)	0.5791			
Category T: T1a-2a T2b-4	35 (10-73) 23 (4-76)	0.0486	42 (16-63) 35 (18-56)	0.0761			
Category N: N0 N1-2	29 (4-76) 28 (5-58)	0.2035	40 (16-63) 34 (19-53)	0.1073			
Histology: Adenocarcinoma S q u a m o u s c e I I carcinoma	27 (4-58) 30 (9-76)	0.6231	34 (16-56) 42 (23-63)	0.0343			
Differentiation: Well or moderate Poor	29 (4-76) 28 (5-58)	0.6879	40 (16-63) 34 (19-53)	0.1487			
Smoking history: Never smokers Current or former smokers	20 (5-47) 30 (4-76)	0.0586	39 (23-56) 38 (16-63)	0.8040			
Performance status: 0 1	17 (13-25) 29 (4-76)	0.2823	48 (36-63) 37 (16-57)	0.1672			

**Table 3.** Association between clinicopathological characteristics and M1 macrophages in tumor nests and stroma.

Baseline clinicopathological Macrophages M1						
characteristics	Tumor islets	Stroma	p-value			
Age: <60 ≥60	17 (3-49) 19 (4-50)	0.4342	10 (2-28) 14 (3-29)	0.1035		
Sex: Female Male	10 (3-22) 20 (6-50)	0.0192	7 (2-25) 12 (2-29)	0.0226		
Stage: IA-IIA IIB-IIIB	15 (4-39) 20 (3-50)	0.1306	11 (2-27) 12 (2-29)	0.5364		
Category T: T1a-2a T2b-4	22 (6-49) 15 (3-50)	0.0973	15 (3-29) 9 (2-26)	0.0205		
Category N: N0 N1-2	16 (3-50) 21 (6-49)	0.1060	10 (2-27) 13 (3-29)	0.0977		
Histology: Adenocarcinoma Squamous cell carcinoma	17 (3-39) 19 (6-50)	0.6681	11 (2-29) 12 (2-28)	0.6048		
Differentiation: Well or moderate Poor	19 (4-50) 17 (3-34)	0.9071	12 (2-28) 11 (2-29)	0.9173		
Smoking history: Never smokers Current or former smokers	12 (3-26) 20 (6-50)	0.0485	8 (2-25) 12 (2-29)	0.0774		
Performance status: 0 1	11 (8-15) 19 (3-50)	0.2307	7 (4-11) 12 (2-29)	0.2815		

**Table 4.** Association between clinicopathological characteristics and M2 macrophages in tumor nests and stroma.

Baseline Macrophages M2							
clinicopathological characteristics	Tumor islets	p-value	Stroma	p-value			
Age: <60 ≥60	13 (6-26) 12 (6-31)	0.5186	25 (9-50) 23 (10-39)	0.5578			
Sex: Female Male	13 (8-26) 13 (6-31)	0.5196	23 (12-33) 24 (9-50)	0.6705			
Stage: IA-IIA IIB-IIIB	12 (6-23) 13 (6-31)	0,8328	24 (9-50) 24 (10-39)	0.8319			
Category T: T1a-2a T2b-4	15 (7-31) 11 (6-26)	0.0639	26 (9-50) 22 (10-37)	0.2652			
Category N: N0 N1-2	12 (6-26) 14 (6-31)	0.4588	23 (9-50) 25 (11-39)	0.4274			
Histology: Adenocarcinoma Squamous cell carcinoma	12 (6-31) 14 (6-24)	0.1924	20 (9-36) 28 (11-50)	0.0060			
Differentiation: Well or moderate Poor	13 (7-26) 12 (6-31)	0.2115	26 (9-50) 21 (11-37)	0.1386			
Smoking history: Never smokers Current or former smokers	13 (8-26) 13 (6-31)	0.5732	25 (12-33) 24 (9-50)	0.7700			
Performance status: 0 1	16 (11-19) 12 (6-31)	0.2388	34 (25-50) 23 (9-39)	0.0510			

total of 19 patients had died, with 18 deaths attributed to lung cancer progression, while 1 patient died due to other causes.

The Cox proportional hazards model was used to evaluate the combined effect of clinical and pathological characteristics on patient survival in NSCLC. Multivariate

**Table 5.** Multivariate Cox proportional hazards model for assessing the impact of clinicopathological characteristics on recurrence-free survival.

Baseline clinicopathological characteristics	HR	95 % CI	p-value
Age (<60 versus ≥60)	0.90	0.70-5.16	0.2030
Sex (female versus male)	0.92	0.07-11.72	0.9550
Stage (IA-IIA versus IIB-IIIB)	0.49	2.46-356.1	0.3300
Category T (Т1а–2а проти T2b–4)	6.79	1.49-30.98	0.0130
Category N (N0 проти N1-2)	6.14	1.90-19.84	0.0020
Histology (adenocarcinoma versus squamous cell carcinoma)	2.78	0.70-10.99	0.1430
Differentiation (well or moderate versus poor)	3.87	1.33-11.24	0.0130
Smoking history (never smokers versus current or former smokers)	2.98	0.32-27.34	0.3330
Performance status (0 versus 1)	0.83	0.06-11.62	0.9840
Surgery type (lobectomy versus pneumonectomy)	1.41	0.47-4.21	0.5320
Adjuvant chemotherapy (yes versus no)	2.85	0.37-26.35	0.1680
Adjuvant radiation therapy (yes versus no)	1.72	0.25-16.11	0.4300
Total macrophages M1 (high versus low)	0.33	0.04-2.65	0.3020
Macrophages M1 in tumor islets (high versus low)	1.01	0.24-4.24	0.0020
Macrophages M1 in stroma (high versus low)	1.91	0.22-16.07	0.5500
Total macrophages M2 (low versus high)	5.14	1.17-22.61	0.0300
Macrophages M2 in tumor islets (low versus high)	0.70	0.20-2.41	0.5790
Macrophages M2 in stroma (low versus high)	0.28	0.07-1.14	0.0770

**Table 6.** Multivariate Cox proportional hazards model for assessing the impact of clinicopathological characteristics on overall survival.

		,
HR	95 % CI	p-value
2.22	0.81-6.06	0.1160
0.86	0.04-17.40	0.9260
0.68	0.18-2.58	0.5770
8.85	0.01-0.62	0.0060
3.63	1.09-12.13	0.0360
2.75	0.66-11.36	0.1600
3.39	1.10-10.39	0.0320
7.51	0.47-188.4	0.1520
0.41	0.03-5.39	0.5020
1.47	0.51-4.21	0.4720
1.12	0.58-4.13	0.5620
0.65	0.22-3.89	0.3860
0.27	0.04-1.74	0.1700
0.87	0.20-3.66	0.8570
2.09	0.29-15.06	0.4630
5.56	1.08-28,57	0.0400
0.83	0.22-3.11	0.7840
0.22	0.05-0.86	0.0300
	2.22 0.86 0.68 8.85 3.63 2.75 3.39 7.51 0.41 1.47 1.12 0.65 0.27 0.87 2.09 5.56 0.83	2.22 0.81-6.06 0.86 0.04-17.40 0.68 0.18-2.58 8.85 0.01-0.62 3.63 1.09-12.13 2.75 0.66-11.36 3.39 1.10-10.39 7.51 0.47-188.4 0.41 0.03-5.39 1.47 0.51-4.21 1.12 0.58-4.13 0.65 0.22-3.89 0.27 0.04-1.74 0.87 0.20-3.66 2.09 0.29-15.06 5.56 1.08-28,57 0.83 0.22-3.11

analysis showed that T category, N category, tumor differentiation, and M1 macrophage infiltration in tumor nests significantly influenced RFS.

Patients with T1a–2a tumors, absence of regional lymph node metastases, well- or moderately differentiated

Vol. 31, №1, Page 37-44

tumors, and high M1 macrophage infiltration in tumor nests had significantly better RFS compared to those with T2b–4 tumors, poorly differentiated tumors, and low M1 macrophage infiltration in tumor nests (Table 5).

OS was affected by T category, N category, tumor differentiation grade, total M2 macrophage levels, and M2 macrophage infiltration in the stroma. Patients with T1a–2a tumors, no regional lymph node metastases, well- or moderately differentiated tumors, low total M2 macrophage levels, and low M2 macrophage infiltration in the stroma had significantly better OS compared to patients with stages IIB–IIIB, T2b–4 tumors, regional lymph node metastases, poorly differentiated tumors, high total M2 macrophage levels, and high M2 macrophage infiltration in the stroma (Table 6).

#### Discussion

The immunosuppressive microenvironment has a negative impact on lung cancer progression. Pro-tumorigenic M2 macrophages hinder immune cell infiltration and suppress the anti-tumor immune response. As a result, lung cancer therapies become less effective, leading to resistance to treatment and poor survival outcomes [26]. In this study, we assessed the infiltration levels of M1 and M2 macrophages in tumor nests and stroma and investigated their prognostic significance in PFS and OS in radically treated NSCLC patients.

Numerous studies have examined the overall expression of M1 and M2 macrophages and their correlation with survival. E. M. Garrido-Martin et al. [7] demonstrated that high M1 macrophage expression in tumor tissue is associated with intense inflammatory infiltration, leading to better treatment outcomes. Meanwhile, R. Sumitomo et al. [22] evaluated the prognostic role of M2 macrophages in relation to their localization and concluded that high expression levels in both the stroma and tumor nests are linked to poor PFS and OS in NSCLC patients.

We believe that it is more appropriate to evaluate not only the overall levels of M1 and M2 macrophage infiltration but also their specific distribution in the stroma and tumor nests. We observed that tumor-associated macrophages were predominantly concentrated in the stroma. Similar findings have been reported by other researchers studying the tumor microenvironment in NSCLC patients. Additionally, M2 macrophages were more abundant in the stroma, where they tend to accumulate in hypoxic, poorly vascularized regions [19, 29].

We found that men had significantly higher M1 macrophage infiltration in both tumor nests and stroma compared to women. This is likely due to the higher prevalence of smoking among men than women. In our study, 94 % of men and 35 % of women were smokers.

Cigarette smoke contributes to chronic inflammation by promoting infiltration of neutrophils, CD8+, CD4+, and B cells, macrophages, and natural killer (NK) cells. Smoking also induces M1-to-M2 macrophage polarization, ultimately increasing the number of M2 macrophages and fostering an

immunosuppressive environment [1].

Macrophages play a crucial role in innate immunity and affect survival in NSCLC patients. Our findings indicate that the level of M1 macrophage infiltration in tumor nests is an independent predictor of RFS – the higher the infiltration, the better the survival outcomes.

F. Dai et al. [6] reached similar conclusions. This effect is primarily attributed to the cytotoxic activity of M1 macrophages in tumor nests, which enhances cellular immune responses [17]. Furthermore, these cells increase lung cancer cell sensitivity to cisplatin, inhibit neoangiogenesis, and reduce metastatic potential [27].

Conversely, our study found that the total number of M2 macrophages and their levels in the stroma are independent predictors of poor overall survival (OS). Higher M2 macrophage levels in the tumor stroma are associated with worse survival outcomes in NSCLC patients. This negative impact is linked to the creation of an immunosuppressive environment, stimulation of angiogenesis, lymphangiogenesis, and metastasis to regional lymph nodes [9].

X. Liu et al. [13] demonstrated that SHP2 receptor expression, which plays a key role in macrophage reprogramming, was higher in M2 macrophages than in M1 macrophages, further supporting their negative effect on OS in NSCLC patients. Additionally, J. Jackute et al. [10] confirmed our findings, showing that low overall M2 macrophage levels and high M1 macrophage infiltration in tumor nests correlate with improved NSCLC survival.

Our study found that squamous cell carcinomas exhibited higher total levels of M2 macrophages, particularly in the tumor stroma. Similar findings were reported by S. Hirayama et al. [8] and S. K. Bisheshar et al. [2]. However, other studies have more frequently associated M2 macrophage infiltration with poor survival in adenocarcinoma patients.

It is believed that high M2 macrophage levels in the tumor stroma indicate adenocarcinoma aggressiveness and are a predictor of disease recurrence [12, 28]. Therefore, regardless of the histological subtype of lung cancer, a high number of M2 macrophages in the tumor stroma appears to be an unfavorable prognostic factor. Beyond their role as prognostic markers, macrophages can also serve as potential therapeutic targets for developing biomarker-based targeted therapies [25]

Current NSCLC treatment options, including chemotherapy, cause systemic toxicity, leading to vomiting, diarrhea, nausea, anemia, and other severe side effects. Moreover, prolonged chemotherapy use often results in resistance and disease progression. Targeted therapies against macrophages may represent a novel approach, with M2 macrophages being a particularly promising target.

Specifically, reprogramming M2 macrophages and shifting their polarization from M2 to M1 is one potential strategy to activate the anti-tumor immune response and improve survival outcomes in NSCLC patients [21].

#### **Conclusions**

- 1. Men have higher M1 macrophage infiltration in tumor nests and stroma than women. Smoking is associated with increased M1 macrophage levels in tumor nests.
- 2. Squamous cell carcinoma has higher total M2 macrophage levels, especially in the tumor stroma, compared

to adenocarcinoma. High M1 macrophage infiltration in tumor nests is associated with better recurrence-free survival. Low overall M2 macrophage levels and low M2 macrophage expression in the stroma correlate with improved overall survival in radically treated NSCLC patients.

#### References

- [1] Bianchi, F., Le Noci, V., Bernardo, G., Gagliano, N., Colombo, G., Sommariva, M., ... & Sfondrini, L. (2024). Cigarette smoke sustains immunosuppressive microenvironment inducing M2 macrophage polarization and viability in lung cancer settings. *PloS one*, 19(5), e0303875. doi: 10.1371/journal.pone.0303875
- [2] Bisheshar, S. K., van der Kamp, M. F., de Ruiter, E. J., Ruiter, L. N., van der Vegt, B., Breimer, G. E., & Willems, S. M. (2022). The prognostic role of tumor associated macrophages in squamous cell carcinoma of the head and neck: A systematic review and meta-analysis. *Oral Oncology*, 135, 106227. doi: 10.1016/j.oraloncology.2022.106227
- [3] Bray, F., Laversanne, M., Sung, H., Ferlay, J., Siegel, R. L., Soerjomataram, I., & Jemal, A. (2024). Global cancer statistics 2022: GLOBOCAN estimates of incidence and mortality worldwide for 36 cancers in 185 countries. CA: a Cancer Journal for Clinicians, 74(3), 229-263. doi: 10.3322/ caac.21834
- [4] Chaft, J. E., Rimner, A., Weder, W., Azzoli, C. G., Kris, M. G., & Cascone, T. (2021). Evolution of systemic therapy for stages I-III non-metastatic non-small-cell lung cancer. *Nature Reviews. Clinical Oncology*, 18(9), 547-557. doi: 10.1038/s41571-021-00501-4
- [5] Cruceriu, D., Baldasici, O., Balacescu, O., & Berindan-Neagoe, I. (2020). The dual role of tumor necrosis factor-alpha (TNF-α) in breast cancer: molecular insights and therapeutic approaches. *Cellular Oncology*, 43(1), 1-18. doi: 10.1007/s13402-019-00489-1
- [6] Dai, F., Liu, L., Che, G., Yu, N., Pu, Q., Zhang, S., ... & You, Z. (2010). The number and microlocalization of tumor-associated immune cells are associated with patient's survival time in non-small cell lung cancer. *BMC Cancer*, 10, 220. doi: 10.1186/1471-2407-10-220
- [7] Garrido-Martin, E. M., Mellows, T. W. P., Clarke, J., Ganesan, A. P., Wood, O., Cazaly, A., ... & Sanchez-Elsner, T. (2020). M1<sup>hot</sup> tumor-associated macrophages boost tissue-resident memory T cells infiltration and survival in human lung cancer. *Journal for Immunotherapy of Cancer*, 8(2), e000778. doi: 10.1136/jitc-2020-000778
- [8] Hirayama, S., Ishii, G., Nagai, K., Ono, S., Kojima, M., Yamauchi, C., ... & Ochiai, A. (2012). Prognostic impact of CD204-positive macrophages in lung squamous cell carcinoma: possible contribution of Cd204-positive macrophages to the tumor-promoting microenvironment. *Journal of Thoracic Oncology: Official Publication of the International Association for the Study of Lung Cancer*, 7(12), 1790-1797. doi: 10.1097/JTO.0b013e3182745968
- [9] Hwang, I., Kim, J. W., Ylaya, K., Chung, E. J., Kitano, H., Perry, C., ... & Hewitt, S. M. (2020). Tumor-associated macrophage, angiogenesis and lymphangiogenesis markers predict prognosis of non-small cell lung cancer patients. *Journal of Translational Medicine*, 18(1), 443. doi: 10.1186/ s12967-020-02618-z

- [10] Jackute, J., Zemaitis, M., Pranys, D., Sitkauskiene, B., Miliauskas, S., Vaitkiene, S., & Sakalauskas, R. (2018). Distribution of M1 and M2 macrophages in tumor islets and stroma in relation to prognosis of non-small cell lung cancer. *BMC Immunology*, 19(1), 3. doi: 10.1186/s12865-018-0241-4
- [11] Jorgovanovic, D., Song, M., Wang, L., & Zhang, Y. (2020). Roles of IFN-γ in tumor progression and regression: a review. *Biomarker Research*, 8, 49. doi: 10.1186/s40364-020-00228-x
- [12] Kaseda, K., Ishii, G., Aokage, K., Takahashi, A., Kuwata, T., Hishida, T., ... & Ochiai, A. (2013). Identification of intravascular tumor microenvironment features predicting the recurrence of pathological stage I lung adenocarcinoma. *Cancer Science*, 104(9), 1262-1269. doi: 10.1111/cas.12219
- [13] Liu, X., Zhang, Z., Yuan, J., Yu, J., & Chen, D. (2024). Spatial interaction and functional status of CD68\*SHP2\* macrophages in tumor microenvironment correlate with overall survival of NSCLC. Frontiers in Immunology, 15, 1396719. doi: 10.3389/fimmu.2024.1396719
- [14] Lu, S., Wu, L., Jian, H., Chen, Y., Wang, Q., Fang, J., ... & Zhang, C. (2022). Sintilimab plus bevacizumab biosimilar IBI305 and chemotherapy for patients with EGFR-mutated non-squamous non-small-cell lung cancer who progressed on EGFR tyrosine-kinase inhibitor therapy (ORIENT-31): first interim results from a randomised, double-blind, multicentre, phase 3 trial. *The Lancet. Oncology*, 23(9), 1167-1179. doi: 10.1016/S1470-2045(22)00382-5
- [15] Matilla, J. M., Zabaleta, M., Martínez-Téllez, E., Abal, J., Rodríguez-Fuster, A., & Hernández-Hernández, J. (2020). New TNM staging in lung cancer (8th edition) and future perspectives. *Journal of Clinical and Translational Research*, 6(4), 145-154.
- [16] Nicholson, A. G., Tsao, M. S., Beasley, M. B., Borczuk, A. C., Brambilla, E., Cooper, W. A., ... & Travis, W. D. (2022). The 2021 WHO Classification of Lung Tumors: Impact of Advances Since 2015. *Journal of Thoracic Oncology: official publication of the International Association for the Study of Lung Cancer*, 17(3), 362-387. doi: 10.1016/j. jtho.2021.11.003
- [17] Ohri, C. M., Shikotra, A., Green, R. H., Waller, D. A., & Bradding, P. (2009). Macrophages within NSCLC tumour islets are predominantly of a cytotoxic M1 phenotype associated with extended survival. *The European Respiratory Journal*, 33(1), 118-126. doi: 10.1183/09031936.00065708
- [18] Qiao, Y., & Fu, E. (2022). Advances in the Study of Tumorassociated Macrophages in Lung Cancer. Zhongguo Fei Ai Za Zhi, 25(1), 34-39. doi: 10.3779/j.issn.1009-3419.2021.102.49
- [19] Rakaee, M., Busund, L. R., Jamaly, S., Paulsen, E. E., Richardsen, E., Andersen, S., ... & Kilvaer, T. K. (2019). Prognostic Value of Macrophage Phenotypes in Resectable Non-Small Cell Lung Cancer Assessed by Multiplex Immu-

Vol. 31, №1, Page 37-44

- nohistochemistry. *Neoplasia*, *21*(3), 282-293. doi: 10.1016/j. neo.2019.01.005
- [20] Rhee, I. (2016). Diverse macrophages polarization in tumor microenvironment. Archives of Pharmacal Research, 39(11), 1588-1596. doi: 10.1007/s12272-016-0820-y
- [21] Sedighzadeh, S. S., Khoshbin, A. P., Razi, S., Keshavarz-Fathi, M., & Rezaei, N. (2021). A narrative review of tumor-associated macrophages in lung cancer: regulation of macrophage polarization and therapeutic implications. *Translational Lung Cancer Research*, 10(4), 1889-1916. doi: 10.21037/tlcr-20-1241 (29)
- [22] Sumitomo, R., Hirai, T., Fujita, M., Murakami, H., Otake, Y., & Huang, C. L. (2019). M2 tumor-associated macrophages promote tumor progression in non-small-cell lung cancer. *Experimental and Therapeutic Medicine*, 18(6), 4490-4498. doi: 10.3892/etm.2019.8068
- [23] Vitale, I., Manic, G., Coussens, L. M., Kroemer, G., & Galluzzi, L. (2019). Macrophages and Metabolism in the Tumor Microenvironment. *Cell Metabolism*, 30(1), 36-50. doi: 10.1016/j.cmet.2019.06.001
- [24] Yi, B., Cheng, Y., Chang, R., Zhou, W., Tang, H., Gao, Y., & Zhang, C. (2023). Prognostic significance of tumor-associated macrophages polarization markers in lung cancer: a pooled analysis of 5105 patients. *Bioscience reports*, 43(2),

- BSR20221659. doi: 10.1042/BSR20221659
- [25] Yin, W., Zhao, Y., Kang, X., Zhao, P., Fu, X., Mo, X., Wang, Y., & Huang, Y. (2020). BBB-penetrating codelivery liposomes treat brain metastasis of non-small cell lung cancer with EGFR<sup>T790M</sup> mutation. *Theranostics*, 10(14), 6122-6135. doi: 10.7150/thno.42234
- [26] Yu, Z., Zou, J., & Xu, F. (2024). Tumor-associated macrophages affect the treatment of lung cancer. *Heliyon*, 10(7), e29332. doi: 10.1016/j.heliyon.2024.e29332
- [27] Yuan, A., Hsiao, Y. J., Chen, H. Y., Chen, H. W., Ho, C. C., Chen, Y. Y., ... & Yang, P. C. (2015). Opposite Effects of M1 and M2 Macrophage Subtypes on Lung Cancer Progression. *Scientific Reports*, 5, 14273. doi: 10.1038/srep14273
- [28] Zhang, B., Yao, G., Zhang, Y., Gao, J., Yang, B., Rao, Z., & Gao, J. (2011). M2-polarized tumor-associated macrophages are associated with poor prognoses resulting from accelerated lymphangiogenesis in lung adenocarcinoma. *Clinics*, 66(11), 1879-1886. doi: 10.1590/s1807-59322011001100006
- [29] Zheng, X., Weigert, A., Reu, S., Guenther, S., Mansouri, S., Bassaly, B., ... & Savai, R. (2020). Spatial Density and Distribution of Tumor-Associated Macrophages Predict Survival in Non-Small Cell Lung Carcinoma. *Cancer Research*, 80(20), 4414-4425. doi: 10.1158/0008-5472.CAN-20-0069

#### РОЗПОДІЛ МАКРОФАГІВ М1 ТА М2 ТА ЇХ ВПЛИВ НА ВИЖИВАНІСТЬ У ХВОРИХ НА НЕДРІБНОКЛІТИННИЙ РАК ЛЕГЕНЬ

Винниченко О. І., Москаленко Ю. В., Піддубний А. М., Москаленко Р. А.

Асоційовані з пухлиною макрофаги відіграють важливу роль у канцерогенезі та метастазуванні. Наше дослідження мало на меті оцінити розподіл макрофагів M1 і M2 в острівцях і стромі пухлини та встановити вплив на безрецидивну виживаність і загальну виживаність у пацієнтів з хірургічно видаленим недрібноклітинним раком легені (НДКРЛ). Із Сумського обласного клінічного онкологічного центру для участі у дослідженні було залучено 42 хірургічно пролікованих пацієнтів, хворих на НДКРЛ. Критеріями включення були вік старше 18 років, стадії ІА-ІІІВ НДКРЛ та відсутність тяжких серцево-судинних, легеневих або аутоімунних захворювань. Антитіла проти CD68+ і CD163+ використовували для визначення фенотипу макрофагів і їх розподілу в острівцях і стромі пухлини. Для кожного зразка аналізували по 6 полів зору діаметром 1 мм, які мали вигляд «гарячих точок» в пухлинній стромі та пухлинних острівцях. Методом середніх значень визначено порогове значення для макрофагів М1 і М2. Граничні значення загальної кількості макрофагів M1 становили 28 клітин/мм², макрофагів M1 в острівцях пухлини — 18 клітин/мм², макрофагів M1 в стромі — 11 клітин/мм², загальної кількості макрофагів M2 — 38 клітин/мм², макрофагів M2 в пухлинних острівцях — 13 клітин/мм², макрофагів М2 у стромі – 24 клітини/мм². Усі дані про клініко-патологічні характеристики пацієнтів збирали з медичної документації. Довгостроковий період спостереження тривав щонайменше 60 місяців. Різницю між досліджуваними групами оцінювали за допомогою t-критерію Стьюдента та критерію Манна-Вітні. Модель пропорційних ризиків Кокса була використана для оцінки впливу кількох клініко-патологічних характеристик на виживання пацієнтів. Встановлено, що найбільше макрофагів M1 і M2 накопичувалося в стромі (p<0,001). Загальна кількість макрофагів M1 була вищою у чоловіків, ніж у жінок (р=0,0082). Прозапальні макрофаги були більш поширені у чоловіків, ніж у жінок, як в острівцях пухлини (р=0,0192), так і в стромі (р=0,0226). Пацієнти з категорією Т1а–2а мали більше загальних макрофагів М1, ніж пацієнти з категорією Т2b–4 (р=0,0486). У стромі пухлини також спостерігалася дана тенденція (р=0,0205). Нинішні та колишні курці мали значно більшу кількість макрофагів М1 в острівцях пухлини (р=0,0485). У плоскоклітинних карциномах загальна кількість макрофагів М2 була вищою, ніж в аденокарциномах (p=0,0343), особливо в стромі пухлини (p=0,0006). Отже, висока інфільтрація пухлинних острівців макрофагами М1 пов'язана з кращою безрецидивною виживаністю. Низька загальна кількість макрофагів М2 та їх низька експресія в стромі пов'язані з кращим загальним виживанням у хірургічно пролікованих пацієнтів із НДКРЛ.

Ключові слова: М1 макрофаги, М2 макрофаги, рак легені, острівці, строма, виживання.

#### Author's contribution

Vynnychenko O. I. - conceptualization, research, methodology and original project writing.

Moskalenko Yu. V. - data visualization, software.

Piddubnyi A. M. - validation.

Moskalenko R. A. – review writing and editing, formal analysis, project administration, supervision.

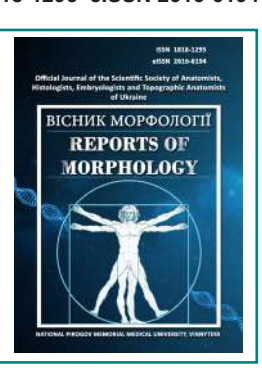
ISSN 1818-1295 eISSN 2616-6194



#### REPORTS OF MORPHOLOGY

Official Journal of the Scientific Society of Anatomists, Histologists, Embryologists and Topographic Anatomists of Ukraine

journal homepage: https://morphology-journal.com



## Morphometric indices of thickness of artificial vagina created from colon

Yakubov M. Z.

Samarkand State Medical University, Samarkand, Uzbekistan

**ARTICLE INFO** 

Received: 19 March 2024 Accepted: 10 December 2024

UDC: 618.215-089.844:612.014.2

#### **CORRESPONDING AUTHOR**

e-mail: yakubovmunis@gmail.com Yakubov M. Z.

#### **CONFLICT OF INTEREST**

The authors have no conflicts of interest to declare.

#### **FUNDING**

Not applicable.

#### **DATA SHARING**

Data are available upon reasonable request to corresponding author.

According to the World Health Organization, congenital defects of female genital organs are more common in families and countries with limited resources. About 94 % of severe developmental disorders occur in low- and middle-income countries, where women often face malnutrition and limited access to quality health care. The aim of the study was to determine the morphometric parameters of the thickness of an artificial vagina created from the colon. Patients who were hospitalized and treated in gynecology for malformations of the genital organs in the period from 2019 to 2023 were considered. For a retrospective analysis, 202 patients (including 36 controls) who were treated for vaginal anomalies and malformations of the genital organs were analyzed: 146 of them underwent histological examination, and 56 - cytological (aged 18 to 40 years). Statistical analysis of the results was performed using the Microsoft Office Excel-2010 software package. When studying morphometric parameters, an increase in the area, volume and surface of goblet cells was established within 1-3 years, which indicates that their activity is at a high level. However, after 4-10 years, the cell parameters sharply decreased, which indicates a weakening of the adaptation process and tissue degradation. In addition, we studied the condition and density of the glands in 1 mm<sup>2</sup> of the mucous membrane in different periods of observation. Thus, over 1-3 years of observation, an increase in the density by 0.91 times, the height by 0.89 times and the diameter of the glands by 0.92 times was noted compared to the control, which indicates the activity of the adaptation process. After 1-3 years of observation, an increase in the density and diameter of the glands by 0.70 times, and the height by 0.68 times compared to the control was noted. These indicators indicate hypertrophy and hyperplasia of the glands. After 4-10 years a significant decrease in all indicators with subsequent degradation and functional disorders was detected. The density of the glands decreased by 1.14 times, the height by 1.49 times and the diameter of the glands by 1.31 times compared to the control, which is a sign of long-term chronic changes and a decrease in the adaptation process leading to atrophic changes in the mucous membrane of the neovagina.

Keywords: neovagina, mucous membrane, epithelium, histology.

#### Introduction

Congenital malformations of female reproductive organs account for 4 % to 14 % of all birth defects. Among them, the most socially significant anomaly is aplasia of the vagina and uterus, occurring in approximately 1 in every 4,500-5,000 newborn girls [8, 15, 16]. Congenital vaginal atresia is a very rare congenital anomaly of the reproductive tract. The main symptoms are abdominal pain, amenorrhea, and breast lumps. MRI examinations reveal an enlarged uterine cavity. After surgery, vaginal restenosis and inflammation occur in 15.9 % (with obstruction) and 40 % (with other types of aplasia) [9]. According to recent studies, patients with

Mayer-Rokitansky-Küster-Hauser syndrome (MRKHS) may develop leiomyoma, adenomyosis, or ovarian edema from the remnants of the uterus and ovaries, which may cause difficulties in differential diagnosis [10]. Uterine leiomyoma is common in medical practice, but is rarely found within syndromes. One case is described in which a 50-year-old woman with MRKHS syndrome was operated on for the presence of leiomyoma [17].

In very rare cases, leiomyoma or adenomyosis may develop in residual Müllerian tissue or rudimentary uterus. MRI reveals leiomyomas arising from residual Müllerian tissue and chronic ovarian dysfunction [8, 12, 13]. A unique case is described in which one patient simultaneously developed two rare pathologies: bilateral ovarian cysts with Sertoli cells and MRKHS [21]. These methods require long periods of dilation and stenting to prevent closure of the canal. Studies have shown that the use of isolated bowel segments gives excellent results, eliminates unnecessary and frequent dilation and provides aesthetic lubrication [2].

Modern surgical techniques for creating an artificial vagina, such as the Vecchetti, Abbe-McIndow, and Davydov methods, are among the most widely used and recognized worldwide. Vaginal vaginoplasty is a well-established procedure that utilizes a thick or thin segment of the vagina. This technique is often used in vaginal agenesis, male-to-female sex reassignment surgery, phallic skin loss, and for revision after unsuccessful primary reconstruction. The use of a pedicled colon segment for vaginal reconstruction after serious complications of the first operation is described [7].

The creation of an artificial vagina is an important achievement in the field of plastic gynecology, providing women with optimal conditions for the natural outflow of menstrual blood after surgery to create a neovagina. The sigmoid colon is usually used as the main material for creating a neovagina, but sometimes other parts of the colon can be used [5].

Earlier studies show that reactive-compensatory processes in the mucous membranes of the urinary tract, especially in the epithelium, develop in accordance with the known classical stages [17]. The traditional process of reactive adaptation is divided into three key stages. The first stage, known as "emergency mobilization," involves the activation of morphofunctional reserves and a response to abrupt changes in external conditions. This is followed by a "plateau" phase, during which the system stabilizes at a new functional level. Long-term exposure to extreme factors can lead to decompensation, followed by an "exacerbation" phase, characterized by disturbances in structural and functional [3]. Such adaptive processes affect all levels of structural organization, monitoring and histology, including subcellular, cellular, tissue and structural-functional units [19].

Despite the creation of neovagina using many types of surgical methods, the morphological changes in it have not been fully studied. For further improvement in this direction, it is necessary to obtain more accurate morphological data by evaluating serial biopsies in the same patients at different times of the postoperative period. It is necessary to regularly monitor the condition of the neovagina after surgery by cytological and histological examination, which allows preventing the prolapse of the neovagina that is often observed in them. Also, to study the condition of the neovagina created from the sigmoid colon by assessing the structural changes during its transformation from a single-layer epithelium to a multilayer epithelium, which makes it possible to predict successful adaptation of the neovagina in patients.

Based on the analysis of the literature, it can be noted that although the structure of the artificial vagina

created from the intestine has been studied clinically, the morphological changes that occur after a certain time and their characteristics have not been deeply studied, which makes this problem of primary importance.

Purpose of the study – to determine the morphometric parameters of the thickness of the artificial vagina created from the colon.

#### Materials and methods

The study material consisted of 202 patients with complications of an artificial vagina, prepared for a dynamic morphometric study of the sigmoid colon tissue used for the plastic surgery of an artificial vagina. The Bioethics Committee of the Ministry of Health of the Republic of Uzbekistan (protocol No. 5/23-1904, 21.06.2024) established that the research does not contradict the basic bioethical standards of the Helsinki Declaration, the Council of Europe Convention on Human Rights and Biomedicine (1977), relevant WHO regulations and the laws of the Republic of Uzbekistan.

A sample of vaginal mucosa was taken to study cytomorphological changes. A comparative analysis of the cytological examination results was conducted. The study was conducted using the classical cytological method in patients 1-10 years after surgery. Using a special tool (brush), a smear was taken from the neovaginal mucosa and applied to a dry bottle, dried in the air, fixed and stained. Staining was done manually using a fixative and Leukodif-200 paint. The smears were processed and stained using the Romanovsky-Giemsa and Pappenheim methods.

For histological examination in order to identify the process of mucus formation, more precisely, the formation of mucopolysaccharides in the goblet cells of the mucous membrane and glands of the submucosal layer, a histochemical study was conducted using mucopolysaccharide staining according to the Schiff reaction. To identify glycolic or aminohydroxyl groups that form dialdehyde in vaginal tissue, a reaction was carried out - PAS (staining with Schiff reagent). For this, paraffin histological sections were washed with water and left in a prepared mixed solution of 0.1 % alcohol and 3 % acetic acid for 5-10 minutes. Then the sections were washed with distilled water and diluted with 0.5 % iodic acid solution for oxidation for 2-5 minutes. Then they were treated with Schiff reagent for 10-15 minutes. After that, they were washed in running water and stained with hematoxylin. Afterwards they were washed again in water, dehydrated in alcohol and xylene and sealed with balsam. As a result, mucoproteins, acidic mucopolysaccharides were stained from blue to light blue, neutral mucopolysaccharides from pink to red, and nuclei were stained blue. The results were assessed semi-quantitatively (in points). Histological and histomorphometric analyses were carried out when studying the micropreparations.

Cytomorphometric and histomorphometric analyses were performed using a scanner on a NanoZoomer microscope (REF

C13140-21.S/N000198/hamamatsu Photonics/431-3196 Japan) using the NDP.VIEV2.0.,QuPath.0.4.0.url program.

Statistical analysis of the results was performed using the Microsoft Office Excel-2010 software package on a personal computer, the statistical analysis package, and Student's t-testing methods (t) were used.

#### Results

According to morphometric changes, over a period of 1 to 3 years, in the mucous membranevagina, plasticized tissue taken from the sigmoid colon, as a result of changing its topical location, morphological adaptation occurs: development of atrophy, hypertrophy, hyperplasia, an increase in the size of secretory cells, which are active cells of the mucous membrane. In the subsequent period (from 3 to 10 years), it was found that a chronic hyperfunctional state causes a change in size and shape due to cell metaplasia. It was found that secretory vacuoles of goblet cells, subjected to the greatest morphofunctional stress, in the period from 1 to 3 years appear as large dark basophils, and in the period from 3 to 10 years these indicators decrease, the size of secretory vacuoles and cellular inclusions decrease, and the number of cells detected in morphometric studies increases. As a result of the hyperfunctionality of the mucous membrane during the first year, it is characterized by an increase in the height of the epithelium of the parenchymatous glands and the mesenchymal cells that make up the nipples.

When analyzing the morphometric parameters of the layers of the artificial vagina wall, it was found that the thickness of the mucous membrane over a period of up to 1 year of observation reached 416.2±21.1  $\mu m$  (p≤0.01), which is 0.87 times more than in the control group (366.3±43.2  $\mu m$ ), in the period up to 3 years – 467.2±11.2  $\mu m$  (0.78 times more) and 10 years of observation it was 301.2±13.1  $\mu m$  and it was noted that during this period it decreased unreliably (1.25 times less) compared to the control group (Table 1, Fig. 1, 2).

**Table 1.**Morphometric indices of the thickness of the artificial vagina ( $M\pm m$ ,  $\mu m$ ).

	Groups							
	control	Up to 1 year	Up to 3 years	10 years				
Mucous membrane	366.3±43.2	416.2±21.1*	467.2±11.2*	301.2±13.1*				
Submucosa	38.41±1.16	44.69±1.89*	63.57±2.21	41.57±1.73*				
Muscular membrane, mm	1869±259	1751±154**	2201±201**	1917±104**				
Serosa/adventitia	122.2±29.1	134.1±11.1*	153.0±21.1*	141.1±24.2*				

**Note:** \* – compared with the control group  $p \le 0.05$  and  $p \le 0.01$ ; \*\* – duration of the postoperative period  $p \le 0.1$ .

The thickness of the submucosa of the neovagina in the control group averaged  $38.41\pm1.16~\mu m$  and significantly increased to  $44.69\pm1.89~\mu m$  (p≤0.01) by 0.85 times over the 1-year observation period. Over the period of up to 3 years in the observation group, these indicators reached  $63.57\pm2.21~\mu m$  (an increase of 0.60 times), and over the 10-year or more observation period  $-41.57\pm1.73~\mu m$ , which is an insignificant decrease of 0.92 times compared to the control

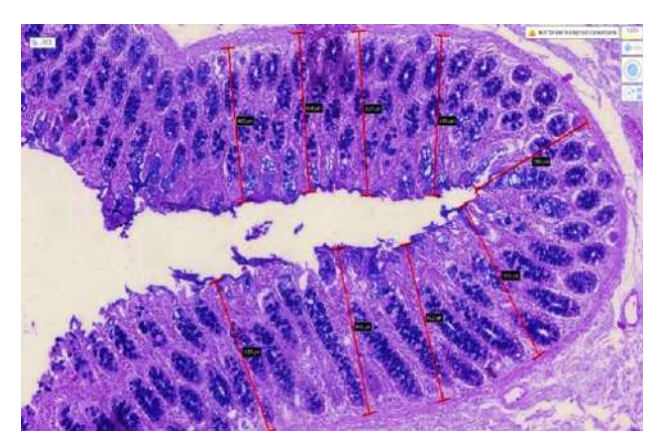


**Fig. 1.** Morphogram of the thickness of the mucous membrane of the artificial vagina. 1st year of observation. Red lines indicate areas of mucosal thickness measurement for morphometric study. PAS stain. ×40.

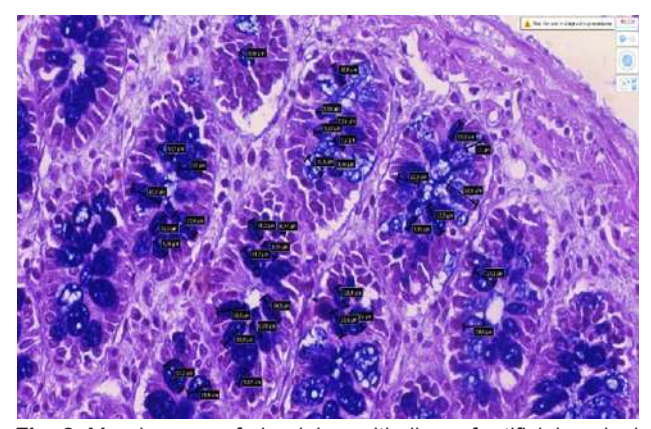


**Fig. 2.** Morphogram of glandular epithelium of artificial vaginal mucosa. 1st year of observation. The areas selected for measuring the planar parameters of goblet cells are highlighted in black. PAS stain. ×400.

group and 1.52 times compared to the 3-year observation group (see Table 1).

When analyzing the morphometric parameters of the area, volume and surface of goblet cells, it was found that the cell area after 1 year in the observation group was 21.81  $\mu m^2$  and increased by 0.86 times compared to the control group (18.92  $\mu m^2$ ). In the period from 1 to 3 years (Fig. 3, 4), this indicator increased to 23.90  $\mu m^2$  (0.79 times more), and in the period from 4 to 10 years it was 13.33  $\mu m^2$  and reliably showed a decrease of 1.42 times.

The volume of goblet cells in the control group was 6751  $\mu$ m³. It was noted that over 1 year of the observation group existence, this indicator increased to 10360  $\mu$ m³ (p≤0.1), (0.65 times), and over 1-3 years – to 13652  $\mu$ m³ (p≤0.1) (0.49 times). Over 4-10 years of observation in the groups, the volume of goblet cells showed a reliable decrease compared to the control group, similar to their area, and decreased by 2.01 times, amounting to 2353  $\mu$ m³ (p≥0.1).

Morphometric indices of the goblet cell surface were  $357.2 \,\mu\text{m}^2$  in the control group, showing a significant increase to  $475.2 \,\mu\text{m}^2$  (p≤0.05) (0.75 times more) after 1 year in the

Vol. 31, №1, Page 45-51

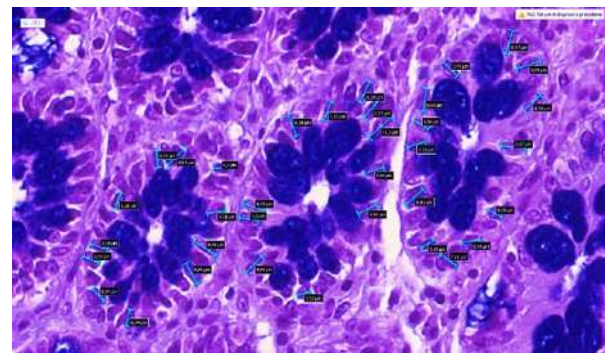


**Fig. 3.** Morphogram of the neovaginal mucosa with measured nuclei.3rd year of observation. Blue lines highlight areas selected for measuring planar parameters of goblet cells. PAS stain. ×400.

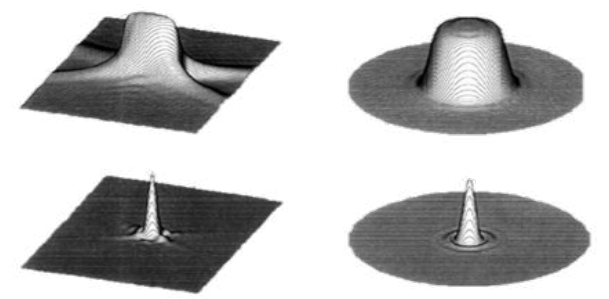


**Fig. 4.** The confocal view is formed using the examples shown in this image to create a three-dimensional spatial pattern in the artificial vaginal mucosa tissue.

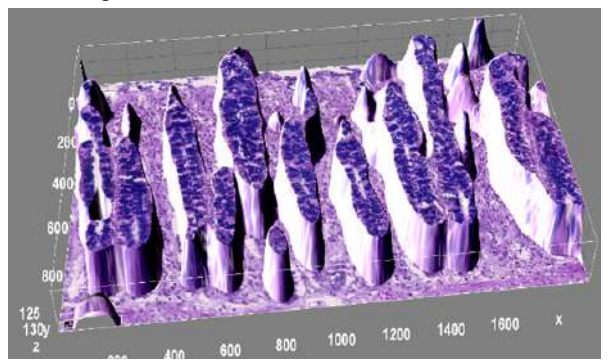


**Fig. 5.** Artificial vaginal mucosa. 1-3 year of observation. Threedimensional confocal morphometric morphogram showing the size of glands in neovaginal tissue. NanoZoomer (JAPAN) is equipped with a scanner.

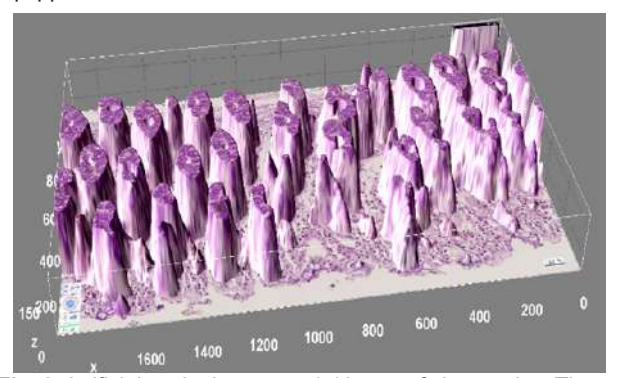


**Fig. 6.** Artificial vaginal mucosa. 4-10 year of observation. Threedimensional confocal morphometric morphogram showing the size of glands in neovaginal tissue. Nano Zoomer (JAPAN) is equipped with a scanner.

observation group and to 571.2  $\mu m^2$  (p≤0.05) (0.62 times more) after 1-3 years of observation. However, during the 4-10 years of observation, these indices were significantly reduced to 176.9  $\mu m^2$  (less than 2.01 times). This is due to the destruction of goblet cells, emptying of the cytoplasm, atrophy and functional insufficiency as a result of hyperfunction and hypersecretion in the early stages of our observation.

In addition, we measured the neovaginal mucosa and the density of glands in 1 mm² of epithelium, as well as morphometric indices of their height and diameter. According to the morphometric indices, the density of glands relative to 1 mm² of the mucous membrane in the control group averaged 5.511±1.545 %. It was found that in the group after 1 year of observation, this index averaged 6.018±1.544 % compared to the control group, which was 0.91 times higher, and significantly increased by 0.70 times in the 1-3 year group (7.816±1.614 %). In the observation group for the period of 4-10 years, the density sharply decreased (by 1.14 times) and averaged 4.815±1.232 % (Fig. 5, 6).

The height of the glands in the mucous membrane of the neovagina after 1 year of observation was 204.7 $\pm$ 19.7 µm (p≤0.05), having increased by 0.89 times, and after 1-3 years the highest value was 266.1 $\pm$ 25.6 µm (p≤0.05), having increased by 0.68 times. After 4-10 years, a significant decrease to 122.8 $\pm$ 19.7 µm (p≤0.01) is observed, which is 1.49 times less than the control value.

The diameter of the glands in the mucous membrane of the neovagina slightly increased in diameter after 1 year of observation (77.98±1.13 µm, p≤0.05) compared to the control group (71.85±1.17 µm), which is 0.92 times more. After 1-3 years of our observation, the maximum value of the diameter of this indicator was recorded - 101.4±1.4 µm (p≤0.05), compared to the control group (increased by 0.70 times). After 4-10 years the glands in the mucous membranes of the neovagina decreased in diameter, averaging 54.58±0.77 µm (p≤0.01), and significantly decreased by 1.31 times.

#### Discussion

Thus, the conducted studies revealed significant structural and functional changes affecting the structural and functional units, the level of cellular differentiation and their synthetic activity. However, these changes occur unevenly at different levels. Regardless of the severity of the reactive changes, they all follow a three-phase process that ultimately leads to accommodation of the intestinal epithelial tissues.

The condition and density of the Lieberkühn glands in 1 mm² of the mucous membrane in different periods of observation. Up to the 1st year of observation, there was an increase in the density by 0.91 times, the height by 0.89 times and the diameter of the glands by 0.92 times compared to the control. This indicates the activity of the adaptation process. After 1-3 years of observation, there was an increase in the density and diameter of the glands by 0.70 times, and the height by 0.68 times compared to the control. These indicators indicated hypertrophy and hyperplasia of the glands. After 4-10 years a significant

decrease in all indicators with subsequent degradation and functional disorders was detected. The density of the glands decreased by 1.14 times, the height by 1.49 times and the diameter of the glands by 1.31 times compared to the control. This is a sign of long-term chronic changes and a decrease in the adaptation process leading to atrophic changes in the mucous membrane of the neovagina.

Vaginal agenesis is a congenital pathological condition in which there is complete underdevelopment of the vagina. It is most often observed in the context of MRKHS. This condition is associated with a developmental defect of the Müllerian duct, which occurs in approximately every 1/4,000 to 10,000 births [11, 27]. Such patients are often encountered in adolescence with complaints of amenorrhea. About 15 % of patients admitted to a gynecological clinic with complaints of amenorrhea have SMPH [14, 20].

To date, many operative and non-operative methods of vaginal construction have been described. A non-operative method (Frank technique) used for rudimentary vagina is serial vaginal dilation. These methods require prolonged dilation and stenting to prevent closure of the canal. The use of isolated bowel segments has been shown to provide excellent results, bypassing the need for regular dilation and providing natural lubrication [11, 21].

Two studies describing the epithelium of neovagina created using the Vecchietti technique evaluated only cytological data. The first study was performed during the first and second months after surgery and showed the presence of inflammatory and parakeratotic cells. The other study, performed 2-12 years after surgery, demonstrated that the mucosa of neovagina obtained using the Vecchietti technique was comparable to the mucosa of a normal vagina [8, 11, 23]. A number of researchers have analyzed biopsies examined using light, scanning, and transmission electron microscopy and have shown slight ultrastructural changes in comparison with normal vaginal mucosal materials from patients operated on using the Vecchietti method [11, 22]. In scanning electron microscopy studies, neovaginal epithelium from three patients with MRKHS who underwent skin grafting using gluteal skin autografts after creation of a vesicorectal pouch showed that the transplanted skin retained keratinized cell maturation and exhibited structures typically found in normal skin despite the different environment and pH [6, 18].

In 1904, Baldwin performed vaginoplasty using a segment of the iliac bone. Baldwin's work was forgotten for a long time due to the high rate of complications, but in 1955, Zangl and in 1961, Pratt demonstrated the use of a pedicled sigmoid colon [17, 24].

#### References

[1] Alimbaeva, G. N. (2018). Нарушение полового развития у подростков: трудности диагностики (клинический случай) [Disorders of sexual development in adolescents: difficulties in diagnosis (clinical case)]. Репродуктивное здоровье детей и подростков = Reproductive Health of Children and Adolescents, 14(4), 67-71. doi: 10.24411/1816-2134-2018-14007

There are no official statistics on this problem in Uzbekistan, but there is an increase in the number of citizens' requests for help with this pathology [1].

Distraction of colonic tissue may result in diversion colitis, a sometimes clinically challenging entity. In sigmoid vaginoplasty, a segment of bowel is diverted from the fecal stream but is not completely defunctionalized, as the operated subjects are able to engage in neovaginal penetrative intercourse. Mild diversion colitis of the sigmoid neovagina has been reported [4, 21, 27].

Possible explanatory factors can be identified in the differences in tissue architecture, vascularization, and innervation of the neovagina compared to the normal vagina. The natal vaginal walls are composed of the SPE and underlying lamina propria of connective tissue, a smooth muscle layer, and the adventitia, which is dense connective tissue that fuses with the surrounding fascia. The lamina propria and underlying connective tissue layers contain a rich blood vessel supply [11, 25, 26].

Similarly, neovagina, created from intestinal segments, is a mucus-secreting epithelium that retains its characteristics for many years [18, 28, 29]. In a series of 15 patients with stratified squamous epithelium who underwent peritoneal neovagina creation, Mhatre performed biopsy in 4 cases and LM analysis. He described, similar to our results, complete re-epithelialization after 6 months of glycogensecreting stratified squamous epithelium. However, given the histochemical approach adopted to identify progenitor cells, the authors concluded that re-epithelialization was the result of indeterminate metaplasia of the sigmoid mucosa rather than colonization by the vaginal introitus epithelium [5].

#### **Conclusions**

- 1. During the period from 1 to 3 years of observation, an increase in the density, height and diameter of the Lieberkühn glands was noted. This indicates the activity of the adaptation process. After 4-10 years a significant decrease in all indicators was detected with subsequent degradation and functional disorders, which is a sign of long-term chronic changes and a decrease in the adaptation process.
- 2. During the first 3 years, the morphometric parameters of the area, volume and surface of the goblet cells of the artificially created vagina from the sigmoid colon increase, indicating that their activity is at a high level. But after 4-10 years, the cell parameters dropped sharply, indicating a weakening of the process of adaptation and tissue degradation.
- [2] Amadou Magagi, I., Adamou, H., Oumarou Garba, S., Halidou, M., Adakal, O., Habou, O., ... & Sani, R. (2020). Sigmoid vaginoplasty in Mayer-Rokitansky-Kuster-Hauser syndrome. *Gynecological Surgery*, 17, 1-6. doi: 10.1186/ s10397-020-01079-y
- [3] Amaratunga, T., Kirkpatrick, I., Yan, Y., & Karlicki, F. (2017). Ectopic pelvic fibroid in a woman with uterine agen-

Vol. 31, №1, Page 45-51

- esis and Mayer-Rokitansky-Küster-Hauser syndrome. *Ultrasound Quarterly*, 33(3), 237-241. doi: 10.1097/RUQ.000000000000284
- [4] Batyrova, Z. K., Uvarova, E. V., Kumykova, Z. Kh., Kruglyak, D. A., Bolshakova, A. S., Sadelov, I. O., ... & Trofimov, D. Yu. (2022). Современные молекулярно-генетические представления о синдроме Майера-Рокитанского-Кюстера-Хаузера [Modern molecular genetic concepts of Mayer-Rokitansky-Küster-Hauser syndrome]. Репродуктивное здоровье детей и подростков = Reproductive Health of Children and Adolescents, 18(2), 25-30. doi: 10.33029/1816-2134-2022-18-2-25-30
- [5] Georgas, K., Belgrano, V., Andreasson, M., Elander, A., & Selvaggi, G. (2018). Bowel vaginoplasty: a systematic review. *Journal of Plastic Surgery and Hand Surgery*, 52(5), 265-273. doi: 10.1080/2000656X.2018.1482220
- [6] Juusela, A. L., Naghi, I., & Thani, S. (2018). Mayer-Rokitansky-Küster-Hauser syndrome with bilateral ovarian Sertoli cell tumors: review of the literature and report of a rare case. *Urogynecology*, 24(5), e32-e34. doi: 10.1097/SPV.00000000000000483
- [7] Khanna, T., & Saran, S. (2021). A 19-Year-Old Female with Primary Amenorrhea: Mayer-Rokitansky-Küster-Hauser Syndrome. *Journal of Medical Ultrasound*, 29(4), 305-306. doi: 10.4103/JMU.JMU\_172\_20
- [8] Kruglyak, D. A., Buralkina, N. A., Ipatova, M. V., & Uvarova, E. V. (2018). Синдром Майера-Рокитанского-Кюстера-Хаузера: современные методики лечения, психологические и социальные аспекты (аналитический обзор) [Mayer-Rokitansky-Küster-Hauser syndrome: modern treatment methods, psychological and social aspects (analytical review)]. Репродуктивное здоровье детей и подростков = Reproductive Health of Children and Adolescents, 14(3), 58-73. doi: 10.24411/1816-2134-2018-13005
- [9] Lee, R., Choi, J. E., Mun, E., Kim, K. H., Choi, S. A., & Kim, H. S. (2024). A case of chromosome 17q12 deletion syndrome with type 2 Mayer-Rokitansky-Küster-Hauser syndrome and maturity-onset diabetes of the young type 5. Children, 11(4), 404. doi: 10.3390/children11040404
- [10] Mahajan, N. N., Tilve, A., Shinde, G., Jnanananda, B., Saifi, S., Srivastava, V., ... & Pophalkar, M. (2023). Minimally invasive vaginal approach to the uterovestibular anastomosis for cervicovaginal aplasia: a case series and review of literature. Archives of Gynecology and Obstetrics, 308(1), 25-34. doi: 10.1007/s00404-022-06708-9
- [11] Матаtkulova, М. D., & Negmadzhanov, В. В. (2022). Оперативное лечение пролапсом неовлагалища после сигмоидального кольпопоэза [Surgical treatment of neovaginal prolapse after sigmoid colpopoiesis]. Проблемы современной науки и образования = Problems of Modern Science and Education, 2(171, 48-52.
- [12] Medvediev, M., Spesyvtsev, D., & Pokrovenko D. (2021). A case of neovagina surgical creation using the uterine cervix remnant in a patient with Mayer-Rokitansky-Küster-Hauser syndrome. Fertility and Sterility, 116(5), 1420-1422. doi: 10.1016/j.fertnstert.2021.06.030
- [13] Mei, L., Zhang, H., Chen, Y., & Niu, X. (2021). Clinical features of congenital complete vaginal atresia combined with cervical aplasia: A retrospective study of 19 patients and literature review. *Congenital Anomalies*, 61(4), 127-132. doi: 10.1111/cga.12417
- [14] Mekhtieva, E. R., Yashchuk, A. G., Musin, I. I., Popova, E. M., Imelbaeva, A. G., & Tyurina, A. A. (2023). Оперативное

- лечение опущения неовлагалища у пациентки с синдромом Майера-Рокитанского-Кюстера-Хаузера (клинический случай) [Surgical treatment of neovaginal prolapse in a patient with Mayer-Rokitansky-Küster-Hauser syndrome (clinical case)]. Практическая медицина = *Practical medicine*, *21*(1), 96-98. doi: 10.32000/2072-1757-2023-1-95-97
- [15] Mikos, T., Gordts, S., & Grimbizis, G. F. (2020). Current knowledge about the management of congenital cervical malformations: a literature review. *Fertility and sterility*, 113(4), 723-732. doi: 10.1016/j.fertnstert.2020.02.006
- [16] Miyake, A., Kobayashi, Y., Imaeda, K., Yoshihama, T., Na-kamura, K., Yokota, M., ... & Aoki, D. (2023). Case Series of Mayer-Rokitansky-Küster-Hauser Syndrome: Analysis of 17 Cases. Clinical and Experimental Obstetrics & Gynecology, 50(1), 1. doi: 10.31083/j.ceog5001001
- [17] Nagaraja, M. R., Gubbala, S. P., Delphine Silvia, C. W., & Amanchy, R. (2019). Molecular diagnostics of disorders of sexual development: an Indian survey and systems biology perspective. Systems Biology in Reproductive Medicine, 65(2), 105-120. doi: 10.1080/19396368.2018.1549619
- [18] Negmadzhanov, B. B., & Mamatkulova, M. D. (2023). Синдром Рокитанского-Кюстера у подростков и тактика его ведения [Rokitansky-Küster syndrome in adolescents and its management tactics]. *International Journal of Education, Social Science & Humanities*, 11(2), 338-342. doi: 10.5281/zenodo.7636204
- [19] Negmadzhanov, B., Davronova, L., Rabbimova, G., Rafikov, S., & Asrorova, Kh. (2021). Диагностика аплазии влагалища от простого к сложному [Diagnosis of vaginal aplasia from simple to complex]. Журнал вестник врача = Journal of the Doctor's Bulletin, 1(2), 167-171. doi: 10.38095/2181-466X-2021992-166-170
- [20] Pandelis, Ts., Vasileos, K., & Efimios, D. (2019). Обследование, тактика ведения и лечение врожденных аномалий влагалища в пубертатном периоде [Examination, tactics of management and treatment of congenital anomalies of the vagina during puberty]. Репродуктивное здоровье детей и подростков = Reproductive Health of Children and Adolescents, 15(2), 25-35. doi: 10.24411/1816-2134-2019-12002
- [21] Triantafyllidi, V. E., Mavrogianni, D., Kalampalikis, A., Litos, M., Roidi, S., & Michala, L. (2022). Identification of genetic causes in Mayer-Rokitansky-Küster-Hauser (MRKH) syndrome: a systematic review of the literature. *Children*, 9(7), 961. doi: 10.3390/children9070961
- [22] Wang, Y. Y., Duan, H., Zhang, X. N., & Wang, S. (2021). Neovagina creation: a novel improved laparoscopic Vecchietti procedure in patients with Mayer-Rokitansky-Küster-Hauster syndrome. *Journal of Minimally Invasive Gynecology*, 28(1), 82-92. doi: 10.1016/j.jmig.2020.04.006
- [23] Yang, X., Liang, J., Li, W., Chen, B., Sun, X., & Xie, Z. (2021). Modified Vecchietti vaginoplasty using self-made single-port laparoscopy in Mayer-Rokitansky-Küster-Hauser syndrome. Fertility and Sterility, 116(1), 266-268. doi: 10.1016/j.fertnstert.2020.10.001
- [24] Yang, X., Zhu, L., Wang, Y. J., Tong, B., Zhong, S., Yang, C., ... & Xie, Z. (2022). Comparison of the modified laparoscopic Vecchietti and Davydov colpoplasty techniques in Mayer-Rokitansky-Küster-Hauser syndrome: A long-term follow-up analysis. *Journal of Obstetrics and Gynaecology Research*, 48(7), 1930-1937. doi: 10.1111/jog.15262
- [25] Yavas Abalı, Z., & Guran, T. (2024). Diagnosis and man-

- agement of non-CAH 46, XX disorders/differences in sex development. *Frontiers in Endocrinology*, *15*, 1354759. doi: 10.3389/fendo.2024.1354759
- [26] Zak, P. W., Chow, I., Zhu, X., Sell Jr, H. W., Rusilko, P. J., & Stofman, G. M. (2021). The use of a Hartmann's pouch for bowel vaginoplasty: a case report. *Plastic and Recon*structive Surgery – Global Open, 9(4), e3546. doi: 10.1097/ GOX.00000000000003546
- [27] Zhang, X., Ding, Y., Hua, K., Liu, S., & Jia, N. (2019). Combined laparoscopic and vaginal cervicovaginal reconstruction using acellular porcine small intestinal submucosa graft in a patient with Mayer-Rokitansky-Küster-Hauser syndrome (U5aC4V4). Journal of Minimally Invasive Gy-
- necology, 26(3), 396-397. doi: 10.1016/j.jmig.2018.06.001 [28] Zhang, X., Qiu, J., Ding, Y., Sun, L., & Hua, K. (2020). Single port laparoscopy combined with vaginal cervicovaginal reconstruction in a patient with congenital atresia of the
- reconstruction in a patient with congenital atresia of the cervix. *Fertility and Sterility*, *113*(3), 681-682. doi: 10.1016/j. fertnstert.2019.11.011
- [29] Zhou, Q., Zhang, X., Li, Y., Hua, K., & Ding, J. (2023). Comparison of Sheares vaginoplasty, vaginoplasty using acellular porcine small intestinal submucosa graft and laparoscopic peritoneal vaginoplasty in patients with Mayer-Rokitansky-Küster-Hauser syndrome. *International urogynecology journal*, 34(2), 499-505. doi: 10.1007/s00192-022-05163-z

### МОРФОМЕТРИЧНІ ПОКАЗНИКИ ТОВЩИНИ ШТУЧНОЇ ПІХВИ, УТВОРЕНОЇ З ТОВСТОЇ КИШКИ Якубов $\mathit{M. 3.}$

За даними Всесвітньої організації охорони здоров'я уроджені дефекти жіночих статевих органів найчастіше зустрічаються у сім'ях та країнах з обмеженими ресурсами. Близько 94 % тяжких порушень розвитку зустрічаються у країнах з низьким та середнім рівнем доходу, де жінки часто мають недостатнє харчування та обмежений доступ до якісної медичної допомоги. Мета дослідження – визначити морфометричні показники товщини штучної піхви, створеної із товстої кишки. До дослідження відібрані пацієнти, які були госпіталізовані та проходили лікування у гінекологічному відділенні з приводу вад розвитку статевих органів у період з 2019 по 2023 рік. Для ретроспективного аналізу було проаналізовано 202 пацієнтки (36 жінок становили контрольну групу), котрі проходили лікування щодо аномалій піхви та вад розвитку статевих органів; 146 випадків підлягали гістологічному дослідженню, а 56 – цитологічному (жінки віком від 18 до 40 років). Статистичний аналіз результатів проводили з використанням пакета програм Microsoft Office Ехсеl-2010. При вивченні морфометричних показників встановлено збільшення площі, обсягу та поверхні бокалоподібних клітин протягом 1-3 років, що свідчить про те, що їхня активність знаходиться на високому рівні. Але через 4-10 років параметри клітин різко знизилися, що свідчить про послаблення процесу адаптації та деградації тканин. Крім того, ми вивчили стан та щільність розташування залоз в 1 мм² слизової оболонки у різні періоди спостереження. Так, протягом 1-3 років спостереження відзначалося збільшення щільності в 0,91 рази, висоти в 0,89 рази та діаметра залоз у 0,92 рази порівняно з контролем, що свідчить про активність процесу адаптації. Після 1-3 років спостереження відзначалося збільшення щільності та діаметра залоз у 0,70 рази, а висоти у 0,68 рази порівняно з контролем. Дані показники свідчать про гіпертрофію та гіперплазію залоз. Через 4-10 років спостерігалося значне зниження всіх показників із подальшою деградацією та функціональними порушеннями. Щільність розташування залоз зменшилася в 1,14 рази, висота в 1,49 рази, діаметр залоз в 1,31 рази порівняно з контролем, що є ознакою тривалих хронічних змін та зниження процесу адаптації, що призводить до атрофічних змін слизової оболонки неовагіни.

Ключові слова: неовагіна, слизова оболонка, епітелій, гістологія.

Vol. 31, №1, Page 45-51 **51** 

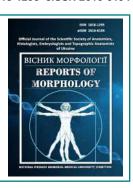
ISSN 1818-1295 eISSN 2616-6194



#### REPORTS OF MORPHOLOGY

Official Journal of the Scientific Society of Anatomists, Histologists, Embryologists and Topographic Anatomists of Ukraine

journal homepage: https://morphology-journal.com



# Studies of changes in rat hepatocytes under conditions of central blockade of luteinizing hormone synthesis with the additional quercetin

Polyviana O. A., Stetsuk E. V., Shepitko V. I., Vilkhova O. V., Boruta N. V., Rud M. V., Pelypenko L. B., Lysachenko O. D., Voloshyna O. V., Dvornyk I. L., Morokhovets H. Yu.

Poltava State Medical University, Poltava, Ukraine

#### **ARTICLE INFO**

Received: 12 March 2024 Accepted: 19 December 2024

**UDC:** 611.36-018.1-06:[615.357:577. 175.6+615.322/.356]-092.9

#### **CORRESPONDING AUTHOR**

e-mail: stetsuk78@gmail.com Stetsuk Ye. V.

#### **CONFLICT OF INTEREST**

The authors have no conflicts of interest to declare.

#### **FUNDING**

Not applicable.

#### **DATA SHARING**

Data are available upon reasonable request to corresponding author.

The nucleus, exchanging information with the cytoplasm of the hepatocyte, controls and coordinates all cell activity: division, growth, intermediate metabolism, protein synthesis and its differentiation. During the cell life cycle the nucleus remains in interphase. The large variation in the size of hepatocyte nuclei is explained by the fact that during postnatal growth, some hepatocytes undergo cytogenetic transformations characterized by gradual polyploidy. Polyploidy, or amplification of the entire genome, refers to cells/organisms containing more than 2 main chromosome sets. The aim of this study is to determine the morphogenesis and dynamics of variability of subtypes of rat hepatocytes, binucleate and with two nucleoli, under conditions of central blockade of luteinizing hormone synthesis with long-term action of triptorelin, with the addition of quercetin to the animal diet. The experiment was conducted on 60 sexually mature white male rats weighing 140-160 g. The animals were divided into 3 groups: group 1 – control, saline solution was administered (10 animals); group 2 was subcutaneously administered triptorelin embonate solution at a dose of 0.3 mg of active ingredient per kg of body weight for 12 months (25 animals); group 3 was administered triptorelin solution at a rate of 0.3 mg of active ingredient per kg of body weight with the addition of quercetin in terms of animal body weight three times a week (25 animals). The animals were removed from the experiment after 1, 3, 6, 9 and 12 months by an overdose of ether anesthesia. A comprehensive study of histological preparations of the liver and quantitative counting of hepatocytes with two nucleoli and binucleate were performed using a light microscope with a digital microfilter and software adapted for these studies. Statistical processing of the study results was performed using Microsoft Office Excel software and the Real Statistics 2019 extension. Pathological processes that occur in liver tissue during experimental oxidative-nitrosative stress caused by the administration of triptorelin lead to both quantitative and qualitative changes. Thus, the number of hepatocytes with two nucleoli significantly increased in group 2 and at the 12th month of observation was 5.291±1.156 cells per field of view at p<0.05. The number of binucleated hepatocytes also tended to change with maxima at the 12th month of observation. Thus, in group 2 at the 9th month, the number of binucleated hepatocytes was 7.012±0.527 cells per field of view at p<0.05, and with the addition of quercetin only 5.311±1.561 cells per field of view at p<0.05. An increased number of mitoses was detected in group 2 at the 6th month of observation, in group 3 it was determined only at the 9th. The study showed that the administration of triptorelin causes oxidative-nitrosative stress, which leads to pathological changes in hepatocytes in the form of quantitative changes in cells with two nucleoli and binucleate cells. Additional administration of quercetin reduces the negative effect on liver hepatocytes, which is confirmed by the indicators in the experimental groups of animals.

**Keywords:** *liver, hepatocyte, binucleated hepatocytes, mitosis, testosterone, luteinising hormone, quercetin, tryptorelin.* 

#### Introduction

According to WHO, the incidence of prostate cancer has been increasing worldwide in recent years. Prostate cancer is the most common cancer in men aged 55 years and older. In Western and Eastern Europe, this disease ranks third among oncological pathologies, and in the Americas it already ranks first [16, 28]. In terms of incidence, prostate cancer is in fourth place in Ukraine. Approximately 6.5 thousand new cases are registered each year. Insufficient testosterone can aggravate liver damage, cause obesity, or even lead to hepatosis [20, 22, 24].

Chronic liver diseases are also quite common in clinical practice. As of 2019, approximately 1.69 billion people worldwide suffered from liver diseases. The liver is crucial for the metabolism of many substances, including sex hormones and lipids [26]. Disturbances in sex hormone, glucose, and lipid metabolism are common complications of chronic liver disease and are high-risk factors for endocrine insufficiency. To date, attention to risk factors for endocrine insufficiency has focused on diabetes mellitus, cardiovascular disease, neurological disease, and psychological factors. Several studies have assessed the prevalence and risk factors for endocrine insufficiency in patients with liver disease [1, 19, 291. The information collected from different literature sources varies to some extent and is often not comparable, due to the different etiology of liver disease, sample size, survey methodologies, and assessment tools used in each study.

Testosterone is known to be a key hormone in the pathology of metabolic diseases such as obesity. Low testosterone levels are associated with increased fat mass (especially central obesity) and decreased lean mass in men. These morphological features are associated with metabolic dysfunction, as testosterone deficiency leads to energy imbalance, impaired glucose control, decreased insulin sensitivity, and dyslipidemia [6, 21]. Androgenic effects on enzymatic pathways of fatty acid metabolism are evident and often tissue-specific, with distinct effects observed in regional adipose tissue, muscle, and liver [11, 15]. Testosterone replacement therapy has been shown to have beneficial effects on obesity indices, partly due to direct metabolic effects on adipose tissue and muscle, and potentially by increasing motivation, vigor, and energy, allowing obese individuals to lead more active lifestyles. The extent of these beneficial changes may depend on the treatment modality. with long-term use often providing greater efficacy.

Quercetin is a common naturally occurring flavonoid, a pigment found in many fruits, vegetables, and seeds. It helps to avoid the development of cardiovascular diseases [8, 33], reduces the risk of oncological pathology and degenerative processes in the brain. This substance has antioxidant properties, protecting the body from free radicals, binding and neutralizing unstable molecules [18, 32, 34]. Triptorelin, a synthetic analogue of the neurohormone gonadotropin-releasing hormone, which suppresses the expression of the receptor in the pituitary gland, but does not change the functioning of the pituitary-testicular complex as a whole.

Central deprivation of luteinizing hormone synthesis leads to the development of oxidative stress [34] in the connective tissue of the testicles of rats, quercetin was used as a pharmacological agent to correct the pathological effect on the interstitial endocrinocytes of the testicles. The question of the effect on liver tissue of long-term inhibition of testosterone synthesis by triptorelin is insufficiently studied.

Therefore, the study of morphological changes in hepatocytes under conditions of central blockade of luteinizing hormone synthesis with the addition of quercetin can help increase the effectiveness of treatment of chronic liver diseases and improve the prognosis for patients.

The aim of this study is to determine the distribution, morphogenesis and dynamics of variability of hepatocyte subtypes, namely binucleolus and binuclear under conditions of central blockade of luteinizing hormone synthesis with long-term action of triptorelin with the addition of quercetin to the animal diet.

#### Materials and methods

The experiment was conducted on 60 sexually mature white male rats weighing 140-160 g. The material for the study was liver tissue. The animals were divided into 3 groups. Group 1 was the control group, which was administered saline (10 animals). Group 2 was subcutaneously administered diphereline (triptorelin embonate) [4] at a dose of 0.3 mg of the active substance per kg of body weight with drug activity for 365 days (25 animals). Group 3 was administered a triptorelin solution at the rate of 0.3 mg of the active substance per kg of body weight with the addition of quercetin to the diet using a gastric tube, calculated on the body weight of the animals three times a week (25 animals). The animals were withdrawn from the experiment after 1, 3, 6, 9 and 12 months by overdose of ether anesthesia. The animals were kept in standard conditions of the vivarium of the Poltava State Medical University. The study is a fragment of the scientific project "Experimental and morphological study of the influence of diphereline, cryopreserved placenta transplants on the morphofunctional state of a number of internal organs", state registration No. 0124U003358.

The Bioethics Committee of Poltava State Medical University (protocol No. 234 dated 01.23.2025) established that all research and euthanasia of experimental animals were carried out in accordance with the provisions of the "European Convention for the Protection of Vertebrate Animals Used for Experimental and Other Scientific Purposes" (Strasbourg, 1986), as well as with the "General Ethical Principles of Animal Experiments" adopted by the First National Congress on Bioethics (Kyiv, 2001).

Small fragments of the liver were fixed according to the generally accepted method and placed in paraffin blocks, from which 4 µm thick sections were made and stained with hematoxylin and eosin [3]. In the complex study of histological preparations, a light microscope BIOREX-3#5605 was used. By visual assessment, using digital microfilters and software adapted for this study, hepatocytes were counted in the

Vol. 31, №1, Page 52-58

field of view. Photography was performed using a digital microphotographic attachment DCM 900 with appropriate software.

As a result of the morphometric study, the actual diameters of hepatocyte nuclei were established. The area of cells and their nuclei (S) was calculated by the formula:  $S=(D_1/2\times D_2\times /2)\times \pi \text{ where } \pi \text{ is a constant value equal to } 3.14; D_1 \text{ is the larger diameter of the cell/nucleus; } D_2 \text{ is the smaller diameter of the cell/nucleus.}$ 

Statistical processing of the study results was carried out using Microsoft Office Excel software and the Real Statistics 2019 extension to it. To determine the statistical significance of differences between groups, the non-parametric Mann-Whitney test was used. The difference was considered statistically significant at p<0.05.

#### Results

When we studied the structural organization of the liver of the control and experimental groups of animals using histological preparations stained with hematoxylin-eosin, the following was established. The liver is an organ with a predominance of the parenchymal component over the stromal one, which are clearly separated from each other with the formation of structural components, namely hepatic lobules. The parenchyma consisted of hepatocytes and non-

hepatocyte cells (endotheliocytes, Ito cells, Kupffer cells, lymphocytes, neutrophils and other cells (Fig. 1). Our study of hepatocytes themselves established that in the intact liver of white rats they are the dominant cells, significantly outnumbering other cellular elements in quantitative terms (see Fig. 1). All cells had clear contours, a polygonal shape, and their average dimensions were: transverse 18.22 $\pm$ 0.91 µm, longitudinal 22.06 $\pm$ 2.33 µm. The average area of hepatocytes was 407.5 $\pm$ 23.9 µm².

The variability of cells was clearly traced from the central vein to the periphery of the hepatic lobule. When we studied the cytoplasm of hepatocytes, we found a change in the reaction with different dyes, in some cases moderate granularity, which, in our opinion, is associated with the functional state of each individual group of cells (Fig. 2). The perinuclear space contained aggregations of basophilic material, which correspond to the localization of the granular endoplasmic reticulum and stand out well against the background of the relatively palely stained cytoplasm. The nuclei had a regular rounded, somewhat less often elliptical shape, were located in the center of the cells and contained from one to two nucleoli.

Most hepatocytes had one nucleus, the relative number of such cells was 77.33 %. Accordingly, 22.67 % of hepatocytes contained two nuclei. We did not detect a greater number of nuclei in hepatocytes in either the control or experimental

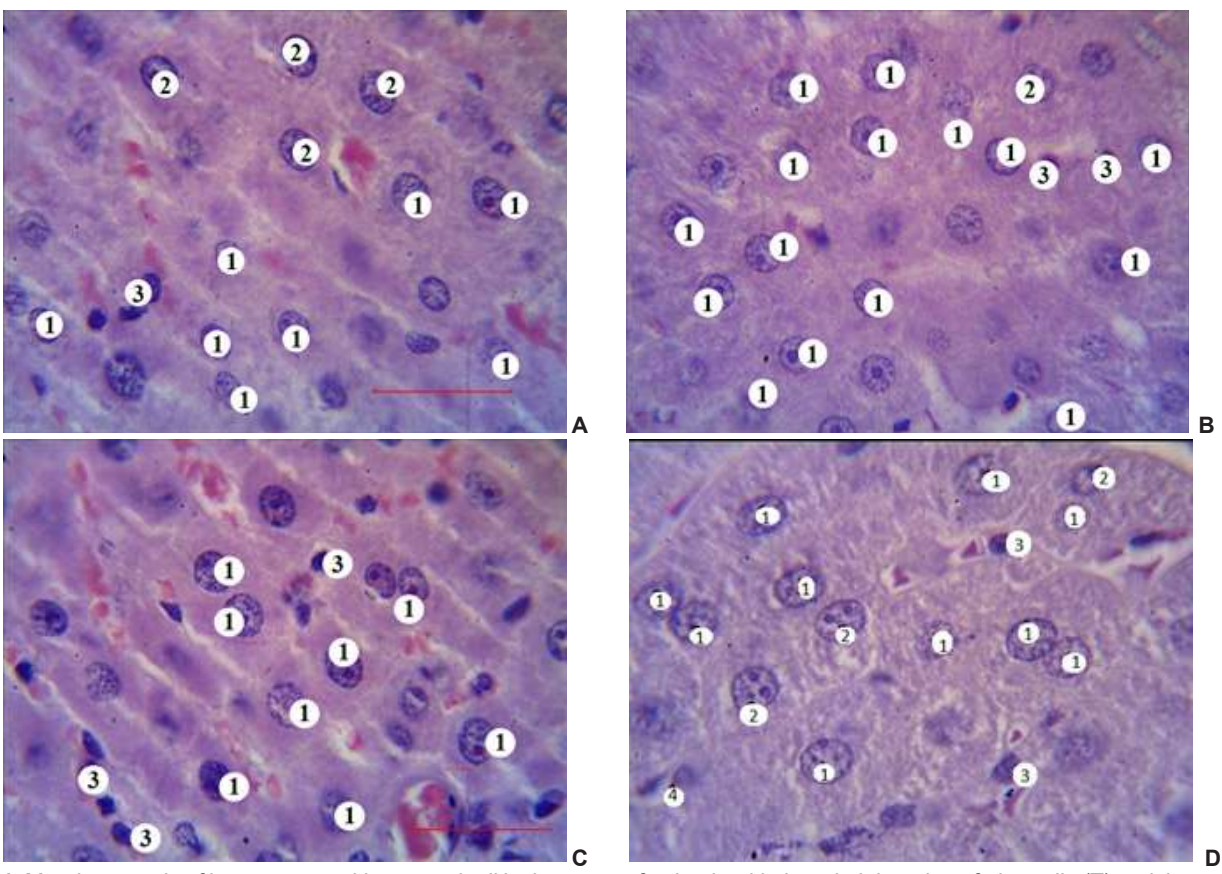


**Fig. 1.** Morphogenesis of hepatocytes with two nucleoli in the group of animals with the administration of triptorelin (T) and the group of animals that were administered quercetin (T+Q) against the background of triptorelin administration at different times of the study. A, C – group with the administration of triptorelin (3rd and 9th months). B, D – group with the administration of quercetin against the background of triptorelin (3rd and 9th months). 1 – mononuclear hepatocytes, 2 – binuclear hepatocytes, 3 – liver macrophages, 4 – Ito cell. Hematoxylin-eosin staining. Lens×40. Eyepiece×15.

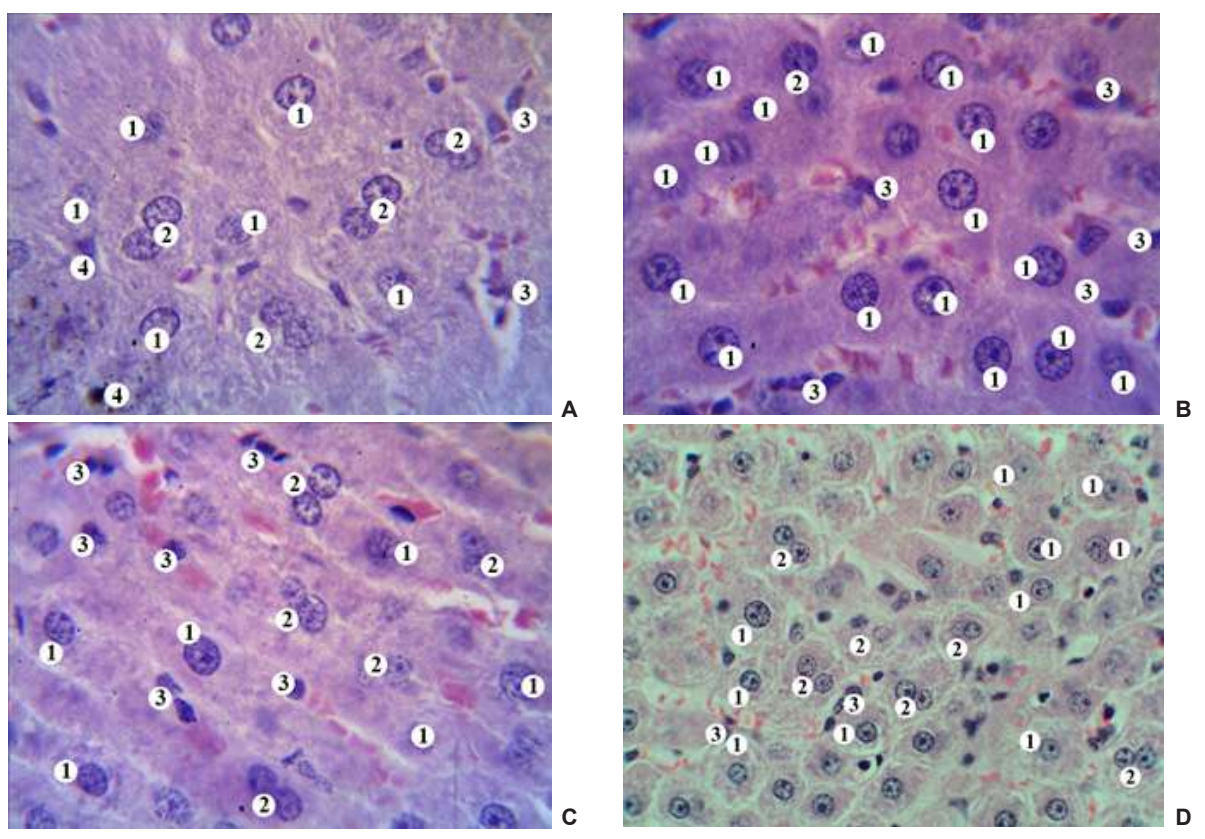


**Fig. 2.** Morphogenesis of binuclear hepatocytes in the group of animals with the administration of triptorelin (T) and the group of animals that were administered quercetin (T+Q) against the background of triptorelin administration at different study periods. A, C – group with the administration of triptorelin (6th and 12th months). B, D – group with the administration of quercetin against the background of triptorelin (6th and 12th months). 1 – mononuclear hepatocytes, 2 – binuclear hepatocytes, 3 – liver macrophages, 4 – Ito cell. Hematoxylin-eosin staining. Lens×40. Eyepiece×15.

groups of animals.

With experimental oxidative-nitrosative stress caused by the administration of triptorelin, quantitative and qualitative changes occur in hepatocytes. The first statistically significant signs are detected from the 3rd month of observation in both experimental groups. Thus, the number of hepatocytes with two nucleoli significantly increased in the group using triptorelin and at the 3rd month was 4.782±1.042, and in the group with the addition of quercetin 3.661±0.798, respectively, at p<0.05 in the field of view. The tendency to increase the number of cells with an increased number of nucleoli (two) persists and at the 12th month of observation was 5.701±1.243 at p<0.05 in the field of view, which is 3.35 times more than in the control group. And in the group with the addition of quercetin, this indicator was statistically significantly higher compared to the control at p<0.05, but less than in the group without quercetin and amounted to 5.291±0.156 cells in the field of view.

In the morphological study of the number of binucleated hepatocytes, we also observed a tendency to changes in the number of such cells with maxima at the 12th month of observation in both experimental groups, but the indicators were significantly different in both experimental groups at the 9th month of observation (Fig. 3). Thus, in the group without the addition of quercetin at the 9th month, the number of binuclear hepatocytes was 7.012±0.527 at p<0.05 in the fields of view, and with the addition of quercetin, only

5.311±0.156 cells in the fields of view at p<0.05, with a difference of 32.00%.

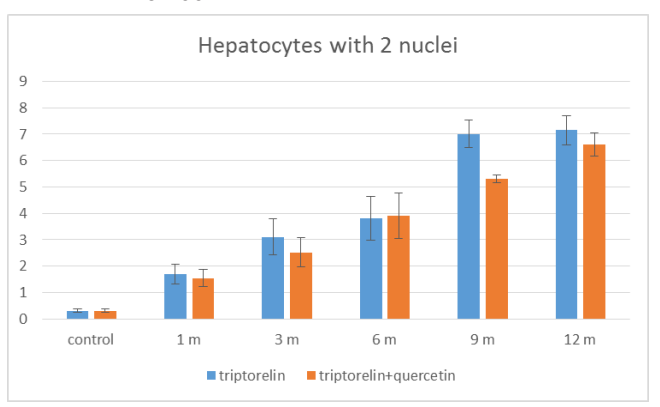


**Fig. 3.** The number of binuclear hepatocytes in the field of view in the group of animals administered triptorelin (T) and the group of animals administered quercetin (T+Q) against the background of triptorelin administration at different study periods.

#### **Discussion**

In this article, we examined the morphofunctional changes in hepatocyte nuclei during long-term (12 months) blocking of the synthesis of releasing hormone caused by the use of the substance triptorelin. The "hypothalamus-pituitary-testis-liver"

Vol. 31, №1, Page 52-58 **55** 

system was studied, namely testosterone – hepatocytes of male rats. Testosterone deficiency and its consequences are increasingly being determined in men in clinical conditions, and this is of increased interest in research worldwide [5, 14, 16].

As is known, the bulk of DNA is concentrated in the nucleus - the carrier of hereditary information and the regulator of metabolic function. The most important matrix processes - DNA replication, transcription (RNA synthesis) and RNA processing (maturation) take place in it. The nucleus transfers genetic information to the cytoplasm to the site of protein synthesis - ribosomes - using mRNA or messenger RNA. The nucleus, exchanging information with the cytoplasm of the hepatocyte, controls and coordinates all cell activity: division, growth, intermediate metabolism, protein synthesis and its differentiation [20]. During the life cycle, the cell nucleus is in interphase. The large variation in the size of hepatocyte nuclei is explained by the fact that during postnatal development, some cells undergo cytogenetic transformation, characterized by gradual polyploidy. Polyploidy, or amplification of the entire genome, is inherent in cells/organisms containing more than 2 main chromosome sets [10, 31]. The proportion of hepatocyte diferon is 60-70 % of cells and 78 % of the volume. Among them, about 25 % of hepatocytes have two nuclei, 70 % of single-nucleated hepatocytes are tetraploid (4n), about 2 % are octaploids (8n) with 4 or 8-fold chromosome sets. Polyploid hepatocytes appear at an early age, their number increases with age. Adults have about 30-40 % of polyploid hepatocytes with a 4-fold set of chromosomes. The increase in nuclear polyploidy is accompanied by an increase in the size of hepatocytes. The volume of hepatocyte nuclei doubles when the DNA content doubles. No significant difference in the volume of polyploid hepatocytes containing one or two nuclei with the same sets of chromosomes has been found [9]. There are several hypotheses to explain polyploidy. Some authors suggest that liver polyploidy is necessary to improve hepatocyte function [13, 30]. A polyploid cell may allow for a two- or four-fold increase in the expression of some genes and thereby enhance certain metabolic functions. However, comparison of gene expression profiles of isolated diploids, tetraploids and octaploids using microarray analysis revealed that only 50 candidate genes from a wide range of different biological processes were differentially expressed [9, 10, 13]. Polyploidy-activated genes are present in all major liver-specific functions, including nitrogen metabolism, protein synthesis, maintenance of the redox state, xenobiotic metabolism and immunity. It has been established that polyploid hepatocytes have a tendency to increase anaerobic energy production by producing ATP from carbohydrates rather than fatty acids, suggesting that polyploidy is associated with the transition of liver-specific functions into an economy mode [7]. According to other hypotheses, polyploidy provides protection of hepatocytes from oxidative stress and genotoxic damage. Polyploid chromosome sets may serve as a buffer against mutations that inactivate genes by DNA-damaging agents. For example, early tumor lesions in the liver are characterized by an increase in the number of diploid cells, which are less protected from mutations than polyploid ones. Notably, a comparison of diploid and polyploid hepatocytes on a genome-wide scale shows that polyploids induce genes directed against pathogens, DNA damage, and oxidative stress, and repress genes that promote apoptosis. In addition, progressive polyploidization allows the liver to adapt to cell loss during the aging process or may be a protective response to the accumulation of damaged DNA. In pathological conditions accompanied by loss of function, the liver is able to compensate for the loss of volume by increasing the number of genomes [19]. Liver polyploidization mainly indicates the severity of the lesion: the higher the observed rate of polyploidization, the greater the injury. However, an increase in diploid cells is a characteristic feature of hepatocellular carcinoma due to their increased proliferative capacity and susceptibility to further mutations [23, 25].

Both basic and clinical studies have shown that testosterone acts on the liver parenchyma both in health and pathology. It is known that testosterone contributes to a global improvement in energy metabolism, the introduction of its excessive amount can cause an excess of reactive oxygen species along with oxidative damage, which indicates electron leakage from the mitochondrial respiratory chain and metabolic uncoupling.

It is assumed that the vasoprotective effects of quercetin are realized due to its ability to reduce the activity of the inflammatory process in the vascular endothelium, enhance the activity of endothelial NO synthase (eNOS), which, in turn, increases the level of nitric oxide in endothelial cells and leads to improved endothelial function [27].

In our work, we observed a tendency to a gradual increase in the number of nucleoli and hepatocyte nuclei at all times of the experiment in both experimental groups. In our opinion, this may indicate a compensatory effect caused by the addition of quercetin to the diet of experimental animals, which, due to its vasoprotective and antioxidant properties, reduces the inflammatory process in the endothelium and in hepatocytes, contributing to an increase in the level of nitric oxide [34].

Our results are consistent with the data of some other experimental and clinical studies, which draw attention to the fact that the use of quercetin leads to antioxidant, anti-inflammatory, hypolipidemic, antisteatotic and antifibrotic effects. The above indicates the potential benefit of this flavonoid in the treatment of various liver diseases, in particular non-alcoholic fatty liver disease, chronic hepatitis of various etiologies and drug-associated liver diseases [9, 10, 13, 35].

Thus, we can assume that changes in the number of nuclei and nucleoli of hepatocytes in the processes of dishormonal disorder protect against oxidative stress and hepatotoxic damage to the cell and increase transcriptional moments in the process of division, growth, intermediate metabolism, protein synthesis and its differentiation. The results obtained by us are a theoretical justification for the development of methods for correcting disorders in the liver during the pathological impact on the body of a dishormonal state of central genesis: "hypothalamus—pituitary—testis—liver". Data on the functional morphology of hepatocyte nuclei at the stages of adaptation to changes in the endocrine

system expand the existing ideas about the causes that cause liver homeostasis disorders.

#### Conclusion

1. Central blocking of the synthesis of releasing hormone and subsequent activation of pituitary gonadotropocytes leads

# to oxidative-nitrosative stress, which causes pathological processes in hepatocytes, primarily in the form of quantitative changes in binucleolus and binuclear cells in the population.

2. Additional administration of quercetin reduces the negative effect on hepatocytes, which is confirmed by changes in parameters in experimental groups of animals.

#### References

- [1] Almomani, A., Hitawala, A. A., Kumar, P., Alqaisi, S., Alshaikh, D., Alkhayyat, M., & Asaad, I. (2022). Prevalence of hypothyroidism and effect of thyroid hormone replacement therapy in patients with non-alcoholic fatty liver disease: A population-based study. World journal of hepatology, 14(3), 551-558. doi: 10.4254/wjh.v14.i3.551
- [2] Alamri, Z. Z. (2019). Effect of luteolin and quercetin on thioacetamide induced hepatic fibrosis in rats. *International Journal of Pharmacology*, 15(7), 863-871. doi: 10.3923/ ijp.2019.863.871
- [3] Bahriy, M. M., Dibrova, V. A., Popadynets, O. H., & Hryshchuk, M. I. (2016). Методики морфологічних досліджень: монографія [Methods of morphological research: monograph]. Вінниця: Нова книга — Vinnytsya: Nova knyha.
- [4] Botté, M. C., Lerrant, Y., Lozach, A., Bérault, A., Counis, R., & Kottler, M. L. (1999). LH down-regulates gonadotropinreleasing hormone (GnRH) receptor, but not GnRH, mRNA levels in the rat testis. *J Endocrinol*, 162(3), 409-415. doi: 10.1677/joe.0.1620409
- [5] Bou-Nader, M., Caruso, S., Donne, R., Celton-Morizur, S., Calderaro, J., Gentric, G., ... & Desdouets, C. (2020). Polyploidy spectrum: a new marker in HCC classification. *Gut*, 69(2), 355-364. doi: 10.1136/gutjnl-2018-318021
- [6] Carteri, R. B., Kopczynski, A., Rodolphi, M. S., Strogulski, N. R., Wannmacher, C. M., Franceschi, I. D., ... & Portela, L. V. (2021). Anabolic-androgenic steroids impair mitochondrial function and redox status in the heart and liver of mice. *Steroids*, 172, 108861. doi: 10.1016/j.steroids.2021.108861
- [7] Chao, H. W., Doi, M., Fustin, J. M., Chen, H., Murase, K., Maeda, Y., ... & Okamura, H. (2017). Circadian clock regulates hepatic polyploidy by modulating Mkp1-Erk1/2 signaling pathway. *Nature communications*, 8(1), 2238. doi: 10.1038/s41467-017-02207-7
- [8] Chekalina, N. I., Shut, S. V., Trybrat, T. A., Burmak, Y. H., Petrov, Y. Y., Manusha, Y. I., & Kazakov, Y. M. (2017). Effect of quercetin on parameters of central hemodynamics and myocardial ischemia in patients with stable coronary heart disease. Wiad Lek, 70(4), 707-711. PMID: 29064791
- [9] Donne, R., Sangouard, F., Celton-Morizur, S., & Desdouets, C. (2021). Hepatocyte Polyploidy: Driver or Gatekeeper of Chronic Liver Diseases. *Cancers (Basel)*, 13(20), 5151. doi: 10.3390/cancers13205151
- [10] Donne, R., Saroul-Aïnama, M., Cordier, P., Celton-Morizur, S., & Desdouets, C. (2020). Polyploidy in liver development, homeostasis and disease. *Nat Rev Gastroenterol Hepatol*, 17(7), 391-405. doi: 10.1038/s41575-020-0284-x
- [11] do Val Lima, P. R., Ronconi, K. S., Morra, E. A., Rodrigues, P. L., Ávila, R. A., Merlo, E., ... & Ribeiro Júnior, R. F. (2023). Testosterone deficiency impairs cardiac interfibrillar mitochondrial function and myocardial contractility while inducing oxidative stress. *Frontiers in Endocrinology*, 14, 1206387. doi: 10.3389/fendo.2023.1206387
- [12] Guo, X., Li, Y., Wang, W., Wang, L., Hu, S., Xiao, X., ... & Zeng, J. (2022). The construction of preclinical evidence for the treatment of liver fibrosis with quercetin: A systematic review and meta-analysis. *Phytotherapy research: PTR*, 36(10), 3774-3791. doi: 10.1002/ptr.7569
- [13] Gupta, S. (2000). Hepatic polyploidy and liver growth

- control. Semin Cancer Biol, 10(3), 161-171. doi: 10.1006/scbi.2000.0317
- [14] Hajam, Y. A., Rani, R., Ganie, S. Y., Sheikh, T. A., Javaid, D., Qadri, S. S., ... & Reshi, M. S. (2022). Oxidative stress in human pathology and aging: molecular mechanisms and perspectives. *Cells*, 11(3), 552. doi: 10.3390/cells11030552
- [15] Kasarinaite, A., Sinton, M., Saunders, P. T. K., Hay, D. C. (2023). The Influence of Sex Hormones in Liver Function and Disease. *Cells*, 12(12), 1604. doi: 10.3390/ cells12121604
- [16] Klaunig, J. E. (2018). Oxidative stress and cancer. Curr Pharm, 24(40), 4771-4778. doi: 10.2174/138161282566 6190215121712
- [17] Kostenko, V., Akimov, O., Gutnik, O., Kostenko, H., Kostenko, V., Romantseva, T., ... & Taran, O. (2023). Modulation of redox-sensitive transcription factors with polyphenols as pathogenetically grounded approach in therapy of systemic inflammatory response. *Heliyon*, 9(5), e15551. doi: 10.1016/j.heliyon.2023.e15551
- [18] Kozaeva, R., Klymenko, M. O., Katrushov, O. V., & Kostenko, V. O. (2022). Bioflavonoids as agents for correcting nitro-oxidative stress and salivary gland functions in rats exposed to alcohol during modeled lipopolysaccharide-induced systemic inflammatory response. *Wiadomosci Lekarskie* (Warsaw, Poland: 1960), 75(3), 685-690. doi: 10.36740/wlek202203121
- [19] Kur, P., Kolasa-Wołosiuk, A., Misiakiewicz-Has, K., & Wiszniewska, B. (2020). Sex Hormone-Dependent Physiology and Diseases of Liver. *International journal of environ*mental research and public health, 17(8), 2620. doi: 10.3390/ ijerph17082620
- [20] Lin, Y. H., Zhang, S., Zhu, M., Lu, T., Chen, K., Wen, Z., ... & Zhu, H. (2020). Mice With Increased Numbers of Polyploid Hepatocytes Maintain Regenerative Capacity But Develop Fewer Hepatocellular Carcinomas Following Chronic Liver Injury. Gastroenterology, 158(6), 1698-1712. doi: 10.1053/j.gastro.2020.01.026
- [21] Lin, H. Y., Yu, I. C., Wang, R. S., Chen, Y. T., Liu, N. C., Altuwaijri, S., ... & Chang, C. (2008). Increased hepatic steatosis and insulin resistance in mice lacking hepatic androgen receptor. *Hepatology (Baltimore, Md)*, 47(6), 1924-1935. doi: 10.1002/hep.22252
- [22] Matsumoto, T. (2022). Implications of Polyploidy and Ploidy Alterations in Hepatocytes in Liver Injuries and Cancers. Int J Mol Sci, 23(16), 9409. doi: 10.3390/ijms23169409
- [23] Mavromati, M., & Jornayvaz, F. R. (2021). Hypothyroidism-Associated Dyslipidemia: Potential Molecular Mechanisms Leading to NAFLD. *International journal of molecular sciences*, 22(23), 12797. doi: 10.3390/ijms222312797
- [24] Miyaoka, Y., Ebato, K., Kato, H., Arakawa, S., Shimizu, S., & Miyajima, A. (2012). Hypertrophy and unconventional cell division of hepatocytes underlie liver regeneration. *Current biology: CB*, 22(13), 1166-1175. doi: 10.1016/j. cub.2012.05.016
- [25] Neshat, S. Y., Quiroz, V. M., Wang, Y., Tamayo, S., & Doloff, J. C. (2021). Liver Disease: Induction, Progression, Immunological Mechanisms, and Therapeutic *Interventions*. Int J Mol Sci, 22(13), 6777. doi: 10.3390/ijms22136777
- [26] Raja, T., Sud, R., Addla, S., Sarkar, K. K., Sridhar, P. S.,

Vol. 31, №1, Page 52-58

- Talreja, V., ... & Patil, K. (2022). Gonadotropin-releasing hormone agonists in prostate cancer: A comparative review of efficacy and safety. *Indian journal of cancer*, *59*(Supplement), S142-S159. doi: 10.4103/ijc.IJC\_65\_21
- [27] Sharifi-Rad, M., Anil Kumar, N. V., Zucca, P., Varoni, E. M., Dini, L., Panzarini, E., ... & Sharifi-Rad, J. (2020). Lifestyle, oxidative stress, and antioxidants: back and forth in the pathophysiology of chronic diseases. *Frontiers in physiol*ogy, 11, 552535. doi: 10.3389/fphys.2020.00694
- [28] Song, M. J., & Choi, J. Y. (2022). Androgen dysfunction in non-alcoholic fatty liver disease: Role of sex hormone binding globulin. *Frontiers in endocrinology*, 13, 1053709. doi: 10.3389/fendo.2022.1053709
- [29] Waxman, D. J., & Kineman, R. D. (2022). Sex matters in liver fat regulation. *Science (New York, N.Y.)*, 378(6617), 252-253. doi: 10.1126/science.ade7614
- [30] Wilkinson, P. D., Alencastro, F., Delgado, E. R., Leek, M. P., Weirich, M. P., Otero, P. A., ... & Duncan, A. W. (2019). Polyploid Hepatocytes Facilitate Adaptation and Regeneration to Chronic Liver Injury. *The American journal of pathology*, 189(6), 1241-1255. doi: 10.1016/j.ajpath.2019.02.008

- [31] Wilkinson, P. D., & Duncan, A. W. (2021). Differential Roles for Diploid and Polyploid Hepatocytes in Acute and Chronic Liver Injury. Seminars in liver disease, 41(1), 42-49. doi: 10.1055/s-0040-1719175
- [32] Xiao, J., & Bai, W. (2019). Bioactive phytochemicals. Critical reviews in food science and nutrition, 59(6), 827-829. doi: 10.1080/10408398.2019.1601848
- [33] Xu, M. X., Wang, M., & Yang, W. W. (2017). Gold-quercetin nanoparticles prevent metabolic endotoxemia-induced kidney injury by regulating TLR4/NF-kB signaling and Nrf2 pathway in high fat diet fed mice. *International journal of* nanomedicine, 5(12), 327-345. doi: 10.2147/IJN.S212318
- [34] Yelins'ka, A. M., Akimov, O. Y., & Kostenko, V. O. (2019). Role of AP-1 transcriptional factor in development of oxidative and nitrosative stress in periodontal tissues during systemic inflammatory response. Український біохімічний журнал=Ukrainian biochemical journal, 91(1), 80-85. doi: 10.15407/ubj91.01.080
- [35] Zhang, S., Lin, Y. H., Tarlow, B., & Zhu, H. (2019). The origins and functions of hepatic polyploidy. *Cell Cycle*, 18(12), 1302-1315. doi: 10.1080/15384101.2019.1618123

### ЗМІНИ В ГЕПАТОЦИТАХ ЩУРІВ ЗА УМОВ ЦЕНТРАЛЬНОЇ БЛОКАДИ СИНТЕЗУ ЛЮТЕЇНІЗУЮЧОГО ГОРМОНУ З ДОДАВАННЯМ КВЕРЦЕТИНУ

Полив'яна О. А., Стецук Є. В., Шепітько В. І., Вільхова О. В., Борута Н. В., Рудь М. В., Пелипенко Л. Б., Лисаченко О. Д., Волошина О. В., Дворник І. Л., Мороховець Г. Ю.

Ядро, обмінюючись інформацією з цитоплазмою гепатоцита, контролює і координує всю активність клітини: поділ, ріст, проміжний обмін речовин, синтез білка і його диференціювання. Протягом життєвого циклу клітини ядро зберігається в інтерфазі. Велика варіація розмірів ядер гепатоцитів пояснюється тим, що при постнатальному зростанні деякі гепатоцити піддаються цитогенетичним перетворенням, що характеризуються поступовою поліплоїдією. Поліплоїдія, або посилення цілого геному, стосується клітин/організмів, що містять більше 2 основних хромосомних наборів. Мета даного дослідження — визначити морфогенез та динаміку мінливості підтипів гепатоцитів щурів, двоядерних та з двома ядерцями, за умов центральної блокади синтезу лютеїнізуючого гормону при довготривалій дії триптореліну, з додаванням в раціон харчування тварин кверцетину. Експеримент проведено на 60 статевозрілих білих щурах самцях масою 140-160 г. Тварин розділили на 3 групи: 1 групі – контрольній, вводився фізіологічний розчин (10 тварин); 2 групі підшкірно вводили розчин триптореліну ембонат у дозі 0,3 мг діючої речовини на кг маси тіла протягом 12 місяців (25 тварин); 3 групі вводили розчин триптореліну із розрахунку 0,3 мг діючої речовини на кг маси тіла з додаванням кверцетину в перерахунку на масу тіла тварин тричі на тиждень (25 тварин). Тварин виводили з експерименту через 1, 3, 6, 9 та 12 місяців шляхом передозування ефірного наркозу. Комплексне дослідження гістологічних препаратів печінки та кількісний підрахунок гепатоцитів з двома ядерцями та двоядерних проводили за допомогою світлового мікроскопа з цифровим мікрофільтром та адаптованого для цих досліджень програмного забезпечення. Статистичну обробку результатів дослідження виконували з використанням програмного забезпечення Microsoft Office Excel та розширення Real Statistics 2019. Патологічні процеси, що виникають у тканині печінки при експериментальному оксидативно-нітрозативному стресі, викликаному введенням триптореліну, призводять як до кількісних, так і якісних змін. Так кількість гепатоцитів з двома ядерцями достовірно збільшувалась в 2 групі і на 12-й місяць спостереження становила 5,291±1,156 клітин в полі зору при р<0.05. Кількість двоядерних гепатоцитів також мала тенденцію до змін з максимумами на 12-й місяць спостереження. Так у 2 групі на 9-й місяць кількість двоядерних гепатоцитів склала 7,012±0,527 клітин в полі зору при p<0,05, а при додаванні кверцетину лише 5,311±1,561 клітин в полі зору при p<0,05. Збільшена кількість мітозів виявлялась у 2 групі на 6-й місяць спостереження, у 3 групі визначалася лише на 9-й. Проведене дослідження показало, що при введенні триптореліну виникає оксидативно-нітрозативний стрес, який призводить до патологічних змін гепатоцитів у вигляді кількісних змін клітин з двома ядерцями та двоядерних. Додаткове введення кверцетину зменшує негативний вплив на гепатоцити печінки, що підтвержується показниками в експериментальних групах тварин.

**Ключові слова:** печінка, гепатоцит, двоядерні гепатоцити, мітоз, тестостерон, лютеїнізуючий гормон, кверцетин, трипторелін.

#### Author's contribution

Polyviana O. A. - data collection and analysis.

Stetsuk Ye. V. - work concept and design.

Shepitko V. I. - final approval of the article.

Vilkhova O. V. - methodology of the original draft.

Boruta N. V. - data visualization.

Rud M. V. - writing of the original draft

Pelypenko L. B. - project administration.

Lysachenko O. D. - review writing and editing.

Voloshyna O. V. – software.

Dvornyk I. L. - critical review.

Morokhovets H. Yu. - responsibility for statistical analysis.

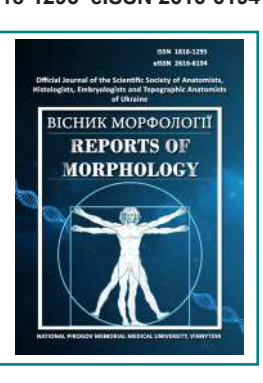
ISSN 1818-1295 eISSN 2616-6194



#### REPORTS OF MORPHOLOGY

Official Journal of the Scientific Society of Anatomists, Histologists, Embryologists and Topographic Anatomists of Ukraine

journal homepage: https://morphology-journal.com



# Discriminant models of the possibility of genital endometriosis in Ukrainian young women depending on the features of the structure and body size

Nyzova O. A.<sup>1</sup>, Chaika H. V.<sup>1</sup>, Berenshtein E. L.<sup>2</sup>, Kryvonis T. G.<sup>1</sup>, Kyrychenko V. I.<sup>1</sup>, Sorokoumov V. P.<sup>1</sup>, Gunas I. V.<sup>1</sup>

<sup>1</sup>National Pirogov Memorial Medical University, Vinnytsya, Ukraine

<sup>2</sup>Core research Facility, The Hebrew University of Jerusalem, Jerusalem, Israel

#### ARTICLE INFO

Received: 17 April 2024 Accepted: 24 December 2024

UDC: 618.1-037-084:616-055.23-

053.7-071.2

#### **CORRESPONDING AUTHOR**

e-mail: olgabojko40g@gmail.com Nyzova O. A.

#### **CONFLICT OF INTEREST**

The authors have no conflicts of interest to declare.

#### **FUNDING**

Not applicable.

#### **DATA SHARING**

Data are available upon reasonable request to corresponding author.

Endometriosis is one of the most common gynecological pathologies, which can significantly affect the reproductive health of women, including young women. Research into factors that may contribute to its development is important for early identification of risk groups and development of preventive measures. Among the possible predictors, anthropometric characteristics that may reflect the endocrine and metabolic characteristics of the body attract attention. The study of these parameters allows us to assess the potential relationship between somatotype and the likelihood of developing the disease, which may contribute to a personalized approach to prevention. The aim of the study is to construct and analyze discriminant models of the possibility of genital endometriosis in Ukrainian young women without and with somatotype, depending on the features of the structure and body size. Clinical, laboratory and anthropo-somatotypological examination were performed on 89 Ukrainian young women (aged 16 to 18 years) with genital endometriosis. Primary anthropo-somatotypological indicators of 78 practically healthy Ukrainian young women of the same age group were taken from the data bank of the National Pirogov Memorial Medical University, Vinnytsya, Ukraine. Discriminant models of the possibility of the occurrence and features of the course of genital endometriosis, depending on the features of the structure and body size, were constructed in the "Statistica 6.0" license package. It was established that when dividing Ukrainian young women into practically healthy and patients with genital endometriosis both without taking into account the somatotype and in representatives of mesomorphic, ectomorphic and ecto-mesomorphic somatotypes, reliable (p<0.001 in all cases) highly informative (correctness of entry into the models of anthropo-somatotypological indicators is from 98.6 % to 100 % of cases; Wilks' Lambda statistics is from 0.084 to 0.039) discriminant models of the possibility of the occurrence of this disease depending on the features of the body structure and body dimensions. The most common components of the constructed models include: in the group without taking into account the somatotype - girth dimensions of the body and trunk diameters of 33.33 % each; in mesomorphs - girth dimensions of the body 42.86 % and trunk diameters 28.57 %; in ectomorphs - girth dimensions of the body 50.00 %, trunk diameters and width of the distal epiphyses of the long tubular bones of the limbs 25.00 % each; in ecto-mesomorphs – girth dimensions of the body in 100 % of cases. Key words: obstetrics and gynecology, genital endometriosis, anthropometry, somatotype, Ukrainian young women, discriminant analysis.

#### Introduction

Endometriosis is a chronic hormone-dependent disease characterized by the presence of endometriotic tissue outside the uterine cavity. It is one of the leading causes of chronic pelvic pain and female infertility. Although the disease has been studied for over a century, its etiology and pathogenesis are still the subject of scientific debate. The main hypotheses for the occurrence of endometriosis are retrograde menstruation, metaplastic theory, genetic predisposition and impaired immune regulation [9, 13, 23].

According to epidemiological studies, the prevalence of endometriosis in women of reproductive age varies from 6 % to 10 %, although among patients with infertility or chronic pelvic pain this figure can reach 50 % [7, 21]. A study conducted in France found that the incidence of hospitalizations for endometriosis is 1.3 cases per 1000 women annually [27]. In Spain, the prevalence of this disease among women aged 15-49 years reached 1.5 % in the general population [3]. Similar data were obtained in studies in Brazil, where the incidence of endometriosis among patients with gynecological complaints was 9.8 % [7]. In the USA, the incidence of diagnosed endometriosis reaches 11.2 %, but the real incidence may be much higher due to the difficulty of diagnosis [23]. A large study conducted on the basis of health insurance companies in Israel showed that the overall prevalence of endometriosis in the country is about 10.8 % among women of reproductive age [11]. In addition, analysis of data from systematic reviews suggests that different forms of endometriosis (subtle, typical, deep) have distinct pathogenetic features and a frequency of detection that varies from 20 % to 40 % in different populations [17].

In addition to reproductive complications, endometriosis has a significant impact on women's quality of life. It is accompanied by chronic pain, dyspareunia, dysuria and other symptoms that can significantly worsen the psycho-emotional state. Studies have shown that women with endometriosis are 2-3 times more likely to suffer from depressive and anxiety disorders, and are also at increased risk of developing eating disorders [16]. An assessment of the economic burden of this disease indicates significant costs for medical care and reduced work productivity. In European countries, direct costs for the treatment of endometriosis exceed 10 billion euros each year, and indirect losses associated with temporary disability are even higher [10].

Given the widespread and multifactorial nature of endometriosis, research into possible predictors of its development is an important area of modern science. Structural features of the body, such as body mass index, anthropometric indicators and features of fat metabolism, can have a significant impact on the likelihood of developing this pathology. Identifying discriminative models that allow predicting the risk of endometriosis can contribute to the development of effective preventive measures and timely diagnosis of this pathology.

The purpose of the study – construction and analysis of discriminant models of the possibility of genital endometriosis in Ukrainian young women depending on the characteristics of the structure and size of the body.

#### Materials and methods

At the Department of Obstetrics and Gynecology of the National Pirogov Memorial Medical University, Vinnytsya, Ukraine, a clinical, laboratory and anthropological

examination of 89 Ukrainian young women (YW) (aged 16 to 18 years) with genital endometriosis was conducted. Committee on Bioethics of National Pirogov Memorial Medical University, Vinnytsya (protocol № 11 from 3.12.2020) found that the studies do not contradict the basic bioethical standards of the Declaration of Helsinki, the Council of Europe Convention on Human Rights and Biomedicine (1977), the relevant WHO regulations and laws of Ukraine.

The diagnosis of genital endometriosis was made according to the updated guidelines of the European Society of Human Reproduction and Embryology (ESHRE) on the management of women with endometriosis [6].

The anthropological examination was performed according to the schemes of Bunak V. V. modified by Shaparenko P. P. [24], somatotypological – according to the Heath-Carter method [8], determination of indicators of the component composition of body mass - according to the formulas of Matiegka J. [18] and the muscle component of body mass according to the formulas of the American Institute of Nutrition [25]. The following distribution of YW patients by somatotype was established: endomorphs - 1; mesomorphs – 45; ectomorphs – 23; ecto-mesomorphs – 12; endo-mesomorphs - 2; average intermediate somatotype - 6. Therefore, further modeling of the possibility of genital endometriosis depending on the features of the structure and size of the body was carried out in groups without taking into account the somatotype, in mesomorphs, in ectomorphs and ecto-mesomorphs.

As a control group, the primary anthropo-somatotypological indicators of 78 practically healthy Ukrainian YW of a similar age group were taken from the data bank of the National Pirogov Memorial Medical University, Vinnytsya, Ukraine.

Discriminant models of the possibility of occurrence and features of the course of genital endometriosis depending on the features of the structure and size of the body were built in the licensed package "Statistica 6.0".

#### Results

When taking into account anthropometric and somatotypological indicators in practically healthy and genital endometriosis Ukrainian YW patients without taking into account somatotype, the discriminant function covers 100 % of practically healthy and 98.9 % of genital endometriosis patients. In general, the model that takes into account indicators of body structure and size in practically healthy and genital endometriosis patients of YW without taking into account somatotype is correct in 99.4 % of cases. The following discriminant variables were established between practically healthy and patients with genital endometriosis Ukrainian YW without taking into account somatotype (Table 1): anteroposterior mid-thoracic diameter (SGK), shoulder girth in a tense state (OBP), shoulder girth in a relaxed state (OBPL), transverse mid-thoracic diameter (PSG), body mass index (IMT), hip girth (OBB), width of the distal epiphysis of the forearm (EPPR), transverse lower thoracic diameter (PNG) and endomorphic component of the somatotype (FX).

The greatest contribution to discrimination (respectively, the smallest values of Partial Lambda) is made by shoulder girths in tense and relaxed states (see Table 1). The set of all anthropometric and somatotypological variables has a very pronounced (Wilks' Lambda statistic=0.076; p<0.001) discrimination between practically healthy and patients with genital endometriosis Ukrainian YW without taking into account somatotype (see Table 1).

**Table 1.** Report of a step-by-step discriminant analysis of practically healthy and patients with genital endometriosis YW without taking into account somatotype depending on the characteristics of body structure and size.

Discriminant Function Analysis Summary (boyko.sta)								
Step 9, N of vars in model: 9; Grouping: GRUP (2 grps)								
	Wilks' Lamb	da: 0.076 a	approx. F(9.1	6)=212.6 <sub> </sub>	0.0000			
	Wilks' Lambda	Partial Lambda	F-remove - 1.16	n-level Inler		1-Toler. (R-Sqr.)		
SGK	0.090	0.843	29.30	0.0000	0.471	0.529		
OBP	0.164	0.461	183.4	0.0000	0.091	0.909		
OBPL	0.128	0.594	107.3	0.0000	0.090	0.910		
PSG	0.094	0.807	37.45	37.45 0.0000		0.817		
IMT	0.093	0.814	35.80	0.0000	0.333	0.667		
OBB	0.090	0.847	28.33	0.0000	0.408	0.592		
EPPR	0.081	0.938	10.32	0.0016	0.799	0.201		
PNG	0.078	0.970	4.811	0.0297	0.172	0.828		
FX	0.078	0.974	4.188	0.0424	0.751	0.249		

**Notes:** in this and subsequent similar tables, Wilks' Lambda – Wilks' Lambda statistic; Partial Lambda – Wilks' Lambda statistic of the single contribution of the variable to the discrimination between populations; F-remove – standard F-criterion associated with the corresponding Partial Lambda; p-level – p-level associated with the corresponding F-remove; Toler. – tolerance (measure of redundancy of the feature); 1-Toler. (R-Sqr.) – coefficient of multiple correlation of the feature with all other features (the indicator is necessary for calculating tolerance).

To determine the classification indicators (Df), which allow to attribute the obtained anthropometric and somatotypological indicators to "typical" for practically healthy or patients with genital endometriosis Ukrainian YW without taking into account the somatotype, the coefficients of the classification discriminant functions for each feature were established. Below are the equations, where the assignment to practically healthy Ukrainian YW without taking into account the somatotype is possible at a Df value close to 159.4; and to patients with genital endometriosis of Ukrainian YW without taking into account the somatotype – at a Df value close to 150.1:

Df (for practically healthy YW without taking into account somatotype) = SGK×1.168 + OBP×7.970 - OBPL×7.197 + PSG×2.996 - IMT×2.609 + OBB×3.893 + EPPR×12.62 - PNG×0.291 - FX×3.115 - 159.4;

Df (for patients with genital endometriosis YW without taking into account somatotype) = SGK×3.763 + OBP×0.777 - OBPL×0.856 + PSG×0.329 - IMT×0.729 + OBB×2.700 + EPPR×17.06 + PNG×0.947 - FX×4.789 - 150.1;

where (here and hereinafter), trunk diameters – in cm; body circumferences – in cm; somatotype components – in points; body mass index – in kg/m²; width of distal epiphyses of long tubular bones of limbs – in cm; somatotype components – in points.

Calculated criterion  $\chi^2$  (=414.0) confirms the statistical significance of the obtained discriminant functions in girls without taking into account somatotype.

When taking into account anthropometric and somatotypological indicators in practically healthy and patients with genital endometriosis Ukrainian YW with a *mesomorphic somatotype*, the discriminant function covers 100% of practically healthy and 97.8 % of patients with genital endometriosis YW. In general, the model that takes into account indicators of body structure and size in practically healthy and patients with genital endometriosis YW with a mesomorphic somatotype is correct in 98.6 % of cases. The following discriminant variables were established between practically healthy and patients with genital endometriosis in Ukrainian YW with a mesomorphic somatotype (Table 2): anteroposterior mid-thoracic diameter (SGK), shoulder girth in a tense state (OBP), shoulder girth in a non-stressed state (OBPL), body mass index (IMT), transverse mid-thoracic diameter (PSG), hip girth (OBB) and width of the distal epiphysis of the forearm (EPPR). The greatest contribution to discrimination (respectively, the smallest values of Partial Lambda) has shoulder girth in a tense state (see Table 2). The set of all anthropometric and somatotypological variables has a very pronounced (Wilks' Lambda statistic=0.084; p<0.001) discrimination between practically healthy and patients with genital endometriosis in Ukrainian YW with a mesomorphic somatotype (see Table 2).

**Table 2.** Report of a step-by-step discriminant analysis of practically healthy and patients with genital endometriosis YW of the mesomorphic somatotype depending on the characteristics of the body structure and dimensions.

Discriminant Function Analysis Summary (boyko.sta)								
	Step 7, N	l of vars in	model: 7; Gr	ouping: GF	RUP (2 grp	s)		
	Wilks' La	mbda: 0.08	34 approx. F(	7.65)=101	.7 p<0.000	0		
	Wilks' Lambda	Partial Lambda	F-remove -1.65	n-level loler		1-Toler. (R-Sqr.)		
SGK	0.098	0.855	11.02	0.0015	0.556	0.444		
OBP	0.213	0.393	100.3	100.3 0.0000 0		0.848		
OBPL	0.153	0.548	53.58	0.0000	0.152	0.848		
IMT	0.113	0.742	22.63	0.0000	0.583	0.417		
PSG	0.103	0.812 15.05		0.0002	0.501	0.499		
OBB	0.103	0.816	14.63	14.63 0.0003 0		0.391		
EPPR	0.093	0.896	7.507	0.0079	0.782	0.218		

Below, in the form of equations, the definition of the Df indicator is given, where the classification of Ukrainian YW with a mesomorphic somatotype as practically healthy is possible with a Df value close to 211.2; and Ukrainian YW with a mesomorphic somatotype as patients with genital endometriosis is possible with a Df value close to 194.4:

Df (for practically healthy YW with a mesomorphic somatotype) = SGK×1.559 + OBP×9.881 - OBPL×6.869

Vol. 31, №1, Page 59-65

- IMT×0.215 + PSG×2.190 + OBB×4.063 + EPPR×7.453 - 211.2;

Df (for patients with genital endometriosis YW with a mesomorphic somatotype) = SGK×3.699 + OBP×2.487 - OBPL×1.027 + IMT×1.918 + PSG×0.777 + OBB×2.814 + EPPR×13.40 - 194.4;

Calculated criterion  $\chi^2$  (=167.4) confirms the statistical significance of the obtained discriminant functions in YW with a mesomorphic somatotype.

Taking into account anthropometric and somatotypological indicators in practically healthy and genital endometriosis patients Ukrainian YW with ectomorphic somatotype, the discriminant function covers 100 % of practically healthy and 100% of genital endometriosis patients of YW. The following discriminant variables were established between practically healthy and genital endometriosis patients of Ukrainian girls with ectomorphic somatotype (Table 3): anteroposterior mid-thoracic diameter (SGK), shoulder girth in a tense state (OBP), shoulder girth in a non-stressed state (OBPL), transverse mid-thoracic diameter (PSG), hip girth (OBB), upper forearm girth (OBPR), width of the distal epiphysis of the forearm (EPPR), width of the distal epiphysis of the shoulder (EPPL). The greatest contribution to discrimination (respectively, the smallest values of Partial Lambda) is made by the anterior-posterior midthoracic diameter and the transverse mid-thoracic diameter (see Table 3). The combination of all anthropometric and somatotypological variables has a very pronounced (Wilks' Lambda statistic=0.060; p<0.001) discrimination between practically healthy and patients with genital endometriosis Ukrainian YW with an ectomorphic somatotype (see Table 3).

**Table 3.** Report of a step-by-step discriminant analysis of practically healthy and patients with genital endometriosis YW of the ectomorphic somatotype depending on the characteristics of the body structure and dimensions.

of the body structure and dimensions.									
Discriminant Function Analysis Summary (boyko.sta)									
	Step 10, N	l of vars in	model: 8; Gr	ouping: GRI	JP (2 grps	)			
	Wilks' Laı	mbda: 0.06	0 approx. F(	8.34)=66.33	p<0.0000				
	Wilks' Lambda	Partial Lambda	F-remove -1,34	p-level Toler.		n-level Toler		1-Toler. (R-Sqr.)	
SGK	0.129	0.466	39.02	0.0000	0.230	0.770			
OBP	0.089	0.679	16.11	0.0003	0.148	0.852			
OBPL	0.087	0.695	14.91	0.0005	0.212	0.788			
PSG	0.115	0.525	30.72	0.0000	0.308	0.692			
OBB	0.080	0.751	11.30	0.0019	0.444	0.556			
OBPR	0.071	0.849	6.025	0.0194	0.286	0.714			
EPPR	0.077	0.777	9.739	0.0037	0.399	0.601			
EPPL	0.070	0.856	5.730	0.0223	0.403	0.597			

Below, in the form of equations, the definition of the Df indicator is given, where the classification of Ukrainian YW with an ectomorphic somatotype as practically healthy is possible with a Df value close to 269.8; and Ukrainian YW with an ectomorphic somatotype as patients with genital endometriosis is possible with a Df value close to 313.6:

Df (for practically healthy YW with an ectomorphic

somatotype) = SGK×7.845 - OBP×2.901 - OBPL×2.515 - PSG×0.050 + OBB×1.076 + OBPR×17.24 + EPPR×21.48 + EPPL×3.647 - 269.8;

Df (for patients with genital endometriosis YW with ectomorphic somatotype) = SGK×16.66 - OBP×10.80 + OBPL×3.980 - PSG×4.236 - OBB×0.754 + OBPR×21.90 + EPPR×35.45 - EPPL×7.366 - 313.6;

Calculated criterion  $\chi^2$  (=104.0) confirms the statistical significance of the obtained discriminant functions in YW with an ectomorphic somatotype.

Taking into account anthropometric and somatotypological indicators in practically healthy and patients with genital endometriosis Ukrainian YW with ecto-mesomorphic somatotype, the discriminant function covers 100% of practically healthy and 100 % of patients with genital endometriosis YW. The following discriminant variables between practically healthy and patients with genital endometriosis Ukrainian YW with ecto-mesomorphic somatotype were established (Table 4): hip circumference (OBB), shoulder circumference in a tense state (OBP), shoulder circumference in a relaxed state (OBPL), chest circumference on exhalation (OBGKH), chest circumference on inhalation (OBGKV). The greatest contribution to discrimination (respectively, the smallest values of Partial Lambda) is made by shoulder circumferences in tense and relaxed states (see Table 4). The set of all anthropometric and somatotypological variables has a very pronounced (Wilks' Lambda statistic=0.039; p<0.001) discrimination between practically healthy and patients with genital endometriosis Ukrainian YW with ecto-mesomorphic somatotype (see Table 4).

**Table 4.** Report of a step-by-step discriminant analysis of practically healthy and patients with genital endometriosis YW of the ecto-mesomorphic somatotype depending on the characteristics of the body structure and dimensions.

Discriminant Function Analysis Summary (boyko.sta)								
	Step 7, N	of vars in m	odel: 5; Gro	uping: GRL	JP (2 grps)	)		
	Wilks' Lan	nbda: 0.039	approx. F(5	5.20)=97.32	p<0.0000			
	Wilks' Lambda	n_level   Toler		1-Toler. (R-Sqr.)				
OBB	0.058	0.681	9.375	0.0062	0.690	0.310		
ОВР	0.189	0.208	75.96	0.0000 0.127		0.873		
OBPL	0.180	0.219	71.44	0.0000	0.095	0.905		
OBGKH	0.059	0.668	9.946	0.0050	0.058	0.942		
OBGKV	0.050	0.783	5.530	0.0291	0.064	0.936		

Below, in the form of equations, the definition of the Df indicator is given, where the classification of Ukrainian YW with an ecto-mesomorphic somatotype as practically healthy is possible with a Df value close to 365.5; and Ukrainian YW with an ecto-mesomorphic somatotype as patients with genital endometriosis is possible with a Df value close to 282.7:

Df (for practically healthy YW with ecto-mesomorphic somatotype) = OBB×10.84 + OBP×6.068 - OBPL×7.861 + OBGKH×4.800 - OBGKV×2.115 - 365.5;

Df (for patients with genital endometriosis YW with ectomesomorphic somatotype) = OBB×7.809 - OBP×6.354 + OBPL×10.61 + OBGKH×0.652 + OBGKV×0.525 - 282.7;

Calculated criterion  $\chi^2$  (=69.49) confirms the statistical significance of the obtained discriminant functions in YW with an ecto-mesomorphic somatotype.

#### **Discussion**

Thus, when dividing Ukrainian YW into practically healthy and patients with genital endometriosis without taking into account the somatotype, a reliable (p<0.001) pronounced discrimination (Wilks' Lambda=0.076) of the obtained classification indicators was established (the correctness of entering the models of anthropo-somatotypological indicators is 99.4 % of cases). The models include trunk diameters (33.33 %), body circumference dimensions (33.33 %), body mass index (11.11 %), the width of the distal epiphyses of the long tubular bones of the limbs (11.11 %) and somatotype components (11.11 %). The greatest contribution to the discrimination between practically healthy and patients with genital endometriosis YW without taking into account the somatotype is shoulder circumferences in tense and unstressed states.

When dividing Ukrainian YW into practically healthy and patients with genital endometriosis of the mesomorphic somatotype, a significant (p<0.001) pronounced discrimination (Wilks' Lambda=0.084) of the obtained classification indicators was established (the correctness of the entry into the models of anthropo-somatotypological indicators is 98.6 % of cases). The models include trunk diameters (28.57 %), body circumference (42.86 %), body mass index (14.29 %) and the width of the distal epiphyses of the long tubular bones of the limbs (14.29 %). The greatest contribution to the discrimination between practically healthy and patients with genital endometriosis of YW of the mesomorphic somatotype has a shoulder girth in a tense state.

When dividing Ukrainian YW into practically healthy and patients with genital endometriosis of the ectomorphic somatotype, a significant (p<0.001) pronounced discrimination (Wilks' Lambda=0.060) of the obtained classification indicators was established (the correctness of the entry into the models of anthropo-somatotypological indicators is 100 % of cases). The models include trunk diameters (25.00 %), girth dimensions of the body (50.00 %) and the width of the distal epiphyses of the long tubular bones of the limbs (25.00 %). The greatest contribution to the discrimination between practically healthy and patients with genital endometriosis of YW of the ectomorphic somatotype is made by the anterior-posterior midthoracic diameter and the transverse mid-thoracic diameter.

When dividing Ukrainian YW into practically healthy and patients with genital endometriosis of the ecto-mesomorphic somatotype, a significant (p<0.001) pronounced discrimination

(Wilks' Lambda=0.039) of the obtained classification indicators was established (the correctness of entering the models of anthropo-somatotypological indicators is 100 % of cases). In all cases, the models include body circumferences (100 %). The greatest contribution to the discrimination between practically healthy and patients with genital endometriosis of YW of the ecto-mesomorphic somatotype is shoulder circumferences in tense and non-tense states.

The results obtained confirm the existence of a relationship between anthropometric characteristics and the risk of developing genital endometriosis in girls. According to the conducted studies, body mass index (BMI), fat tissue distribution and overall body structure may play a key role in shaping the predisposition to this disease. Several large-scale epidemiological studies have demonstrated that an increased BMI is associated with a lower risk of developing endometriosis, which may be due to the hormonal characteristics of fat tissue and its effect on estrogen levels [4, 5, 14].

However, the data on the relationship between body weight and the risk of endometriosis are contradictory. A meta-analysis conducted by Yong L. & Weiyuan Z. [28] showed that underweight women (BMI<18.5) have a higher risk of developing endometriosis, while obese women demonstrate a lower level of this disease. Similar results were obtained in the study by Aarestrup J. et al. [1], which demonstrated that low body weight in childhood and short stature are associated with an increased risk of endometriosis in the future. This suggests that factors related to early development may influence susceptibility to this disease in adulthood.

Studies by Omiyale W. et al. [19] and Sponholtz T. R. et al. [26] demonstrated that fat distribution is more important than overall BMI in determining the risk of endometriosis and endometrial cancer. In particular, central obesity was associated with an increased risk of endometrial cancer, while peripheral fat distribution had a protective effect. This may explain the different endocrine mechanisms associated with the localization of fat tissue and its effect on circulating estrogen levels.

Another important aspect is the role of metabolic factors in the development of endometriosis. Studies by Backonja U. et al. [5] confirmed that total adipose tissue, independent of BMI, can be a predictor of risk for this disease. In addition, a review by Pantelis A. et al. [20] indicates a complex interaction between obesity, hormonal balance and the development of endometriosis.

In the study of Aune D. et al. [2], it was demonstrated that tall stature is associated with an increased risk of endometrial cancer, which may indicate similar mechanisms of hormonal influence in endometriosis. At the same time, the study of Farland L. V. et al. [12] did not find significant associations between stature and endometriosis, which indicates the need for further research in this direction.

Thus, the results obtained indicate the multifactorial nature of genital endometriosis, in the development of which

Vol. 31, №1, Page 59-65

both genetic and metabolic factors play a role. Established anthropometric predictors may be useful for developing individualized approaches to early diagnosis and prevention of this disease.

#### Conclusions

1. Based on the characteristics of body structure and size, reliable (p<0.001 in all cases) discriminant models were developed, which allow with a high probability to predict the possibility of genital endometriosis in Ukrainian YWs without taking into account the somatotype (the classification matrix covers 99.4 % of cases, Wilks' Lambda statistics=0.076), representatives of the mesomorphic somatotype (the

classification matrix covers 98.6 % of cases, Wilks' Lambda statistics=0.084), ectomorphic somatotype (the classification matrix covers 100 % of cases, Wilks' Lambda statistics=0.060) and ecto-mesomorphic somatotype (the classification matrix covers 100 % of cases, Wilks' Lambda statistics=0.039).

2. The most common components of the constructed models are trunk diameters (33.33 % in the group without taking into account somatotype; 28.57 % in mesomorphs; 25.00 % in ectomorphs), body circumferences (33.33 % in the group without taking into account somatotype; 42.86 % in mesomorphs; 50.00 % in ectomorphs; 100 % in ectomesomorphs) and the width of the distal epiphyses of the long tubular bones of the limbs (25.00 % in ectomorphs).

#### References

- [1] Aarestrup, J., Jensen, B. W., Ulrich, L. G., Hartwell, D., Trabert, B., & Baker, J. L. (2020). Birth weight, childhood body mass index and height and risks of endometriosis and adenomyosis. *Annals of human biology*, 47(2), 173-180. doi: 10.1080/03014460.2020.1727011
- [2] Aune, D., Rosenblatt, D. N., Chan, D. S. M., Vingeliene, S., Abar, L., Vieira, A. R., ... & Norat, T. (2015). Anthropometric factors and endometrial cancer risk: a systematic review and dose–response meta-analysis of prospective studies. *Annals of Oncology*, 26(8), 1635-1648. doi: 10.1093/ annonc/mdv142
- [3] Ávalos Marfil, A., Barranco Castillo, E., Martos García, R., Mendoza Ladrón de Guevara, N., & Mazheika, M. (2021). Epidemiology of endometriosis in Spain and its autonomous communities: a large, nationwide study. *International Journal of Environmental Research and Public Health*, 18(15), 7861. doi: 10.3390/ijerph18157861
- [4] Backonja, U., Hediger, M. L., Chen, Z., Lauver, D. R., Sun, L., Peterson, C. M., & Buck Louis, G. M. (2017). Beyond body mass index: using anthropometric measures and body composition indicators to assess odds of an endometriosis diagnosis. *Journal of Women's Health*, 26(9), 941-950. doi: 10.1089/jwh.2016.6128
- [5] Backonja, U., Louis, G. M. B., & Lauver, D. R. (2016). Overall adiposity, adipose tissue distribution, and endometriosis: a systematic review. *Nursing research*, 65(2), 151-166. doi: 10.1097/NNR.000000000000146
- [6] Becker, C. M., Bokor, A., Heikinheimo, O., Horne, A., Jansen, F., Kiesel, L., ... & Vermeulen, N. (2022). ESHRE guideline: endometriosis. *Human reproduction open*, 2022(2), hoac009. doi: 10.1093/hropen/hoac009
- [7] Cardoso, J. V., Machado, D. E., Silva, M. C. D., Berardo, P. T., Ferrari, R., Abrão, M. S., & Perini, J. A. (2020). Epidemiological profile of women with endometriosis: a retrospective descriptive study. *Revista Brasileira de Saúde Materno Infantil*, 20(4), 1057-1067. doi: 10.1590/1806-93042020000400008
- [8] Carter, J. L., & Heath, B. H. (1990). Somatotyping development and applications. Cambridge University Press.
- [9] Chapron, C., Marcellin, L., Borghese, B., & Santulli, P. (2019). Rethinking mechanisms, diagnosis and management of endometriosis. *Nature Reviews Endocrinology*, 15(11), 666-682. doi: 10.1038/s41574-019-0245-z
- [10] Darbà, J., & Marsà, A. (2022). Economic implications of endometriosis: a review. *Pharmacoeconomics*, 40(12), 1143-1158. doi: 10.1007/s40273-022-01211-0

- [11] Eisenberg, V. H., Weil, C., Chodick, G., & Shalev, V. (2018). Epidemiology of endometriosis: a large population-based database study from a healthcare provider with 2 million members. BJOG: An International Journal of Obstetrics & Gynaecology, 125(1), 55-62. doi: 10.1111/1471-0528.14711
- [12] Farland, L. V., Missmer, S. A., Bijon, A., Gusto, G., Gelot, A., Clavel-Chapelon, F., ... & Kvaskoff, M. (2017). Associations among body size across the life course, adult height and endometriosis. *Human Reproduction*, 32(8), 1732-1742. doi: 10.1093/humrep/dex207
- [13] Greene, A. D., Lang, S. A., Kendziorski, J. A., Sroga-Rios, J. M., Herzog, T. J., & Burns, K. A. (2016). Endometriosis: where are we and where are we going?. *Reproduction* (*Cambridge, England*), 152(3), R63-R78. doi: 10.1530/ REP-16-0052
- [14] Holdsworth-Carson, S. J., Dior, U. P., Colgrave, E. M., Healey, M., Montgomery, G. W., Rogers, P. A., & Girling, J. E. (2018). The association of body mass index with endometriosis and disease severity in women with pain. *Journal* of Endometriosis and Pelvic Pain Disorders, 10(2), 79-87. doi: 10.1177/2284026518773939
- [15] Kliemann, N., Ould Ammar, R., Biessy, C., Gicquiau, A., Katzke, V., Kaaks, R., ... & Gunter, M. J. (2022). Metabolically defined body size phenotypes and risk of endometrial cancer in the European prospective investigation into cancer and nutrition (EPIC). Cancer Epidemiology, Biomarkers & Prevention, 31(7), 1359-1367. doi: 10.1158/1055-9965. EPI-22-0160
- [16] Koller, D., Pathak, G. A., Wendt, F. R., Tylee, D. S., Levey, D. F., Overstreet, C., ... & Polimanti, R. (2023). Epidemiologic and genetic associations of endometriosis with depression, anxiety, and eating disorders. *JAMA network open*, 6(1), e2251214. doi: 10.1001/jamanetworkopen.2022.51214
- [17] Koninckx, P. R., Ussia, A., Keckstein, J., Wattiez, A., & Adamyan, L. (2016). Epidemiology of subtle, typical, cystic, and deep endometriosis: a systematic review. *Gynecologi*cal Surgery, 13, 457-467. doi: 10.1007/s10397-016-0970-4
- [18] Matiegka, J. (1921). The testing of physical efficiency. Am. J. Phys. Antropol, 2(3), 25-38. doi: 10.1002/ajpa.1330040302
- [19] Omiyale, W., Allen, N. E., & Sweetland, S. (2020). Body size, body composition and endometrial cancer risk among postmenopausal women in UK Biobank. *International journal* of cancer, 147(9), 2405-2415. doi: 10.1002/ijc.33023
- [20] Pantelis, A., Machairiotis, N., & Lapatsanis, D. P. (2021). The formidable yet unresolved interplay between endometriosis and obesity. *The Scientific World Journal*, 2021(1), 6653677.

- doi: 10.1155/2021/6653677
- [21] Parazzini, F., Esposito, G., Tozzi, L., Noli, S., & Bianchi, S. (2017). Epidemiology of endometriosis and its comorbidities. European Journal of Obstetrics & Gynecology and Reproductive Biology, 209, 3-7. doi: 10.1016/j.ejogrb.2016.04.021
- [22] Rossi, H. R., Nedelec, R., Jarvelin, M. R., Sebert, S., Uimari, O., & Piltonen, T. T. (2021). Body size during adulthood, but not in childhood, associates with endometriosis, specifically in the peritoneal subtype—population-based life-course data from birth to late fertile age. Acta Obstetricia et Gynecologica Scandinavica, 100(7), 1248-1257. doi: 10.1111/aogs.14090
- [23] Shafrir, A. L., Farland, L. V., Shah, D. K., Harris, H. R., Kvaskoff, M., Zondervan, K., & Missmer, S. A. (2018). Risk for and consequences of endometriosis: a critical epidemiologic review. Best practice & research Clinical obstetrics & gynaecology, 51, 1-15. doi: 10.1016/j.bpobgyn.2018.06.001
  [24] Shaparenko, P. P. (2000). Антропометрія [Anthropometry].

- Вінниця: ВДМУ ім. М. І. Пирогова=Vinnytsia: VDMU іm. М. І. Ругодоva.
- [25] Shephard, R. J. (2005). Body composition in biological anthropology. Cambridge University Press, Cambridge, UK; New York.
- [26] Sponholtz, T. R., Palmer, J. R., Rosenberg, L., Hatch, E. E., Adams-Campbell, L. L., & Wise, L. A. (2016). Body size, metabolic factors, and risk of endometrial cancer in black women. *American Journal of Epidemiology*, 183(4), 259-268. doi: 10.1093/aje/kwv186
- [27] von Theobald, P., Cottenet, J., Iacobelli, S., & Quantin, C. (2016). Epidemiology of endometriosis in France: a large, nation-wide study based on hospital discharge data. *BioMed Research International*, 2016(1), 3260952. doi: 10.1155/2016/3260952
- [28] Yong, L., & Weiyuan, Z. (2017). Association between body mass index and endometriosis risk: a meta-analysis. Oncotarget, 8(29), 46928-46936. doi: 10.18632/oncotarget.14916.

## ДИСКРИМІНАНТНІ МОДЕЛІ МОЖЛИВОСТІ ВИНИКНЕННЯ ГЕНІТАЛЬНОГО ЕНДОМЕТРІОЗУ В УКРАЇНСЬКИХ ДІВЧАТ У ЗАЛЕЖНОСТІ ВІД ОСОБЛИВОСТЕЙ БУДОВИ ТА РОЗМІРІВ ТІЛА

Низова О. А., Чайка Г. В., Беренштейн Е. Л., Кривоніс Т. Г., Кириченко В. І., Сорокоумов В. П., Гунас І. В.

Ендометріоз є однією з найпоширеніших гінекологічних патологій, що може значно впливати на репродуктивне здоров'я жінок, у тому числі й молодого віку. Дослідження факторів, які можуть сприяти його розвитку, є важливим для раннього виявлення груп ризику та розробки профілактичних заходів. Серед можливих предикторів увагу привертають антропометричні характеристики, які можуть відображати ендокринні та метаболічні особливості організму. Вивчення цих параметрів дозволяє оцінити потенційний зв'язок між соматотипом та ймовірністю розвитку захворювання, що може сприяти персоналізованому підходу до профілактики. Мета дослідження – побудова та аналіз дискримінантних моделей можливості виникнення генітального ендометріозу в українських дівчат без та з урахуванням соматотипу у залежності від особливостей будови та розмірів тіла. У 89 українських дівчат (віком від 16 до 18 років), хворих на генітальний ендометріоз, проведено клініко-лабораторне та антропо-соматотипологічне обстеження. Первинні антропо-соматотипологічні показники 78 практично здорових українських дівчат аналогічної вікової групи отримані з банку даних науково-дослідного центру Вінницького національного медичного університету ім. М. І. Пирогова. Дискримінантні моделі можливості виникнення та особливостей перебігу генітального ендометріозу в залежності від особливостей будови та розмірів тіла побудовані в ліцензійному пакеті «Statistica 6.0». При розподілі українських дівчат на практично здорових та хворих на генітальний ендометріоз як без урахування соматотипу, так і у представниць мезоморфного, ектоморфного та екто-мезоморфного соматотилів побудовані достовірні (р<0,001 в усіх випадках) високоінформативні (коректність входження до моделей антропо-соматотипологічних показників складає від 98,6 % до 100 % випадків; статистика Wilks' Lambda дорівнює від 0,084 до 0,039) дискримінантні моделі можливості виникнення даного захворювання в залежності від особливостей показників будови та розмірів тіла. Найбільш часто до складу побудованих моделей входять: в групі без урахування соматотипу – обхватні розміри тіла та діаметри тулуба (по 33,33%); у мезоморфів – обхватні розміри тіла (42,86%) та діаметри тулуба (28,57%); у ектоморфів – обхватні розміри тіла (50,00 %), діаметри тулуба та ширина дистальних епіфізів довгих трубчастих кісток кінцівок по (25,00 %); у ектомезоморфів – обхватні розміри тіла (в 100 % випадків).

**Ключові слова:** акушерство та гінекологія, генітальний ендометріоз, антропометрія, соматотип, українськи дівчата, дискримінантний аналіз.

#### **Author's contribution**

Nyzova O. A. – research, methodology and writing of the original draft, formal analysis and validation.

Chaika H. V. – conceptualization, supervision.

Berenshtein E. L. - software, review writing and editing.

Kryvonis T. G. – data visualization, review writing and editing.

Kyrychenko V. I. – validation, review writing and editing.

Sorokoumov V. P. - resources, review writing and editing.

Gunas I. V. – project administration.

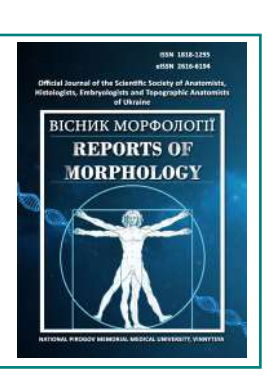
Vol. 31, №1, Page 59-65



#### REPORTS OF MORPHOLOGY

Official Journal of the Scientific Society of Anatomists, Histologists, Embryologists and Topographic Anatomists of Ukraine

journal homepage: https://morphology-journal.com



# A correlation between cartilage degradation and inflammation of the synovial membrane of shoulder joint in a rabbit model of collagenase-induced osteoarthritis

Strafun S. S.<sup>1</sup>, Bohdan S. V.<sup>1</sup>, Savosko S. I.<sup>2</sup>, Yuriychuk L. M.<sup>3</sup>

<sup>1</sup>SI "The Institute of Traumatology and Orthopedics" by NAMS of Ukraine, Kyiv, Ukraine

<sup>2</sup>Bogomolets National Medical University, Kyiv, Ukraine

<sup>3</sup>Regional Clinical Hospital of Ivano-Frankivsk Regional Council, Ivano-Frankivsk, Ukraine

#### **ARTICLE INFO**

Received: 3 May 2024 Accepted: 8 January 2025

UDC: 616.728.2-007.24:616-018.2

#### **CORRESPONDING AUTHOR**

e-mail: s.i.savosko@gmail.com Savosko S. I.

#### **CONFLICT OF INTEREST**

The authors have no conflicts of interest to declare.

#### **FUNDING**

Not applicable.

#### **DATA SHARING**

Data are available upon reasonable request to corresponding author.

Osteoarthritis is a degenerative disease of articular cartilage. Numerous studies have expanded our understanding of the pathophysiology of the disease, yet there remain controversial questions regarding the relationship between mechanical loads on the joint, inflammation, and biochemical changes in cartilage tissue that lead to its degradation. The question of the primary cause of cartilage tissue damage remains unresolved, as synovitis and contracture may result from cartilage injury, while cartilage degeneration can concurrently arise in the presence of synovitis. Animal models play a key role in studying these changes, as they allow for the identification of the structural basis and characteristics of joint tissue disorders. Our hypothesis is that non-mechanical damage to cartilage tissues, through the introduction of collagenase into the synovial cavity, provokes a slow, progressive development of changes in the capsule and articular cartilage. The aim of the work was to investigate changes in cartilage and capsule of the shoulder joint under the conditions of modeling collagenase-induced joint damage. Collagenase was injected into the shoulder joint and saline was injected into the contralateral joint. After 4 months, the articular cartilage of the humerus head and scapula, the joint capsule, was examined. The morphometric method measured the thickness of the capsule, the condition of the cartilage by scale method and correlated between changes in the studied structures of the joint to establish the relationship between the degeneration of cartilage tissue and fibrous changes in the synovial membrane. The statistical analysis of the results was performed using non-parametric methods. The introduced enzyme induced degenerative changes in the shoulder joint cartilage after 3 months, accompanied by an inflammatory reaction in the synovial membrane and signs of connective tissue remodeling in the capsule. The results suggest that inflammation of the synovial membrane correlates with cartilage degradation (for the humeral head, r=0.74, p=0.02, and for the glenoid cavity, r=0.71, p=0.03), which likely represents an early event in the initiation and progression of articular cartilage damage. Damage to the synovial membrane and capsule thickness showed a direct correlation (r=0.87, p=0.001). Although mechanical damage remains the primary risk factor for osteoarthritis, the slow, "sluggish" progression of cartilage-degrading changes provided new insights into the relationship between changes in the cartilage, synovial membrane, and shoulder joint capsule. The model of osteoarthritis described in this study serves as a valid model for investigating the pathogenesis and treatment of the inflammatory and degenerative changes of the shoulder joint.

Keywords: shoulder joint, arthritis, collagenase, inflammation.

#### Introduction

Osteoarthritis is the degenerative joint disease, characterized by the gradual degeneration of articular

cartilage, changes in the subchondral bone, and the development of chronic inflammation [6, 28]. Although

osteoarthritis is traditionally considered a disease of the elderly, its prevalence among younger populations is increasing due to risk factors such as injury, excess weight, and genetic predisposition [17, 21, 25]. There are numerous theories regarding the disease development, focusing on the idea that cartilage damage is a combination of interactions between mechanical stress on the joint, inflammation, and biochemical changes in the tissues, leading to a disruption of cartilage tissue homeostasis [7, 8]. Fibrotic changes in the capsule, synovitis, and contractures can result from cartilage impairment, but alternatively, cartilage degeneration can arise in the context of synovitis [16], or adhesive capsulitis [26].

Animal models allow for the faster and easier acquisition of factual material during the dynamic progression of pathology and in its various forms, because the reproduction of cartilage and joint capsule in animals is relatively simple from a technical standpoint, enabling the rapid collection of sufficient observations for biostatistical analysis, unlike in clinical settings, where finding similar cases can be a challenging task [23, 24]. However, the outcomes of open mechanical joint injuries in experiments are well-documented, develop quickly, and are predictable and well-understood [4, 15]. Our hypothesis is that non-mechanical damage to cartilage tissue may provoke a slow, prolonged development of changes in the capsule. Reproducing a model, where cartilage is primarily affected, has proven to be guite a challenging task. We hypothesized that such changes could be iatrogenic. It is known that saline or Hartmann's solution, which are used in arthroscopy, cause chondrocyte swelling and cartilage damage due to their slightly different osmolarity compared to the extracellular matrix of the cartilage [5, 14, 19]. Inducing non-isolated cartilage damage with matrix breakdown can be achieved by injecting a sufficient amount of enzyme into the joint to disrupt the homeostasis of the cartilage and synovial membrane, triggering disturbances characteristic of the inflammatory process [8, 27]. The inflammatory cell infiltration also secretes enzymes, including collagenase, so one or two injections of the enzyme into the joint should cause degenerative changes in the cartilage, as shown in the model of osteoarthritis of the knee joint [1, 11, 29]. Identifying the relationship between changes in cartilage tissue and capsule tissue should help confirm our hypothesis regarding the role of primary cartilage damage in fibrotic changes of the shoulder joint.

The aim of the study is to investigate changes in the cartilage and capsule of the shoulder joint under conditions of collagenase-induced joint injury modeling.

#### Materials and methods

The study was conducted as part of scientific cooperation on the experimental development of models for various types of traumatic injuries to the musculoskeletal system. This is a component of the fundamental research project titled "The study of tissue reactions in different parts of the nervous system and internal organs to injuries of various origins and their modulation. Pedagogical aspects of histology teaching,"

project number 0123U101051. The implementation period is 2023-2025.

The experiments were conducted on 9 rabbits, aged 2-2.5 years and weighing 4.2-4.5 kg. The experimental model involved inducing shoulder joint damage in the animals with minimal traumatic impact. Considering the literature [2]. which reports age-related changes in the joint cartilage of rabbits older than 1 year, older animals were selected for reproducing the joint injury model. For this, a solution of microbial collagenase enzyme (Clostridium histolyticum, C5138, Sigma-Aldrich Chemie GmbH) was injected into the shoulder joint in a volume of 200 µl, which contained 1500 collagenase units. The enzyme was injected once, with a second injection administered after 1 month; 20 µl of saline was administered into the contralateral joint. Three months after the second injection, the animals were euthanized (lethal dose of sodium thiopental) in accordance with the provisions of the EU Directive 2010/63/EU "On the protection of animals used for scientific purposes" and the Law of Ukraine of February 21, 2006, No. 3447-IV "On the protection of animals from cruelty". The study was approved by the Ethics Committee of Bogomolets National Medical University (Protocol No. 192 dated 24.02.2025).

The shoulder joint was removed from the animals. The joint capsule, humeral head, and articular surface of the scapula were fixed in a 10 % formalin solution (pH 7.4). After fixation, a strip 2-3 mm thick was cut from the joint surfaces and placed in a decalcifying solution, OsteoFast 1 (BioGnost, Croatia). The samples were then rinsed from the solution, dehydrated in isopropanol (4 changes, 1 hour each), and embedded in paraffin (Leica-Paraplast Regular, Leica Biosystems Inc., USA). The capsule was embedded in paraffin following a similar protocol, but without the decalcifying solution. Microsections were prepared using a Thermo Microm HM 360 microtome and stained with Sirius Red, Alcian Blue (pH=2.5) (BioGnost, Croatia). The stained micro-preparations were examined under an Olympus BX51 microscope, and images were captured using an Olympus C3040ZOOM digital camera with Olympus DP-Soft 3.2 software (Olympus, Tokyo, Japan). The morphology of the capsule was assessed using a developed scale that includes histological changes and their degree of severity. The scale consists of three parameters: changes in capsule thickness, the condition of the synovial membrane, and signs of inflammation. To determine the capsule thickness, the method of linear morphometry was applied, and 25 points at 200 um intervals from each sample were measured using Carl Zeiss software (AxioVision SE64 Rel.4.9.1).

For the scale and correlation analysis, linear changes in thickness were converted into scores: 0 - no significant difference, 1 - an increase of 25-50 %, 2 - 75-100 %, 3 - more than 100 %. The following classifier was introduced for changes in the synovial membrane: 0 - no changes, 1 - altered but epithelial layer continuity is preserved, 2 - epithelium is disrupted with mild signs of fibrosis, 3 - moderate signs of fibrosis, 4 - significant signs of fibrosis.

Vol. 31, №1, Page 66-72

The inflammation factor was classified as follows: 0 – absent, 1 – focal cell-inflammatory infiltration, 2 – moderate, 3 – severe. Each sample received a total scale score by summing the points for each morphological parameter.

The condition of the articular cartilage was assessed using a modified Mankin histological score [20]. The scoring system included four morphological features and their degrees of severity: cartilage (matrix) condition from 0 to 6, cartilage cellularity from 0 to 3, staining intensity (Alcian blue dye) from 0 to 4, and the tidemark between cartilage and bone. Each score was calculated as the sum of the points for each morphological parameter.

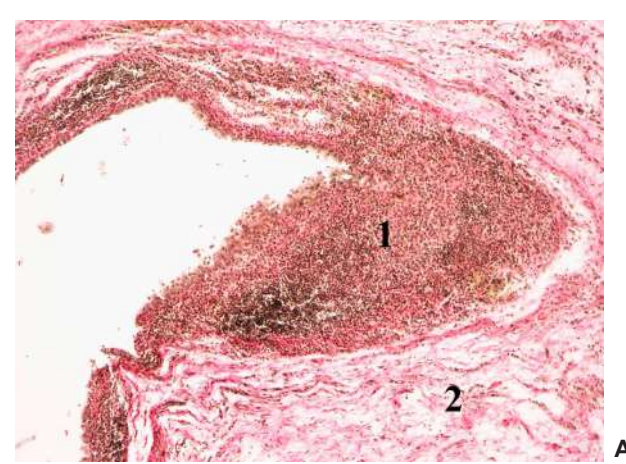
Statistical analysis was conducted using analysis of variance (ANOVA), followed by a Bonferroni post-hoc test and Mann-Whitney test. Data processing was performed using StatPlus software, version 7.3.0 (AnalystSoft Inc., USA). The correlation between joint parameters in each sample was assessed using Spearman's rank correlation (Spearman's rho). A p-value of 0.05 or less was considered statistically significant.

#### Results

Histological changes in the shoulder joint capsule

According to the results of the enzyme-induced shoulder ioint iniury model, the capsule was visually enlarged, and its wall was found to be thickened upon cross-section. An increase in capsule thickness was observed due to increased cellularity in the connective tissue, particularly fibroblasts, leading to enhanced collagenogenesis. The density of newly formed collagen beneath the synovial membrane significantly increased, with foci of newly formed thin fibers spreading almost throughout the length of the capsule. The remodeling of the fibrous structure of the capsule showed quite a varied picture, while the intact capsule was characterized by the presence of thick bundles of collagen fibers in the connective tissue. Meanwhile, the synovial membrane of the capsule suffered significant damage, predominantly due to inflammatory infiltration (monocytes/macrophages, lymphocytes) (Fig. 1). The morphological damage to the villi of the synovial membrane involved a reduction in their length and cellularity, while the thickness of the villi was markedly increased (visibly protruding into the joint cavity), with bloodfilled, congested vessels. Vascular stasis was often observed but did not have a clear correlation with focal or extensive inflammation in the capsule. However, areas of reduced cellular density in the synovial membrane were also noted.

Morphometric analysis showed a significant increase in capsule thickness (intact cartilage 1.588±0.489 mm vs model 2.571±0.209 mm, p<0.05 according to ANOVA, Bonferroni test). An attempt was made to differentiate the nature of changes in the joint capsule, categorizing cases into those with signs of newly formed tissues in the synovial membrane and cavity (these changes were evaluated as possible morphological evidence of connective tissue formation on the inner side of the capsule, akin to synovitis) and those without such signs (4 vs 5). It was found that a



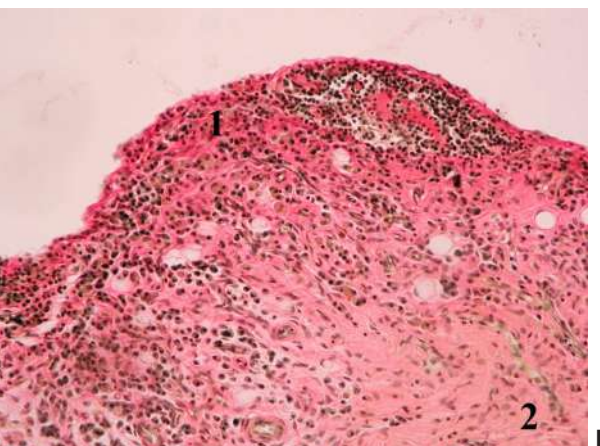


**Fig. 1.** Structural changes in the shoulder joint capsule under conditions of a collagenase-induced model of shoulder joint injury. A – pronounced cellular-inflammatory infiltration at the level of the synovial membrane, ×100; B – cellular-inflammatory infiltration in the synovial membrane, ×200. 1 – cellular infiltration, 2 – subintimal connective tissue. Picrosirius red staining with Weigert's hematoxylin.

greater degree of damage was associated with an increase in capsule thickness (model 2.400±0.289 mm vs model + inflammation 3.020±0.128 mm, p<0.05 according to the Mann-Whitney test).

We introduced a classifier (Table 1) for assessing morphological changes in the joint capsule to detail the changes in its layers considering inflammatory cell infiltration. In almost all cases, disturbances in the morphology of the synovial membrane were observed (loss of villi, inflammatory infiltration, and less frequently, cellular reduction), while in 3 samples (33.3 %), significant development of connective tissue was noted, which was assessed as a manifestation of fibrous changes. Inflammatory cell infiltration comprising macrophages and lymphocytes was equally classified as moderate or pronounced. These changes were primarily concentrated in the synovial membrane. Consequently, a higher score was observed in samples with histologically confirmed inflammation and damage to the synovial membrane (intact cartilage 1.588±0.489 mm vs model

 $2.601\pm0.509$  mm vs model + inflammation  $6.502\pm0.921$  mm, p<0.05 according to the Mann-Whitney test).

**Table 1.** Scale for assessing morphological changes in the joint capsule.

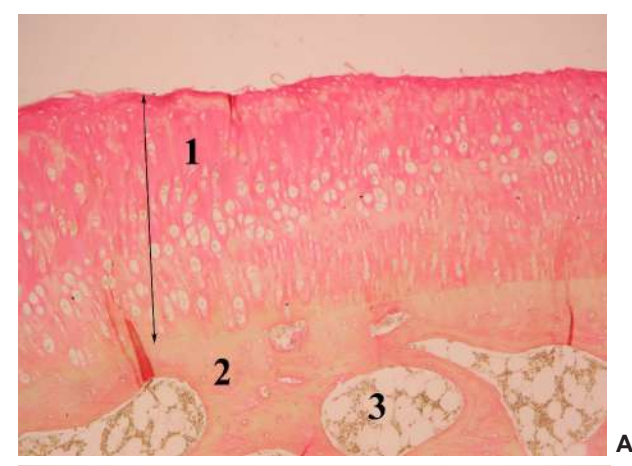
Scale indicator		Π	-	٩nir	ma	l n	um	ber		П
1		2	3*	4*	5	6	7*	8*	9	
thickening of the	none =0					0				
capsule	25-50% =1	1	1				1			
	75-100% =2			2					2	
	<100% =3				3			3		3
condition of	normal =0	0				Г				П
the synovial membrane	changed but preserved =1		1			1	1		1	1
Internbrane	mild signs of fibrosis =2	Г	Г	П	Г	Г		2	П	П
	moderate signs of fibrosis =3			3	3	Г				П
	severe signs of fibrosis =4									П
signs of	none =0					0			0	0
inflammation	mild and focal =1	1	1			Г	1			
	moderate =2				2	Г		2		П
	severe =3			3						
Total		2	3	8	8	1	3	7	3	4

Note:\* signs of synovitis

Degenerative changes in the shoulder joint cartilage

The study of the morphology of articular cartilage and its quantitative assessment using the Mankin scale convincingly demonstrated significant damage to the cartilage tissue (Fig. 2). The main changes observed in the cartilage included a reduction in histochemical detection of glycosaminoglycans, damage to the surface layers of the cartilage, and in some cases even to the middle layers of the cartilage, degeneration of chondrocytes, and the appearance of acellular regions. In samples with inflammatory cell infiltration, where the formation of fibrous connective tissue was observed, the emergence of connective tissue on the surface of the damaged cartilage was noted. We suggest that these changes reflect, to some extent, the stages of cartilage damage, ranging from superficial erosion and histochemical changes in the cartilage matrix to deeper erosion with fibrous changes near the surface of the articular cartilage. We observed a numerical, but statistically nonsignificant, increase in the degree of damage to the cartilage of the humeral head (intact cartilage: 6.555±0.668 points vs. model: 5.601±0.678 points vs. model + inflammation: 7.74±0.92 points, p>0.05 according to the Mann-Whitney test) and the cartilage of the glenoid surface (intact cartilage: 8.333±0.745 points vs. model: 7.400±0.678 points vs. model + inflammation: 9.500±1.322 points, p<0.05 according to the Mann-Whitney test) in cases of greater capsule damage.

The data on the morphology of articular cartilage did not have a significant correlation with the results of the joint capsule morphology scale (humeral head: r=0.41, p=0.28; glenoid cavity: r=0.57, p=0.11), but it showed a significantly strong positive correlation with the level of damage to the synovial membrane (r=0.74, p=0.02 and r=0.71, p=0.03), as well as a tendency or significant dependence regarding the factor of inflammatory cell infiltration detection in the capsule (r=0.63, p=0.07 and r=0.79, p=0.01) (Table 2). Despite the



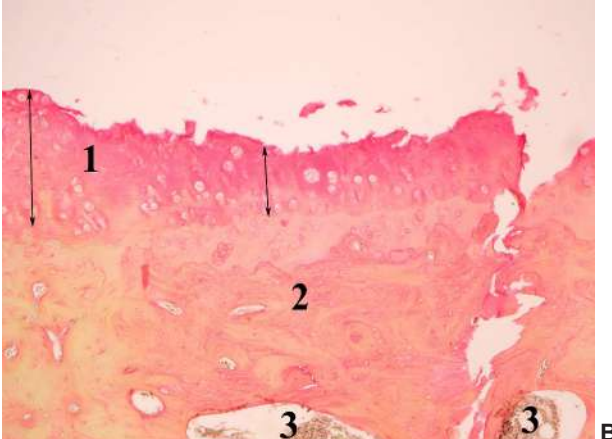


**Fig. 2.** Damage to the articular cartilage of the humeral head. A – nearly unchanged cartilage thickness, with edema and cell death present; B – erosion of the glenoid cartilage. 1 – cartilage; 2 – bone tissue; 3 – lacunae with bone marrow; arrow – cartilage thickness. Picrosirius red staining with Weigert's hematoxylin, ×100.

direct relationship between synovial membrane damage and capsule thickness (r=0.87, p=0.001), the thickness measurement introduced some dispersion in the statistical analysis. Therefore, the analysis of the relationship between joint damage and the synovial membrane turned out to be the most sensitive for studying the patterns of pathological changes in the shoulder joint. Based on these studies, the conclusion is made that the assessment of capsule morphology using the developed scale is more sensitive and significant compared to the linear morphometry of the capsule wall.

#### **Discussion**

Our experimental study showed that shoulder joint synovitis and degenerative processes in the articular cartilage are a common pathogenetic pattern of osteoarthritis. We were unable to reliably determine limb function with changes in the shoulder joint tissues, but histologically, we proved damage to the joint surface and synovial membrane with the development of inflammation. Structural changes

Vol. 31, №1, Page 66-72

in the capsule are mainly localized within the synovial membrane. We have demonstrated damage to the cells of the synovial membrane and cellular-inflammatory infiltration with remodeling of the subintimal connective tissue layer of the synovial membrane. A positive correlation was established between these changes, as well as between changes in the synovial membrane and capsule thickness. That is, changes in homeostasis in the synovial membrane are a significant factor in the remodeling of the connective tissue of the capsule and the potential development of fibrosis. At the same time, these changes under collagenase action on joint tissues have a prolonged development and a non-bacterial nature of inflammation. Clearly, the local appearance of collagenase in the synovial fluid did not cause significant tissue damage in the joint and only initiated changes, as no functional disorders of the joint were observed within 30 days. The repeated injection of collagenase also became a factor in the prolonged development of disorders, which after 3 months reached a state that was visually observed in the form of articular cartilage erosion and tissue density changes in the shoulder joint capsule.

Similarly, in the model of cold injury to the joint, it was found that the longer the time after injury, the more severe the fibrosis of the capsule and muscles [13]. If we simplify the molecular basis for the onset of the inflammatory response and fibrosis, the products from degraded hyaline cartilage likely initiate damage to the synovial membrane and synovial inflammation [9]. Cells of the synovial intima respond to these changes by secreting various cytokines and growth factors that attract immune cells, which in turn release enzymes to remodel the extracellular matrix.

This was clearly observed in the intima and subintimal layer of the capsule, where altered connective tissue density, newly formed fine collagen networks, and increased vascular density were detected. It is important to understand that there are mutual inductive forces between the synovial membrane cells and immune cells, which involve both types of cells secreting enzymes capable of degrading all components of the extracellular matrix of the cartilage and capsule, not just collagen degradation. Moreover, activated chondrocytes in the cartilage, which also produce enzymes such as MMP-13 that degrade proteoglycans, contribute to this pathophysiological cycle. Thus, a dual cellular effect occurs in the destruction of the articular cartilage matrix [3, 10]. Hypothetically, this may occur in the foci of chondrocyte clustering, which are found in the hyaline cartilage near areas of degradation and erosion. Histological studies have shown that in these areas there may be a significant increase in the number of chondrocytes, likely through proliferation, forming large lacunae, larger than the lacunae of isogenic groups in intact cartilage. Further damage to chondrocytes in these cellular clusters leads to the formation of large acellular lacunae and, eventually, to rapid progression of matrix erosion. Proteoglycans and collagens are the main high-molecular components of the cartilage matrix, and their degradation inevitably leads to the loss of cartilage tissue. Evidence of these processes has been found in clinical studies, where the expression of degrading enzymes MMP-1 and MMP-9 was increased in the synovial fluid in arthritis compared to healthy individuals [12, 30]. Therefore, inflammation plays a critical role in the erosion of articular cartilage and the damage to the synovial membrane. Changes in the synovial membrane and fluid lead to a decrease in the concentration of cartilage protective factors, tissue inhibitors of metalloproteinases, and an increase in the production of factors that promote matrix degradation, ultimately leading to a vicious cycle of capsule inflammation and osteoarthritis development [18, 22].

The pathogenic mechanism of this cycle remains unclear, although a vast amount of data regarding the tissue damage mechanisms has already been discovered. Any updated information about new factors and their correlation with already known phenomena will also be beneficial for further study and treatment of osteoarthritis. A promising area of research on joint damage is the role of stem cells. Our study was not focused on detecting stem cells or their immunophenotypic characterization, but we predict their appearance based on already known studies [31]. Systematic literature analyses only report changes in the clinical presentation of patients, whereas morphological evidence of the involvement of endogenous mesenchymal stem cells is extremely scarce. It is assumed that influencing the activity of stem cell appearance in the damaged joint will stop the progression of degenerative changes and potentially promote regenerative processes. It is evident that stem cells will enter the damaged synovial membrane without significant barriers and differentiate into connective tissue cells. However, their potential ability to differentiate into cartilage cells has not yet been sufficiently confirmed by research. There is a need to study this aspect of osteoarthritis development using animal models with immunophenotypic characterization of endogenous mesenchymal stem cells.

#### Conclusions

- 1. Histological signs of connective tissue remodeling in the capsule and an increase in its thickness suggest the potential development of shoulder joint contracture in the presence of inflammatory cellular infiltration of the synovial membrane.
- 2. A strong positive correlation has been established between the degradation of articular cartilage, changes in the morphology of the synovial membrane, and the adjacent connective tissue of the joint capsule. It should be noted that changes in the cartilage did not always depend on the thickness of the capsule but were determined by the damage to its inner membrane.
- 3 The collagenase-induced osteoarthritis model is an effective model for studying the pathogenesis of the disease, as the slow progression of cartilage-degrading changes provides new insights into the interaction of tissues between cartilage, the synovial membrane, and the shoulder joint capsule.

#### References

- [1] Adães, S., Almeida, L., Potes, C. S., Ferreira, A. R., Castro-Lopes, J. M., Ferreira-Gomes, J., & Neto, F. L. (2017). Glial activation in the collagenase model of nociception associated with osteoarthritis. *Molecular Pain*, 13. doi: 10.1177/1744806916688219
- [2] Arzi, B., Wisner, E. R., Huey, D. J., Kass, P. H., Hu, J., & Athanasiou, K. A. (2011). A proposed model of naturally occurring osteoarthritis in the domestic rabbit. *Lab* Animal, 41(1), 20-25. doi: 10.1038/laban0112-20
- [3] Bendele, A. M., Neelagiri, M., Neelagiri, V., & Sucholeiki, I. (2021). Development of a selective matrix metalloproteinase 13 (MMP-13) inhibitor for the treatment of Osteoarthritis. *European Journal of Medicinal Chemistry*, 224, 113666. doi: 10.1016/j.ejmech.2021.113666
- [4] Buckwalter, J. A., Anderson, D. D., Brown, T. D., Tochigi, Y., & Martin, J. A. (2013). The Roles of Mechanical Stresses in the Pathogenesis of Osteoarthritis: Implications for Treatment of Joint Injuries. *Cartilage*, 4(4), 286-294. doi: 10.1177/1947603513495889
- [5] Bush, P. G., & Hall, A. C. (2001). The osmotic sensitivity of isolated and in situ bovine articular chondrocytes. *JOR*, 19(5), 768-778. doi: 10.1016/S0736-0266(01)00013-4
- [6] Chainani, A., Matson, A., Chainani M., Colon, A. J., Toth, A. P., Garrigues, G. E., & Little D. (2020). Contracture and transient receptor potential channel upregulation in the anterior glenohumeral joint capsule of patients with end-stage osteoarthritis. *J Shoulder Elbow Surg*, 29(7), e253-e268. doi: 10.1016/j.jse.2019.11.013
- [7] Dieppe, P. A., & Lohmander, L. S. (2005). Pathogenesis and management of pain in osteoarthritis. *Lancet*, 365(9463), 965-973. doi: 10.1016/S0140-6736(05)71086-2
- [8] Dwivedi, G., Flaman, L., Alaybeyoglu, B., Struglics, A., Frank, E. H., Chubinskya, S., ... & Grodzinsky, A. J. (2022). Inflammatory cytokines and mechanical injury induce post-traumatic osteoarthritis-like changes in a human cartilage-bone-synovium microphysiological system. Arthritis Research & Therapy, 24(1), 198. doi: 10.1186/s13075-022-02881-z
- [9] Fang, T., Zhou, X., Jin, M., Nie, J., & Li, X. (2021). Molecular mechanisms of mechanical load-induced osteoarthritis. *International Orthopaedics*, 45(5), 1125-1136. doi: 10.1007/ s00264-021-04938-1
- [10] Hu, Q., & Ecker, M. (2021). Overview of MMP-13 as a Promising Target for the Treatment of Osteoarthritis. *International Journal of Molecular Sciences*, 22(4), 1742. doi: 10.3390/ijms22041742
- [11] Huh, J. E., Baek, Y. H., Kim, Y. J., Lee, J. D., Choi, D. Y., & Park, D. S. (2009). Protective effects of butanol fraction from Betula platyphyla var. japonica on cartilage alterations in a rabbit collagenase-induced osteoarthritis. *Journal* of Ethnopharmacology, 123(3), 515-521. doi: 10.1016/j. jep.2008.08.028
- [12] Kumar, S., Kumar, H., Mittal, A., Singh, P. P., Yadav, V., Kumar, D., ... & Mishra, V. (2023). Correlation Between Synovial Fluid Levels of Matrix Metalloproteinase's (MMP-1, MMP-3, and MMP-9) and TNF-α with the Severity of Osteoarthritis Knee in Rural Indian Population. *Indian Journal of Orthopaedics*, 57(10), 1659-1666. doi: 10.1007/s43465-023-00974-8
- [13] Liu, L., Cheng, S. D., Cheng, Y., Peng, S. C., Ge, C., & Wang, S. H. (2024). Zhongguo gu shang. China Journal of Orthopaedics and Traumatology, 37(4), 392-398. doi: 10.12200/j.

- issn.1003-0034.20221303
- [14] Lo, L., Koenig, S., Leong, N. L., Shiu, B. B., Hasan, S. A., Gilotra, M. N., & Wang, K. C. (2021). Glenoid bony morphology of osteoarthritis prior to shoulder arthroplasty: what the surgeon wants to know and why. *Skeletal Radiology*, 50(5), 881-894. doi: 10.1007/s00256-020-03647-x
- [15] Lou, Y., Song, F., Kang, Y., & Xu, Y. (2023). Periodic Mechanical Stress Inhibits the Development of Osteoarthritis via Regulating ATF3-Akt Axis. *Journal of Inflammation Research*, 16, 5613-5628. doi: 10.2147/JIR.S419186
- [16] MacFarlane, L. A., Yang, H., Collins, J. E., Jarraya, M., Guermazi, A., Mandl, L. A., ... & MeTeOR Investigator Group (2019). Association of Changes in Effusion-Synovitis With Progression of Cartilage Damage Over Eighteen Months in Patients With Osteoarthritis and Meniscal Tear. Arthritis & Rheumatology (Hoboken, N.J.), 71(1), 73-81. doi: 10.1002/ art.40660
- [17] Marigi, E. M., Statz, J. M., Sperling, J. W., Sanchez-Sotelo, J., Cofield, R. H., & Morrey, M. E. (2020). Shoulder arthroplasty in patients with cerebral palsy: a matched cohort study to patients with osteoarthritis. *JSES*, 29(3), 483-490. doi: 10.1016/j.jse.2019.07.018
- [18] Mehana, E. E., Khafaga, A. F., & El-Blehi, S. S. (2019). The role of matrix metalloproteinases in osteoarthritis pathogenesis: An updated review. *Life Sciences*, 234, 116786. doi: 10.1016/j.lfs.2019.116786
- [19] Menendez, M. E., Puzzitiello, R. N., Moverman, M. A., Kirsch, J. M., Little, D., Jawa, A., & Garrigues, G. E. (2022). The association between anterior shoulder joint capsule thickening and glenoid deformity in primary glenohumeral osteoarthritis. *JSES*, 31(9), e413-e417. doi: 10.1016/j. jse.2022.02.011
- [20] Moody, H. R., Heard, B. J., Frank, C. B., Shrive, N. G., & Oloyede, A. O. (2012). Investigating the potential value of individual parameters of histological grading systems in a sheep model of cartilage damage: the Modified Mankin method. *Journal of Anatomy*, 221(1), 47-54. doi: 10.1111/j.1469-7580.2012.01513.x
- [21] Nedunchezhiyan, U., Varughese, I., Sun, A. R., Wu, X., Crawford, R., & Prasadam, I. (2022). Obesity, Inflammation, and Immune System in Osteoarthritis. *Frontiers in immunology*, 13, 907750. doi: 10.3389/fimmu.2022.907750
- [22] Noh, K. C., Park, S. H., Yang, C. J., Lee, G. W., Kim, M. K., & Kang, Y. H. (2018). Involvement of synovial matrix degradation and angiogenesis in oxidative stress-exposed degenerative rotator cuff tears with osteoarthritis. *JSES*, 27(1), 141-150. doi: 10.1016/j.jse.2017.08.007
- [23] Sanchez-Lopez, E., Coras, R., Torres, A., Lane, N. E., & Guma, M. (2022). Synovial inflammation in osteoarthritis progression. *Nature reviews. Rheumatology*, 18(5), 258-275. doi: 10.1038/s41584-022-00749-9
- [24] Shen, D., Sun, S., Song, Y., Guo, D., & Dong, Y. (2024). Correlation of lower limb alignment with medial mensical extrusion in knee osteoarthritis. Archives of Orthopaedic and Trauma Surgery, 144(11), 4819-4826. doi: 10.1007/ s00402-024-05568-z
- [25] Smith, G. C. S., Geelan-Small, P., & Sawang, M. (2022). A predictive model for the critical shoulder angle based on a three-dimensional analysis of scapular angular and linear morphometrics. *BMC Musculoskeletal Disorders*, 23(1), 1006. doi: 10.1186/s12891-022-05920-7
- [26] Sudah, S. Y., Menendez, M. E., Moverman, M. A., Puzzitiello,

Vol. 31, №1, Page 66-72

- R. N., Little, D., Nicholson, A. D., & Garrigues, G. E. (2022). The role of the anterior shoulder joint capsule in primary glenohumeral osteoarthritis. *JSES Reviews, Reports and Techniques*, *3*(1), 21-27. doi: 10.1016/j.xrrt.2022.09.005
- [27] Troeberg, L., & Nagase, H. (2012). Proteases involved in cartilage matrix degradation in osteoarthritis. *Biochimica* et *Biophysica Acta*, 1824(1), 133-145. doi: 10.1016/j.bbapap.2011.06.020
- [28] Wang, X., Guo, Z., Wang, M., & Xiang, C. (2024). Association between body roundness index and risk of osteoarthritis: a cross-sectional study. *Lipids in Health and Disease*, 23(1), 334. doi: 10.1186/s12944-024-02324-5
- [29] Xiao, S. Q., Cheng, M., Wang, L., Cao, J., Fang, L., Zhou, X. P., ... & Hu, Y. F. (2023). The role of apoptosis in the pathogenesis of osteoarthritis. *International orthopaedics*, 47(8), 1895-1919. doi: 10.1007/s00264-023-05847-1
- [30] Zeng, G. Q., Chen, A. B., Li, W., Song, J. H., & Gao, C. Y. (2015). High MMP-1, MMP-2, and MMP-9 protein levels in osteoarthritis. *Genetics and Molecular Research: GMR*, 14(4), 14811-14822. doi: 10.4238/2015.November.18.46
- [31] Zhu, C., Wu, W., & Qu, X. (2021). Mesenchymal stem cells in osteoarthritis therapy: a review. Am J Transl Res, 13(2), 448-461. PMID: 33594303

## КОРЕЛЯЦІЯ МІЖ ДЕГРАДАЦІЄЮ ХРЯЩА ТА ЗАПАЛЕННЯМ СИНОВІАЛЬНОЇ ОБОЛОНКИ В ІНДУКОВАНІЙ КОЛАГЕНАЗОЮ МОДЕЛІ ОСТЕОАРТРИТУ ПЛЕЧОВОГО СУГЛОБУ У КРОЛИКІВ

Страфун С. С., Богдан С. В., Савосько С. І., Юрійчук Л. М.

Остеоартроз є дегенеративним захворюванням суглобового хряща. Багато досліджень розширили наше розуміння патофізіології захворювання, але досі є дискусійні питання щодо зв'язку між механічним навантаженням на суглоб, запаленням та біохімічними змінами у тканинах хряща, які призводять до його руйнування. Питання першопричини пошкодження хрящової тканини залишається невирішеним, оскільки синовіт та контрактура можуть бути наслідком пошкодження хряща, і, одночасно, дегенерація хряща виникає на тлі синовіту. Тваринні моделі відіграють ключову роль у вивченні цих змін, тому що дають можливість виявити структурні основи та характеристику розвитку порушень тканин суглобу. Наша гіпотеза полягає у тому, що немеханічне пошкодження тканин хряща шляхом введення колагенази до синовіальної порожнини провокує повільний, тривалий розвиток змін у капсулі та суглобовому хрящі. Метою роботи було дослідити зміни хряща та капсули плечового суглобу за умов моделювання колагеназо-індукованого пошкодження суглобу. Кролям у плечовий суглоб вводили колагеназу, а у контралатеральний суглоб фізіологічний розчин. Через 4 місяці досліджували суглобовий хрящ головки плечової кістки і лопатки, капсулу суглобу. Морфометричним методом вимірювали товщину капсули, стан хряща напівкількісно за шкалою і проводили кореляційний аналіз між змінами у досліджуваних структурах суглобу для встановлення залежності між дегенерацією хрящової тканини і фіброзними змінами у синовіальній оболонці. Статистична обробка результатів виконана з використанням непараметричних методів. Введений фермент викликав дегенеративні зміни хрящів плечового суглоба через 3 місяці і це поєднувалося із запальною реакцією у синовіальній мембрані, ознаками ремоделювання сполучної тканини капсули. Результати проведеного дослідження показали, що запалення синовіальної оболонки корелює з деградацією хряща (для головки плечової кістки r=0,74, p=0,02 та заглибини лопатки r=0,71, p=0,03), що скоріше є ранньою подією під час ініціації та прогресування пошкодження суглобових хрящів. Параметри пошкодження синовіальної мембрани та товщина капсули мали пряму кореляцію (r=0,87, p=0,001). Незважаючи на те, що механічне пошкодження є основним фактором ризику остеоартроза, саме повільний, «млявий» розвиток деградуючих змін хряща дав більше нових даних про зв'язок змін у хрящі, синовіальній оболонці та капсулі плечового суглобу. Таким чином, описана у цій роботі модель структурних змін суглобу спричинених колагеназою, є ефективною моделлю для вивчення патогенезу та лікування запальних і дегенеративних процесів плечового суглобу.

Ключові слова: плечовий суглоб, артроз, колагеназа, запалення.

#### Author's contribution

Strafun S. S. - conceptualization, administration.

Bohdan S. V. - resources, review writing and editing.

Savosko S. I. - supervision, software.

Yuriychuk L. M. – data visualization, project administration, research, formal analysis and validation, methodology and writing of the original draft.

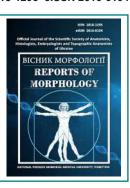
ISSN 1818-1295 eISSN 2616-6194



#### REPORTS OF MORPHOLOGY

Official Journal of the Scientific Society of Anatomists, Histologists, Embryologists and Topographic Anatomists of Ukraine

journal homepage: https://morphology-journal.com



# Morphological changes in the cingulate gyrus in rats with various neurocognitive disorders after traumatic brain injury

Mizyakina K. V., Dzyak L. A., Tverdokhlib I. V.

Dnipro State Medical University, Dnipro, Ukraine

#### **ARTICLE INFO**

Received: 20 May 2024 Accepted: 14 January 2025

UDC: 591.481.1-001:57.012.4

#### **CORRESPONDING AUTHOR**

e-mail: ivt@dmu.edu.ua Tverdokhlib I. V.

#### **CONFLICT OF INTEREST**

The authors have no conflicts of interest to declare.

#### **FUNDING**

Not applicable.

#### **DATA SHARING**

Data are available upon reasonable request to corresponding author.

Information about the sensitivity of different neurons and neuroglia cells to injury and their ability to recover depending on the location of the damage and the nature of microcirculation changes in the post-traumatic period require significant clarification. The study aims to study the tissue and cellular posttraumatic changes in the structure of the cingulate gyrus of the brain frontal lobe of rats with various neurocognitive disorders at different times after severe traumatic brain injury. A "shock acceleration model" was used to reproduce severe traumatic brain injury in rats. According to the results of neurological tests, the rats were divided into three groups: the first – animals after trauma with neurocognitive disorders and memory disorders; the second animals after trauma with neurocognitive disorders without memory disorders; the third comparison group - animals after trauma without neurocognitive disorders. A histological, morphometric and immunohistochemical study of the cingulate gyrus of the frontal lobe was carried out using the markers β-tubulin. Synaptophysin. GAP43, NCAM1, N-cadherin, GFAP. Statistical processing of the obtained results was carried out in the licensed software package "Statistica v6.1" using parametric and nonparametric methods. In animals with neurocognitive disorders, a moderate decrease in the total content of neurons of different types in the cingulate cortex is observed, while in animals without cognitive deficits, the density of neurocytes does not differ from the normal level. The suppressed expression of Synaptophysin in the cingulate cortex in rats with neurocognitive disorders does not change significantly 20 and 40 days after injury and remains at a low level. In animals of the comparison group, the density of p38-positive synapses is restored during the post-traumatic period. 10 days after injury, in animals of all groups, a moderate accumulation of CD56- and N-cadherin-positive protoplasmic astrocytes in the pericapillary spaces is observed, which is often associated with foci of edema and increased mitotic activity of gliocytes. In animals with neurocognitive disorders, in some cases, astroglia form cell layers on the surface of microvessels in the form of dense couplings, which indicates the blockage of transendothelial transport. 40 days after injury, the number of damaged microvessels with layers of astrocytes on the outer surface is significantly reduced. Thus, 10 days after injury, moderately pronounced neurodegenerative and destructive changes occur in the cingulate cortex and adjacent infralimbic cortex due to the posttraumatic cytotoxic cascade. 20 and 40 days after injury, signs of neuroinflammation are reduced regardless of the degree of cognitive deficit.

**Keywords:** traumatic brain injury, rats, neurocognitive disorders, cingulate gyrus, morphology.

#### Introduction

Disorders of higher mental functions are of particular importance among the reasons that determine the degree of disability after traumatic brain injury (TBI). It has been proven that the pathognomonicity of psychopathological consequences depends little on the severity of the injury, the depth of neurological disorders, the features of

macrostructural brain damage and can be formed both in the acute and in the remote period of TBI. A wide range of neurocognitive disorders is formed in the majority of patients with TBI, and in 3-10 % of victims who have a history of severe TBI, dementia develops [10, 13].

The study of pathomorphological mechanisms that

determine the nature of the formation and dynamics of neurocognitive disorders at different times after the injury is of particular interest in solving numerous issues related to the treatment and rehabilitation of patients with TBI. It has been shown that after TBI, the inflammatory response, toxicity of alutamate and other mediators, the formation of free radicals. ionic imbalance and activation of apoptotic processes cause massive secondary neuronal death, meanwhile leading to brain edema, axonal damage and anoxia, destruction of the blood-brain barrier (BBB), increased inflammation, oxidative stress and neurodegeneration, which causes aggravation of cognitive impairment [3, 26, 28]. The main cause of neurocognitive impairment is damage to nerve cells, but astrocytes, oligodendrocytes and microglia are also activated. Astrocyte activation causes hyperplasia of the glial scar after TBI and a number of other macroglial rearrangements [4]. Damaged oligodendrocytes can affect myelin, thus causing dysfunction of nerve conduction [14]. In addition, activated microglial cells participate in phagocytosis and functional recovery, and then initiate further changes in vascular permeability, which causes a cellular anoxia response [1, 26]. It has also been shown that activation of the immune system after TBI leads to the migration of macrophages and monocytes into the damaged area of the brain, with the subsequent release of inflammatory mediators (IL-1β and IL-6) and additional damage to nerve cells [22].

Excitotoxic damage leads to impaired cognitive functions (arousal, speed of information processing, attention, memory, etc.), which are implemented with the participation of the affected brain areas [15, 27]. As the acute neurotransmitter imbalance gradually reduces or transforms, a long-term deficit develops in the cerebral cholinergic systems and, possibly, also in the catecholaminergic structures, which prolongs or deepens the cognitive impairment. It is also reported that there is a close relationship between neurodestructive processes, cognitive impairment and synaptic transmission [8, 9, 12, 23]. Thus, until now, the ideas about the relationship between the sequence of pathogenetic mechanisms of traumatic injury and the nature of cognitive impairment after TBI remain fragmentary. Currently, the data on the dynamics of remote post-traumatic changes in intercellular interactions in different parts of the brain are controversial. The information on the sensitivity of various neurons and neuroglial cells to injury and their ability to recover depending on the localization of damage and the nature of hemomicrocirculation rearrangements in the posttraumatic period requires significant clarification.

The study aims to determine tissue and cellular posttraumatic changes in the structure of the cingulate gyrus in rats with various neurocognitive disorders at different times after severe traumatic brain injury.

#### Materials and methods

To TBI modeling in adult nonlinear male rats (aged 4 to 6 months) weighing 300-400 g, the "shock acceleration model" was used [7, 17]. Before the injury, a 2 cm sagittal scalp

incision was made along the midline under general anesthesia, exposing the bregma and lambda, and a 1 cm diameter steel coin was fixed using cyanoacrylate glue. Standardized TBI was inflicted by freely falling a 450 g weight from a height of 170 cm. Before TBI modeling, as well as 10, 20, and 40 days after it, rats underwent a comprehensive general and neurological examination, which included: 1) assessment of neurological deficit using the mNSS (Modified Neurological Severity Scores) scale with tests of balance on the tube, asymmetry of paw extension, and placement; 2) open field test; 3) conditioned passive avoidance response test [2].

According to the results of neurological tests, the rats were divided into three groups: the first - animals after TBI with neurocognitive disorders and memory impairments; the second - animals after TBI with neurocognitive disorders without memory impairments; the third comparison group - animals after TBI without neurocognitive disorders. The control group consisted of intact rats aged 4.8±0.6 months and weighing 347±28 g. All studies with laboratory animals were conducted in compliance with the provisions of the "European Convention for the Protection of Vertebrate Animals Used for Experimental and Other Scientific Purposes" (Strasbourg, 1986), the Vancouver Declaration on Animal Experiments, the Resolution of the First National Congress on Bioethics (Kyiv, 2001), the Regulation on Bioethics of the Ministry of Health of Ukraine dated November 1, 2000. No. 281, Law of Ukraine "On the Protection of Animals from Cruelty" No. 3446-IV of February 21, 2003 in accordance with the EU Council Directive 2010/63/EU on the enforcement of regulations, laws, administrative provisions of the EU Member States on the protection of animals used for scientific purposes [5, 6].

For pathomorphological examination, the rat brain was removed from the cranial cavity after euthanasia, the condition of the soft tissues, relief, presence of hemorrhages and localization of the slaughter foci were macroscopically assessed. The cerebrum was fixed for 24 hours in a 10 % buffered formalin solution. After fixation, the brain was cut in the frontal plane into slices at the level of the limbic lobe with subsequent manufacture of paraplast blocks. Histological sections 5-7 µm thick with Nissl staining (thionin with the addition of cresyl violet) or silver impregnation [18, 24] were studied using an AxioSkope A1 light-optical microscope ("Carl Zeiss", Germany).

Immunohistochemical study using primary antibodies ( $\beta$ -tubulin, Synaptophysin, GAP43, NCAM1, N-cadherin, GFAP – "Thermo Scientific", USA) was performed in accordance with the protocol, which included the following steps. Histological sections fixed on slides were unmasked for 20 minutes in a microwave oven at +100 °C in citrate buffer (pH 6.0). To assess the specificity of immunohistochemical staining, control reactions were performed. At the next stage, using the Lab Visison Quanto visualization system ("Thermo Scientific", USA), slides and brain preparations were treated with each reagent for 10 minutes with intermediate washing in Trisbuffered solution. 3,3'-Diaminobenzidine ("DakoCytomation",

Denmark) was used as a chromogen. To differentiate cortical structures, the sections were additionally stained with Mayer's hematoxylin according to standards [16, 19].

The studied areas of the cingulate gyrus of the limbic lobe of the cerebrum were photographed using a digital camera Axiocam ERc 5s ("Carl Zeiss", Germany). The obtained micrographs were processed using the AxioVs40 V 4.6.3.0 software ("Carl Zeiss Imaging Solutions GmbH", Germany). The numerical density of neurocytes, the average diameter of the perikaryon of pyramidal neurons, the numerical density of macrogliocytes, microgliocytes and hemocapillaries of the cortex were calculated using the ImageJ 1.47v software package [21].

The statistical processing of the obtained results was carried out taking into account the Student's t criterion. In the event that the empirical distribution obtained in the study did not correspond to the normal law, the assessment of differences between samples was assessed using the nonparametric Wilcoxon test for related samples and Mann-Whitney for unrelated samples or using the Van der Waerden rank test according to standard procedures [11]. When conducting statistical processing of the obtained quantified results, all necessary calculations were performed in the Excel spreadsheet using the appropriate formulas and using the licensed software package "Statistica v6.1" (Statsoft Inc., USA) (serial number AGAR909E415822FA).

#### Results

10 days after the injury in the cingulate cortex and adjacent infralimbic cortex in animals of all groups, cytoarchitectonics was preserved, the ratio between the layers of neurocytes did not differ from the group of intact animals. Moderately expressed neurodegenerative and destructive changes in small areas of gray matter were observed due to the post-traumatic cytotoxic cascade. In some areas of the cortex, signs of moderate intercellular and perivascular edema were observed (Fig. 1). Necrotically or apoptotically altered neurocytes were not detected. Damage to the microcirculatory bed was observed around a small number of hemocapillaries in the form of thickening and compaction of the endothelial basement membrane. 20 and 40 days after TBI, single "shadows" of neurocytes were observed in the cingulate cortex against the background of optically unchanged neuropil without signs of neuroinflammation.

When morphometrically determining the numerical density of  $\beta$ -tubulin-positive cells 10 days after injury, a moderate decrease in the total content of neurons of different types was observed in the cingulate cortex in rats of the first and second groups – by 33.8 % (p<0.05) and 41.1 % (p<0.05), respectively, while in the comparison group the parameter did not differ statistically from the level of intact animals (Table 1). 20 days after TBI in the first and second groups of animals, the numerical density of neurons moderately increased relative to the previous period due to the reduction of pericellular and perivascular edema and other tissue signs of neurodestruction, although

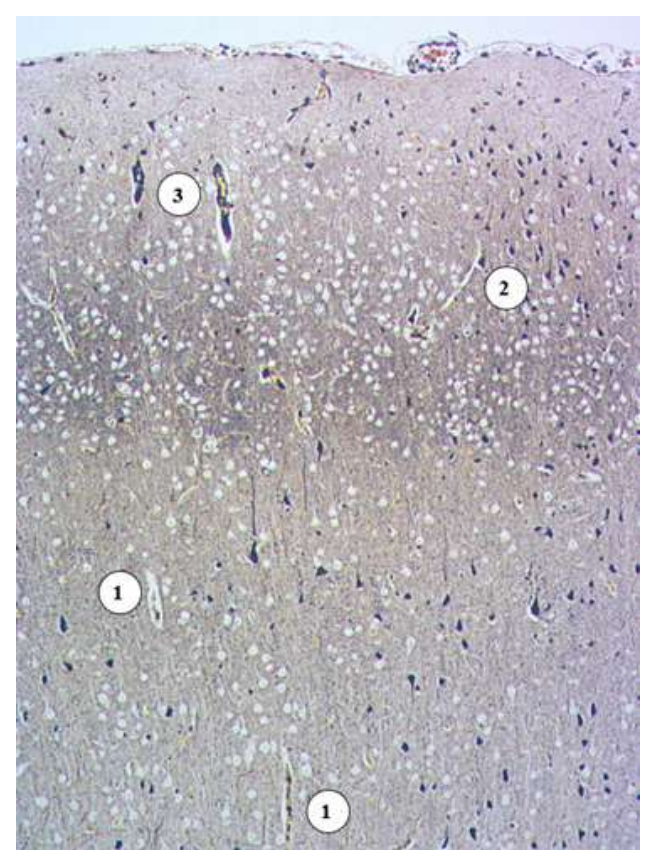


**Fig. 1.** The rat cingulate cortex in the 2nd experimental group 10 days after TBI. Perivascular edema (1), intercellular edema (2), damaged microvessels (3). Silver impregnation. ×100.

it was significantly lesser to the normal level – by 24.7 % (p<0.05) and 26.6 % (p<0.05), respectively. After 40 days of the experiment, the numerical density of neurocytes in the cingulate cortex of the first and second experimental groups did not change significantly compared to the previous period, yielding to the indicator of intact animals by 28.9 % (p<0.05) and 23.2 % (p<0.05), respectively.

Table 1. Numerical density of neurocytes in the cingulate cortex,  $\times 10^2$  mm $^{-2}$  (M±m).

Time after injury	Study groups		
	First	Second	Comparison
10 days	20.96±1.55* **	18.63±1.34* **	27.58±2.21
20 days	23.82±1.34*	23.27±2.02*	28.33±2.66
40 days	22.49±1.96*	24.26±2.17*	29.85±2.12

**Notes:** \* – p<0.05 when compared with the value in the intact group (31.63 $\pm$ 2.14 ×10<sup>2</sup> mm<sup>-2</sup>); \*\* – p<0.05 when compared with the value corresponding to the term in the comparison group.

Morphological features of small multipolar neurocytes and excitatory stellate neurons of the granular layer of the cingulate cortex in all studied experimental groups did not differ significantly from the characteristics of the intact group of animals at all stages of the experiment. Some pyramidal neurons 10 days after injury had signs of partial chromatolysis and reduced dendrites. In some cases, figures of apoptosis or

Vol. 31, №1, Page 73-81

"shadows" of neurons, hyperchromic pyramids with winding neurites or signs of chromatolysis were found. The most majority of neurocytes after TBI retained a characteristic conical shape. 20 and 40 days after the injury, damaged neurocytes in the pyramidal layer were not detected in any of the experimental groups.

Morphometric analysis showed that the size of the neurons of the pyramidal layer did not differ significantly between the three experimental groups, but were significantly lesser to the normal value of the average diameter of the perikaryon of intact rats 10 days after the application of TBI (Table 2). The most pronounced decrease in the size of the perikaryons was observed in the first group of animals – by 28.6 % (p<0.05). In animals of the second group, the parameter was lesser to the normal level by 28.1 % (p<0.05), in animals of the comparison group – by 26.4 % (p<0.05). 20 and 40 days after injury, the size of the neurons of the pyramidal layer in animals of all study groups did not differ statistically from the indicator of intact animals.

**Table 2.** Average diameter of the perikaryon of pyramidal neurons of the cingulate cortex, µm (M±m).

Time after injury	Study groups		
	First	Second	Comparison
10 days	4.063±0.386*	4.082±0.318*	4.184±0.341*
20 days	5.452±0.314	5.356±0.401	5.498±0.415
40 days	5.587±0.353	5.515±0.415	5.458±0.433

**Note:** \* – p<0.05 when compared with the value in the intact roup (5.681 $\pm$ 0.417  $\mu$ m).

When analyzing the effect of TBI on the synaptic apparatus of the cingulate gyrus and adjacent infralimbic cortex using monoclonal antibodies to Synaptophysin (p38), animals of all experimental groups showed a moderate decrease in the expression of this marker 10 days after injury compared to intact animals. The diffuse distribution of the immunohistochemical label of the p38 marker did not differ between the studied groups of animals (Fig. 2). 20 and 40 days after TBI, the expression of Synaptophysin in the rat cingulate cortex in the first and second experimental groups did not change significantly, remaining at a low level. On the contrary, in animals of the comparison group, the density of p38-positive synapses was restored during the post-traumatic period (Fig. 3).

The study of the synaptic marker GAP43, which reflects the remodeling of axon terminals, showed the absence of GAP43-positive structures in the cingulate cortex both in intact rats and in all three experimental groups of animals during the studied post-traumatic period.

In animals of the three experimental groups after TBI using the markers NCAM1 and N-cadherin, it was found that the intensity of the immunohistochemical label on the surface of the perikaryons of most neurons of the cingulate cortex did not differ from the expression of these markers on the membranes of intact neurons, although the overall intensity of immunohistochemical staining of the sections was noticeably lower after TBI compared to intact animals due

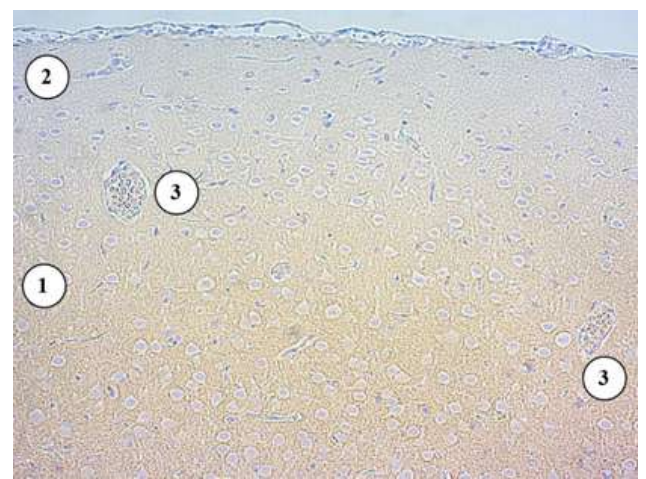


**Fig. 2.** The rat cingulate cortex in the 1st experimental group 10 days after TBI. Diffuse expression of synaptophysin of low intensity around pyramidal neurons (1), lack of expression in the superficial layers of the cortex (2), damaged microvessels (3). Immunohistochemistry with antibodies against p38. Additional staining with Mayer's hematoxylin. ×200.

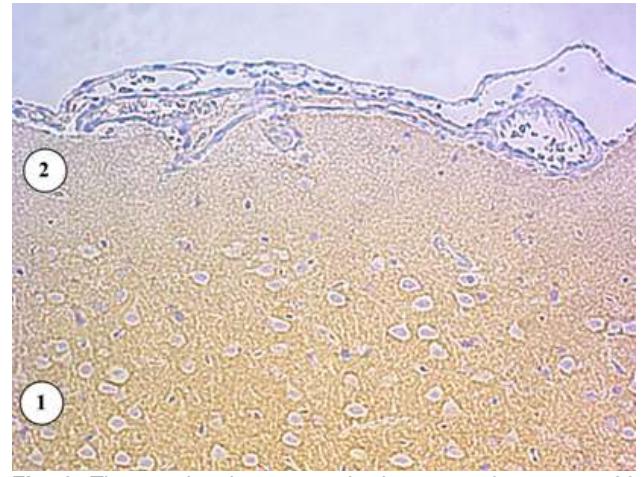


**Fig. 3.** The rat cingulate cortex in the comparison group 20 days after TBI. Diffuse expression of synaptophysin of moderate intensity around pyramidal neurons (1), low expression in the superficial layers of the cortex (2). Immunohistochemistry with antibodies against p38. Additional staining with Mayer's hematoxylin. ×200.

to the death of a portion of neurons. The distribution pattern of CD56-positive and N-cadherin-positive neurocytes in rats of the experimental groups did not change during the entire post-traumatic period.

When studying the cingulate cortex TBI, characteristic signs of apoptotic death of a small number of pyramidal neurons were observed in animals of the studied groups at all times of the experiment, which indicated a limited neurodegenerative process in this brain localization. Necrotically altered neurons in the cingulate gyrus and adjacent infralimbic cortex were not detected in any group of animals at all times after injury. Manifestations of autophagy of large pyramidal neurocytes were rare, their frequency did not depend on the time after injury.

The study of the glial component of the cortex of the cingulate gyrus and adjacent infralimbic cortex revealed significant morphogenetic rearrangements of macrogliocytes both in terms of the pattern of their spatial redistribution and proliferative properties. In particular, 10 days after TBI, animals of all experimental groups showed a moderate increase in the number of protoplasmic astrocytes, but macrogliocytes of other types did not change compared to intact animals. The accumulation of astrocytes was observed mainly in the pericapillary spaces, which was often associated with foci of edema and increased mitotic activity of gliocytes 10 days after injury. The density of fibrous astrocytes in the neuropil did not differ from the typical architectonics of intact rats. Astrocytes with branched processes contacted each other. 20 and 40 days after TBI, animals of all experimental groups did not show significant pathomorphological changes or rearrangements of the structural organization of macroglia in the studied localization.

Immunohistochemical determination of markers CD56 (NCAM1) and N-cadherin, which are responsible for intercellular cooperation not only of neurocytes, but also of the glial component of nervous tissue, showed certain features of the label distribution in the rat cingulate cortex in all studied groups. 10 days after the application of TBI, protoplasmic astrocytes around a small number of hemocapillaries intensively accumulated the label of both specified markers. The neuropil between microvessels contained a significantly lower density of CD56- and N-cadherin-positive cells. During the studied post-traumatic period, the distribution pattern of immunohistochemical label did not change and did not become equal between the three experimental groups.

Morphometric analysis of macrogliocytes using monoclonal antibodies against GFAP showed that 10 days after the start of the experiment, the average numerical density of cells in the rat cingulate cortex was lesser to the normal value in the first group by 26.4 % (p<0.05), in the second – by 22.6 % (p<0.05), in the comparison group – by 18.3 % (p<0.05). 20 days after the injury in animals of the first and second experimental groups, the degree of astrocytic deficiency did not significantly change compared to the previous period; in rats of the comparison group – it disappeared when compared with the norm (Table 3). 40 days after TBI in animals of the first and second groups, the parameter returned to normal values, not differing from the indicator of the comparison group.

**Table 3.** Numerical density of macrogliocytes in the cingulate cortex, ×10<sup>2</sup> mm<sup>-2</sup> (M±m).

Time after injury	Study groups		
	First	Second	Comparison
10 days	168.9±176.4*	177.5±12.1*	187.6±16.4*
20 days	174.5±13.4* **	167.8±13.5* **	205.1±15.7
40 days	217.7±22.3	211.0±18.3	218.7±26.6

**Notes:** \* – p<0.05 when compared with the value in the intact group (229.5±18.1 ×102 mm-2); \*\* – p<0.05 when compared with the value corresponding to the term in the comparison group.

The morphology of microgliocytes was not the same in different layers of the rat cingulate cortex in the studied groups. The most majority of cells had a flattened shape and complexly branched processes that were immersed between neurons or in the depth of the neuropil. Also, near the hemocapillaries, spherical microgliocytes with single long wavy processes were found, which contacted the BBB elements. In some observations, typical circulating macrophages and single lymphocytes were located perivascularly in the pyramidal layers, which indicated residual manifestations of the inflammatory process without signs of edema.

When morphometry of the numerical density of microgliocytes of the cingulate gyrus in all studied animals 10 days after TBI, a significantly increased level of cell density with macrophage activity by 91-106 % was noted compared to intact animals (Table 4). After 20 and 40 days after TBI, a gradual decrease in the density of microgliocytes was observed, but even at the end of the studied post-traumatic period, their number exceeded the indicator of intact animals: in the first group – by 44.4 % (p<0.05), in the second group – by 29.9 % (p<0.05), in the comparison group – by 25.7 % (p<0.05). Statistically significant differences of the parameter in the first and second groups from the indicators of the comparison group were not observed throughout the entire post-traumatic period.

**Table 4.** Numerical density of microgliocytes of the cingulate cortex,  $\times 10^2$  mm<sup>-2</sup> (M±m).

ſ	Time after injury	Study groups		
		First	Second	Comparison
	10 days	2.704±0.452*	2.508±0.339*	2.635±0.366*
	20 days	2.187±0.324*	2.112±0.403*	1.942±0.299*
	40 days	1.891±0.357*	1.704±0.346*	1.655±0.313*

**Note:** \* - p<0.05 when compared with the value in the intact group (1.312±0.166 ×10² mm $^2$ ).

When studying the microcirculation of the cingulate cortex 10 days after TBI in animals of all experimental groups the majority of hemocapillaries had an intact wall structure and formed a typical BBB structure. Some microvessels with signs of intravascular microthrombosis were detected surrounded by small foci of secondary hemorrhages, with plasmatic infiltration of the hemocapillary wall and perivascular space. In animals with neurocognitive disorders, pathologically altered microvessels with astrocyte layers on the outer surface were detected (Fig. 4, 5), while in animals of the comparison group, astrocytes did not form any cell conglomerates near microvessels (Fig. 6). Hemocapillaries with necrosis, destruction or fragmentation of the endothelial wall were not detected. 20 and 40 days after the injury, the number of pathologically altered microvessels and foci of diapedetic hemorrhages in the cortical tissue significantly decreased in all animals.

When morphometrically determining the numerical density of hemocapillary vessels in the cingulate cortex 10 days after TBI, a significantly increased level of the parameter was observed compared to the intact one: in animals of the

Vol. 31, №1, Page 73-81

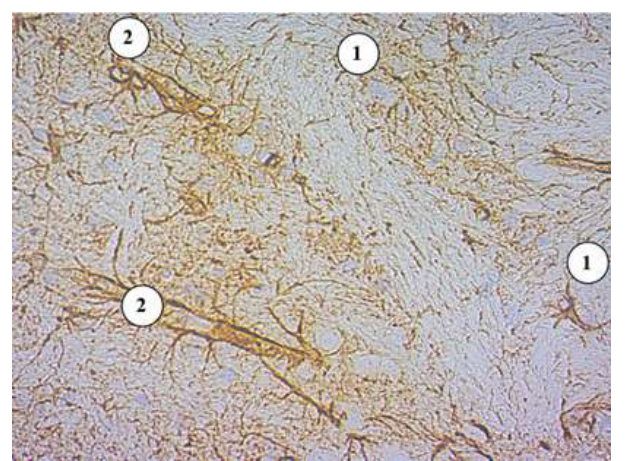


**Fig. 4.** The rat cingulate cortex in the 1st experimental group 10 days after TBI. Fibrous astrocyte (1), astrocytic conglomerate around the hemocapillaries (2). Immunohistochemistry with antibodies against GFAP. Additional staining with Mayer's hematoxylin. ×400.

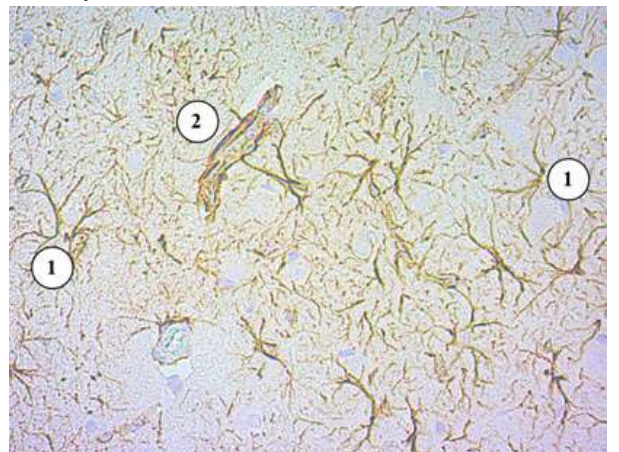
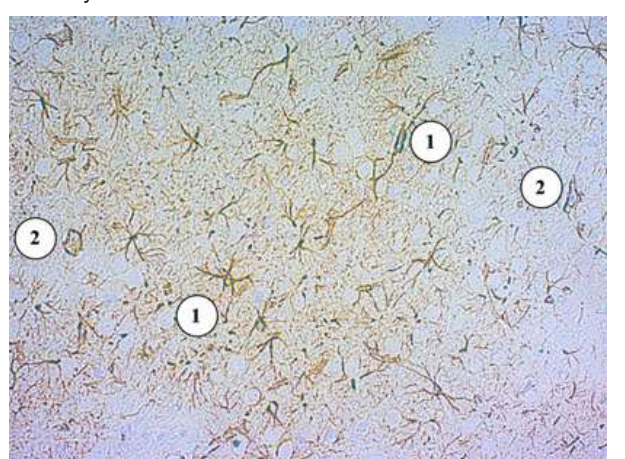


Fig. 5. The rat cingulate cortex in the 2nd experimental group 10 days after TBI. Fibrous astrocyte (1), astrocytic conglomerate around the hemocapillaries (2). Immunohistochemistry with antibodies against GFAP. Additional staining with Mayer's hematoxylin. ×400.



**Fig. 6.** The rat cingulate cortex in the comparison group 10 days after TBI. Fibrous astrocyte (1), hemocapillary (2). Immunohistochemistry with antibodies against GFAP. Additional staining with Mayer's hematoxylin. ×200.

first group – by 34.9 % (p<0.05); in the second group – by 39.0 % (p<0.05); in the comparison group – by 40.4 % (p<0.05). 20 and 40 days after the experimental injury, the density of microvessels in the cingulate cortex returned to normal levels in all experimental groups of animals (Table 5).

**Table 5.** Numerical density of hemocapillaries in the cingulate cortex, mm<sup>-2</sup> (M±m).

Time after injury	Study groups		
	First	Second	Comparison
10 days	63.16±7.41*	65.03±8.17*	65.71±7.56*
20 days	53.22±5.55	50.86±6.65	53.75±6.28
40 days	51.16±6.84	48.63±5.31	50.94±7.22

**Note:** \* - p<0.05 when compared with the value in the intact group (46.83±5.38  $\mathrm{MM}^{-2}$ ).

#### **Discussion**

TBI causes a complex set of primary and secondary reactions that damage brain areas that serve certain cognitive functions. Focal injuries cause persistent cognitive impairments, the types of which are relatively easy to understand on the basis of modern neuroanatomical concepts [20]. In addition, axonal damage in combination with cytotoxic processes is the most common pathomorphological cause of post-traumatic cognitive impairments and has the greatest impact on the speed and efficiency of information processing [8, 15]. In this regard, the specific topological features of the structural reorganizations of different parts of the brain that occur during the remote post-traumatic period and are associated with the nature of neurocognitive disorders are of interest.

Our study analyzed reversible and stable morphological changes in the rat cingulate gyrus and adjacent infralimbic cortex for 40 days after the application of standardized symmetric severe TBI in the shock acceleration model. It was shown that 10 days after the injury, moderately pronounced neurodegenerative and destructive changes in gray matter occur in the cingulate cortex. In animals with neurocognitive disorders, a moderate decrease in the total content of neurons of different types is observed, while in animals without cognitive deficits, the density of neurocytes does not differ from the normal level. 20 and 40 days after TBI, signs of neuroinflammation in the cingulate cortex are reduced regardless of cognitive deficit degree.

According to the results of the immunohistochemical study, it was found that the suppressed expression of Synaptophysin in the cingulate cortex in rats with neurocognitive disorders 20 and 40 days after TBI does not change significantly and remains at a low level. In animals of the comparison group, the density of p38-positive synapses is restored during the post-traumatic period. 10 days after TBI, a moderate accumulation of CD56- and N-cadherin-positive astrocytes in the pericapillary spaces is observed in the cingulate cortex in animals of all groups, which is often associated with foci of edema and increased mitotic activity of gliocytes. At the same time, significant areas of neuropil with a low density of fibrous astrocytes are formed. After 20 and

40 days of post-traumatic period, foci of astrocytic deficiency persist in animals with neurocognitive disorders, while they are very rare in rats of the comparison group.

Our data quantitatively characterize and explain numerous information in the scientific literature that the destruction and tension of axons causes a sharp increase in the level of most cerebral neurotransmitters, and the traumatically induced excess of glutamate and acetylcholine is the most neurotoxic [23]. The destructive consequences of such an excess of neurotransmitters are greatest in those areas where these neurotransmitters are localized together – in the structures of the hippocampal complex, the basal forebrain, the frontal cortex and the cortex of the limbic lobe.

It is noteworthy that after TBI, the inflammatory reaction, glutamate toxicity, and activation of apoptotic processes cause massive secondary neuronal death, while leading to neurodegeneration, which causes cognitive impairment [3, 26, 28]. Our study shows that in the cingulate cortex distant from the injury zone in animals with neurocognitive disorders, a significant increase in the number of newly formed hemocapillaries with a typical endothelial wall structure is observed, but on the surface of some damaged capillaries, a large number of densely packed protoplasmic astrocytes are found. In these cases, astroglia form cellular layers on the surface of microvessels in the form of dense couplings, which indicates the blockage of transendothelial transport. In our opinion, the presence of such pathologically altered hemocapillaries in the cingulate gyrus may be one of the morphological components of persistent neurocognitive deficit.

#### **Conclusions**

1. 10 days after injury, moderately pronounced neurodegenerative and destructive changes in gray matter occur in the cingulate cortex and adjacent infralimbic cortex due to the post-traumatic cytotoxic cascade. In animals with

neurocognitive disorders, a moderate decrease in the total content of cortical neurons is observed (in the first group – by 33.8 %, in the second group – by 41.1 %), while in animals without cognitive deficits, the density of neurocytes does not differ from the normal level. 20 and 40 days after TBI, signs of neuroinflammation in the cingulate cortex are reduced regardless of cognitive deficit degree.

- 2. Suppressed expression of Synaptophysin in the cingulate cortex in rats with neurocognitive disorders does not change significantly 20 and 40 days after TBI and remains at a low level. In animals of the comparison group, the density of p38-positive synapses is restored during the post-traumatic period.
- 3. 10 days after TBI, in the cingulate cortex in animals of all groups, a moderate accumulation of CD56- and N-cadherin-positive protoplasmic astrocytes in the pericapillary spaces is observed, which is often associated with foci of edema and increased mitotic activity of gliocytes. At the same time, significant areas of neuropil with a low density of fibrous astrocytes are formed. After 20 and 40 days of the post-traumatic period, foci of astrocytic deficiency are preserved in animals with neurocognitive disorders, while in rats of the comparison group they are very rare.
- 4. 10 days after TBI, animals with neurocognitive disorders show a significant increase in the number of newly formed hemocapillaries with a typical endothelial wall structure and normal blood filling, accompanied by astrocytic glia and with a formed BBB. A large number of densely packed protoplasmic astrocytes are found on the surface of single damaged capillaries. In some cases, astroglia form cell layers on the surface of microvessels in the form of dense couplings, which indicates the blockage of transendothelial transport. 40 days after injury, the number of damaged microvessels with layers of astrocytes on the outer surface is significantly reduced.

#### References

- [1] Bachstetter, A. D., Zhou, Z., & Rowe, R. K. (2016). MW151 Inhibited IL-1β Levels after Traumatic Brain Injury with No Effect on Microglia Physiological Responses. *PLoS One*, *11*(2), e0149451. doi: 10.1371/journal.pone.0149451
- [2] Bureš, J., Burešová, O., & Huston, J. P. (2016). Techniques and basic experiments for the study of brain and behavior. Second edition. Amsterdam – New York: Elsevier science publishers BV.
- [3] Chary, K., Nissi, M. J., Nykänen, O., Manninen, E., Rey, R. I., Shmueli, K., Sierra, A., & Gröhn, O. (2021). Quantitative susceptibility mapping of the rat brain after traumatic brain injury. NMR Biomed, 34(2), e4438. doi: 10.1002/nbm.4438
- [4] Di Giovanni S., Movsesyan, V., & Ahmed, F. (2005). Cell cycle inhibition provides neuroprotection and reduces glial proliferation and scar formation after traumatic brain injury. *Proc Natl Acad Sci USA*, 102(23), 8333-8338. doi: 10.1073/ pnas.0500989102
- [5] Directive 2010/63/EU of the European Parliament and of the Council of 22 September 2010 on the protection of animals used for scientific purposes. (2010). Official Journal of the European Union, 53(L276), 33-79.

- [6] de l'Europe, C. (1986). European Convention for the protection of vertebrate animals used for experimental and other scientific purposes/Convention européenne sur la protection des animaux vertébrés utilisés à des fins expérimentales ou à d'autres fins scientifiques:[Strasbourg, 18. III. 1986]. Conseil de l'Europe Section des publications.
- [7] Foda, M. A., & Marmarou, A. (1994). A new model of diffuse brain injury in rats. Part II: Morphological characterization. *J Neurosurg*, 80(2), 301-313. doi: 10.3171/ jns.1994.80.2.0301
- [8] Griffiths, D. R., Law, L. M., Young, C., Fuentes, A., Truran, S., Karamanova, N., ... & Lifshitz, J. (2022). Chronic Cognitive and Cerebrovascular Function after Mild Traumatic Brain Injury in Rats. *J Neurotrauma*, 39(19-20), 1429-1441. doi: 10.1089/neu.2022.0015
- [9] Gu, Y. L., Zhang, L. W., & Ma, N. (2014). Cognitive improvement of mice induced by exercise prior to traumatic brain injury is associated with cytochrome C oxidase. *Neurosci Lett*, 570, 86-91. doi: 10.1016/j.neulet.2014.04.004
- [10] Howlett, J. R., Nelson, L. D., & Stein, M. B. (2022). Mental Health Consequences of Traumatic Brain Injury. Biol Psy-

Vol. 31, №1, Page 73-81

- *chiatry*, *91*(5), 413-420. doi: 10.1016/j.biopsych.2021.09.024 [11] Hruzieva, T. S., Lekhan, V. M., Ohniev, V. A., Haliienko, L. I.,
- [11] Hruzieva, T. S., Lekhan, V. M., Ohniev, V. A., Haliienko, L. I., Kriachkova, L. V., & Palamar, B. I. (2020). Біостатистика [Biostatistics]. Вінниця: Нова книга=Vinnytsia: New Book.
- [12] Hui, Y., Zhao, H., Shi, L., & Zhang, H. (2023). Traumatic Brain Injury-Mediated Neuroinflammation and Neurological Deficits are Improved by 8-Methoxypsoralen Through Modulating PPARγ/NF-κB Pathway. Neurochem Res, 48(2), 625-640. doi: 10.1007/s11064-022-03788-6
- [13] James, S. L., Theadom, A., & Ellenbogen, R. G. (2019). Global, regional, and national burden of traumatic brain injury, 1990-2016 a systematic analysis for the Global Burden of Disease Study 2016. *Lancet Neurol*, 18(1), 56-87. doi: 10.1016/S1474-4422(18)30415-0
- [14] Jones, N. C., Cardamone, L., Williams, J. P., Salzberg, M. R., Myers, D., & O'Brien, T. J. (2008). Experimental traumatic brain injury induces a pervasive hyperanxious phenotype in rats. *J Neurotrauma*, 25(11), 1367-1374. doi: 10.1089/neu.2008.0641
- [15] Macks, C., Jeong, D., Bae, S., Webb, K., & Lee, J. S. (2022). Dexamethasone-Loaded Hydrogels Improve Motor and Cognitive Functions in a Rat Mild Traumatic Brain Injury Model. *Int J Mol Sci*, 23(19), 11153. doi: 10.3390/ijms231911153
- [16] Magaki, S., Hojat, S. A., Wei, B., So, A., & Yong, W. H. (2019). An Introduction to the Performance of Immunohistochemistry. *Methods Mol Biol*, 1897, 289-298. doi: 10.1007/978-1-4939-8935-5\_25
- [17] Marmarou, A. I., Foda, M. A., & van den Brink, W. (1994). A new model of diffuse brain injury in rats. Part I: Pathophysiology and biomechanics. *J Neurosurg*, 80(2), 291-300. doi: 10.3171/jns.1994.80.2.0291
- [18] Mulish, M., & Welsh, U. (2010). Romeis Mikroscopiche technic. Heidelberg: Spektrum Akademischer Verlag. doi: 10.1007/978-3-8274-2254-5
- [19] Nguyen, T. (2022). Immunohistochemistry: A Technical Guide to Current Practices. Cambridge: Cambridge University Press.
- [20] Nie, L., He, J., Wang, J., Wang, R., Huang, L., Jia, L., ... & Wang, J. (2023). Environmental Enrichment for Stroke and

- Traumatic Brain Injury: Mechanisms and Translational Implications. *Compr Physiol*, *14*(1), 5291-5323. doi: 10.1002/cphy.c230007
- [21] Poslavska, O. V. (2016). Визначення лінійних розмірів та площ окремих морфологічних об'єктів на мікрофотографіях за допомогою програми ImageJ. [Determination of linear dimensions and areas of individual morphological objects on photomicrographs using the ImageJ program]. Морфологія=Morphologia, 10(3), 377-381.
- [22] Shaw, B. C., Anders, V. R., Tinkey, R. A., Habean, M. L., Brock, O. D., Frostino, B. J., & Williams, J. L. (2023). Immunity impacts cognitive deficits across neurological disorders. *J Neurochem*, 10(1111), jnc.15999. doi: 10.1111/jnc.15999
- [23] Song, H., Chen, C., Kelley, B., Tomasevich, A., Lee, H., Dolle, J. P., ... & Smith, D. H. (2022). Traumatic brain injury recapitulates developmental changes of axons. *Prog Neurobiol*, 217, 102332. doi: 10.1016/j.pneurobio.2022.102332
- [24] Suvarna, S. K., Layton, C., & Bancroft, G. D. (2019). Bancroft's Theory and Practice of Histological Techniques, 8th Edition. Elsevier. doi: 10.1016/B978-0-7020-6864-5.00008-6
- [25] Wu, M., Wang, C., Gong, Y., Huang, Y., Jiang, L., Zhang, M., ... & Dang, B. (2023). Potential mechanism of TMEM2/CD44 in endoplasmic reticulum stress-induced neuronal apoptosis in a rat model of traumatic brain injury. *Int J Mol Med*, 52(6), 119. doi: 10.3892/ijmm.2023.5322
- [26] Wu, W., Tian, R., Hao, S., Xu, F., Mao, X., & Liu, B. (2014). A pre-injury high ethanol intake in rats promotes brain edema following traumatic brain injury. *Br J Neurosurg*, 28(6), 739-745. doi: 10.3109/02688697.2014.915007
- [27] Yang, Z., Zhu, T., Pompilus, M., Fu, Y., Zhu, J., Arjona, K., ... & Febo, M. (2021). Compensatory functional connectome changes in a rat model of traumatic brain injury. *Brain Commun*, 3(4), 244. doi: 10.1093/braincomms/fcab244
- [28] Zohar, O., Lavy, R., Zi, X., Nelson, T. J., Hongpaisan, J., Pick, C. G., & Alkon, D. L. (2011). PKC activator therapeutic for mild traumatic brain injury in mice. *Neurobiol Dis*, 41(2), 329-337. doi: 10.1016/j.nbd.2010.10.001

### МОРФОЛОГІЧНІ ЗМІНИ ПОЯСНОЇ ЗВИВИНИ У ЩУРІВ З РІЗНИМИ НЕЙРОКОГНІТИВНИМИ РОЗЛАДАМИ ПІСЛЯ ЧЕРЕПНО-МОЗКОВОЇ ТРАВМИ

Мізякіна К. В., Дзяк Л. А., Твердохліб І. В.

Потребують суттєвих уточнень відомості про чутливість різних нейронів і клітин нейроглії до травми та їх здатність до відновлення в залежності від локалізації ушкоджень та характеру перебудов гемомікроциркуляції в посттравматичному періоді. Метою дослідження було визначення тканинних і клітинних посттравматичних змін структури поясної звивини лімбічної частки головного мозку щурів з різними нейрокогнітивними розладами у різні терміни після тяжкої черепно-мозкової травми. Для відтворення тяжкої черепно-мозкової травми у щурів застосовували «модель ударного прискорення». За результатами неврологічних тестів щури були розподілені на три групи: перша – тварини після травми з нейрокогнітивними розладами і порушеннями пам'яті; друга — тварини після травми з нейрокогнітивними розладами без порушень пам'яті; третя група порівняння – тварини після травми без нейрокогнітивних розладів. Проводили гістологічне, морфометричне та імуногістохімічне дослідження поясної звивини з використанням маркерів β-tubulin, Synaptophysin, GAP43, NCAM1, N-cadherin, GFAP. Статистичну обробку отриманих результатів проводили в ліцензійному програмному пакеті «Statistica v6.1» з використанням параметричних і непараметричних методів. У тварин з нейрокогнітивними розладами спостерігається помірне зменшення сумарного вмісту нейронів різних типів поясної кори, в той час як у тварин без когнітивного дефіциту щільність нейроцитів не відрізняється від нормального рівня. Пригнічена експресія синаптофізину у корі поясної звивини щурів з нейрокогнітивними розладами через 20 і 40 діб після травми суттево не змінюється та залишається на низькому рівні. У тварин групи порівняння відбувається відновлення щільності р38-позитивних синапсів протягом посттравматичного періоду. Через 10 діб після травми у тварин всіх груп спостерігається помірне накопичення CD56- і N-кадгерин-позитивних протоплазматичних астроцитів у перикапілярних просторах, що часто асоційовано з осередками набряку і підвищенням мітотичної активності гліоцитів. У тварин з нейрокогнітивними розладами в окремих випадках астроглія утворює клітинні нашарування на поверхні мікросудин у

вигляді щільних муфт, що вказує на блокування трансендотеліального транспорту. Через 40 діб після травми суттєво зменшується кількість ушкоджених мікросудин з нашаруваннями астроцитів на зовнішній поверхні. Таким чином, через 10 діб після нанесення травми у складі кори поясної звивини та прилеглої інфралімбічної кори відбуваються помірно виражені нейродегенеративні та деструктивні зміни внаслідок посттравматичного цитотоксичного каскаду. Через 20 і 40 діб після травми ознаки нейрозапалення редукуються незалежно від ступеня когнітивного дефіциту. Ключові слова: черепно-мозкова травма, щури, нейрокогнітивні розлади, поясна звивина, морфологія.

#### Author's contribution:

Mizyakina K. V. - research, review writing and editing.

Dzyak L. A. - conceptualization.

Tverdokhlib I. V. – methodology, resources, project administration.

Vol. 31, №1, Page 73-81

Signed for print 18.03.2025 Format 60x84/8. Printing offset. Order № 1973. Circulation 100. Vinnytsia. Printing house "TVORY", Nemyrivske shose St., 62a, Vinnytsya, 21034 Phone: 0 (800) 33-00-90, (096) 97-30-934, (093) 89-13-852,

(098) 46-98-043

e-mail: tvory2009@gmail.com http://www.tvoru.com.ua